THE PETROLOGY AND GEOCHEMISTRY OF THE KAROO SEQUENCE BASALTIC ROCKS IN THE NATAL DRAKENSBERG AT SANI PASS

by

Vijay Rajlal Ramluckan

Submitted in part fulfillment of the requirements for the degree of

MASTER OF SCIENCE

in the Department of Geology in the faculty of Science at the
University of Durban-Westville.

Supervisor: Dr A A Mitchell

Joint Supervisor: Dr J N Dunlevey

Date Submitted: 18 December 1992

DECLARATION

All work in this thesis is the original work of the author except where specific acknowledgement is made to the work of others.

SIGNED: 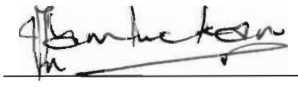

V R Ramluckan
Department of Geology
University of Durban-Westville
Private Bag X54001
DURBAN
4000

December 1992

ABSTRACT

The Sani Pass in the Natal Drakensberg is situated in the north-eastern sector of the Lesotho Highlands which forms a major Karoo-age basaltic massif in the Karoo Igneous Province. The volcanic section exposed in the pass is approximately 800m thick, and comprises a succession of regularly stratified, massive and amygdaloidal lavas which were extruded mainly by fissure-type eruptions. Dolerite dykes, which now occupy the fissures, form a network of predominantly NE-SW and NW-SE trending topographic features.

During post-eruption cooling hydrothermal solutions percolated through the volcanic succession and produced an amygdale zonation which was controlled predominantly by ambient pressure and temperature conditions. An original maximum thickness of 1 820m of the volcanic succession has therefore been estimated and an average fossil geothermal gradient of 111°C/km is conceived to have persisted during amygdale formation.

New electron microprobe data are presented for the silicate phases in the Sani Pass basalts and dolerites. These data do not effectively separate the Sani Pass volcanic succession into different geochemical units. Microprobe analyses for olivine, albeit limited, are in the forsterite range and indicate that a proportion of olivine in the high-MgO basalts is due to cumulus enrichment. The pyroxenes are predominantly augite and minor pigeonite, with some of the augites displaying a tholeiitic trend similar to that recognised at Skaergaard. Plagioclase is mainly in the labradorite to bytownite range, the phenocrysts being slightly enriched in anorthite compared to the groundmass.

The use of whole-rock geochemistry for 67 basalts and 8 dolerites has permitted the recognition of five geochemically distinct magma types, namely, the Giant's Cup, Agate Vale, Sakeng, Mkhomazana and the Phinong. The Phinong basalts comprise the upper two-thirds of the volcanic succession and although are generally homogeneous, there is a slight tendency for the more evolved rocks to be found higher up in the stratigraphic sequence. The remaining magma types precede the Phinong succession and are generally enriched in silica and have higher Zr/Nb and lower P/Zr ratios than the Phinong basalts. Within the pre-Phinong succession the Giant's Cup basalts are generally depleted in the compatible elements, while the overlying Agate Vale basalts are enriched in incompatible elements. Except for a marginally lower Na_2O and Sr content, the chemistry of the Sakeng basalts is variable, generally overlapping with the other magma types. The Mkhomazana basalts are slightly enriched in MgO, Ni, Cr and Sc compared to all other pre-Phinong basalts. The dolerites in the area adjacent to the Sani Pass are geochemically similar to the Phinong basalts.

The Phinong magma type is considered to be equivalent to the Lesotho magma type, based on their geochemical and stratigraphical similarities. In terms of discriminant diagrams the Giant's Cup, Sakeng and Mkhomazana basalts generally show some compositional overlap with the Phinong, or plot in incoherent fields, but the Agate Vale basalts are distinctly different and might indicate a new magma type within the Karoo Central area. Broad compositional overlap between the Phinong basalts and those preserved at Kirwan and Heimefrontfjella, Antarctica, indicates juxtaposition of Antarctica along the southern African east coast in a reconstructed Gondwanaland.

Petrogenesis of the Sani Pass basalts has been examined in terms of alteration, open and closed system fractional crystallization, partial melting procesess and a heterogeneous source. Although limited alteration and conduit contamination have occurred, the most feasible mechanism responsible for the geochemical variation lies in the existance of inhomogeneities in the upper mantle at the time of generation of the Sani Pass magmas.

TABLE OF CONTENTS

Page

ABSTRACT i

LIST OF FIGURES ix

LIST OF TABLES xi

LIST OF PLATES xii

1. INTRODUCTION 1

1.1. General 1

1.2. Previous Investigations 2

1.3. Sampling and Analytical Techniques 5

1.4. Aims 6

2. GEOLOGICAL HISTORY AND BASALT STRATIGRAPHY 7

2.1. Introduction 7

2.2. Geological History 7

2.3. Basalt Stratigraphy and Stratigraphic Nomenclature 10

2.3.1. Giant's Cup magma type 11

2.3.2. Agate Vale magma type 11

2.3.3. Sakeng Magma Type 12

2.3.4. Mkhomazana Magma Type 13

2.3.5. Phinong Magma Type 13

2.4. Summary 14

3. MACROSCOPIC FEATURES OF THE LAVAS 16

3.1. Introduction 16

3.2. Amygdales 16

3.2.1. Spherical Amygdales 16

3.2.2. Pipe Amygdales 17

3.2.3. Cone Amygdales 17

3.3. Pahoehoe Surface and Toes 18

3.4. Auto-Intrusive Dykes 18

3.5. Pillow Lavas 18
3.6. Xenoliths 19
3.7. Sedimentary Features 19
3.8. Summary 20
4. PETROGRAPHY 21
4.1. Silicates 21
4.1.1. Introduction 21
4.1.2. The Giant's Cup magma type 21
4.1.3. Agate Vale magma type 23
4.1.4. Sakeng magma type 24
4.1.5. Mkhomazana magma type 25
4.1.6. Phinong magma type 26
4.1.7. Dolerites 28
4.2. Ore Mineralogy 29
4.2.1. Introduction 29
4.2.2. Giant's Cup Magma Type 29
4.2.3. Agate Vale Magma Type 31
4.2.4. Sakeng Magma Type 31
4.2.5. Mkhomazana Magma Type 32
4.2.6. Phinong magma type 32
4.3. Summary 34
5. MINERAL CHEMISTRY 35
5.1. Introduction 35
5.2. Olivine 35
5.3. Pyroxene 38
5.4. Plagioclase Feldspar 42
5.5. Summary 44
6. ZEOLITES AND OTHER SECONDARY MINERALS 46
6.1. Introduction 46

6.2. Morphology of the Secondary Minerals 47
6.3. Mineralogy 48
6.4. Distribution of the Zeolites 48
6.5. Causes of Zeolite Zonation 50
6.6. Summary 53
7. **BASALT CLASSIFICATION** 55
7.1. Introduction 55
7.2. Review of Basalt Nomenclature 55
7.3. Normative Mineralogy 57
7.3.1. Norm calculation and the Fe_2O_3/FeO ratio 57
7.3.2. Basalt Tetrahedron 58
7.4. Alkali-Silica Diagram 61
7.5. Anorthite-Alumina Diagram 61
7.6. AFM Diagram 62
7.7. Tectonic Discrimination 63
7.8. Summary 65
8. **WHOLE-ROCK MAJOR AND TRACE ELEMENT GEOCHEMISTRY** 67
8.1. Introduction 67
8.2. Major Element Geochemistry 67
8.2.1. Introduction 67
8.2.2. SiO_2 68
8.2.3. TiO_2 69
8.2.4. Al_2O_3 70
8.2.5. Total iron 71
8.2.6. MnO 72
8.2.7. MgO 73
8.2.8. CaO 74
8.2.9. Na_2O 75
8.2.10. K_2O 76

8.2.11. P_2O_5 77

8.3. Trace Element Geochemistry 77

8.3.1. Introduction 77

8.3.2. Strontium (Sr) 78

8.3.3. Rubidium (Rb) 78

8.3.4. Barium (Ba) 80

8.3.5. Yttrium (Y) 81

8.3.6. Zirconium (Zr) 81

8.3.7. Niobium (Nb) 82

8.3.8. Lanthanum (La) 82

8.3.9. Cobalt (Co) 83

8.3.10. Nickel (Ni) 84

8.3.11. Chromium (Cr) 85

8.3.12. Vanadium (V) 86

8.3.13. Scandium (Sc) 87

8.3.14. Zinc (Zn) 87

8.3.15. Copper (Cu) 88

8.4. Dolerites: Comparison with lavas 89

8.5. Stratigraphic Variations 90

8.6. Summary of Whole-Rock Geochemistry 95

9. DISCRIMINATION AND CHARACTERIZATION OF THE DIFFERENT MAGMA TYPES IN THE SANI PASS 96

9.1. Introduction 96

9.2. Canonical Discrimination Function Analyses 96

9.3. Incompatible Interelement Ratios 97

9.4. Relative Abundance of Incompatible Elements 99

9.5. Summary 101

10. PETROGENESIS OF THE KAROO BASALTS OF THE SANI PASS 103

10.1. Introduction 103

10.2. Alteration and its effect on whole-rock geochemistry 103

10.2.1. Introduction 103

10.2.2. Petrographic and field evidence 104

10.2.3. Oxidation Ratio 105

10.2.4. Chemical Index of Alteration 109

10.2.5. Albitisation 111

10.3. Crystal Fractionation 112

10.3.1. Closed system low pressure fractionation 113

10.3.2. Trace element variations 116

10.3.3. High Pressure Fractionation 118

10.3.4. Open System Low-Pressure Fractional Crystallization 121

10.3.5. Crustal Contamination 123

10.4. Partial Melting Models 128

10.5. Mantle Heterogeneity 132

10.6. Summary 134

11. THE SANI PASS VOLCANIC SUCCESSION IN RELATION TO THE KAROO IGNEOUS PROVINCE 136

11.1. Introduction 136

11.2. Geochemical Provinciality of the Sani Pass Magma Types 137

11.3. The Sani Pass magmas compared to magma types in the southern province 138

11.4. Summary 143

12. COMPARISON WITH OTHER MESOZOIC BASALTS OF GONDWANALAND 145

12.1. Introduction 145

12.2. Overview of basalts in Dronning Maud Land, Antarctica 145

12.3. Geochemical Comparison of the Dronning Maud Land basalts with the Sani Pass basalts 147

12.4. Summary 149

13. CONCLUSIONS 151

ACKNOWLEDGEMENTS 155

REFERENCES 156

APPENDIX 1 - Sample localities and experimental work 168

APPENDIX 2 - X-ray flouresence spectrometry 169

APPENDIX 3 - Electron microprobe 170

APPENDIX 4 - X-ray diffraction analyses 171

APPENDIX 5 - Distribution coefficients 172

LIST OF FIGURES

Figure	1.1	Locality map of study area
	2.1	Distribution of Karoo-age outcrops in southern Africa
	2.2	Simplified sections of the main stratigraphic units in the Central Area
	2.3	Stratigraphic section of the Sani Pass volcanic succession
	3.1	Idealized cross-section of a basaltic flow
	5.1	Ni versus MgO for olivines in the Phinong basalts
	5.2	Ni/MgO mineral chemistry for olivines in the Phinong basalts
	5.3a-b	Chemistry of pyroxenes in terms of Wo-En-Fs endmembers
	5.4a-b	Ionic Mn versus Mg for pyroxenes in the Agate Vale and Phinong
	5.5	Ionic Cr versus Al for pyroxenes in the Agate Vale and Phinong
	5.6a-b	Ionic Cr versus Mg for pyroxenes in the Agate Vale and Phinong
	5.7a-b	Ionic Ti versus Mg for pyroxenes in the Agate Vale and Phinong
	5.8a-b	Ionic Al versus Mg for pyroxenes in the Agate Vale and Phinong
	5.9a-c	Feldspar compositions in terms of An-Ab-Or endmembers
	5.10	Variation of molecular % Or with An
	6.1	Distribution of amygdales in the Sani Pass
	6.2	Distribution of amygdale zones in the Sani Pass
	6.3	Lebombo volcanic succession in relation to the Sani Pass succession
	7.1	Basalt and dolerite data plotted on normative basalt tetrahedron
	7.2	SiO_2 versus total alkalies variation diagram
	7.3	Anorthite versus alumina variation diagram
	7.4	AFM diagram for basalts and dolerites
	7.5	Ti-Zr-Y tectonic discrimination diagram
	7.6	Ti-Zr-Sr tectonic discrimination diagram
	7.7	Spidergram of Sani Pass basalts normalized by CAB
	8.1	Histogram of silica frequency
	8.2a-i	SiO_2 variation diagrams for all major elements
	8.3a-n	SiO_2 variation diagrams for all trace elements
	8.4a-i	Stratigraphic variation diagrams for selected elements
	9.1	Discriminant function analysis diagram
	9.2a-d	Incompatible trace element discrimination diagrams
	9.3	Ti-P-Zr discrimination diagram
	9.4	Spidergram of Sani Pass basalts normalized to average Lesotho
	10.1	Variation of FeO and Fe_2O_3 concentrations
	10.2	Variation of the chemical index of alteration
	10.3a-f	Between magma type composition trends and phase extract vectors

Figure 10.4 Basalt compositions compared to the 1 atmosphere cotectic
10.5 SiO_2 versus Mg#
10.6a-b Ni variation diagrams in terms of K_2O and Rb
10.7a-b Cr variation diagrams in terms of K_2O and Rb
10.8a-d Stepped histograms for selected trace elements ratios
10.9a-c Zr variation diagram for selected trace element ratios
11.1 Spidergram comparision for Sani Pass basalts and SRBF
11.2 Summary diagram of stratigraphic relations in the Central area
11.3a-d Comparision of Central area magmas on selected trace element discrimination diagrams
12.1 Karoo-age magmatic provinces in Gondwanaland
12.2 Distribution of basalt outliers in Dronning Maud
12.3a-e Spidergrams comparing average Sani Pass compositions and Dronning Maud Land basalt compositions
A1.1 Stratigraphic column of the Sani Pass indicating sample localities
A1.2 Geological map of the Sani Pass area indicating sample locations of the dolerite dykes

LIST OF TABLES

Table 5.1 Microprobe analyses of olivine

5.2 Microprobe analyses of pyroxene

5.3 Microprobe analyses of plagioclase feldspar

6.1 Secondary minerals of the Sani Pass

6.2 Distribution of zeolites with stratigraphy

6.3 Bounding temperatures for zeolites

10.1 Mixing calculations

10.2 Comparison of observed and calculated trace element compositions for the Rayleigh fractionation model

11.1 Average compositions of some Karoo magma types

12.1 Average compositions of some Dronning Maud Land basalts

A1.1 List of experimental work done on the Sani Pass rocks

A2.1 Analytical conditions for XRF analyses

A2.2 Unnormalised major element data for the Sani Pass volcanics

A2.3 Unnormalised major element data for the Sani Pass dolerites

A2.4 Normalised major and unnormalised trace element data for the Sani Pass volcanics

A2.5 Normalised major and unnormalised trace element data for the Sani Pass dolerites

A2.6 CIPW weight percent norms for the Sani Pass volcanics

A2.7 CIPW weight percent norms for the Sani Pass dolerites

A4.1 Amygdales from the Sani Pass analysed by X-ray diffraction

A5.1 Selected partition coefficients for trace elements in the basaltic assemblage

LIST OF PLATES

Plate	3.1	Pipe vesicles at the base of a flow
	3.2	Plan of cone amygdales
	3.3	Pahoehoe flow surface
	3.4	Pillow lavas
	3.5	Basaltic xenolith
	4.1	Glomeroporphyritic texture of the Giant's Cup basalts
	4.2	Apparent seriate texture in the Agate Vale basalts
	4.3	Resorbed plagioclase
	4.4	Hourglass zoning in augite
	4.5	Large single plagioclase phenocryst
	4.6	Prismatic laths of pyroxene
	4.7	Subophitic texture in the Phinong basalts
	4.8	Glomeroporphyritic texture in the Phinong basalts
	4.9	Pigeonite mantled by augite
	4.10	Olivine macrophenocrysts
	4.11	Ophitic texture in the dolerites
	4.12	Acicular ilmenite laths
	4.13	Subhedral magnetite with inclusions of entrapped melt
	4.14	Development of minor ilmenite around magnetite
	4.15	Ilmenite oxidation-exsolution lamellae
	4.16	Alteration of magnetite to hematite
	4.17	Mantling of earlier-formed ilmenite by later-Ti magnetite

CHAPTER 1

1. INTRODUCTION

1.1. General

This study is concerned with the Karoo-age volcanic rocks of an approximately 40km^2 area centred on the Sani Pass, which crosses the Lesotho-Natal border between the Drakensberg peaks of Phinong and Sakeng (Fig. 1.1). The lavas form the prominent Drakensberg Escarpment, which is regularly stratified and often terraced, owing to alternations of compact and resistant lavas with amygdaloidal, and therefore easily erodable varieties. In the vicinity of the Lesotho border the escarpment attains an altitude of 2 874m.

In the foothills of the Drakensberg massif, and occurring directly below the volcanics, is a succession of horizontally bedded aeolian sandstones of the Clarens Formation. These sediments are extensively intruded by dolerite sills and dykes, and are characterized by distinctive erosional patterns.

Forming a major watershed between the drainage systems of Natal and Lesotho, the Drakensberg is characterised by strongly trellised drainage. Stream directions are controlled by prominent NE-SW trending joints. Most streams are perennial, due to the high mean annual rainfall and frequent winter snowfalls. Temperatures up to 23°C can be expected during the wet summer months.

Access to the study area is via Sani Pass, which is the only road access to Lesotho from the east. This steep and tortuous 8km pass is open only to four-wheel drive vehicles, and is often closed as a result of heavy rain and snowfalls. Access to the area in the vicinity of Sani Pass is facilitated by numerous hiking trails. However, permission must be obtained from the Department of Forestry for use of these trails.

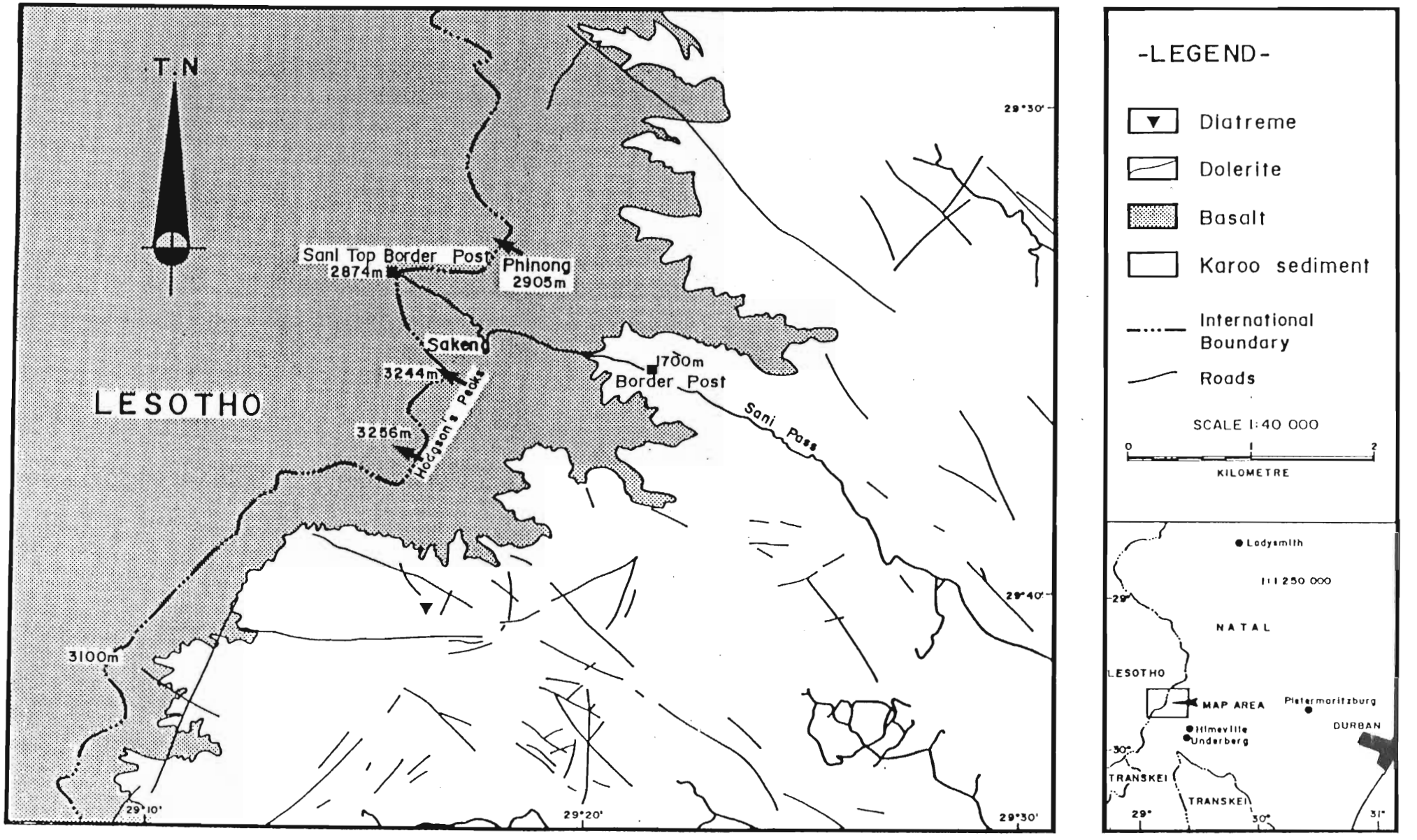

Fig 1.1 Locality map of the study area, showing the basal contact of the lavas and the predominantly NE-SW and NW-SE trending dolerite dykes. A single diatreme is located in the Karoo sediments. The geological features were identified from aerial photographs, followed by field verification.

1.2. Previous Investigations

The lavas of the central Karoo area are generally described with respect to two areas; firstly those of the Stormberg area, in the north-eastern Cape, and secondly, those of the Drakensberg escarpment or the Lesotho plateau (Marsh and Eales, 1984; Cox and Hornung, 1966).

The petrology and field relationships of the Stormberg area are well documented by the pioneering works of Du Toit (1904, 1911) and Gevers (1928). These early workers recognised an initial explosive eruptive stage, expressed physically by the numerous diatremes which dot the north-eastern Cape Province. Lock *et al.*, (1974), believed that the diatremes represent phreatic activity. Stockley (1940, 1947), from his detailed study of the geology of Lesotho (formerly Basutholand), observed that the diatremes are mainly confined to southern and eastern Lesotho, and that none of the seventy-two vents he examined occurred below the Molteno Formation sediments. Gevers (1928) also noted the absence of vents in the Beaufort Group and underlying beds, and consequently proposed that the vents had been produced by volcanic processes operative during, or immediately prior to, Molteno sedimentation. This initial phase of volcanism was complex, with periods of explosive activity from central volcanic vents producing pyroclastics and compositionally heterogeneous lavas (Lock *et al.*, 1974; Mitchell, 1980). In some instances these eruptions culminated in caldera collapse, as at Kelvin Grove (Lock *et al.*, 1974) and Brosterlea (Mitchell, 1980), in the north-eastern Cape. The central eruptions eventually gave way to fissure-type eruptions of highly mobile lava, which produced the compositionally uniform basaltic sequence designated the Lesotho-type magma by Marsh and Eales (1984). At the base of the basalt succession, numerous sedimentary lenses and pillow lavas occur (McCarthy, 1970; Lock *et al.*, 1974; present study), probably indicating periods of non-eruption and hence sedimentation, and the emplacement of lavas into ephemeral lakes and streams respectively.

Lock *et al.*, (1974) subdivided the volcanic sequence in the Barkly East area into a sequence of mappable units. However, in the Giant's Castle area in the northern

Drakensberg, no significant field and mineralogical differences exist to justify subdivision of the Drakensberg volcanic succession into lithostratigraphic units (Botha and Lindström, 1976).

The distinctive field and stratigraphic characteristics of the basalts of the north-eastern Cape persist into their chemistry, as demonstrated by Pemberton (1978), Mitchell (1980), and Marsh and Eales (1984).

Regional studies of the Karoo volcanics by Cox *et al.*, (1967), established the existence of distinct geochemical provinces within the basaltic lavas and doleritic dykes. The northern province consisted of the basaltic lavas of Zimbabwe, characterized by abnormally high concentrations of K, Ti, P, Ba, Sr and Zr, whilst a southern province, which incorporated the lavas of Lesotho, Swaziland and the north-eastern Cape, was characterized by a normal continental tholeiitic geochemistry. The province boundaries proposed by Cox *et al.* (1967) did not correspond in any way to tectonic environments. Rhodes and Kröhn (1972), argued for a strong relationship between the Karoo basalts and dolerites and the regional tectonics of the Karoo basin, suggesting the existence of a central basin, corresponding to the Lesotho and Stormberg areas, and distinct from the neighbouring marginal zone of the Lebombo-Nuanetsi region. The Karoo Geodynamics Project (Erlank, 1984) has subsequently shown that the Lesotho magma type can be recognized well beyond the margins of the Karoo sedimentary basin. Rhodes and Kröhn (1972) suggested that compositional differences between marginal and central basalts resulted from derivation from different mantle levels, related to different tectonic regimes. Woolley and Garson (1970) attributed changes in Karoo magma composition to increasing degrees of fractionation. On the basis of geographical distribution and geochemistry, Duncan and Erlank (1979) grouped the Karoo volcanics into four major "provinces" or magma types:

1. The Atlantic type, incorporating the lavas of northern Namibia-Etendeka and the Cape Cross area and equivalent basaltic lavas in South America;
2. The Central Karoo magma type, comprising the Stormberg, Drakensberg, Springbok and Mariantal lava fields and the Central Karoo dolerites;

3. The southern Lebombo type, comprising lavas of the southern Lebombo and Swaziland; and

4. The northern Lebombo type, comprising the lavas in Zimbabwe.

These different magma types were attributed to heterogeneous mantle source areas (Erlank *et al.*, 1980).

The volcanics occurring in northwestern Namibia (Etendeka) have been described in detail by Erlank *et al.*, (1984). These rocks differ from all the other Karoo volcanics by virtue of their Cretaceous age, as well as their stratigraphy, mineralogy, geochemistry and isotopic composition (Erlank *et al.*, 1984), and are, in fact, more appropriately associated with the Parana CFB Province of South America than with the Karoo Province (Duncan *et al.*, 1990).

The geology of the Lebombo-Nuanetsi-Sabi zone has been described in outline by Eales *et al.*, (1984). The geology of specific areas of the Lebombo has been comprehensively dealt with by many authors: southern Lebombo (Bristow, 1976; Bristow and Saggerson, 1983), Rooi Rand (Saggerson *et al.*, 1983; Armstrong *et al.*, 1984), Swaziland (Cleverly, 1977, 1979; Betton, 1978), northern Lebombo picrites and nephelinites (Bristow, 1980, 1984), low-MgO basalts of the Sabi River Basalt Formation (Bristow, 1980; Cox and Bristow, 1984; Sweeney, 1988). The dolerites, which are the subsurface expression of the Karoo volcanic episode, were described in detail by Walker and Poldervaart (1949).

The stratigraphy and geochemistry of the Central area has been well established by Lock *et al.*, (1974) (Barkly East), Pemberton (1978) (Barkly East and Naude's Nek) and Mitchell (1980) (Jamestown and Molteno). Expanding on the work of Lock *et al.*, (1974), Pemberton (1978), and Mitchell (1980), Marsh and Eales (1984) showed that a number of compositionally distinct basalt magma types exist in the Central area. The Lesotho magma type constitutes the bulk of the intrusive dolerites and the flood lava sequence. Other basalt types are minor in volume, and are located at the base of the volcanic succession. Cox and Hornung (1966) concluded that the Lesotho basalts represent the same series of magma as the Karoo dolerites. Marsh and Eales (1984) using completely different suites of basalt and

dolerite, reached similar conclusions. Cox and Hornung (1966) noted that in the Letele Pass section (north-western Lesotho) the Fe/Mg index increased with height, and concluded that "there is a slight tendency for more fractionated rocks to be found stratigraphically higher". This is confirmed by Pemberton's (1978) detailed geochemistry of the Drakensberg Formation in the Naude's Nek Pass. His study shows that the uppermost basalts of the Lesotho Formation are clearly enriched in Fe_2O_3, P_2O_5, Ce, La and Zr, and are lower in Ni, Cr and Mg-number compared with those lower in the succession. There is also a suggestion of an increase in the Sr isotope initial ratio through the Naude's Nek section.

Initial K-Ar dating on the Lesotho basalts exposed in the Bushman's Pass (northern Lesotho) suggested that Karoo volcanism commenced about 187 my ago, and continued intermittently until 155 my (Fitch and Miller, 1971). Subsequent K-Ar age determinations based on more refined techniques of sample preparation indicated that volcanism in the Central Karoo area commenced about 193 ± 5 my ago (Fitch and Miller, 1984). Intrusive dolerites in Lesotho have yielded dates of 167 to 193 my (Fitch and Miller, 1984).

1.3. Sampling and Analytical Techniques

Field work was conducted during the period March, 1988 to February, 1989. The initial phase of field work entailed the identification of individual lava flows on the basis of differing texture and field appearance. The contacts of these flows were mapped, each flow was sampled, and flow thickness measured. The problem of weathering and poor outcrop is a very real one in this area, and an attempt was made to obtain at least one sample suitable for geochemical analysis of every flow unit exposed in the section. The second phase of the field work was a mapping exercise in the area immediately adjacent to the Sani Pass (Fig. 1.1), preceded by an aerial photographic interpretation of the geology of the area (using 1:30 000 air photos). Only limited sampling was performed during this second phase.

Seventy five representative samples of basalts and dolerites (excluding very amygdaloidal varieties) were analysed for major and trace elements by the technique described in Appendix 2. A comprehensive geochemical coverage has therefore been obtained of the

Sani Pass stratigraphic section.

In addition to the whole rock chemical analysis, electron probe microanalyses of plagioclase, pyroxene and olivine were performed on selected samples of basalt by the procedure described in Appendix 3.

Fifty eight amygdale mineral samples were analysed by X-ray diffraction (Appendix 4). Only the most abundant amygdale type of each flow was analysed.

Fifteen basalt samples, which are representative of the individual magma types, were subjected to reflected light studies.

1.4. Aims

Although substantial data are available for the Karoo volcanics in other parts of South Africa, there is a notable scarcity of data for the Karoo-aged basalts of the Natal Drakensberg. The volcanic history, stratigraphy and geochemistry of the north-eastern Cape, in particular, are already known. It is important that the stratigraphic correlation between the north-eastern Cape and Sani Pass, on opposite sides of the Drakensberg massif, be attempted.

The aims of this study were, therefore, to:

1. produce a geological map of the area, detailing lithological contacts and any large-scale structures such as volcanic vents and faults,
2. establish the stratigraphy of the lavas utilizing field, microscopic and geochemical techniques,
3. note and interpret the physical features of the lavas, conditions under which eruptions took place, and the time sequence of the igneous events in the area,
4. interpret the magmatic processes involved in the production and evolution of the lavas, and,
5. relate the Drakensberg volcanic rocks to other parts of the Karoo volcanic province and other major flood basalt provinces in the context of the breakup of Gondwanaland.

CHAPTER 2

2. GEOLOGICAL HISTORY AND BASALT STRATIGRAPHY

2.1. Introduction

The fragmentation of the Gondwanaland supercontinent extended from the late Triassic-early Jurassic to the early Cretaceous, and was accompanied by increased igneous activity, which is represented in South Africa by the Karoo volcanic event (Tankard *et al.*, 1982). Similar volcanic sequences are preserved in Antarctica (Jurassic), Tasmania (Jurassic), South America (late Jurassic to early Cretaceous) and India (late Cretaceous to early Tertiary).

In the southern African sub-continent Karoo volcanism followed, without any major hiatus, the extensive and prolonged sedimentation of the Karoo Supergroup. Outliers of an originally extensive volcanic field cover an area in excess of 3,5 million km^2 in southern Africa (Fig. 2.1). In addition, the underlying Karoo sedimentary sequence is host to an extensive intrusive suite of dykes and sills. Simplified stratigraphic sections of the principal areas of extensive volcanics are diagrammatically represented in Fig. 2.2.

2.2. Geological History

The main phase of Karoo volcanism was preceded by infilling of a retro-arc foreland basin by the Karoo Sequence sediments (Johnson, 1991).

The Karoo-age sedimentary succession in the Sani Pass culminates in the buff-coloured sandstones of the Clarens Formation, which immediately underlie the basalts, and are up to 150 m thick. The hiatus between Karoo sedimentation and the volcanic episode in the Sani Pass is indicated by erosional features developed on the Clarens Formation sandstones directly below the volcanics. From hand samples, it is obvious that silicification of the

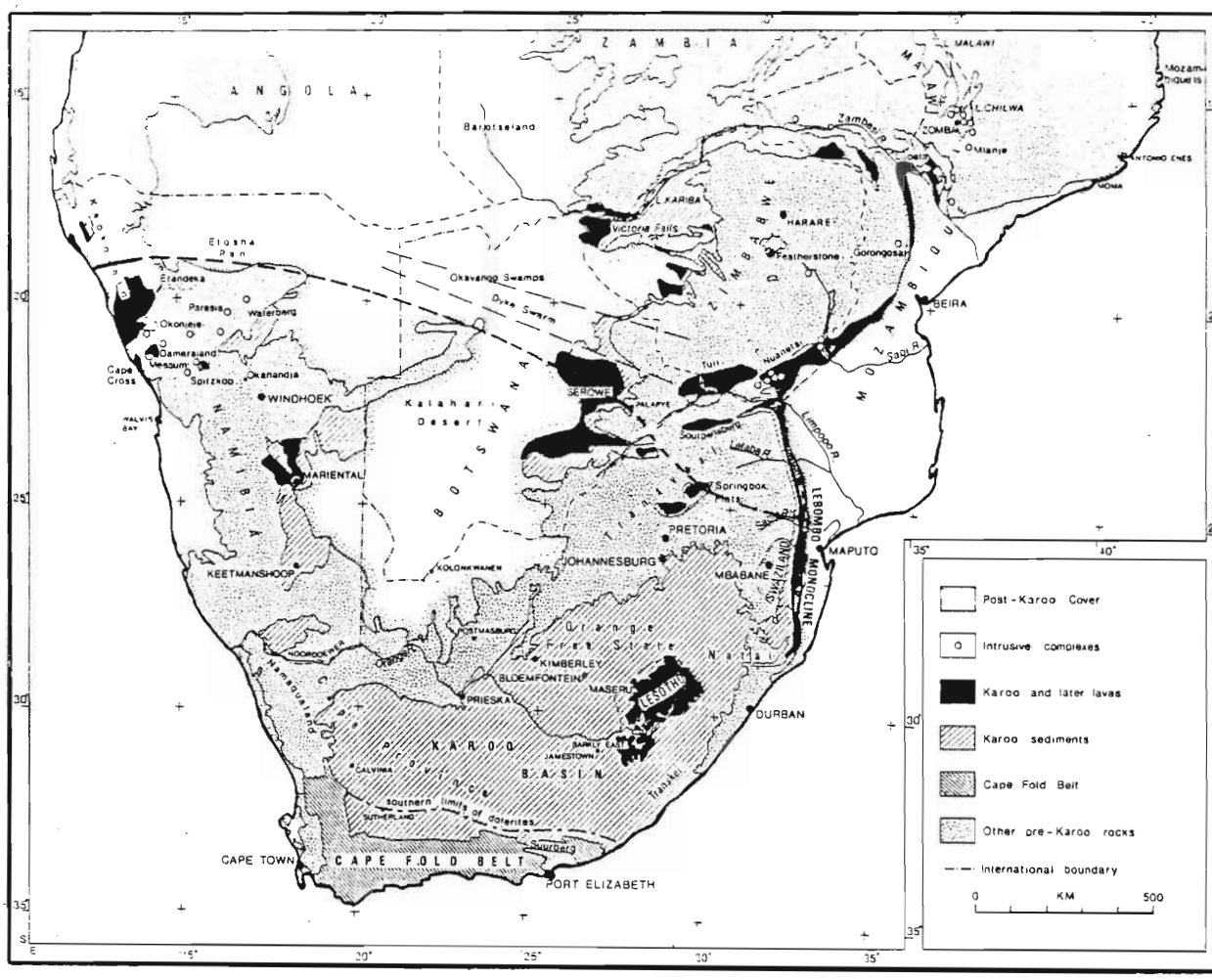

Fig. 2.1 Simplified geological map showing the distribution of Karoo-age basalt outcrops in southern Africa (Fig. 1, after Eales *et al.*, 1984). The dashed line represents the current best estimate for the boundary between the northern and southern Karoo magmatic provinces (after Erlank *et al.*, 1990b).

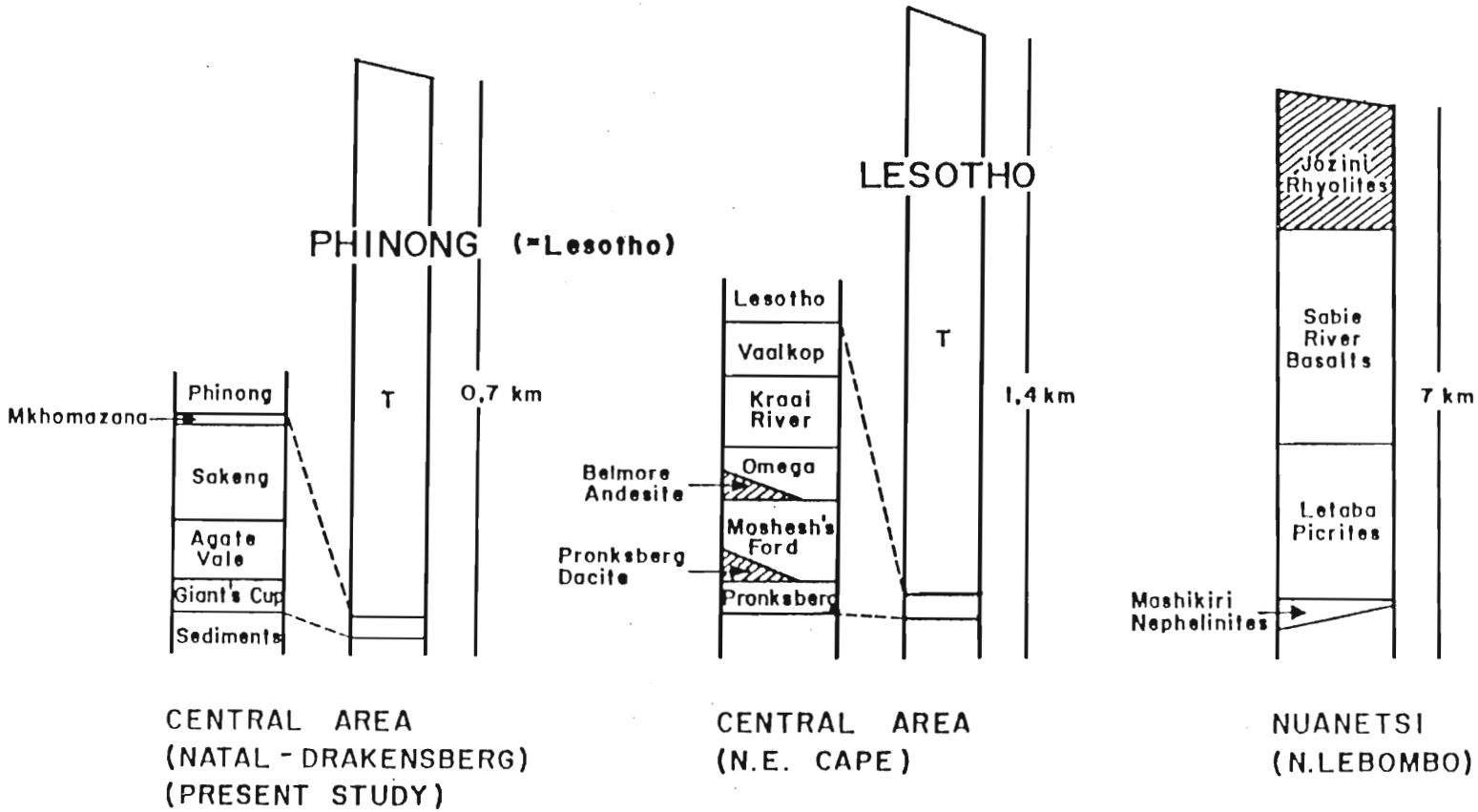

Fig. 2.2 Simplified sections of the main stratigraphic units recognized in the Central area (NE Cape and Natal-Drakensberg) and Nuanetsi-north Lebombo. The NE Cape and Lebombo sections were extracted from Fig. 2 in Hawkesworth *et al.*, (1984).

uppermost Clarens Formation sandstones as a consequence of volcanism is only developed within the upper half a metre or so. The Clarens Formation is underlain by maroon to grey mudstones and subordinate sandstones of the Elliot Formation. Below the Elliot Formation are the alternating coarse-grained sandstones and mudstones of the Molteno Formation. This sedimentary succession extends to just before the Sani Pass Hotel and forms the foothills to the Drakensberg Escarpment. South of the hotel, the Beaufort Group forms the relatively flat topography that extends into the town of Himeville.

Volcanic activity prior to the eruption of the Karoo lavas, indicated by volcaniclastic material in the underlying sediments (Botha and Theron, 1967; Fuller, 1970; Martini, 1974; Elliot and Watts, 1974; Lock and Johnson, 1974; Lock and Wilson, 1975; McLachlan and Jonker, 1990), probably was an important component of Karoo volcanism (Bristow and Saggerson, 1983). These volcaniclastic units have been documented mainly in the Ecca and Beaufort Formations. During the present study, systematic sampling of the upper ten meters of the Clarens Formation in the Sani Pass area revealed no evidence of volcaniclastic activity.

Following the precursive phase of essentially phreatic activity, volcanism in the north-eastern Cape apparently commenced at discrete centres which built up lava shields and through periods of explosive activity deposited thick sequences of pyroclastics over wide areas (Lock *et al.*, 1974; Mitchell, 1980). The eruptions from the central complexes led, in places, to caldera collapse along outer ring fractures through which further diatremes and volcanic plugs penetrated. In the Sani Pass area, no pyroclastics were observed, and only one diatreme within the Elliot Formation was identified (Fig. 1.1). The inference, therefore, is that the initial central-vent phase of volcanism was virtually non-existent in this area. However, tuffs have been identified in sample AV113, which was taken from the boundary between the Agate Vale- and Sakeng magma types. This might indicate activation of vent eruptions at the close of Agate Vale magmatism. Thus, it appears that vent eruptions in the Sani Pass area were active, albeit shortlived, after the initial fissure-type eruptions and did not precede the initial fissure-type eruptions as in the north-eastern Cape. It is generally believed that, in the north-eastern Cape, the central vent phase of eruption was brought to

an end by the onset of a long period of non-explosive fissure-type continental flood basalt (CFB) eruptions, lavas from which blanketed the vents (Lock *et al.*, 1974; Mitchell, 1980; Marsh and Eales, 1984). The volcanic succession in the Sani Pass area may have formed by similar fissure-type eruptions. Lavas ejected from these fissures were highly mobile, and laterally extensive flows can be traced for many kilometres. Norry and Fitton (1983) noted that "most flood basalt provinces appear to have been fed by fissures, with central vent-type volcanoes being relatively unimportant".

Dolerite dykes, which now occupy the fissures probably were feeders to the overlying layers of basalt. Many bear a cross-cutting relationship to the lavas, and when traced through the basalts, the dolerite dykes form negative topographic features. In some instances where the dolerites cut the basalts, no prominent cross-cutting relationship is seen, except for amygdales developed along the margins of the dyke. The dykes have a predominantly NE-SW, NE-SW orientation which may be controlled by pre-existing basement structures (Fig. 1.1).

The early volcanic activity in the Sani Pass area was periodically interrupted by short diastems, which are indicated by the numerous sedimentary lenses. In addition, pillow lavas indicate localised aqueous environments during the early volcanic activity. A change from a totally desert environment (Clarens Formation) to a more seasonal climate is therefore envisaged. This is in accordance with Ericksson's (1979) belief that towards the close of Clarens Formation sedimentation, the climate in the Natal Drakensberg was marginal desert, with a combination of high temperatures and torrential rain.

Subsequent to eruption of the volcanics in the Central Karoo Province no major deformation has affected the rocks. The only structural features present in the Sani Pass section are post-volcanic faults.

2.3. Basalt Stratigraphy and Stratigraphic Nomenclature

Uncertainty exists at present as to the exact stratigraphic status of the volcanic rocks occurring above the sedimentary succession of the Karoo Sequence. Du Toit (1904, 1954), designated these volcanics the Drakensberg or Volcanic Beds of the Stormberg Series. Maintaining the boundaries and conceptual framework of Du Toit (1954), Lock *et al.*, (1974) allocated the volcanic succession to the Volcanic Group, comprising the Drakensberg and Lebombo Subgroups. Lock *et al.* (1974) subdivided the Drakensberg Subgroup in the Barkly East area into a number of lithological units to which they assigned formation status, namely:

3. Lesotho Formation
2. Kraai River Formation
1. Moshesh's Ford Formation.

The South African Committee for Stratigraphy (SACS, 1980), tentatively suggested that these latter units be regarded as members, in which case the Drakensberg Formation/Group would retain formation status throughout its outcrop area. Botha and Lindström (1976) suggested that the name "Champagne Castle Formation" of the Drakensberg Group be used to describe the succession of lavas in the Giant's Castle area. The Karoo Task Group for SACS, however, suggested formation status be maintained for the Drakensberg volcanics (A Christie, *pers. comm.*, 1989).

Adhering to the recommendations of SACS (1980) and the Karoo Task Group, the following stratigraphy and stratigraphic nomenclature is adopted in this work:

Karoo Sequence

- Drakensberg Formation
- Clarens Formation
- Elliot Formation
- Molteno Formation
- Beaufort Group
- Ecca Group
- Dwyka Formation

Pemberton (1978), Mitchell (1980) and Marsh and Eales (1984) demonstrated that the field and stratigraphic characteristics of the Karoo-age volcanic rocks in the north-eastern Cape persist into their geochemistry. This has led to the concept of "magma types" in the Central Karoo Province. In this context the use of the terms "magma type" is not meant to imply that any such magma is a primary magma. A detailed field description of each magma type in the Sani Pass succession is given below.

2.3.1. Giant's Cup magma type

The Giant's Cup magma type occurs as a thin succession (14m thick) of basaltic rocks, erupted directly on Clarens Formation sandstone (Fig. 2.3). The sandstone-basalt contact is clearly identifiable on the hillslopes adjacent to the Sani Pass, by the contrast between the light buff-coloured sandstones and the darker greyish black volcanics. Individual flows increase in thickness upward (Fig. 2.3). All flows are amygdaloidal, with poorly developed pipe amygdales at the base of flow GC360. Calcite is the predominant amygdale infilling.

In hand specimen, the basalts of the Giant's Cup magma type are aphanitic, greyish black and highly altered. With the exception of sample GC370, these basalts are plagioclase-phyric. The phenocrysts are highly altered.

In the field, the Giant's Cup magma type is terminated by a 2m thick meta-sedimentary lens. Yellowish brown scree from this sedimentary lens is clearly observable on the hillslopes where it outcrops.

2.3.2. Agate Vale magma type

The detailed stratigraphy of the Agate Vale magma type is shown in Fig. 2.3. It consists essentially of tholeiitic basaltic rocks, characterised by a higher alkali content than any of the other types, except the Mkhomazana magma type. In addition the Agate Vale magma type has higher Zr and Ba contents than the other magma types.

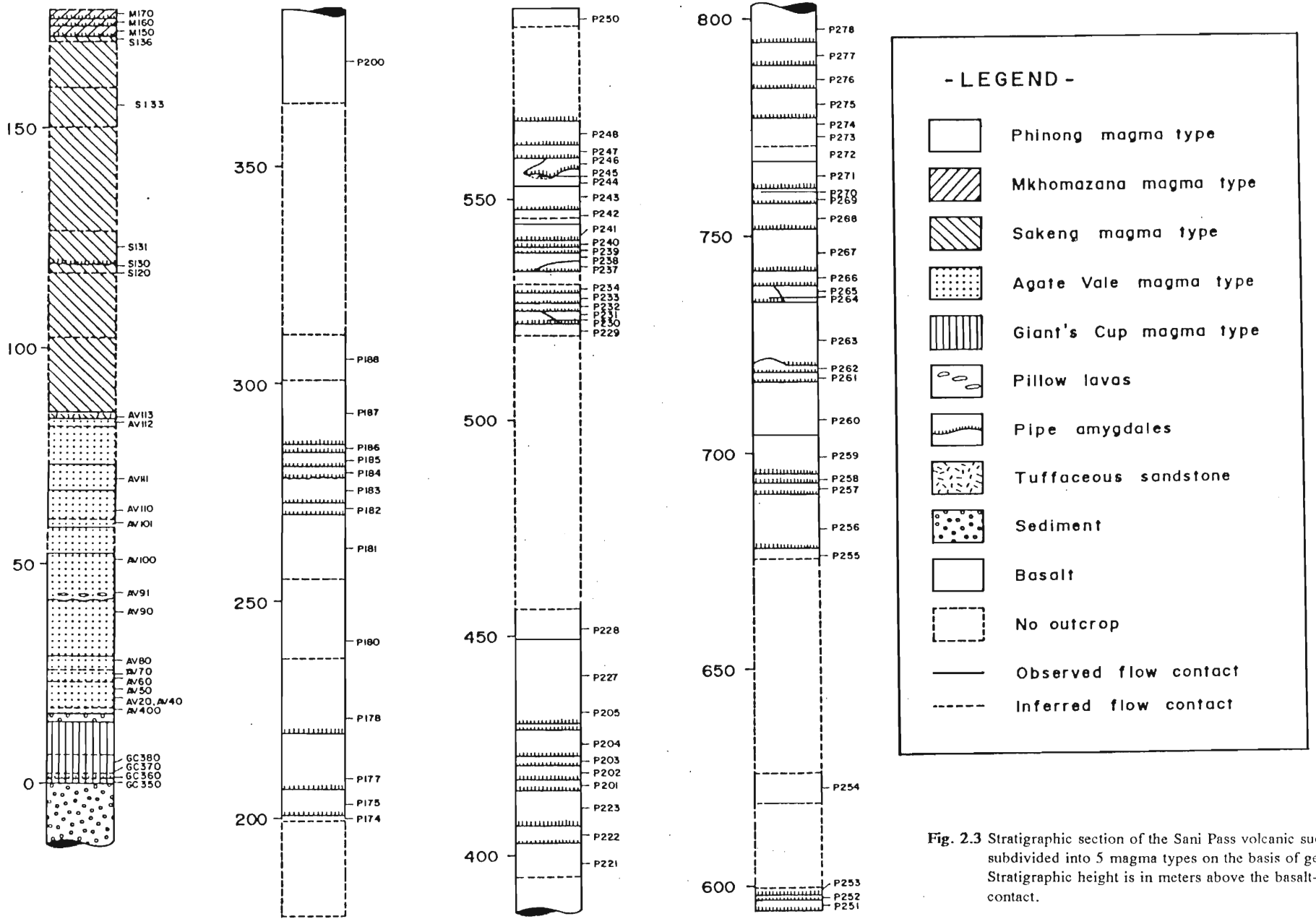

Fig. 2.3 Stratigraphic section of the Sani Pass volcanic succession, subdivided into 5 magma types on the basis of geochemistry. Stratigraphic height is in meters above the basalt-sandstone contact.

With a vertical extent of approximately 70m, the Agate Vale basalts build the steep-sided foothills of the escarpment in the lower reaches of the Sani Pass. Individual flows within this geochemical unit are thicker than those of the underlying Giant's Cup magma type and extend up to 15m. Most of the flows are characterized by amygdaloidal flow tops, which are typically eroded to form rounded scarps. A small outcrop of pillow lava at 45m from the base indicates the existence of bodies of water such as playa lakes and ephemeral streams during volcanism. A prominent bole surface underlies the pillow lavas (Plate 3.4).

In hand specimen, the basaltic rocks of the Agate Vale magma type are aphanitic, dark greyish black and a combination of plagioclase-phyric and aphyric. Thick flows normally consist of a massive central portion characterized by angular weathering. The top contact of this geochemical unit is only poorly exposed in the field, and a massive, dark greenish black tuffaceous sandstone exposed 70m from the base of the unit is considered to be the upper contact.

2.3.3. Sakeng Magma Type

The detailed stratigraphy of the Sakeng magma type is given in Fig. 2.3. This magma type is tholeiitic and has a chemistry similar to that of the Agate Vale magma type. The division between these two magma types is on the basis of the alkali, Zr and Ba content, which is significantly higher in the Agate Vale magma type, as well as the tuffaceous sandstone layer between the two units.

The Sakeng type basalts have a vertical extent of 84m. Individual flow thicknesses were not obtained because the majority of this unit is poorly exposed. Numerous sedimentary lenses occur irregularly distributed within this magma type. These lenses are not laterally persistent and occur on a millimeter to centimetre scale. Quartz-filled pipe amygdales are developed at the base of flow S130. The Sakeng type basalts are aphanitic, dark greyish black and poorly porphyritic.

The top contact of the Sakeng magma type is clearly exposed in the field. It is marked by an oxidized yellowish brown flow top, which displays a pahoehoe texture (Plate 3.3).

2.3.4. Mkhomazana Magma Type

Only three flows constitute the Mkhomazana magma type (Fig. 2.3). The chemistry of this magma type is distinctly different from the rest of the basaltic magma types, in that it shows enriched Na_20 and depleted CaO contents.

The Mkhomazana magma type has an estimated thickness of 6m and individual flows range from 1.6 to 2.8m thick. All the flows are amygdaloidal and are characterized by pipe amygdales at the base. The amygdales are mainly zeolites, quartz and calcite. This unit is cut by a 1m thick dyke, which is very fine-grained, dark greyish black and is plagioclase-phyric.

In handspecimen the rocks of the Mkhomazana magma type are aphanitic and light blueish grey. They have a speckled appearance due to the presence of greenish black glassy mesostasis, which is made conspicuous by the lighter colour of the rock. Glomeroporphyritic aggregates of altered creamish white feldspar are clearly visible in hard specimens of samples M160 and M170.

The upper contact of the Mkhomazana magma type is not exposed in the field area and the total exposed thickness is taken as the true thickness of this geochemical unit.

2.3.5. Phinong Magma Type

The detailed stratigraphy of the Phinong magma type is shown in Fig. 2.3. This magma type constitutes the bulk of the Drakensberg Formation in the Sani Pass, and is characterised by a normal tholeiitic geochemistry analogous to the Lesotho-type basalt of Marsh and Eales (1984), with which it is correlated (Chapter 11).

Owing to alternations of compact and amygdaloidal basalt flow units, a great number of individual lava flows can be recognised in the Phinong magma type, especially when this succession is viewed from a distance. Unlike the discrete, distinguishable flows of the preceding magma types, the apparently thick flows of the Phinong magma type are made up of several smaller flows. Flow units range from 0.3m to 20m in thickness. Some of the

thicker flow units in the upper parts of the succession exhibit well-developed vertical columnar jointing in the entablature. Sedimentary lenses and rheomorphic dykes are poorly developed, and above 415m from the base of the volcanics none are present. Volcanological features include auto-intrusive dykes and pahoehoe toes.

Occurring 60m from the base of the Phinong magma type is a thick flow (P180) (30m) which is doleritic in appearance. The presence of scree above this flow precludes any conclusions being drawn as to its origin. However, from the available field evidence it is tentatively suggested to be a flow. Marsh and Eales (1984) noted that doleritic textures are common in the interior of many thick flows, accordingly yielding few criteria for separating intrusive and extrusive equivalents in the absence of adequate field evidence.

In handspecimen, the Phinong type basalts are aphanitic to fine-grained, greyish black and rarely visibly plagioclase-phyric. Amygdales become widespread within this magma type, and the zeolites increase in abundance.

The Phinong magma type attains a thickness of about 615m in the study area, but is believed to extend beyond this thickness in the highlands of Lesotho.

2.4. Summary

Detailed geological mapping in the Sani Pass has indicated a lack of volcaniclastic material in the Clarens Formation sandstones as well as any pyroclastics immediately above the sedimentary succession. However, a tuffaceous lens at 70m from the base of the volcanic succession indicates short-lived explosive eruptions, possibly from central vents. Thus, it appears that only minor vent eruptions might have been operational after a period of fissure-type eruptions. The explosive episode, however, was extremely short-lived and was overcome by the fissure-type eruptions responsible for the major volume of the Sani Pass basalts. Evidence for the fissure-type eruptions is preserved by dolerite dykes, which presumably served as feeders to the basaltic succession. Eruptions were separated by periods of quiescence, as shown by sedimentary lenses, bole surfaces and pillow lava.

The geochemical subdivision of the Sani Pass volcanic succession can be substantiated by field relationships, except for the separation between the Mkhomazana and Phinong magma types. A metasedimentary lens separates the Giant's Cup and Agate Vale magma types, while a tuffaceous sandstone lens indicates a break in fissure volcanism between the Agate Vale and Sakeng magma types and an oxidized flow top separates the Sakeng and Mkhomazana magma types.

CHAPTER 3

3. MACROSCOPIC FEATURES OF THE LAVAS

3.1. Introduction

The Drakensberg Formation exposed in the Sani Pass consists almost entirely of basalts (*sensu lato*) and associated dolerites with minor interbedded sedimentary lenses and related rheomorphic veins. Although these basalts were erupted in the early Jurassic period, numerous volcanological features such as amygdales, pillows and pahoehoe toes are still well preserved in the study area.

3.2. Amygdales

During extrusion of a magma, dissolved gases form bubbles as a result of reduced confining pressure. This produces numerous cavities or vesicles, which are now filled by secondary minerals and termed amygdales. Secondary minerals may form during the extrusion of the magma by the migration and concentration of late stage residual liquids, or may be deposited by the later circulation of warm or cold ground-water in the lava pile (Chapter 6). Differential cooling and flowage of lava flows produces different mineral assemblages which occur in different zones within the flows (Fig. 3.1).

3.2.1. Spherical Amygdales

Commonly, the originally spherical to almost circular amygdales are stretched out by flowage of the surrounding magma during cooling, and assume a more or less ellipsoidal

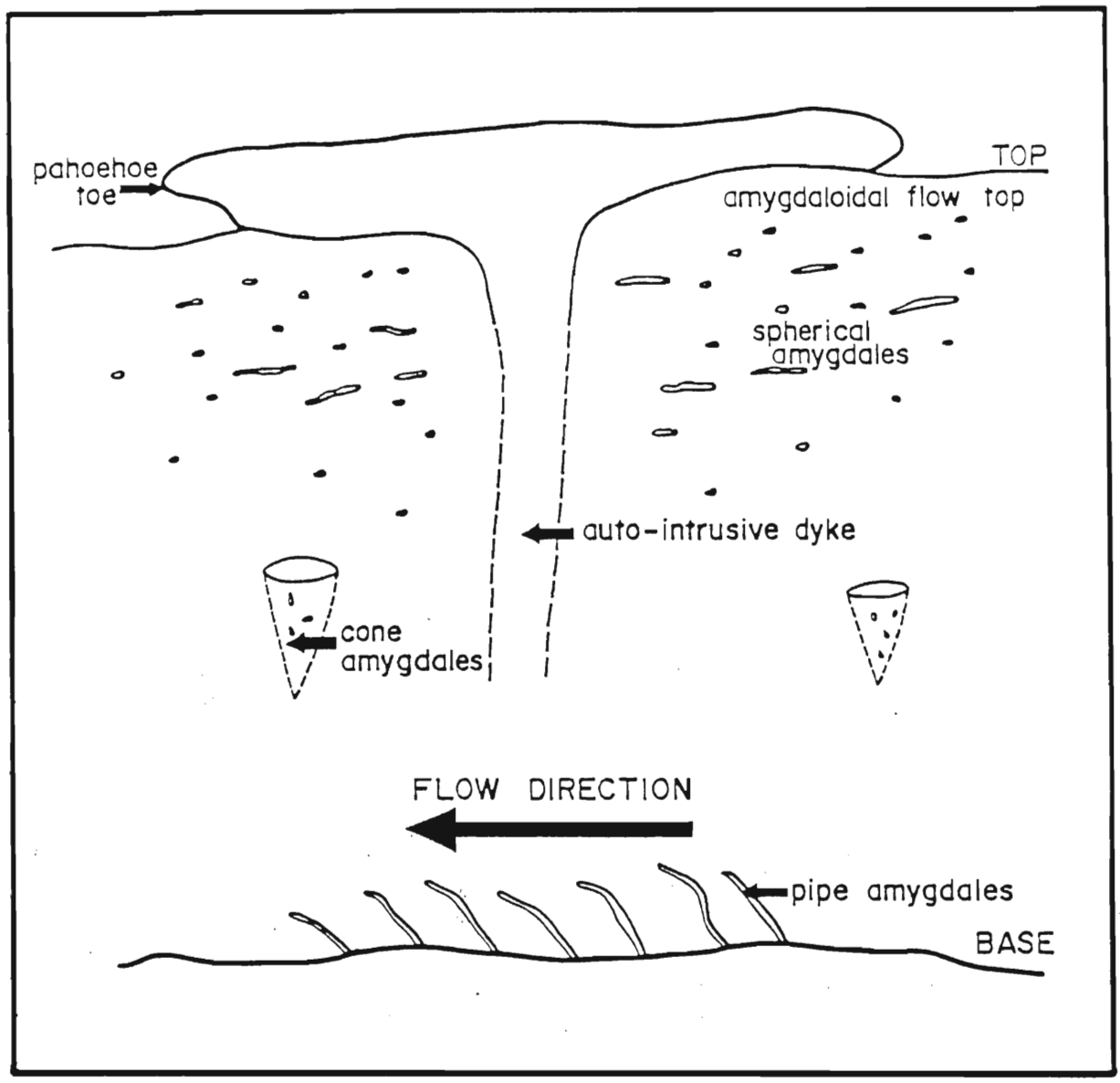

Fig. 3.1 An idealized cross-section of a basaltic flow, indicating various volcanological features preserved by the Sani Pass basalts. Diagram is not drawn to scale and has been adopted from MacDonald (1967).

shape (in cross-section) (Fig. 3.1). It is not uncommon to find lenticular amygdales, sometimes disjointed, parallel to flow direction and ranging in size from a few tens of mm up to about 400mm in length. Spherical amygdales are common in the thin flows and the top and bottom of thicker flows. In thick flows the central portion, termed the entablature (nomenclature after Long and Davidson, 1981), cools slowly, allowing most of the volatiles to escape, therefore inhibiting vesicle formation, while rapid cooling of the margins promotes the preservation of cavities.

3.2.2. Pipe Amygdales

Typically, the pipe amygdales are up to 100mm in length and 5 to 10mm in diameter (Plate 3.1). They are well developed in the thick flows and are normally restricted to the lower 300mm of the flows (lower colonnade). Pipe amygdales form by the uprise of steam from the moist surface over which the lava flows (Waters, 1960; MacDonald, 1967). Due to differential flow rates at the bottom of the lava flow, the pipes are commonly bent in the direction of flow (Plate 3.1). In ascertaining lava flow direction from pipe amygdales, it is important to use a pipe exposed in three dimensions.

3.2.3. Cone Amygdales

Cone amygdales are not common, and only a few occurrences have been observed in the lower part of the volcanic succession (Plate 3.2). In cross-section the cone amygdales define ellipsoidal patterns of amygdales tapering downward (Fig. 3.1). Similar conical arrangements were noted by Du Toit (1907) in the Ventersdorp lavas.

Cone amygdales occur in the lower portion of the entablature, and form due to an decrease in confining pressure from a central nucleation point (Fig. 3.1). Occasionally the volatiles do not disperse outwards, resulting in straight, disjointed pipe-like amygdales.

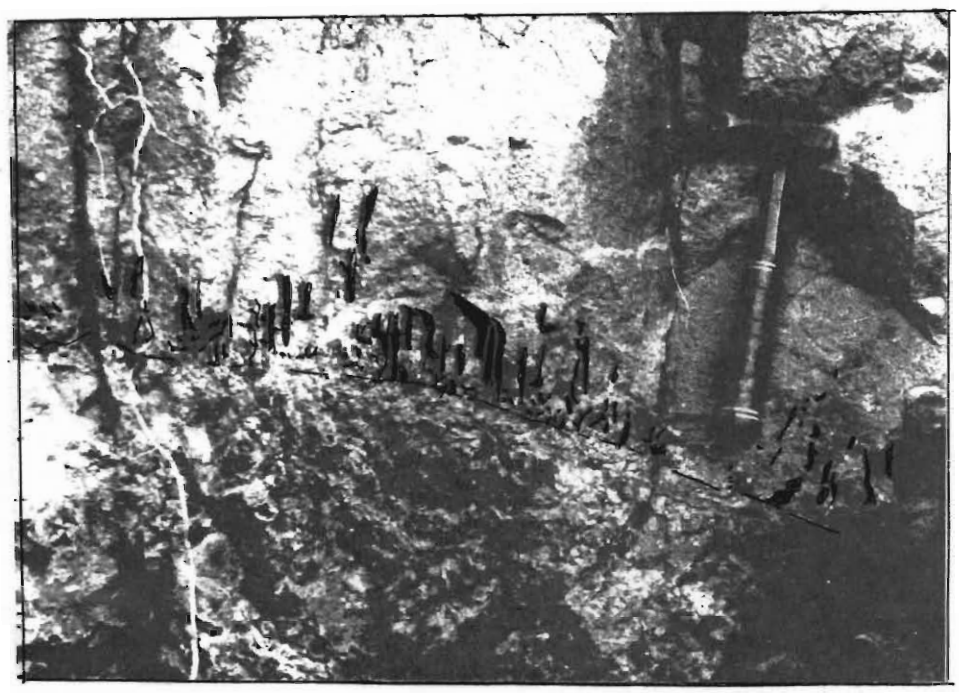

Plate 3.1 Pipe vesicles at the base of flow. These pipes may be up to 100mm in length and are best developed in the lowest 300mm of the flow.

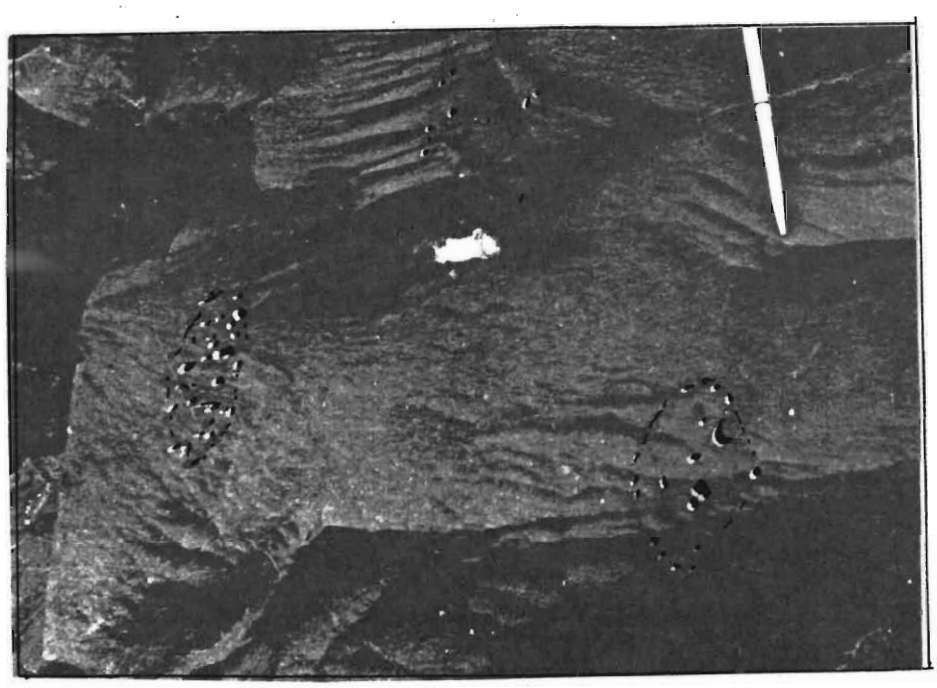

Plate 3.2 A plan of cone amygdales indicating the more or less ellipsoidal pattern. In cross-section the amygdales taper downward to a point describing a cone-like feature.

3.3. Pahoehoe Surface and Toes

Most of the flow tops are even and almost parallel, and only three occurrences of pahoehoe or "ropy lava" have been observed (Plate 3.3). The curvature of these surfaces is characteristically convex in the direction of flow of the lava. In the Sani Pass the observed surfaces clearly indicate a south-westerly palaeoflow direction. However, this flow direction may indicate only local movement due to local turbulance and eddies, and a much larger number of measurements is required to determine a regional direction of lava palaeoflow. Pahoehoe surfaces result from the dragging of cooler plastic crust by the movement of liquid lava beneath (MacDonald, 1972).

In some of the thicker flows, pahoehoe toes are present. These normally project as lobes from the edge of the advancing flow front and form from retardation of the basal part of the flow, causing the upper portions to override it (MacDonald, 1972) (Fig. 3.1).

3.4. Auto-Intrusive Dykes

Numerous small scale auto-intrusive dykes (up to 1m in vertical cross-section) are present. These are normally cone-shaped in cross-section, and seem to spread out at the flow contact (Fig. 3.1). These dykes generally have an irregular morphology and frequently amygdaloidal margins.

3.5. Pillow Lavas

Pillow lavas are more or less ellipsoidal bodies formed when basaltic lava is extruded subaqueously and accumulate by molding one on top of another, frequently resembling pahoehoe toes. In the basal portion of the Drakensberg Formation pillow lavas have been documented in the north-eastern Cape and Natal (Botha, 1971; Lock *et al.*, 1974; McCarthy, 1970).

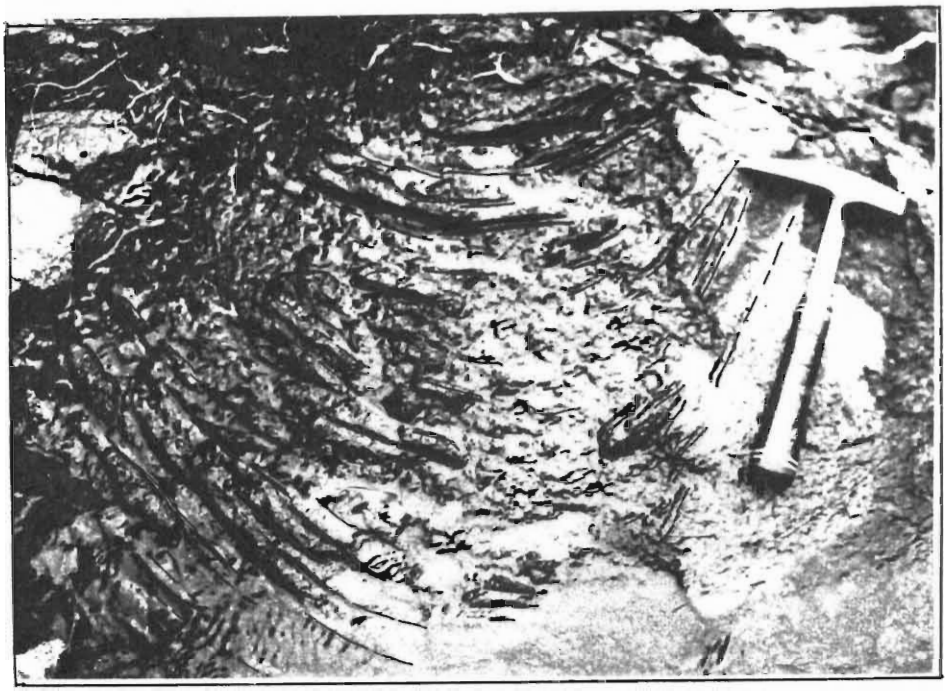

Plate 3.3 Pahoehoe or "ropy lava" at the top of flow S136. The curvature of the pahoehoe surface is normally in the direction of flow of the lava.

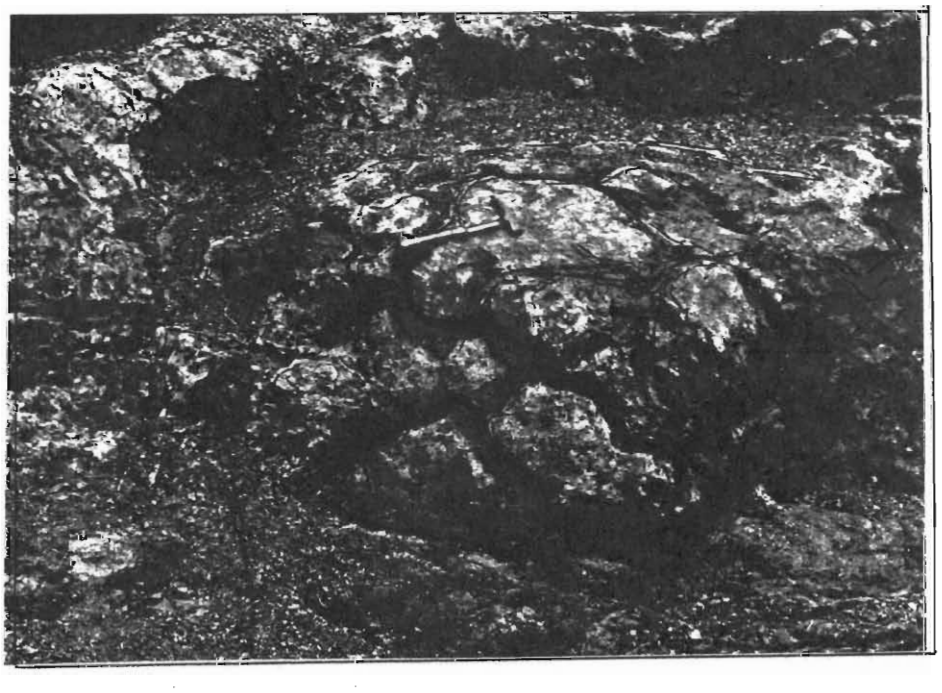

Plate 3.4 Pillow lavas at the base of flow AV91. Note the negative weathering pattern of the glassy material between individual pillows as well as the unconformable relationship between the pillows and the underlying flow (AV90).

During the present study, only one occurrence of pillow lavas was observed, 45m from the base of the volcanics and within the Agate Vale magma type (Plate 3.4) The pillows are underlain by a prominent bole surface, grade upwards into massive lavas over a distance of 2m, and have a lateral outcrop extent of 30m. In the field, the pillows are very fine-grained and more resistant to weathering than the glassy interstitial material between them.

The similarity of pillow basalts to pahoehoe toes has in some cases led to confusion between the two features. However, the slight radial elongation of the amygdales and the glassy material filling the interstices between the pillows suggests that the lavas exposed in the Sani Pass are actually pillows rather than pahoehoe toes. The geochemistry of a pillow basalt from the Sani Pass is given in Appendix 2 (sample AV91).

3.6. Xenoliths

A single occurrence of a tabular basaltic xenolith was noted in flow P232 (Plate 3.5). The xenolith is disjointed and therefore occurs as separate upper and lower parts, subparallel to the lava flow contacts. The contacts between the country rock and the xenolith are clearly discernable, and no apparent assimilation has occurred. The xenolith has a cross-section length of about a metre. It is light brown with a slight pinkish hue, and is aphanitic.

3.7. Sedimentary Features

Numerous sandstone and siltstone lenses and associated rheomorphic veins occur within the lower 415m of the volcanic succession. The sedimentary outcrops range from 70mm to 2m in thickness and are mostly concordant with the lava flows. The thinner lenses are very localised and impersistant, but the thicker ones are laterally more extensive. Sedimentary structures such as cross-bedding and laminations are well developed in some of the sediments. Sample AV113 (70m from the base of the volcanic succession) is a tuffaceous sandstone, containing tiny glass shards and lapilli which may be wind-blown material from neighbouring vent eruptions.

Plate 3.5 Disjointed, tabular basaltic xenolith in flow P232. The xenolith is subparallel to the flow contacts and does not show evidence of assimilation.

Associated with the sedimentary lenses are rheomorphic dykes which are irregularly distributed in the volcanic pile. The individual rhemorphic dykes are up to 300mm thick and are very fine-grained.

3.8. Summary

Volcanological features such as amygdales, auto-intrusive dykes as well as pahoehoe toes and surfaces are well preserved within the Sani Pass volcanic succession. These features are not restricted to any specific magma type within the basaltic stratigraphy. However, features associated with an aqueous environment, such as pillow lavas and sedimentary lenses, are restricted to the lower 415m of the basaltic sequence. The distribution of such features in the lower 415m of the volcanic succession might be as a consequence of changing conditions of eruption, from spurts interrupted by quiescence, to prolonged continuous eruption.

CHAPTER 4

4. PETROGRAPHY

4.1. Silicates

4.1.1. Introduction

In keeping with the approach adopted by recent workers in the Karoo igneous province, the basaltic rocks of the Drakensberg Formation exposed in the Sani Pass have been subdivided on the basis of geochemistry. This subdivision has defined five distinct magma types (Fig. 2.3). Each magma type has its type locality in the Sani Pass and has been designated a local geographical name. Although the lateral extent of each magma type is unknown, basaltic flows of the Phinong magma type can be traced for many kilometers.

The petrography of basalts exposed in the Sani Pass section is summarised for each of the different magma types. Included in the discussion are the associated dolerites. Anorthite concentrations of feldspars referred to in this chapter have been determined by optical means, unless otherwise stated.

4.1.2. The Giant's Cup magma type

The Giant's Cup magma type is geochemically heterogeneous and constitutes the initial flows of the Drakensberg Formation in the Sani Pass. The basalts are very limited in volume and this 14m thick unit constitutes less than 0.5% of the volcanic succession exposed in the Sani Pass.

In thin section rocks of the Giant's Cup type are fine-grained, hyalocrystalline and glomeroporphyritic, the clusters of plagioclase phenocrysts being clearly visible in handspecimen. In contrast to rocks of the overlying magma types, the rocks of the Giant's Cup unit, especially flows GC350 and GC360, are highly altered. Plagioclase is the only phenocryst phase, and is set in a groundmass of plagioclase, pyroxene and devitrified glass (Plate 4.1). The lowest flows, GC350 and GC360, have an intersertal groundmass texture that grades into intergranular in samples GC370 and GC380 (Plate 4.1).

Plagioclase occurs as subhedral to euhedral laths in the groundmass and as larger grains up to 2.5mm in length in the glomeroporphyritic aggregates. Twinning in the plagioclase is predominantly by the albite, and combined albite-Carlsbad, twin laws and indicates a compositional range of An_{58} to An_{60} for the phenocrysts, whereas a range of An_{48} to An_{54} is typical of the smaller (0.4 to 0.6mm) groundmass crystals. Alteration of the feldspar is intense, especially in the phenocrysts, and in samples GC350 and GC360 the feldspars are almost completely saussuritized. Some of the groundmass plagioclase show well developed quench textures, such as sheaf-like growths of acicular crystals and hollow sections, indicative of rapid cooling during extrusion.

Pyroxene occurs as small subhedral to anhedral crystals in the groundmass (Plate 4.1). In the two lowermost flows the pyroxene has been completely replaced by epidote and chlorite. Less altered pyroxenes, which frequently show twinning, yield a 2V angle of approximately 50°, implying an augitic composition.

Brownish-black glass frequently occurs as random patches interstitial to the plagioclase; in some instances the glass has devitrified with the release of a reddish brown oxide. Within this glassy mesostasis randomly orientated, needle-like oxide grains are conspicuously distributed and cut across all silicate minerals (Plate 4.12). Amygdales are relatively common, and mainly calcite and lesser quartz infillings are typical, frequently with a rim of chlorite and a bright reddish brown oxide.

4.1.3. Agate Vale magma type

Most of the basalts of the Agate Vale magma type are glomeroporphyritic. The groundmass plagioclase grains are gradational in size between the phenocryst range and the groundmass range. This feature often imparts an apparent seriate texture to the rock (Plate 4.2). Groundmass textures are mainly intersertal; intergranular and hyalophitic textures are poorly represented. Sample AV90, which occurs 40m above the base of the succession, is the only sample within this magma type characterized by a subophitic to poikilophitic groundmass texture. All the basalts, except sample AV90 are amygdaloidal in varying degrees.

Plagioclase occurs as both groundmass and phenocryst phases. The plagioclase phenocrysts often occur in a glomeroporphyritic arrangement within which individual laths may be up to 1.8mm in length. The phenocrysts range in composition from An_{57} to An_{65}. Plagioclase in sample AV400 is highly saussuritized, precluding any compositional assessment. Two generations of groundmass plagioclase are present namely:

1. subhedral to anhedral laths up to 0.8mm long,
2. zoned stubby subhedral to euhedral crystals up to 0.6mm in length.

The anorthite content of the groundmass plagioclase ranges from An_{50} to An_{58}. The hyalophitic samples (AV80, AV91) display quench textures (Plate 4.3) which may be indicative of rapid cooling, heterogeneous nucleation (Lofgren, 1983) or differential flow in the magma (Kouchi *et al.* 1986). Within the large phenocrysts resorption is indicated by internal melting, preserved as pores now filled by residual glassy material (Plate 4.3). Cox *et al.*, (1979) suggested that such resorptional features are characteristic of thermal or compositional disequilibrium within a magma chamber.

Augite is the predominant pyroxene and occurs as subhedral to anhedral grains up to 0.6mm in diameter. Augite also occurs as a groundmass phase, except in sample AV91 where glomeroporphyritic clusters of euhedral grains arranged parallel to (001) are present. A number of flows also contain subordinate pigeonite both as individual grains and cores to augite grains. Hourglass zoning is common within the pyroxenes (Plate 4.4).

Plate 4.1 **Giant's Cup (GC380).** Characteristic glomeroporphyritic texture of the Giant's Cup basalts, in which plagioclase occurs as the phenocryst phase, set in a groundmass of plagioclase, pyroxene and devitrified glass. In this sample the groundmass is intergranular (crossed nicols).

Plate 4.2 **Agate Vale (AV100).** Plagioclase in the Agate Vale basalts is variable in size, between the phenocryst and groundmass size range. This feature imparts an apparent seriate texture to the rock. Frequently the groundmass texture is intersertal, as in this case (crossed nicols).

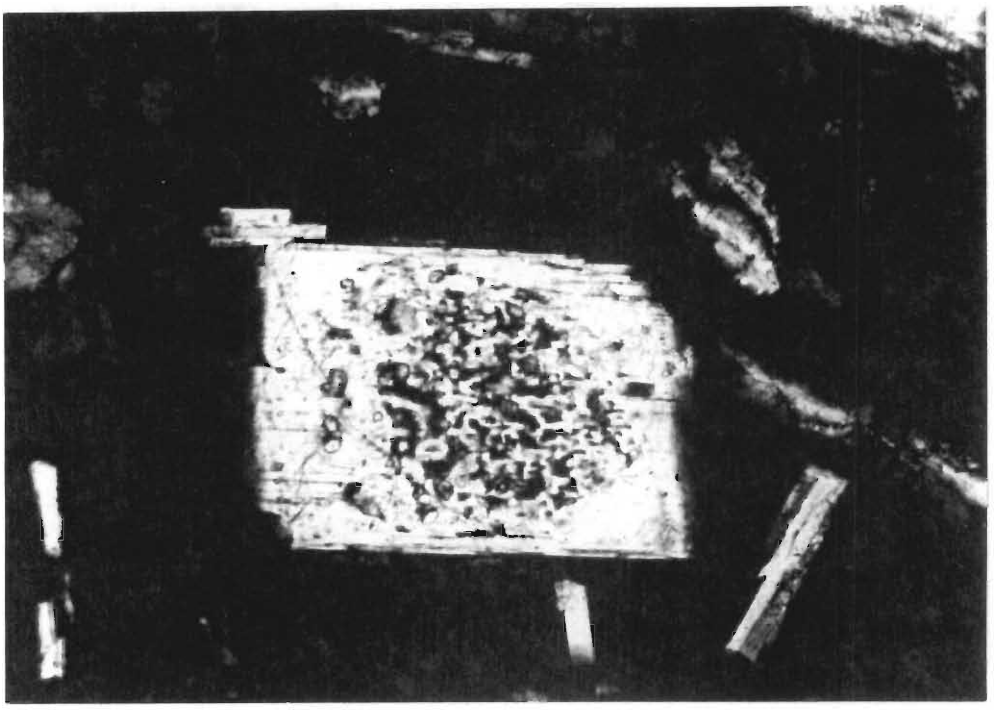

Plate 4.3 **Agate Vale (AV91).** Chill margin of pillow lava, displaying a hyalophitic texture, possibly indicative of rapid cooling, heterogeneous nucleation or differential flow. The large plagioclase phenocryst indicates resorption by pores now filled by residual glassy material (crossed nicols).

Plate 4.4 **Agate Vale (AV90).** Hourglass zoning in augite. In this sample, plagioclase and pyroxene occur subophitically as the groundmass (crossed nicols).

Within the Agate Vale magma type, olivine is present only as small inclusions in the pyroxene and very sparse single crystals. Most of the olivine has been completely altered, the common alteration product being serpentine.

The opaque ore minerals comprise mainly magnetite octahedra and skeletal ilmenite/ magnetite set in a glassy mesostasis. In sample AV91 the magnetite shows resorptional textures similar to those in the plagioclase. Amygdale compositions are predominantly, calcite with minor agate and chlorite.

4.1.4. Sakeng magma type

The very fine-grained basalts (<0.5mm) of the Sakeng magma type are characterised by intersertal and hyalophitic textures, while the coarser-grained (2.0 to 2.5mm) samples are subophitic to poikilophitic. The poorly developed glomeroporphyritic texture is only developed in the fine-grained samples as clusters of plagioclase. Plagioclase, pyroxene and olivine constitute the main mineral components of the Sakeng-type basalts, but only plagioclase and olivine occur as phenocryst phases.

In the glomeroporphyritic samples plagioclase is present as euhedral to subhedral laths up to 0.3mm in length. In addition to glomeroporphyritic plagioclase, rare single plagioclase phenocrysts, up to 1.4mm in length, are present (Plate 4.5). The average composition of the large phenocrysts is An_{55}. In the basalts having a glassy component, rapid cooling is indicated by the abundant small acicular plagioclase crystals having swallow tail edges. Spherulitic bundles of plagioclase are also present and are best developed in the vicinity of the amygdales.

Augite is restricted to the groundmass and occurs as equigranular, anhedral to subhedral grains which comprise up to 20% of the rock. In the coarser-grained samples plagioclase is subophitically to poikilophitically enclosed by larger (2.5 to 2.8mm diameter) pyroxene crystals. Hourglass zoning is well developed in the large pyroxene crystals. Pigeonite is present within the Sakeng basalts mainly as cores to individual augite grains.

Pseudomorphs after olivine (up to 1.3mm in diameter), are well represented in the Sakeng-type basalts. They occur as inclusions mainly within the pyroxene. Serpentine and associated oxides are common alteration products.

Patches of a greenish black isotropic interstitial material appears to have replaced glass. The replacement mineral has similar characteristics to chlorophaeite, which has been observed as an alteration product of glass in the Thingmuli tholeiites (Carmichael, 1964), the Deccan Traps (Sukheswala *et al.*, 1974) and the Columbia River basalts (Hooper, 1988). The ore phases comprising large (up to 0.25mm) subhedral to anhedral magnetite grains and smaller skeletal ilmenite laths riddle the greenish brown glassy mesostasis. Chlorite is the most abundant amygdale infilling with lesser proportions of agate and calcite. The amygdales are frequently rimmed by reddish brown iron oxides (Plate 4.5).

4.1.5. Mkhomazana magma type

The Mkhomazana magma type exhibits a mineralogy which is different from the other magma types within the Sani Pass volcanic succession. However, the basaltic rocks of this unit are texturally similar to those of the underlying magma types in having glomeroporphyritic and seriate textures.

Plagioclase occurs as aggregates of phenocrysts as well as individual crystals in the groundmass. Both generations of plagioclase are highly sausuritized, which imparts a dusty appearance to these crystals. The composition of the phenocrysts range from An_8 to An_{10}, and the groundmass crystals from An_2 to An_4; both compositions being in the range of albite. A few grains of Carlsbad-twinned alkali feldspar were observed in the groundmass. Two generations of pyroxene are present namely:

1. subhedral to anhedral grains which are intergranular to the plagioclase and occasionally enclose the latter subophitically,
2. larger subhedral prismatic laths which are less abundant and formed later (Plate 4.6).

The pyroxenes are highly altered and often completely chloritized. No fresh olivine is present, but serpentine pseudomorphs after olivine are present.

Plate 4.5 **Sakeng (S130).** Large single plagioclase phenocryst in an intersertal to intergranular groundmass. These single phenocrysts are extremely rare. Note the reddish brown oxide rim around the amygdales (crossed nicols).

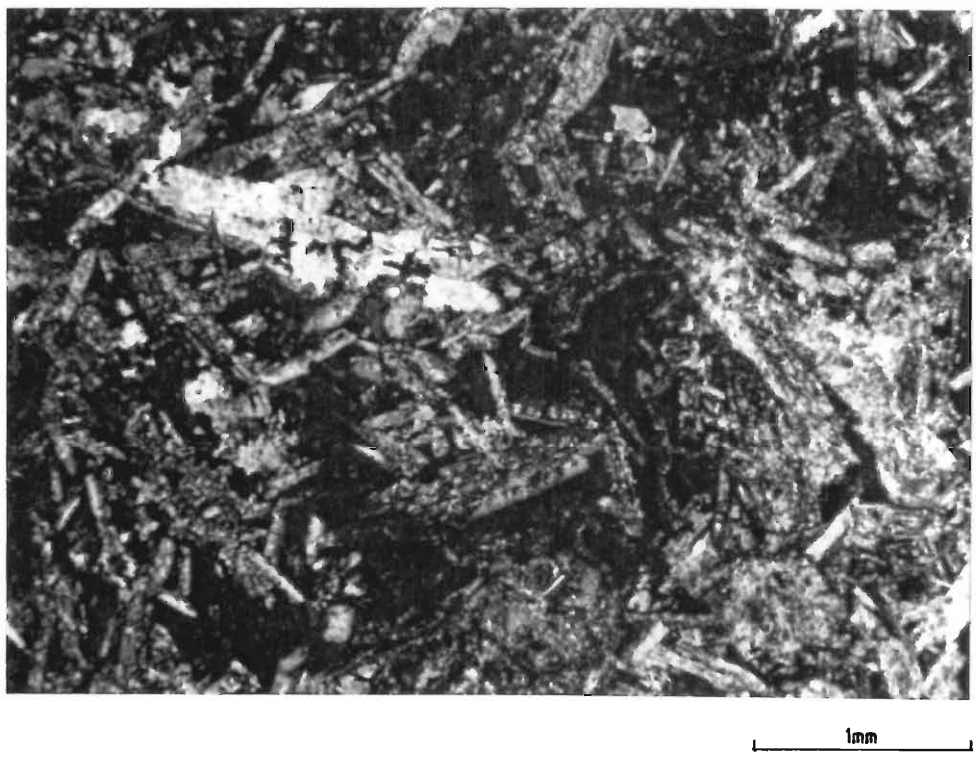

Plate 4.6 **Mkhomazana (M160).** Late-formed subhedral prismatic laths of pyroxene. Smaller, subhedral to anhedral grains occur intergranular to the plagioclase. Note the large degree of alteration of this sample especially the glomeroporphyritic plagioclase (in lower right hand corner) and the groundmass plagioclase (crossed nicols).

Glass occurs intersertally and contains abundant ilmenite microlites. Magnetite occurs as euhedral to subhedral grains and is less well developed than the ilmenite. A large proportion of the glass has been altered to a greenish brown material. Amygdales are abundant and filled mainly with chlorite and to a lesser extent calcite and zeolite, and are frequently rimmed by brown iron oxides and quartz (chalcedony).

4.1.6. Phinong magma type

Although the basalts of the Phinong magma type are geochemically uniform, this uniformity is less well developed in the petrography, as reflected by the variation in texture. The lower flows are characterized by a seriate to subophitic texture (Plate 4.7), while those higher in the stratigraphy have a well developed glomeroporphyritic texture (Plate 4.8). Similar textural variations have been observed in the Roodehoek basalt type of the north-eastern Cape (Mitchell, 1980), but no stratigraphic pattern has been ascribed to the occurrence of the two petrographic types in the Roodehoek unit. Similar textures were also reported by Cox and Hornung (1966) in the Lesotho basalts, they also noted that the central massive portions of flows are rather coarse, with large groundmass plagioclase which often obscures any porphyritic texture.

Plagioclase is the most abundant mineral and occurs both as phenocrysts and small crystals in the groundmass. Plagioclase phenocrysts occur as single large grains (up to 2.0mm in length), as well as in glomeroporphyritic association, where individual crystals may be as large as 3.0mm (Plate 4.8).

Three generations of plagioclase have been observed in the groundmass, namely:

1. tabular laths slightly smaller than the phenocryst generation,
2. smaller skeletal laths which may be poikilophitically included in large pyroxene grains or in the glassy mesostasis. Plagioclase laths having the latter occurrence generally show quench textures, and
3. subhedral to anhedral stubby crystals which are larger than (2) but often smaller than (1). This generation of plagioclase is the least abundant.

Plate 4.7 **Phinong (P200).** Typical subophitic texture in the lower flows of the Phinong magma. This texture is characterized by pyroxene plates that partially enclose the plagioclase laths (crossed nicols).

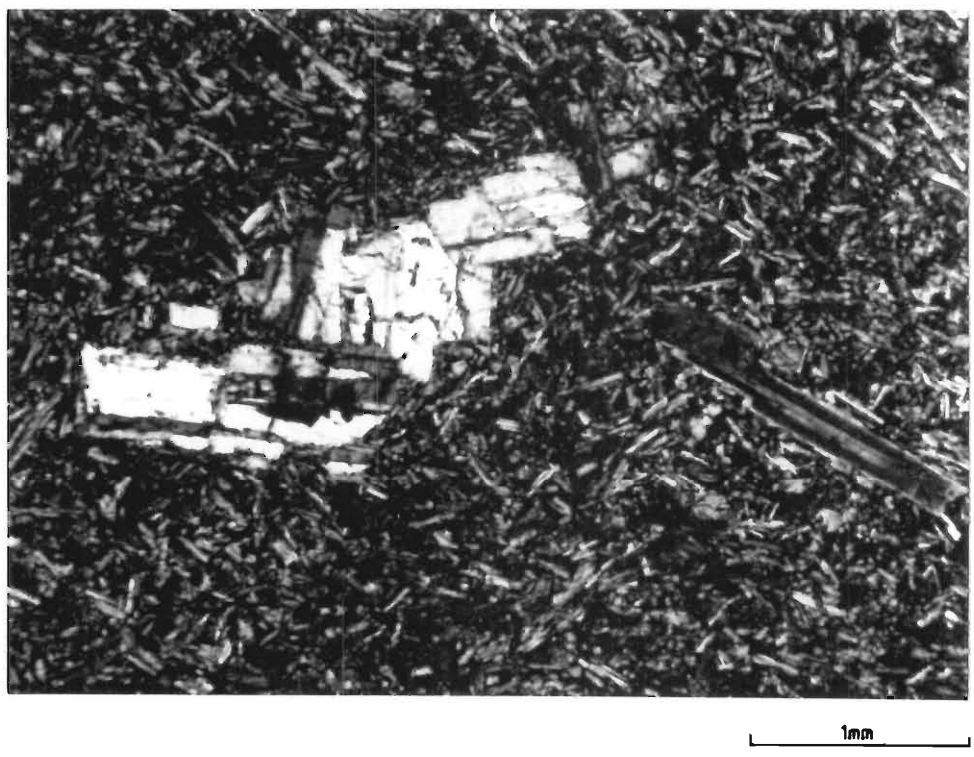

Plate 4.8 **Phinong (P273).** A glomeroporphyritic texture is characteristic of flows higher up in the Phinong succession. This texture type is characterized by early-formed plagioclase that accumulates in a fine-grained groundmass (crossed nicols).

Augite with a 2V angle of 40 to 52° is the dominant pyroxene, and occurs as subhedral to anhedral grains up to 3.0mm in diameter. In the coarser-grained basalts augite occurs in subophitic to poikilophitic relationship with the plagioclase (Plate 4.7). In the more glomeroporphyritic rocks, characteristic of flows higher in the volcanic succession, pyroxene is intergranular to plagioclase and occurs as a groundmass phase (Plate 4.8). Pigeonite, usually in accessory amounts, has been detected both as cores to the augite grains (Plate 4.9) and as smaller single grains. The pyroxenes are frequently twinned and occasionally show well developed hourglass zoning.

Olivine is widespread throughout the Phinong magma type and constitutes up to 15% of the rock in sample P227. In the majority of the higher magnesium rocks only pseudomorphs of olivine are preserved. Olivine is always pseudomorphed by serpentine or a mixture of serpentine and magnetite. Fresh olivine is preserved in the lower flows as large (up to 2.5mm diameter) euhedral to subhedral phenocrysts (Plate 4.10). Smaller olivine grains, frequently completely altered, occur as inclusions in the pyroxene.

Glass is an essential constituent and represents the residual liquids which finally solidified in the form of small patches between crystals. This glass is present in variable proportions in the different flows, being slightly more abundant in the lower flows. The patches of glass generally contain needles of opaque ore (ilmenite) and microlites of feldspar. The opaque oxides are generally unevenly distributed and vary in proportion amongst the individual flows.

Two generations of magnetite have been observed:

1. ragged, angular magnetite that occurs interstitially to the groundmass pyroxene and plagioclase, is common in the lower olivine-rich flows, and
2. larger, equant grains occurring as phenocrysts in the upper flows.

Amygdales are common and their infillings include calcite, iron oxides and a variety of zeolites.

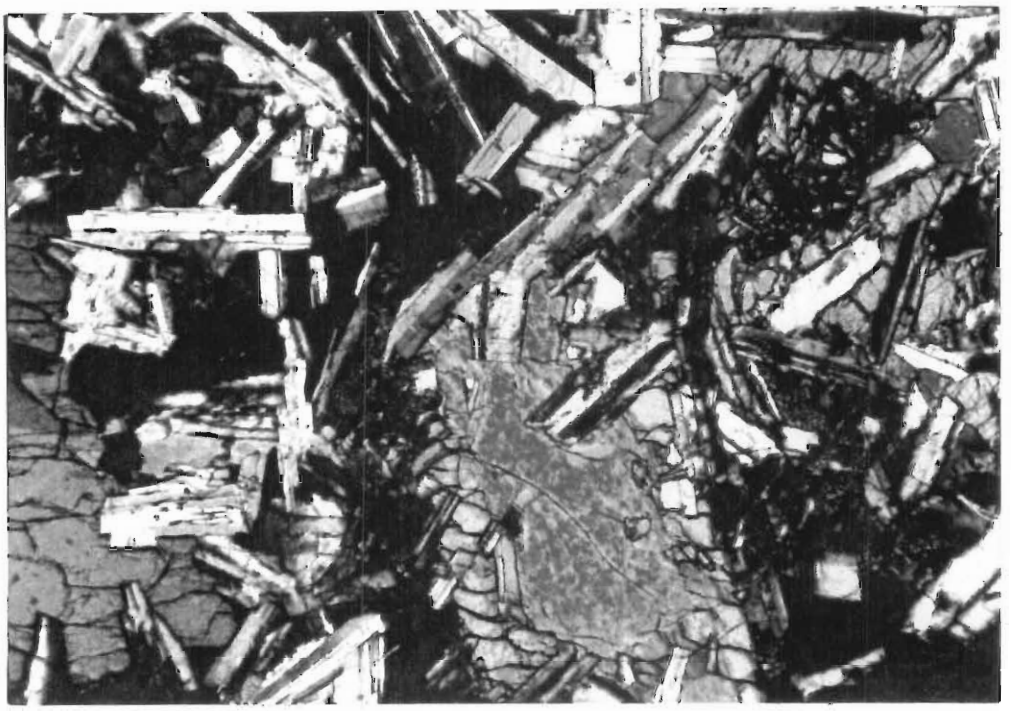

Plate 4.9 **Phinong (P180).** Photomicrograph of pigeonite mantled by augite. Note the relatively well formed augite rim on the central pigeonite core (crossed nicols).

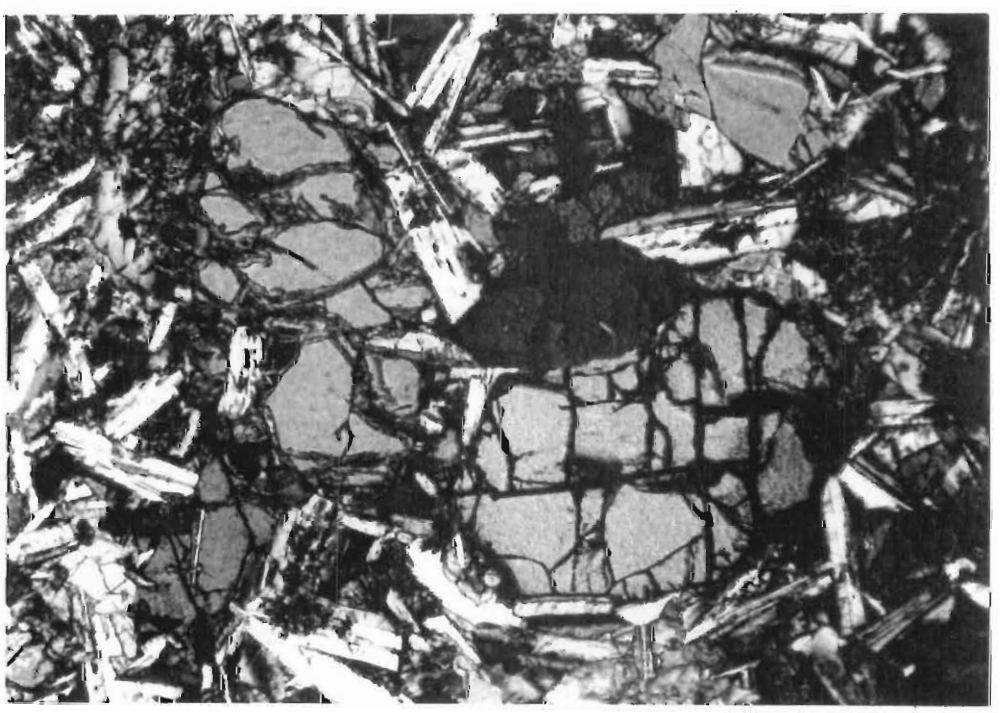

Plate 4.10 **Phinong (P227).** Photomicrograph of olivine macrophenocrysts in a groundmass of plagioclase and pyroxene. Alteration of the olivine on the left of the photograph has advanced along fractures, the alteration product being serpentine.

4.1.7. Dolerites

The dolerites are characterized by glomeroporphyritic plagioclase set in an intergranular groundmass. Samples from the central portions of dykes exhibit well-developed subophitic and poikilophitic textures (Plate 4.11). As in the basalts, plagioclase constitutes the most abundant mineral phase, followed by pyroxene and olivine. In comparison with the basalts, the dolerites are less altered. The plagioclase phenocrysts occur as bladed and stubby laths, up to 1.5mm in length, and range in composition from An_{50} to An_{62}. This large anorthite compositonal range reflects the prominent zoning in the plagioclase grains. The earlier formed plagioclase grains are poikilitically to ophitically included in the larger later-formed plagioclase. The groundmass plagioclase is seriate, ranging from larger stubby and bladed laths to small, almost skeletal grains. Commonly, the large plagioclase crystals occur in a subophitic arrangement with the pyroxene.

Pyroxene, which occurs interstitially to the plagioclase crystals, is subhedral and the grains are 0.2 to 0.3mm in diameter. Augite is the predominant pyroxene with only minor amounts of pigeonite. In dolerites that have a subophitic texture, the augite grains are up to 3.0mm in diameter, and riddled with poikilophitic plagioclase (Plate 4.11).

Only pseudomorphs after olivine phenocrysts are preserved, and constitute up to 8% of the rock. Generally the pseudomorphs are small (0.15 to 0.30mm), but grains up to 1.5mm have been observed. Cracks in the olivine pseudomorphs are filled by serpentine, while iron oxides occur as stringers of small grains. The reddish brown alteration product, iddingsite, is abundant.

Subhedral to anhedral magnetite is the dominant ore mineral, with skeletal ilmenite occurring in accessory amounts. Magnetite is present as a phenocryst phase as well as an alteration phase. When magnetite occurs as phenocrysts, it is frequently corroded.

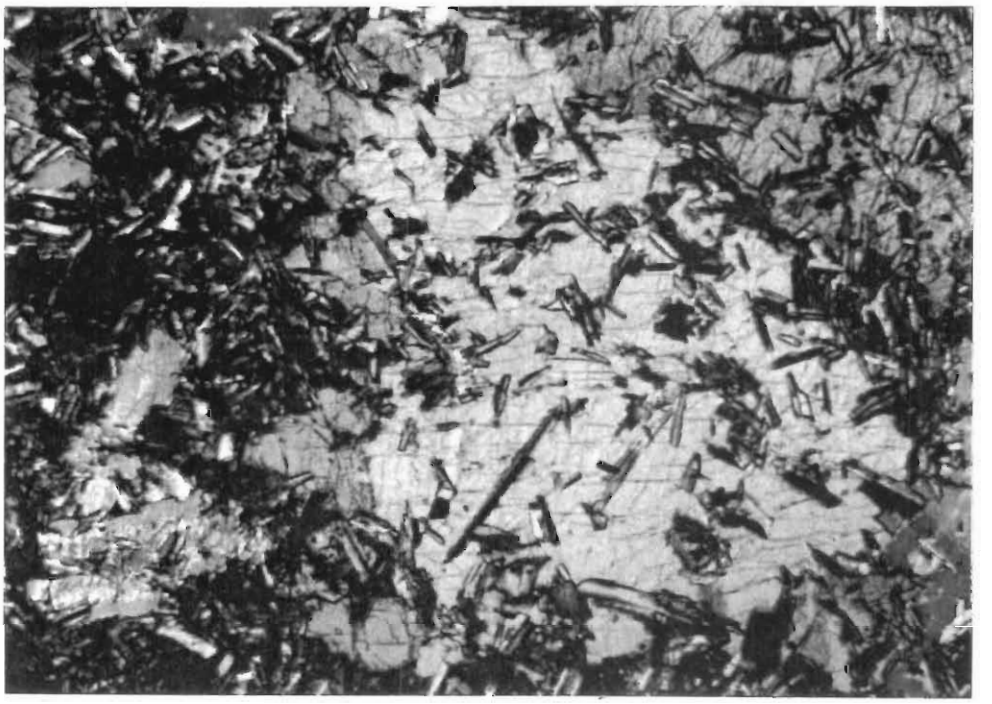

Plate 4.11 Dolerite (D51). Smaller plagioclase grains completely enclosed in a large pyroxene grain, classic example of an ophitic texture.

4.2. Ore Mineralogy

4.2.1. Introduction

The opaque minerals of the Sani Pass basalts occur as accessory phases, comprising between 0.5 to 2.0 volume percent. Oxides constitute the major proportion of the opaque mineralogy, with subordinate sulphide phases. The oxide minerals belong to the spinel and hematite groups and their associated oxidation products. Oxides are prone to post crystallization effects such as further oxidation, hydration and exsolution, hence it is important that these processes are considered as they may change the primary mineralogy, and the whole-rock geochemistry.

Eales *et al.* (1980) noted that primary ilmenite and titaniferous magnetite (Ti-magnetite) are both late crystallizing phases in the Karoo Province basalts and dolerites, and nucleate after about two-thirds of the parent magma has solidified. These minerals therefore provide useful information on the later crystallization stages and subsequent cooling histories of their host rocks. Thus, the ratio of primary ilmenite/magnetite has been used as a qualitative indicator of oxygen fugacity (fO_2) in Karoo dolerites (Reynolds, 1983), as well as an indication of the whole- rock chemistry of the melts from which the Sabi River basalts and dolerites crystallized (Sweeney, 1988).

This chapter therefore provides an ore mineralogy description of 15 polished sections from the Sani Pass basalt and dolerite suite. In addition, late stage alteration phenomena are described as well as aspects of the subsolidus behaviour of the ore phases.

4.2.2. Giant's Cup Magma Type

Ilmenite and magnetite are the major opaque phases in the Giant's Cup basalts, with only minor sulphides being identified in sample GC360. Ilmenite occurs as the major oxide in samples GC350 and GC360 while magnetite is predominant in GC380.

Ilmenite is present in two forms, namely as individual grains (up to 0.5mm) as well as an exsolution/oxidation phase. The primary ilmenite phase exhibits a variety of morphologies, with the skeletal type being most common (Plate 4.12). The skeletal ilmenites seem to be best developed interstitial to the silicates, in areas now occupied by highly altered glassy mesostasis. Reynolds (1983) recorded similar skeletal ilmenites in the chill zones of some Karoo dolerites (Eastern Cape and southern Orange Free State areas) and ascribed their morphology to a rapid cooling rate. J H Henckel (pers, comm. 1992) however, suggested that the smaller ilmenite laths might represent remnant ilmenite exsolutions from a magnetite host, that has been completely altered, as similar alteration textures have been observed in titaniferous magnetites of the Bushveld Complex Main Zone (von Groenewald *et al.*, 1985). The exsolution/oxidation ilmenite phase in the Giant's Cup basalts is preserved as networks of trellis lamellae and sparse occurrences of sandwich lamellae in a titaniferous magnetite host. The ilmenite lamellae are oriented parallel to (111) planes of the host magnetite. Alteration of the ilmenites varies from "fresh" to completely altered, as in sample GC360, in which the ilmenite is altered to rutile and iron oxides. Incipiant rutile alteration of ilmenite has been observed to occur along grain boundaries, possibly testifying to deuteric alteration.

Magnetite occurs as an early-formed phase, characterized by euhedral to subhedral crystal morphology (<0.25mm) and no exsolution lamellae of ilmenite, and a later titaniferous rich variety, characterized by ilmenite lamellae. Buddington and Lindsley (1964) and Haggerty (1976) interpreted such ilmenite intergrowths as having developed in response to differences in oxygen fugacity and cooling rate during subsolidus cooling. These authors also indicated that the ilmenite intergrowths possibly resulted from contemporaneous oxidation/exsolution of magnetite-ulovöspinel solid solution during cooling under high oxygen fugacity conditions.

Sulphides in sample GC360 are the major opaque phases, with pyrite being most abundant. The pyrite is present as large (*ca* 0.25mm) idiomorphic grains that commonly nucleate on prexisting silicates and along amygdale boundaries, submicroscopic abhorescent grains preserved mainly in the groundmass, and postcumulus vein pyrite. The large

idiomorphic pyrites frequently have a core of pyrrhotite, that was progressively replaced with an increase in the sulphur/iron ratio.

4.2.3. Agate Vale Magma Type

Opaque minerals in the Agate Vale basalts constitute less than 1.5 volume percent, and comprise predominantly oxides with minor sulphide grains. Immediately apparent in this unit is the almost total absence of acicular ilmenite grains, thus establishing magnetite as the predominant oxide phase. The magnetite grains occur mainly as skeletal and arborescent grains, frequently containing inclusions of entrapped melt (Plate 4.13). Martitization, that is, the alteration of magnetite to hematite as a result of oxidation, is present; and in some of the grains has reached an advanced stage. This replacement texture seems to be preferentially developed along cleavage directions in the magnetite. Oxidation/exsolution lamellae of ilmenite in magnetite are very poorly developed and might indicate low fO_2 conditions during crystallization. However, the almost total absence of ilmenite should be accompanied by a low bulk rock TiO_2 content. This, however, is not the case for the polished sections examined (TiO_2 = 1.06 (AV 40); 1.05 (AV91) weight percent), and might therefore indicate that a proportion of the TiO_2 is in the silicate minerals.

In sample AV91 sulphides are extremely well developed along the chill margins of the pillow lava, and in other cases pyrite occurs as granular rims around amygdales.

4.2.4. Sakeng Magma Type

Only a single polished section has been examined for the Sakeng-type basalts, and the opaque minerals comprise approximately 0.5% of the total mineralogy for this magma type, with almost equal proportions of oxides and sulphides present.

Very fine-grained skeletal ilmenites reappear in the Sakeng magma type and, as in the Giant's Cup basalts, these grains are randomly distributed in the groundmass. Magnetite is rare, and only a single grain of magnetite (without any exsolutions) was observed.

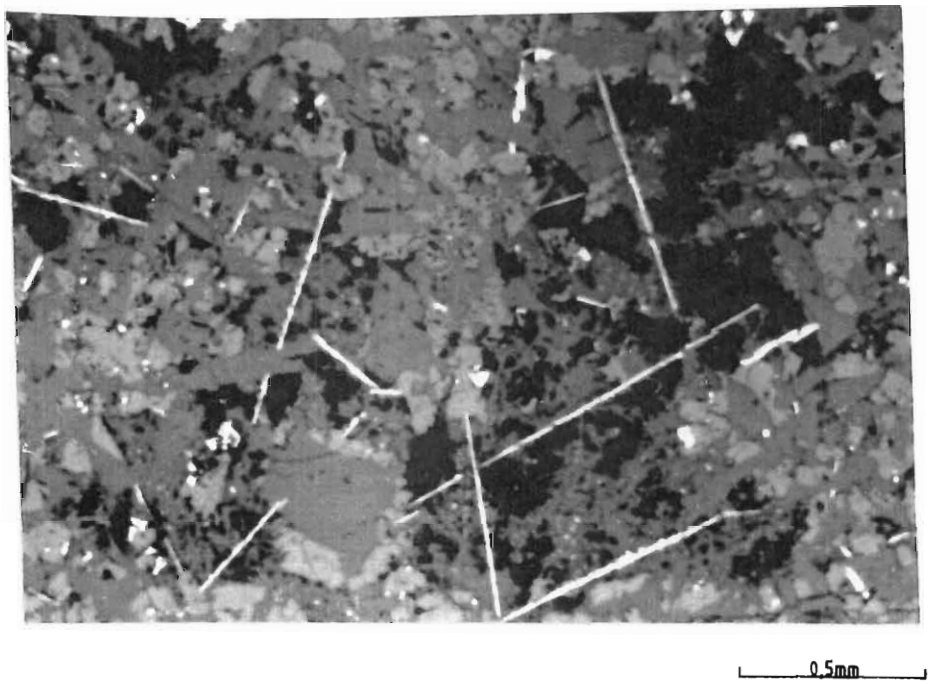

Plate 4.12 Giant's Cup (GC380). Photomicrograph of acicular ilmenite laths. Although randomly developed, these laths show a preference for the mesostasis. Incident light, no oil immersion.

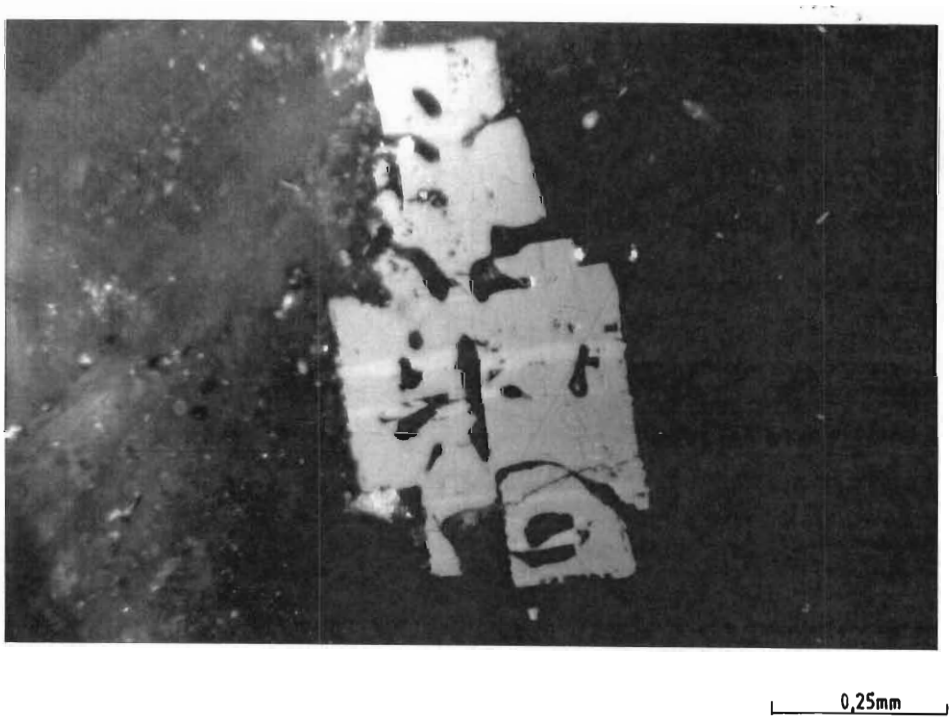

Plate 4.13 Agate Vale (AV40). Photomicrograph showing subhedral magnetite crystal containing inclusions of entrapped melt. These inclusions cut across pre-existing ilmenite exsolutions (very light coloured). Incident light, oil immersion.

Although not totally representative, the lack of Ti-rich exsolutions in the single polished section from this magma type, might indicate low fO_2 during fractional crystallization. Alteration of the oxides is intense, the alteration products being pseudobrookite, anatase, leucoxene and rutile.

The sulphides are present as earlier-formed subhedral to anhedral pyrite grains (up to 0.2mm), and as later sulphide-filled micro-veins that cut pre-existing silicates and oxide grains. A strong possibility therefore exists for sulphur being an important component in post-solidification hydrothermal fluids, which might account for the observed replacement of pyrrhotite by pyrite.

4.2.5. Mkhomazana Magma Type

For the Mkhomazana magma type, a single polished section from the central portion of the succession was examined. Although both oxides and sulphides are present in this magma type, the sulphides are very sparse.

Very fine-grained skeletal ilmenite and magnetite are present in almost equal proportions, and are preferentially located in the glassy groundmass. The ilmenite grains show intense alteration, mainly to rutile, while the magnetite is preferentially altered along twin planes to pseudobrookite, after exsolved ilmenite. The predominance of magnetite with Ti-rich exsolutions over magnetite without Ti-rich exsolutions (only one occurrence), suggests a high oxygen fugacity.

4.2.6. Phinong magma type

The Phinong magma type is the volumetrically dominant type in the Sani Pass volcanic succession, and hence displays a variety of textures in the oxide and sulphide minerals. Ilmenite and magnetite frequently predominate over the sulphide phases.

Skeletal textures that are common in the underlying magma types are poorly developed in the Phinong basalts. Rather, the opaque minerals in the Phinong basalts are more subhedral to euhedral. This feature of a more euhedral shape in the Phinong magma type, might be attributed to the cooling history of individual lava flows, since thin and therefore rapidly cooled flows were sampled in the Giant's Cup, Agate Vale, Sakeng, and Mkhomazana magma types in contrast to the thicker and slower cooled flows of the Phinong magma type.

The influence of bulk-rock chemistry on oxide mineralogy is well illustrated in the Phinong magma type. The olivine-enriched flows, and hence high MgO flows, contain predominantly magnetite with minor ilmenite and no sulphides. The magnetite in these high-MgO rocks (P180) occurs as small homogeneous, subhedral inclusions in the olivine and is considered to be chromium-enriched. Thus, the high whole rock chromium content in sample P180 (Cr = 477ppm) possibly reflects the presence of chromium-enriched magnetite. The chromium-enriched magnetites do not exhibit any exsolution features, reflecting the low TiO_2 whole-rock content (0.68 weight percent) and indicating low fO_2 conditions during their formation. Minor ilmenite has been observed along the margins of some chromium-enriched magnetite grains (Plate 4.14). Buddington and Lindsley (1964) suggested that such a feature represents either a late overgrowth nucleated on magnetite, or an externally exsolved phase produced by high-temperature oxidation. Eales *et al.*, (1980) suggested that magnetite in contact with such rims holds generally low levels of TiO_2 ($\pm 10\%$).

Samples characterised by a normal whole-rock MgO content (5 to 8 weight percent) commonly have a predominance of ilmenite over magnetite, or both minerals occur in about equal proportions. The magnetite is light pinkish brown and exhibit a variety of Ti-rich exsolution features (Plate 4.15). These rocks are generally also marked by a higher whole-rock TiO_2 content (0.84 to 1.12 weight percent). Trellis and sandwich lamellae of ilmenite occur, with the trellis lamellae being orientated parallel to (111) in the magnetite. Ramdohr (1980) suggested that ilmenite unmixing in magnetite takes place between 400 and 700°C. Martitization is widespread in the magnetite grains (Plate 4.16). In some instances early-formed ilmenite grains act as nucleation points for titaniferous magnetite (Plate 4.17).

4.3. Summary

Primary minerals in the basaltic rocks of the five magma types defined from the Sani Pass are: plagioclase and pyroxene (usually augite, and subordinate pigeonite), lesser olivine and accessory amounts of opaque minerals. A variety of textures are exhibited by these rocks, with the pre-Phinong basalts being mainly glomeroporphyritic, whilst the lower portion of the Phinong succession is subophitic, grading into glomeroporphyritic in the uppermost part.

The opaque minerals, which constitute less than 2% by volume of the rock, are dominated by magnetite and ilmenite, with minor sulphides. Numerous subsolidus exsolution and replacement features, which possibly occurred at temperatures between 400 to 700°C, are exhibited by these minerals. Evidence of late-stage deuteric alteration is also preserved. The ratio of ilmenite to magnetite indicates that oxygen fugacity conditions may have fluctuated considerably during the late-stage crystallization of the Sani Pass basalts.

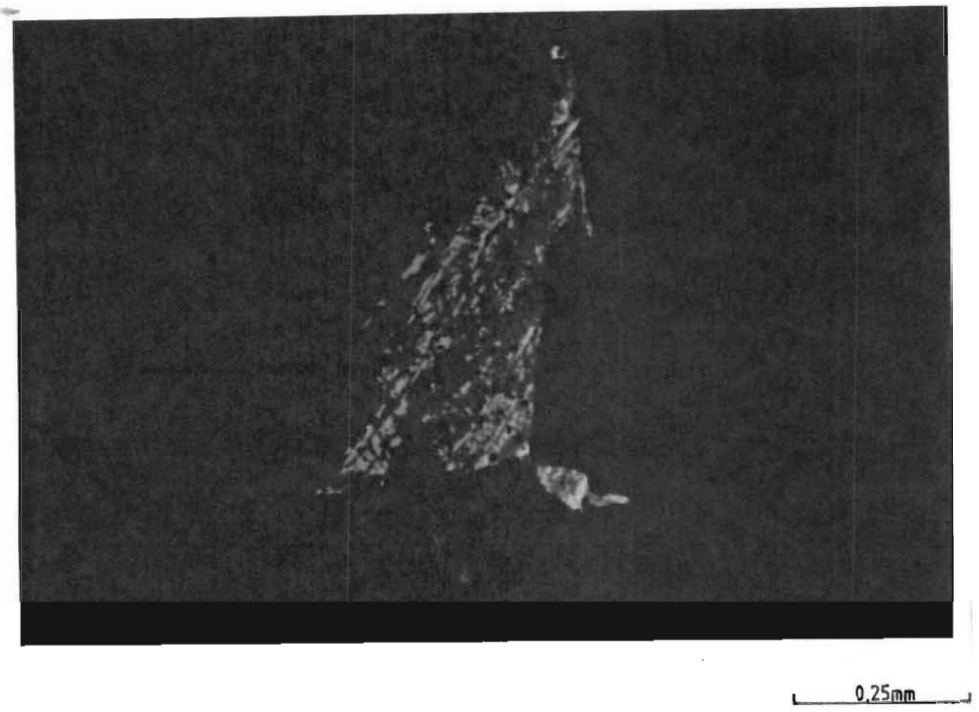

Plate 4.16 Phinong (P278). Photomicrograph showing the incipient alteration of magnetite to hematite (martitization). Incident light, oil immersion.

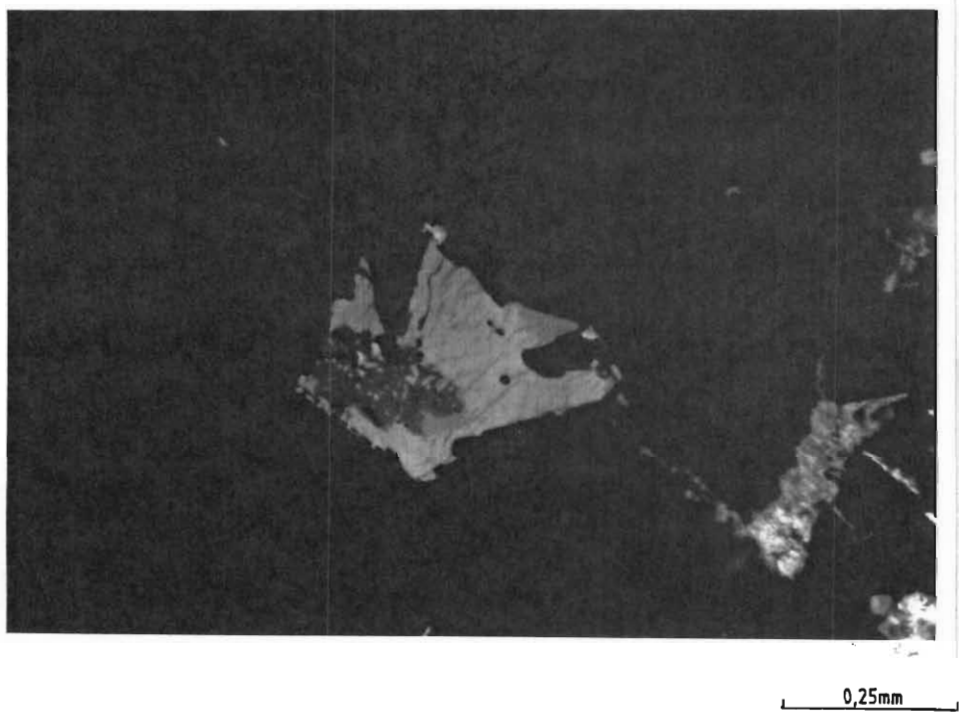

Plate 4.17 Phinong (P278). Photomicrograph illustrating the mantling of earlier-formed ilmenite (dark grey) by later Ti-magnetite (light grey). Incident light, oil immersion.

CHAPTER 5

5. MINERAL CHEMISTRY

5.1. Introduction

Quantitative microprobe studies on lavas of the Central Karoo Province are limited (Mitchell, 1980; Marsh and Eales, 1984), although some earlier data based on optical determinations exists (Walker and Poldervaart, 1949). Electron probe microanalysis of selected plagioclase, pyroxene and olivine from basalts of the Drakensberg Formation exposed in the Sani Pass are presented. The objective of this chapter is to determine whether consistent differences in mineral chemistry exist within and between the different magma types in the Sani Pass volcanic succession. Each of the mineral phases analysed is considered individually. Details of microprobe analytical conditions are provided in Appendix 3.

5.2. Olivine

Olivine is orthorhombic with a structure consisting of independent SiO_4 tetrahedra linked by divalent atoms in octahedral co-ordination. The SiO_4^{4+} tetrahedra are linked by Mg and Fe ions, each of which has six nearest oxygen neighbours. The oxygens are arranged in six-fold co-ordination and lie in sheets parallel with the (100) plane, and the SiO_4^{4+} tetrahedra point alternately in the X and Y directions. The Mg and Fe ions, which approach random distribution between the unco-ordinated M1 and M2 sites (Birle *et al.*, 1968) are located at centres of symmetry and on reflection planes.

The common ferromagnesian olivines show complete diadochy between Mg and Fe, hence forming a solid solution series between the end members forsterite (Mg_2SiO_4) and fayalite (Fe_2SiO_4), with minor substitution of Ni, Cr, Mn and Ca for Fe and Mg. The distribution of these minor elements between olivine and liquid is normally expressed in terms of distribution coefficients, which may be considerably affected by temperature (Irving, 1978; Leeman and Lindström, 1978; Ray *et al.*, 1983), pressure (Mysen and Kushiro, 1979) and liquid composition (Watson, 1977).

The partitioning of nickel into olivine, in particular, has received much attention (Sato, 1977; Hart and Davies, 1978; Leeman and Lindström, 1978) and estimated olivine/liquid distribution coefficients range between 4.8 and 34 (Leeman and Lindström, 1978).

Mitchell (1980) demonstrated a decline in Ni with decreasing MgO content in olivines by combining the data of both intrusive (Elephant's Head picrites) and extrusive rocks (Drumbo Basalt member) from the Karoo Central area. The variation of Ni in relation to the MgO content of olivines from the Sani Pass appears to fit into the overall trend indicated by olivine compositions from other Karoo-age intrusive and extrusive rocks (Fig. 5.1). This Ni/MgO relationship in olivines, is an expression of the high distribution coefficient of Ni for olivine relative to the silicate melt, which results in a rapid depletion of Ni in residual melts, and consequently in a lower Ni content for olivine crystallized from more fractionated liquids.

Selected olivine microprobe analyses for sample P227 are listed in Table 5.1. Since only olivines from a single sample (P227) were analysed by microprobe, the results presented in Table 5.1 are not representative of all the magma types in the Sani Pass. The range in measured forsterite composition in olivines from P227 is Fo_{66} to Fo_{75} (Table 5.1); however, this limited range might be a function of a limited number of analyses.

The presence of olivine in the Sani Pass basalts is directly related to their whole-rock MgO content. For example, sample P227 contains 12.09 weight percent MgO and contains 15% modal olivine, while samples with a MgO content of 5.0 to 8.0 weight percent generally contain less than 4% modal olivine. The whole-rock MgO content of P227 is outside the 5.0 to 8.0 weight percent range that Eales and Marsh (1979) considered typical

Table 5.1 Microprobe analyses of olivine

	P227/1a	P227/1b	P227/2a	P227/2b
SiO_2	37.48	38.07	36.10	37.52
FeO	28.17	24.20	30.44	23.37
MnO	0.34	0.27	0.42	0.31
MgO	35.15	38.22	33.71	39.48
CaO	0.29	0.27	0.29	0.31
NiO	0.10	0.12	0.07	0.11
TOTAL	101.53	101.15	101.03	101.10

Atomic proportions calculated using 4 oxygens:

Si	0.989	0.989	0.972	0.974
Fe	0.622	0.526	0.685	0.507
Mn	0.008	0.006	0.010	0.007
Mg	1.382	1.480	1.352	1.527
Ca	0.008	0.008	0.008	0.008
Ni	0.002	0.003	0.002	0.002
Sum	3.011	3.012	3.029	3.025
Measured Fo	69.0	73.8	66.4	75.1
*Calculated Fo	86.5	86.5	86.5	86.5

* Olivine composition calculated from whole-rock data according to the method of Roeder & Emslie (1970)

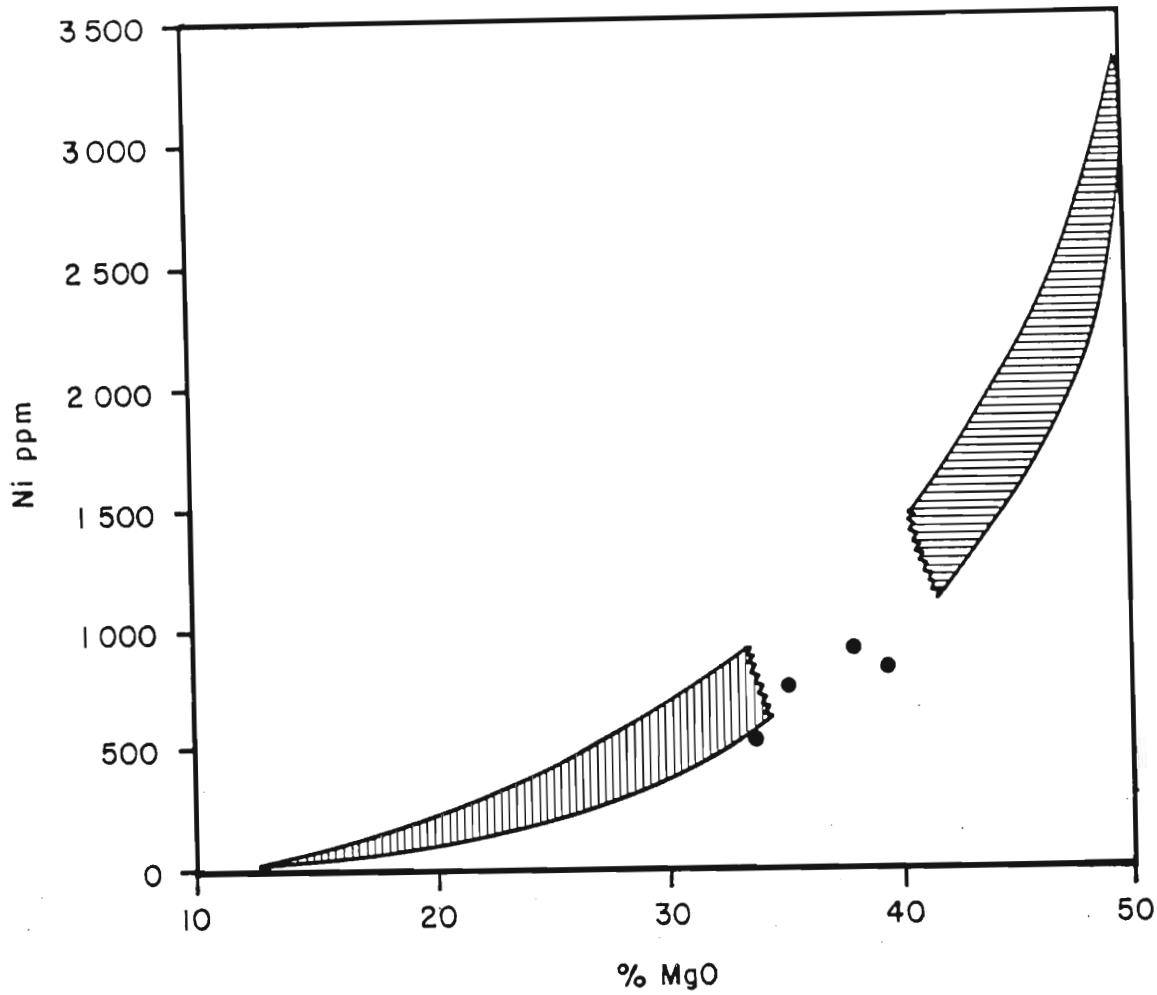

Drumbo Basalt Member

Various Karoo-age Intrusives

Phinong Magma-Type

Fig. 5.1 Plot of Ni (ppm) vs MgO (wt percent) for olivines from the Phinong magma type (sample P227). The stippled area represents analyses for various Karoo-age intrusive and extrusive rocks. The high distribution coefficient of Ni for olivine is exhibited by the decline in Ni with decreasing MgO. Data for the stippled area are from Mitchell (1980).

of "normal" (non olivine-enriched) Karoo magmas. This high-MgO content, therefore, might indicate a component of cumulus olivine, in which case modelling the fractionation history of sample P227 along olivine mixing lines becomes problematic.

A MgO/Ni mixing line, indicates by lever rule calculations that approximately 17% olivine enrichment would be required to derive the composition of sample P227 from an average Lesotho-type parent (designated A, in Fig. 5.2, data from Marsh and Eales, 1979). This is compatible with the petrography, indicating a modal olivine content of about 15%. In addition, Fig. 5.2 indicates that the whole rock composition of sample P227 (designated B) falls only slightly off the mixing line (AM) linking the hypothetical average Lesotho-type parent magma and the average olivine composition of sample P227 (designated M).

Using Roeder and Emslie's (1970) distribution coefficient (K_D) of 0.30 for the distribution of Fe^{2+} and Mg^{2+} between a melt and olivine, the forsterite content of olivine crystallizing from a liquid with the whole-rock composition of sample P227 is calculated as having a composition of Fo_{86} (Table 5.1). This calculated forsterite content far exceeds the measured forsterite content (Fo_{66} to Fo_{75}). This discrepancy between the observed and measured forsterite contents, supports the idea that a component of cumulus olivine is present in sample P227, causing the anomalously high MgO content.

Since the olivines analysed are reasonably unaltered, alteration as a mechanism causing low Fo values can be discarded. The more fractionated composition of the olivines relative to that predicted for the whole-rock host (P227) may be the result of a process such as compensated crystal settling (Cox and Bell, 1972; Krishnamurthy and Cox, 1977), whereby the olivine crystallized in a more Fe-rich portion of a magma chamber and settled into its present position. Mitchell (1980) noted features similar to those in sample P227 in the Roodehoek basalts, and suggested that iron enrichment of the olivines by sub-solidus re-equilibration with the host rock to a more Fe-rich composition may have prevailed during their formation. During this process Mg is released to the rock, and has the effect of inhibiting iron enrichment of the other mineral phases (for example in pyroxene) and at the same time increasing the bulk MgO content of the rock. The high distribution coefficient

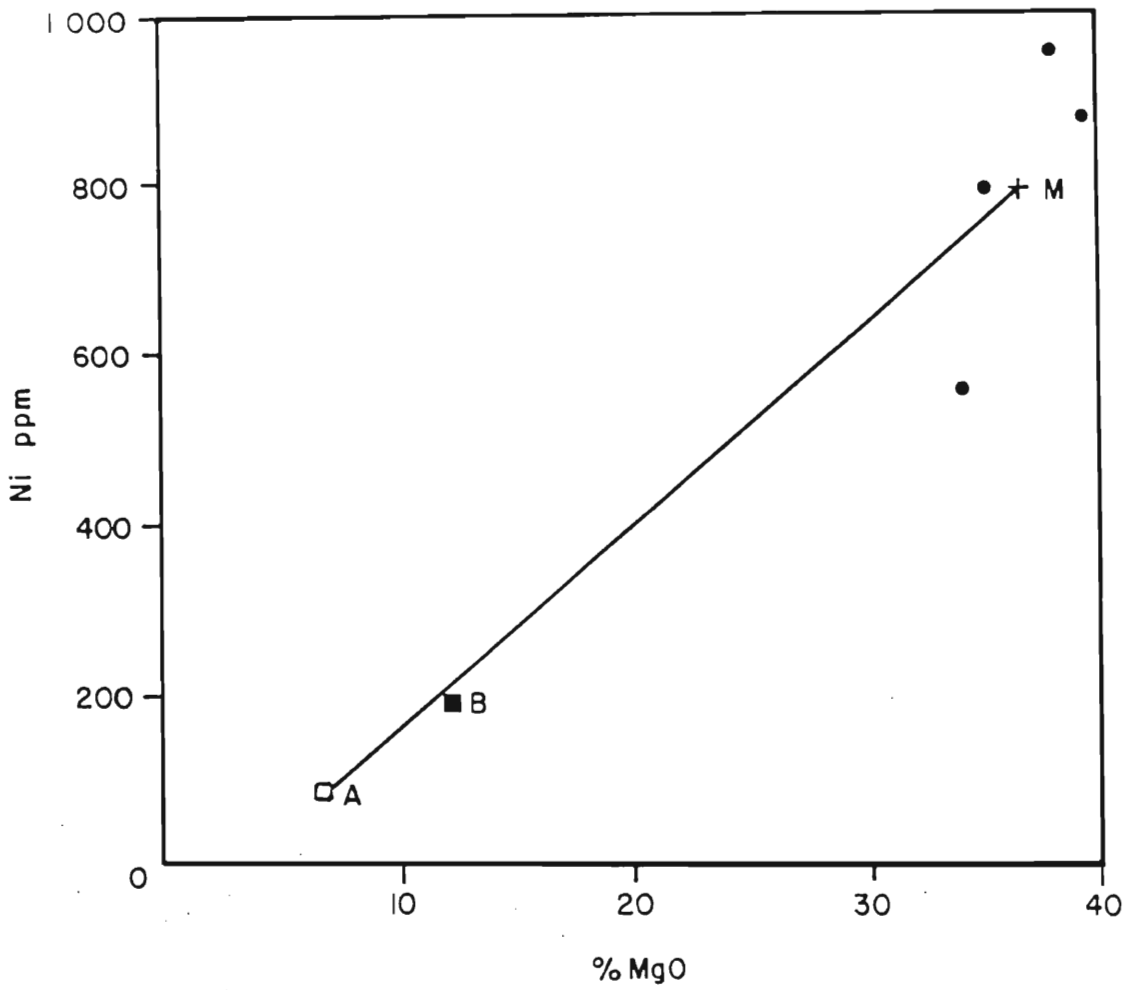

Fig. 5.2 Ni/MgO relationship of the Phinong magma type (sample P227) olivines. A is an average Karoo basalt (data from Eales and Marsh, 1979), B represents the whole-rock composition of P227. Olivine compositions of P227 are designated by shaded dots, the average composition being m. B falls only slightly off the mixing line of an average Lesotho-type basalt enriched in cumulus olivine.

of Ni for olivine inhibits cation-exhange reactions, thus effectively freezing in the primary Ni content of the olivines. The above conclusions are in agreement with Eales and Marsh (1979), who suggested that high-Mg rocks within the central Karoo Province are not a true magma type, but the result of cumulus olivine enrichment. Cumulus olivine enrichment possibly occurred by some form of flowage differentiation (Bhattercharji, 1967).

5.3. Pyroxene

Pyroxenes may be either orthorhombic or monoclinic and, in their simplest form are composed of chains of linked SiO_3^{2-} tetrahedra. The chains are linked laterally by cations bonded to the unshared oxygens. In all pyroxenes the SiO_3^{2-} chains run parallel to the crystallographic c axis and are arranged parallel to (100).

The general chemical formula for the pyroxenes is a function of the disposition of the cations, and is indicated by the formula $M2M1T_2O_6$, where the M1 and M2 sites have a pseudo-octahedral co-ordination, and T is tetrahedrally co-ordinated. Cations which occupy the M2 site include Na; Ca; Mn^{2+}; Fe^{2+}; Mg and more rarely Li; while Mg, Fe^{3+}, Al, Cr and Ti occupy the smaller M1 site and Si and Al occupy the tetrahedral T-site (Cameron and Papike, 1981).

The common rock-forming pyroxenes form a wide range of solid solutions of the Ca-Mg-Fe pyroxenes and can be expressed in the pyroxene quadrilateral in the system $Mg_2Si_2O_6$ (Enstatite) - $Fe_2Si_2O_6$ (Ferrosillite) - $CaMgSi_2O_6$ (Diopside) - $CaFeSi_2O_6$ (Hedenbergite).

Clinopyroxene compositions of the Sani Pass basalts are displayed in the Ca-Mg-Fe ternary diagrams in Fig. 5.3a-b and representative analyses are listed in Table 5.2. The pyroxenes of both the Agate Vale and Phinong magma types display a fairly large compositional range, plotting mostly in the augite field and a few samples in the pigeonite field. Compositional ranges for the augites and pigeonites of the Agate Vale basalts are $Wo_{39}En_{51}Fs_{10}$ to $Wo_{31}En_{29}Fs_{40}$ and $Wo_9En_{64}Fe_{27}$ respectively, whilst equivalent ranges in the Phinong basalts are $Wo_{27}En_{52}Fs_{21}$ to $Wo_{42}En_{49}Fs_9$ and $Wo_{10}En_{44}Fs_{46}$ to $Wo_8En_{63}Fs_{29}$.

The significant chemical variations found within the individual clinopyroxenes are reflected by oscillatory and hour-glass zoning (Plate 4.4), features which are considered to imply crystal growth within a rapidly changing physico-chemical environment (Augustithus, 1978).

Augite from the Agate Vale basalts, particularly samples AV90 and AV50, display a tholeiitic trend similar to that identified by Brown and Vincent (1963) at Skaergaard and Eales and Booth (1974) at Bird's River (Fig. 5.3a). This trend shows an initial Ca-depletion, followed by moderate Ca-enrichment as the iron content of the pyroxenes increases. This trend is in contrast to very little depletion in Ca as the iron content increases, as displayed by augites hosted by alkali basalts (Barberi *et al.*, 1971). Although these trends are very poorly developed in the Sani Pass pyroxenes, augite in the Phinong basalts show a more distinct trend of Ca-depletion than the Agate Vale augites. Mitchell (1980) observed a similar Ca depletion trend in the Roodehoek lavas of the north-eastern Cape Province. He suggested that this trend is not a primary fractionation effect, but due to the presence of submicroscopic intergrowths of calcium-poor pyroxene and calcium-enriched pyroxene to produce composite analyses of pigeonite and augite in varying proportions respectively. Support for this theory is the presence, albeit sparse, of pigeonite cores surrounded by augite overgrowths in the Phinong basalt (Plate 4.9) which have been recognised by optical means. According to Barberi *et al.*, (1971) it is characteristic for a tholeiitic suite to have a two-pyroxene assemblage, one Ca-rich and the other Ca-poor.

A limitation of the Ca-Mg-Fe ternary diagram is that pyroxene with significant amounts of cations other than Mg, Fe^{2+}, and Ca cannot be accurately represented. The most important cations in this category are Mn, Cr, Ti, Na and Al. Ionic proportions of these elements are plotted against ionic Mg as a measure of differentiation in Figs. 5.4a-b, 5.6 to 5.8a-b.

The behaviour of Mn^{2+} in a melt has been documented by Campbell and Borley (1974), who noted that Mn^{2+} partitions between coexisting pyroxenes in favour of the Ca-poor variety, and that the Mn^{2+} content should increase with decreasing enstatite content.

TABLE 5.2: Electron microprobe analyses of pyroxene

	P180/1a	P180/1b	P180/1c	P180/1d	P180/2a	P187/1a	P187/1b	P187/1c	P187/1d	P187/1e	P200/1a	P200/1b	P200/1c	P205/1a	P205/1b
SiO_2	53.13	52.68	54.35	53.40	51.65	53.16	54.00	52.07	50.52	52.24	53.20	52.74	53.18	52.64	51.61
TiO_2	0.66	0.41	0.32	0.37	1.12	0.47	0.28	0.37	0.39	0.46	0.45	0.51	0.41	0.41	0.71
Al_2O_3	1.35	2.11	0.97	1.55	1.70	1.46	0.63	2.65	0.40	0.76	1.64	1.55	0.82	1.94	1.48
FeO	10.02	7.18	13.70	7.38	10.48	10.07	18.66	6.02	28.18	21.25	9.63	10.39	21.06	6.90	12.18
MnO	0.30	0.20	0.36	0.18	0.19	0.23	0.49	0.16	0.55	0.47	0.33	0.25	0.47	0.16	0.27
MgO	17.65	17.89	24.17	17.63	15.66	17.53	22.96	17.52	15.12	20.67	17.21	16.61	20.30	17.29	15.91
CaO	16.97	17.78	5.84	19.07	18.93	16.52	4.07	19.38	4.55	4.53	16.69	16.89	4.25	20.29	17.12
Na_2O	0.24	0.23	0.09	0.23	0.34	0.19	0.07	0.27	0.06	0.07	0.18	0.20	0.07	0.21	0.20
Cr_2O_3	0.06	0.54	0.07	0.29	0.02	0.03	0.01	1.03	0.02	0.02	0.03	0.00	0.00	0.21	0.00
NiO	0.07	0.02	0.04	0.07	0.00	0.00	0.03	0.00	0.01	0.00	0.02	0.02	0.03	0.00	0.00
TOTAL	100.45	99.04	99.91	100.17	100.09	99.66	101.20	99.47	99.80	100.47	99.38	99.16	100.59	100.05	99.48
Structural formula based on six oxygens:															
Si	1.954	1.946	1.975	1.957	1.926	1.966	1.973	1.918	1.970	1.954	1.970	1.966	1.978	1.935	1.941
Ti	0.018	0.011	0.009	0.010	0.031	0.013	0.008	0.010	0.011	0.013	0.013	0.014	0.012	0.011	0.020
Al	0.059	0.092	0.041	0.067	0.075	0.064	0.027	0.115	0.018	0.033	0.072	0.068	0.036	0.084	0.066
Fe	0.308	0.222	0.416	0.226	0.327	0.311	0.570	0.185	0.919	0.665	0.298	0.324	0.655	0.212	0.383
Mn	0.009	0.006	0.011	0.006	0.006	0.007	0.015	0.005	0.018	0.015	0.010	0.008	0.015	0.005	0.008
Mg	0.967	0.984	1.309	0.962	0.870	0.966	1.250	0.962	0.879	1.152	0.950	0.923	1.125	0.948	0.891
Ca	0.669	0.704	0.227	0.749	0.756	0.654	0.159	0.764	0.190	0.182	0.662	0.674	0.169	0.799	0.690
Na	0.017	0.016	0.006	0.017	0.025	0.013	0.005	0.020	0.004	0.005	0.013	0.015	0.005	0.015	0.015
Cr	0.002	0.016	0.002	0.008	0.001	0.001	0.000	0.030	0.001	0.001	0.001	0.000	0.000	0.006	0.000
Ni	0.002	0.001	0.001	0.002	0.000	0.000	0.001	0.000	0.000	0.000	0.001	0.001	0.001	0.000	0.000
SUM	4.005	3.998	3.997	4.004	4.017	3.995	4.008	4.009	4.010	4.020	3.990	3.993	3.996	4.015	4.014
At% Fe	15.85	11.61	21.33	11.67	16.73	16.12	28.81	9.70	46.23	33.26	15.61	16.85	33.60	10.83	19.50
At% Mg	49.76	51.55	67.03	49.68	44.55	50.01	63.15	50.31	44.20	57.66	49.73	48.04	57.71	48.37	45.39
At% Ca	34.39	36.84	11.64	38.65	38.72	33.87	8.04	39.99	9.57	9.08	34.66	35.11	8.69	40.80	35.11

TABLE 5.2: Electron microprobe analyses of pyroxene

	P205/1c	P205/1d	P205/1e	P205/1f	P205/1g	P223/1a	P223/1b	P223/1c	P223/1d	P223/1e	P223/1f	P227/1a	P227/1b	P227/1c	P227/1d	P227/2a
SiO_2	53.05	52.17	52.65	52.76	53.08	52.99	52.56	53.08	52.49	52.84	52.33	53.29	53.32	53.56	53.17	53.43
TiO_2	0.32	0.37	0.43	0.40	0.35	0.29	0.40	0.28	0.52	0.32	0.41	0.84	0.56	0.42	0.45	0.47
Al_2O_3	1.43	2.13	1.15	1.76	1.35	1.78	1.18	1.78	1.02	0.55	0.65	1.61	1.70	1.93	1.93	1.74
FeO	6.39	6.15	9.08	7.39	7.17	6.39	10.45	6.86	18.21	19.53	20.69	10.51	8.28	6.68	6.72	7.08
MnO	0.15	0.13	0.21	0.18	0.13	0.20	0.30	0.22	0.44	0.44	0.47	0.26	0.25	0.23	0.20	0.15
MgO	17.76	17.28	17.52	17.77	17.56	17.77	18.00	18.77	21.15	21.81	20.73	17.17	17.53	17.88	17.56	17.48
CaO	20.01	20.54	18.62	18.99	20.09	19.94	17.00	18.56	6.39	4.49	4.57	17.86	19.02	19.44	19.88	20.28
Na_2O	0.21	0.21	0.18	0.20	0.20	0.21	0.18	0.22	0.09	0.06	0.07	0.22	0.22	0.22	0.22	0.20
Cr_2O_3	0.26	0.48	0.01	0.20	0.09	0.42	0.01	0.55	0.00	0.00	0.00	0.02	0.05	0.23	0.20	0.14
NiO	0.00	0.00	0.00	0.00	0.00	0.02	0.01	0.00	0.02	0.02	0.05	0.00	0.00	0.02	0.00	0.07
TOTAL	99.58	99.46	99.85	99.65	100.02	100.01	100.09	100.32	100.33	100.06	99.97	101.78	100.93	100.61	100.33	101.11
Structural formula based on six oxygens:																
Si	1.953	1.927	1.950	1.944	1.952	1.943	1.946	1.937	1.948	1.966	1.962	1.942	1.946	1.949	1.944	1.945
Ti	0.009	0.010	0.012	0.011	0.010	0.008	0.011	0.008	0.014	0.009	0.012	0.023	0.015	0.011	0.012	0.013
Al	0.062	0.093	0.050	0.077	0.059	0.077	0.051	0.077	0.045	0.024	0.029	0.069	0.073	0.083	0.083	0.075
Fe	0.197	0.190	0.281	0.228	0.220	0.196	0.324	0.209	0.565	0.608	0.649	0.320	0.253	0.203	0.205	0.215
Mn	0.005	0.004	0.006	0.005	0.004	0.006	0.009	0.007	0.014	0.014	0.015	0.008	0.008	0.007	0.006	0.005
Mg	0.974	0.951	0.967	0.976	0.962	0.971	0.993	1.021	1.170	1.210	1.158	0.932	0.953	0.969	0.956	0.947
Ca	0.789	0.813	0.739	0.750	0.791	0.783	0.675	0.726	0.254	0.179	0.184	0.697	0.744	0.758	0.779	0.790
Na	0.015	0.015	0.013	0.014	0.014	0.015	0.013	0.016	0.007	0.004	0.005	0.015	0.015	0.015	0.016	0.014
Cr	0.007	0.014	0.000	0.006	0.003	0.012	0.000	0.016	0.000	0.000	0.000	0.001	0.001	0.007	0.006	0.004
Ni	0.000	0.000	0.000	0.000	0.000	0.001	0.000	0.000	0.001	0.000	0.001	0.000	0.000	0.001	0.000	0.002
SUM	4.011	4.017	4.018	4.011	4.015	4.012	4.022	4.017	4.018	4.014	4.015	4.005	4.008	4.003	4.007	4.010
At% Fe	10.03	9.72	14.16	11.66	11.17	10.04	16.26	10.70	28.41	30.44	32.59	16.42	12.95	10.53	10.59	11.02
At% Mg	49.70	48.68	48.65	49.96	48.74	49.80	49.87	52.19	58.81	60.59	58.19	47.81	48.90	50.22	49.29	48.52
At% Ca	40.27	41.60	37.19	38.38	40.09	40.16	33.87	37.11	12.78	8.97	9.22	35.77	38.15	39.25	40.12	40.46

TABLE 5.2: Electron microprobe analyses of pyroxene

	P227/2b	P227/2c	P227/2d	P227/2e	P227/1f	P227/1g	P246/1a	P246/1b	P246/1c	P246/1d	P271/1a	P271/1b	P271/1c	P271/1d
SiO_2	52.77	51.54	52.78	52.41	53.00	52.65	53.23	52.81	53.50	52.56	53.74	53.47	53.55	53.20
TiO_2	0.66	0.39	0.36	0.56	0.43	0.61	0.31	0.44	0.28	0.48	0.31	0.25	0.32	0.46
Al_2O_3	1.72	2.59	1.51	1.73	1.47	1.49	1.20	1.95	1.33	1.39	1.22	1.33	1.29	1.39
FeO	8.96	6.77	6.79	8.68	7.84	10.26	7.73	7.50	7.20	11.90	8.01	7.52	7.73	13.43
MnO	0.24	0.18	0.17	0.26	0.18	0.25	0.20	0.14	0.18	0.35	0.21	0.21	0.18	0.33
MgO	17.30	18.04	18.04	17.76	17.69	18.17	17.80	16.97	18.02	17.14	18.27	18.66	17.93	18.23
CaO	18.71	18.58	19.97	18.38	19.14	16.48	18,40	19.41	18.91	15.34	18.20	18.13	19.25	13.52
Na_2O	0.21	0.24	0.21	0.20	0.18	0.19	0.17	0.21	0.20	0.17	0.16	0.18	0.16	0.15
Cr_2O_3	0.05	0.69	0.21	0.04	0.09	0.01	0.08	0.10	0.16	0.02	0.15	0.27	0.12	0.05
NiO	0.03	0.06	0.07	0.04	0.05	0.07	0.02	0.01	0.01	0.00	0.02	0.07	0.07	0.09
TOTAL	100.65	99.08	100.11	100.06	100.07	100.18	99.14	99.54	99.79	99.35	100.29	100.09	100.60	100.85
Structural formula based on six oxygens:														
Si	1.938	1.909	1.938	1.934	1.949	1.943	1.969	1.949	1.964	1.962	1.965	1.957	1.957	1.959
Ti	0.018	0.011	0.010	0.016	0.012	0.017	0.009	0.012	0.008	0.014	0.008	0.007	0.009	0.013
Al	0.075	0.113	0.066	0.075	0.064	0.065	0.053	0.085	0.057	0.061	0.053	0.058	0.056	0.060
Fe	0.275	0.210	0.209	0.268	0.241	0.316	0.239	0.231	0.221	0.371	0.245	0.230	0.236	0.413
Mn	0.007	0.006	0.005	0.008	0.006	0.008	0.006	0.004	0.006	0.011	0.007	0.007	0.006	0.010
Mg	0.947	0.996	0.987	0.976	0.969	0.999	0.981	0.933	0.986	0.954	0.996	1.018	0.976	1.000
Ca	0.736	0.737	0.786	0.726	0.754	0.651	0.729	0.768	0.744	0.613	0.713	0.711	0.754	0.533
Na	0.015	0.017	0.015	0.014	0.013	0.013	0.012	0.015	0.014	0.013	0.012	0.013	0.011	0.011
Cr	0.001	0.020	0.006	0.001	0.003	0.000	0.002	0.003	0.005	0.001	0.004	0.008	0.003	0.001
Ni	0.001	0.002	0.002	0.001	0.001	0.002	0.001	0.000	0.000	0.000	0.000	0.002	0.002	0.003
SUM	4.013	4.021	4.024	4.021	4.012	4.014	4.001	4.000	4.005	4.000	4.003	4.011	4.010	4.003
At% Fe	14.06	10.80	10.53	13.58	12.27	16.09	12.27	11.98	11.33	19.16	12.55	11.75	12.01	21.23
At% Mg	48.35	51.25	49.82	49.55	49.34	50.79	50.33	48.30	50.54	49.19	50.95	51.96	49.66	51.39
At% Ca	37.59	37.95	39.65	36.87	38.39	33.12	37.40	39.72	38.13	31.65	36.50	36.29	38.33	27.38

A bimodal distribution of Mn is observed for the Agate Vale augites (Fig. 5.4a). This bimodality is attributed to the presence of groundmass and phenocryst analyses. The small interstitial, groundmass pyroxenes (AV50/3, AV90/4 and AV90/5) are characterized by a higher Mn content (0.012 to 0.015 ionic proportions) than the earlier-formed larger pyroxenes (0.005 to 0.009 ionic proportions). These groundmass pyroxenes are also characterized by lower Mg and marginally lower Ca contents than the earlier-formed phenocryst pyroxenes (Fig. 5.3a). A single pigeonite analysis (AV20/3) and a composite analyses of augite and pigeonite (AV50/6) have a Mn content in the range of the groundmass augite, but are enriched in Mg (1.279 to 1.152 ionic proportions) relative to the groundmass and phenocryst populations.

Figure 5.4b, which is a plot of ionic Mn against ionic Mg indicates a decreasing Mn content with increasing Mg in pigeonites of the Phinong basalts. These pigeonites show a slight enrichment in Mn and Mg relative to the augites of these magma types. Bordering on the lower limit of the pigeonite field (*sensu stricto*) in Fig. 5.4b are two analyses, namely, P180/Ic and P223/1d, that represent composite analyses of pigeonite and augite. The Mn content for augites in the Phinong basalts increases over a restricted Mg range (0.9 to 1.1 ionic proportions) (Fig. 5.4b).

Chromium (Cr^{3+}) partitions strongly into early-formed pyroxenes, resulting in an inverse relationship between Cr^{3+} and progressive time of crystallization. This relationship is regarded as a typical tholeiitic trend (Schweitzer *et al.*, 1979), whereas pyroxenes in alkalic basalts have consistently low Cr^{3+} contents. Cr^{3+} substitutes for divalent cations in the octahedral sites in pyroxenes. This results in a charge excess that is counterbalanced by the substitution of Al^{3+} for Si^{4+} in the tetrahedral site. On this basis, there should be a more or less linear correlation between Al_2O_3 and Cr_2O_3 in the pyroxenes. This relationship is somewhat diffuse for the augites in the Phinong and Agate Vale basalts, and the pigeonites shallow out considerably at low Al_2O_3 content (Fig. 5.5). The displacement of pigeonites from this somewhat linear trend (described by the augites) has also been noted by Mitchell (1980) in the basalts from the Molteno-Jamestown area, and it was suggested that substitution of small proportions of Fe^{3+} for Al may have lowered the Al content of the

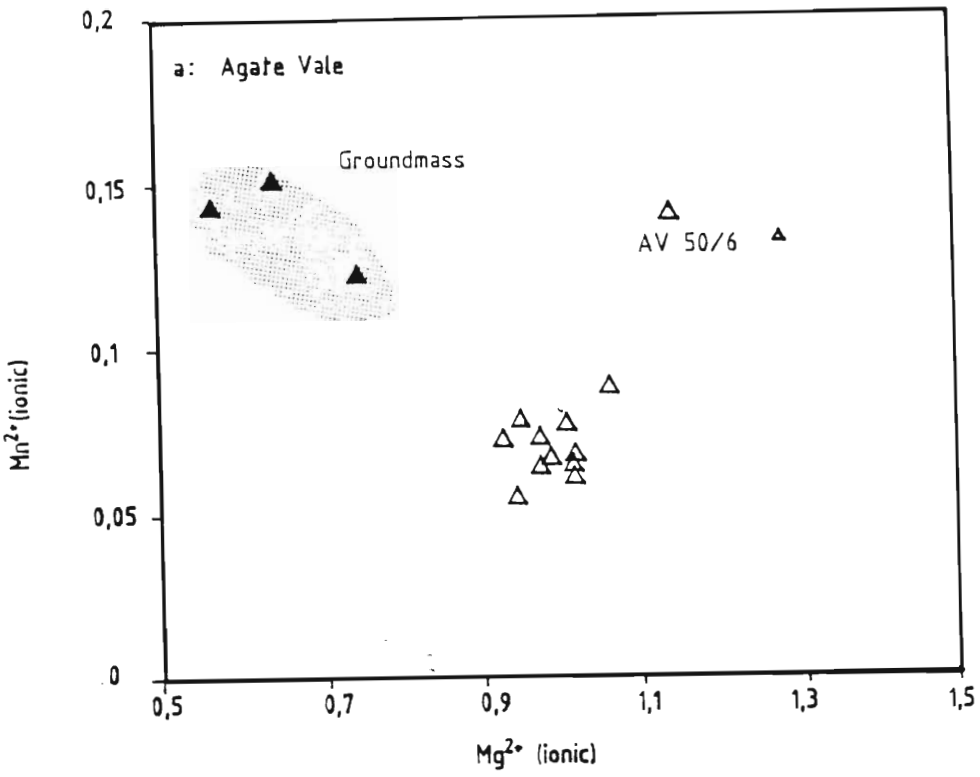

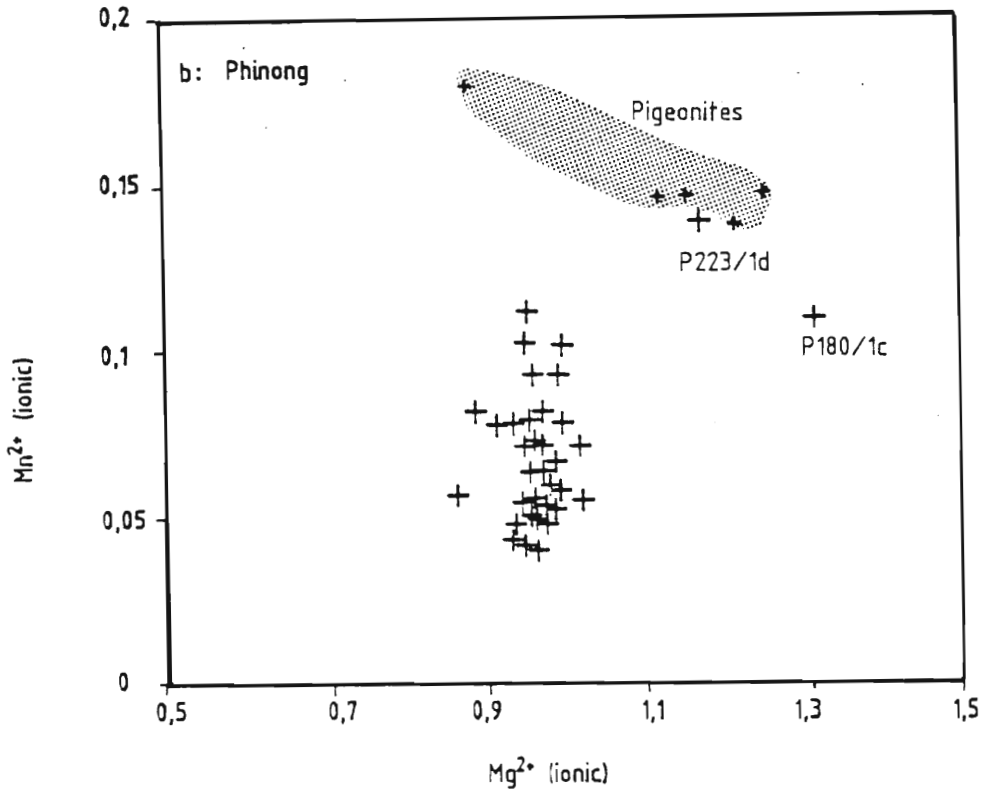

Fig. 5.4a-b Mn (ionic) versus Mg (ionic) for augites and pigeonites from the Agate Vale (Fig. 5.4a) and Phinong basalts (Fig. 5.4b). Fig. 5.5a indicates the bimodal distribution of Mn, which is enriched in the groundmass augites (light stipple) and more depleted in the phenocrysts. In the Phinong augites, Mn increases over a restricted Mg range. The pigeonites (dark stipple), however, decrease in Mn as Mg increases. Pigeonite compositions are indicated by small symbols, and augite compositions by the larger symbols.

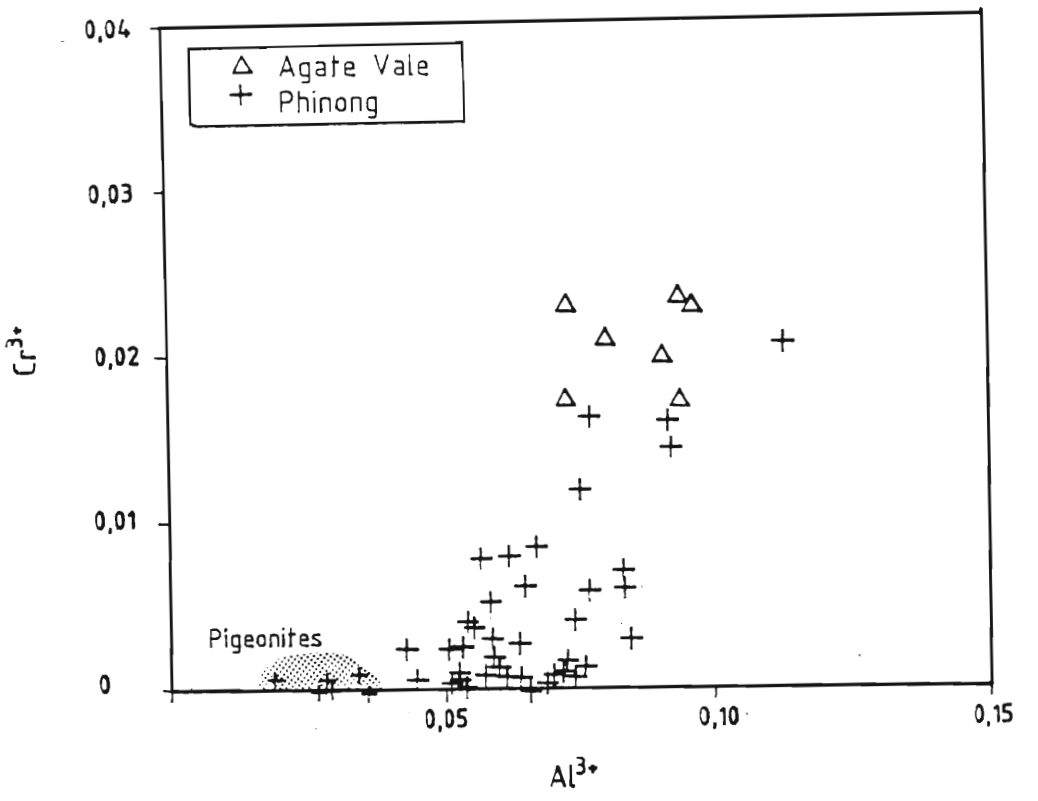

Fig. 5.5 Cr (ionic) versus Al (ionic) for pyroxenes from the Agate Vale and Phinong basalts. A poorly developed positive trend is indicated by augites from the Agate Vale and Phinong basalts, and offset from this trend, are pigeonites occurring at very low Cr contents.

pigeonites relative to the Cr content.

Augites from the Phinong basalts show a very slight inverse correlation between Cr^{3+} and Mg^{2+} (Fig. 5.6b). This trend is not apparent for augites from the Agate Vale basalts (Fig. 5.6a). Instead pyroxenes from this magma type show a large cluster of data above 0.01 Cr^{3+} (ionic proportions) and the 3 groundmass augites (AV50/3; AV90/4; AV90/5) have low Cr^{3+}, between 0.001 and 0.002 ionic proportions. The single pigeonite analysis (AV20/4) shows no Cr^{3+}.

Figures 5.7a-b indicate an increase in Ti content of the Agate Vale and Phinong pyroxenes with decreasing Mg^{2+}. However, this relationship is poorly developed in the Phinong clinopyroxenes with a scatter of Ti values despite a very limited range of Mg content (Fig. 5.7b). The lower concentration of Ti in the early-formed pyroxenes is due to its relatively low crystal field stabilization energy (C.F.S.E). This means that Ti cannot compete with Cr for charge-deficient octahedral sites, and Ti only becomes an important constituent of pyroxene once Cr is significantly depleted in the melt (Campbell and Borley, 1974). This relationship is verified by a comparison of Fig. 5.6 with Fig. 5.7.

As in the case for Mn^{2+} and Cr^{3+}, Ti^{4+} content in pyroxenes of the Agate Vale magma type also display a bimodal distribution, the high-Ti pyroxenes being groundmass and lower-Ti pyroxenes being phenocrysts (Fig. 5.7a). Pyroxene data for the Phinong basalts indicate that Ti-enrichment occurs at a Mg content varying between 0.879 and 1.021 ionic proportions (excluding composite and pigeonite analyses) but in the Agate Vale pyroxenes this Ti enrichment occurs between 0.567 and 1.019 (excluding AV20/3 and AV50/6) (<0.55 to 1.06 ionic proportions). This relates directly to whole-rock MgO content which ranges from 4.34 to 6.75 weight percent for the Agate Vale basalts and 5.91 to 12.09 weight percent for the Phinong basalts.

Barberi *et al.*, (1971) noted that the entry of Ti into clinopyroxenes is directly controlled by the Al and Si content of the pyroxenes which are related to the silica activity of the melt. Data for the Phinong and Agate Vale pyroxenes plot as a large scatter of values with no clear Al/Ti trend. Gibb (1973) and Campbell and Borley (1974) found that as the Al content of pyroxenes increases, so does the amount in excess of that required solely to fill the Si-

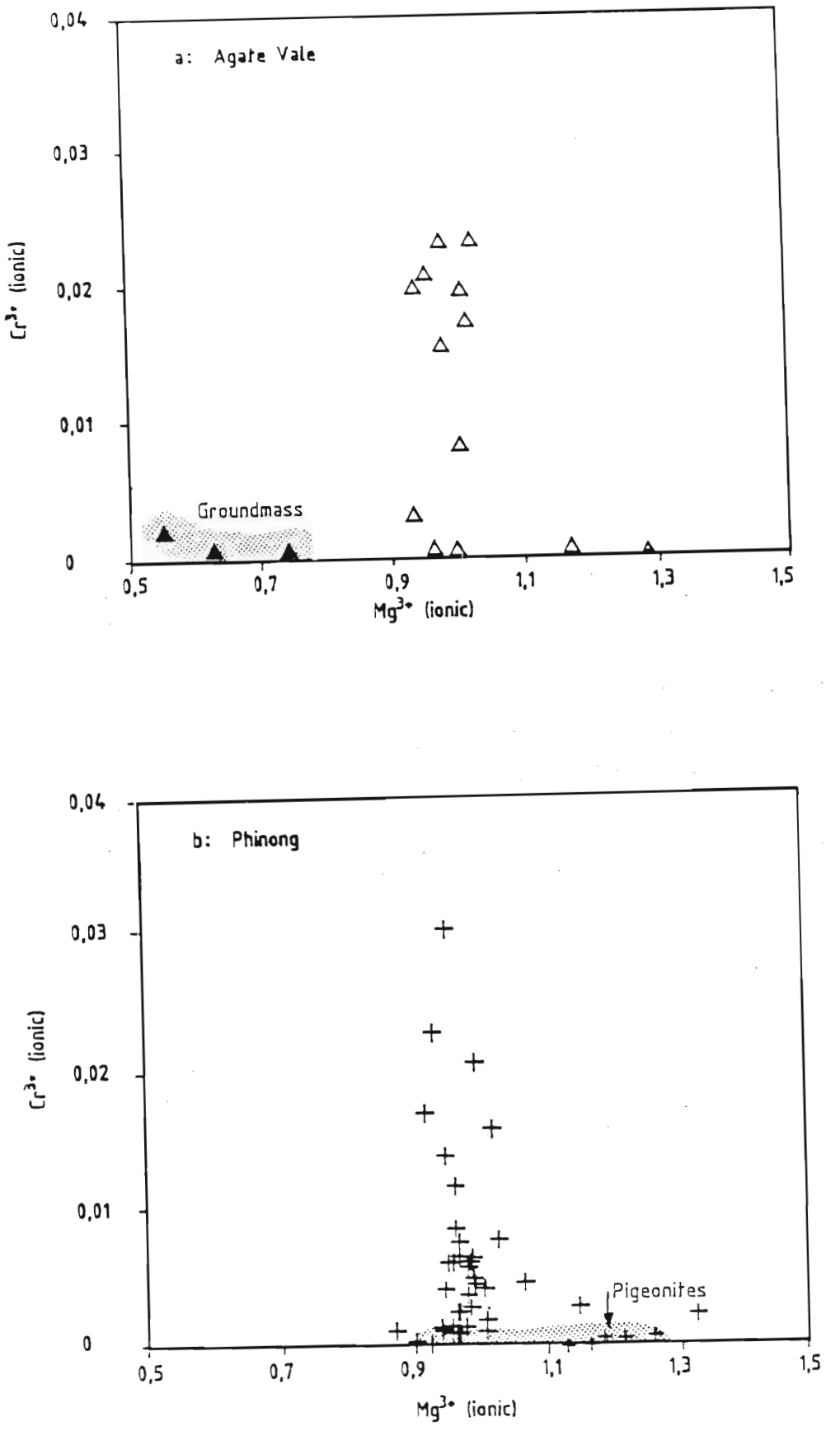

Fig. 5.6a-b Cr^{3+} (ionic) versus Mg^{3+} (ionic) for pyroxenes in the Agate Vale (Fig. 5.6a) and Phinong basalts (Fig. 5.6b). The expected trend of increasing Cr^{3+} with increasing Mg^{2+} is not apparent in the pyroxenes from the Agate Vale and Phinong basalts. The stippled field in Fig. 5.6a, representing the groundmass pyroxenes occurs at low Cr^{3+} and Mg^{2+} contents. The pigeonites are generally depleted in Cr contents relative to the augites.

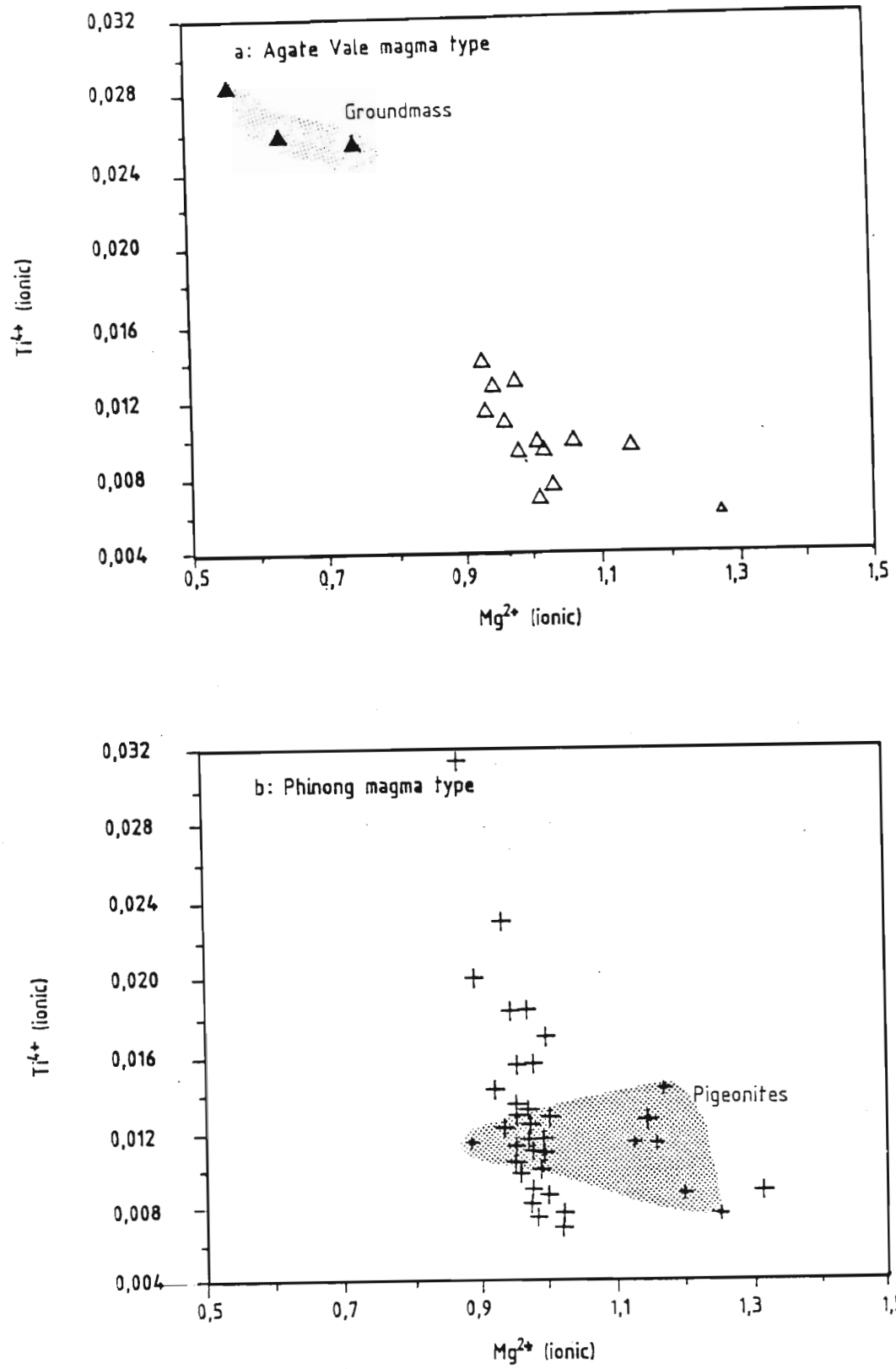

Fig. 5.7a-b Ti^{4+} (ionic) versus Mg^{2+} (ionic) for augites and pigeonites from the Agate Vale (Fig. 5.7a) and Phinong (Fig. 5.7b) basalts. The pyroxenes show decreasing Ti^{4+} with increasing Mg^{2+}, albeit poorly developed in the Phinong pyroxenes. The groundmass pyroxenes in the Agate Vale basalts (shown as the stippled area in Fig. 5.7a) has high Ti^{4+} contents.

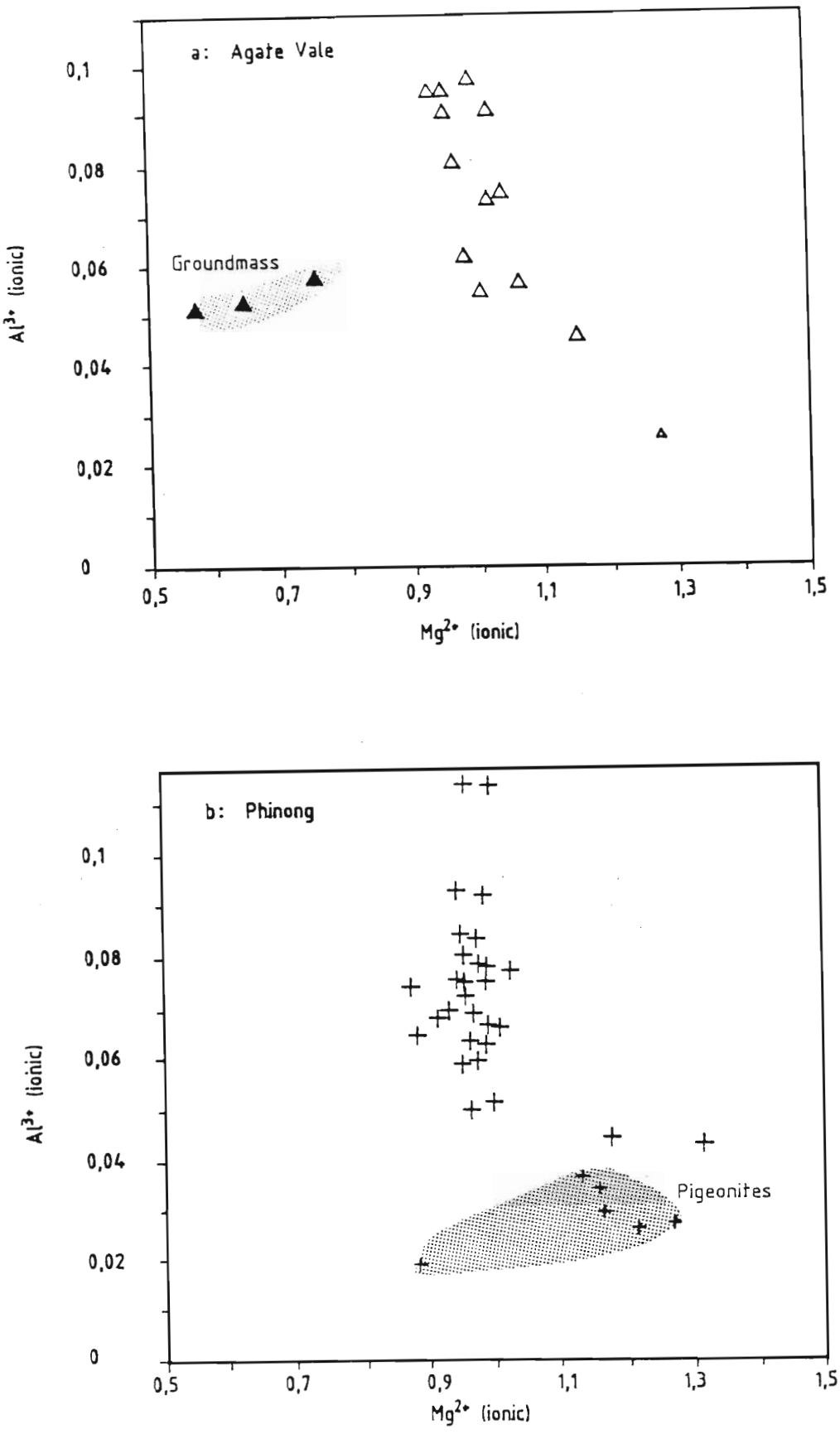

Fig. 5.8a-b Al^{3+} (ionic) versus Mg^{2+} (ionic) for the pyroxenes from the Agate Vale and Phinong basalts. Al^{3+} increases over a restricted Mg^{2+} content for the Agate Vale and Phinong pyroxenes. The single plageonite analysis from the Agate Vale magma, as well as those from the Phinong basalts are depleted in Al relative to the augites.

deficient tetrahedral sites. This might, therefore, be the case for the Agate Vale and Phinong clinopyroxenes which show increasing Al^{3+} content over a very restricted Mg^{2+} range (Fig. 5.8a-b).

5.4. Plagioclase Feldspar

The crystal structure of feldspar is an aluminosilicate framework, in which interstitial alkali and alkali-earth elements occur in tetrahedral co-ordination with oxygen. The ideal formula of feldspar is MT_4O_8, where M is either a monovalent atom (Na; K) or divalent atom (Ca; Ba), whilst the T site may be filled primarily by Al and Si, with minor substitutions of Ba; Ga; Ge and Fe^{3+} (Deer *et al.*, 1966). At high temperature, Na and K, or Na and Ca in all proportions can occur interstitially, whilst only partial substitution occurs for K and Ca. Hence, there are two principal series of feldspars, the alkali feldspars and the plagioclase feldspars, which meet at the composition of albite. The feldspars can be classified chemically as members of the ternary system $KAlSi_3O_8$ (Orthoclase) - $NaAlSi_3O_8$ (Albite) - $CaAl_2Si_2O_8$ (Anorthite).

Microprobe analyses of feldspars from the Sani Pass basalts and a single dolerite from the vicinity of Sani Pass are presented in Table 5.3. The recalculated molecular percentages based on 32 oxygens are plotted in terms of the albite, anorthite and orthoclase end-members in Fig. 5.9a-c. The plagioclase composition of the basalts and dolerite range from An_{43} to An_{82}, with most of the analyses falling in the range labradorite to bytownite. The individual magma types in the Sani Pass do not show unique feldspar compositions.

Within each magma type, a bimodal distribution is exhibited by the plagioclase-phyric rocks, with phenocrysts substantially more calcic than the groundmass plagioclase (Fig. 5.9a-c). Microprobe analysis of a single Giant's Cup type sample (sample GC380) indicates a phenocryst range of An_{72} to An_{73}, while the more variable groundmass ranges from An_{45} to An_{65} (Fig. 5.9a). Except for sample AV91, which shows reverse zoning, the Agate Vale magma type plagioclase phenocrysts range in anorthite composition from An_{60} to An_{72}, while the compositional range for the groundmass is An_{38} to An_{56} (Fig. 5.9a). In

the Sakeng magma type (sample S120), the phenocryst compositions range from An_{52} to An_{82} (Fig 5.9a). Phenocryst and groundmass anorthite compositions in the Phinong magma type range from An_{60} to An_{82} and An_{36} to An_{72} respectively (Figs. 5.9b-c). A single dolerite sample (D20) has a groundmass range of An_{36} to An_{38} and a phenocryst range of An_{40} to An_{80} (Fig. 5.9a).

Normal zoning is common in the plagioclase phenocrysts, and is indicated by a decrease in calcium from core to margin, for example, An_{82} to An_{52} (sample S120). The accompanying alkali enrichment from core to margin indicates a normal fractionation effect. Loomis (1982) suggested that normal zoning might be promoted by rapid cooling, contemporaneous crystallization of other phases, and the absence of volatiles. Generally, the phenocrysts have rather variable rim compositions, some of which are similar to groundmass analyses in the same rock (Fig. 5.9a). Zoning in a single phenocryst of sample P180 (Phinong magma type) is very slight. This suggests some degree of equilibrium crystallization, or possibly subsolidus reequilibrium, since the sample was removed from the central portion of the flow, which presumably cooled relatively slowly.

A single plagioclase feldspar from sample AV91, which is a pillow lava from the Agate Vale magma type, exhibits reverse zoning (Fig. 5.10a). This effect is marked by an increase in alkalies in the core relative to the margin. Cox *et al.*(1979), have indicated that compositional disequilibrium within a magma chamber could result in reverse zoning. In this scenario sodic plagioclase which formed at higher levels in the magma chamber could sink to lower levels and be in disequilibrium with the coexisting liquid. Within this higher temperature environment it is common for calcic plagioclase to form a mantle around the sodic core. The reverse zoned phenocryst in AV91 possibly formed in such an environment envisaged by Cox *et al.*, (1979), and may therefore be xenocrystic.

Mitchell (1980) characterized the various basalt types of the north-eastern Cape in terms of the orthoclase content of the plagioclases. A similar approach has been attempted for the Sani Pass basalts and dolerites and is depicted in Fig. 5.10, as a plot of molecular percent orthoclase against molecular percent anorthite. Only plagioclase-phyric samples are represented on this figure. Except for a single plagioclase (molecular percent orthoclase

Table 5.3 Electron microprobe analyses of plagioclase feldspar

Sample #	1	2	3	4	5	6	7	8	9	10	11	12	13	14	15	16	17	18	19
SiO_2	51.37	53.47	53.12	53.14	53.03	56.05	54.90	54.02	53.63	53.33	53.34	57.58	52.66	49.11	57.20	48.51	53.27	54.65	54.21
Al_2O_3	30.04	28.93	28.96	29.20	29.19	26.88	28.01	28.69	28.73	29.01	28.75	25.65	29.30	31.33	26.00	32.09	28.99	27.68	27.55
FeO	0.59	0.64	0.61	0.56	0.52	0.73	0.60	0.49	0.47	0.51	0.47	0.82	0.60	0.58	0.82	0.50	0.65	0.73	0.63
CaO	14.10	12.89	13.17	13.13	13.23	10.41	11.57	12.41	12.71	12.85	12.59	9.39	12.28	15.58	9.86	16.02	12.08	11.19	11.30
Na_2O	3.56	4.14	4.05	3.96	3.86	5.43	4.96	4.49	4.32	4.20	4.32	6.02	4.09	2.37	5.81	2.22	4.24	5.22	5.25
K_2O	0.28	0.17	0.16	0.16	0.14	0.28	0.21	0.16	0.16	0.13	0.15	0.39	0.17	0.08	0.36	0.06	0.18	0.32	0.28
TOTAL	99.94	100.24	100.07	100.15	99.97	99.78	100.25	100.26	100.02	100.03	99.62	99.85	99.10	99.05	100.05	99.40	99.41	99.79	99.22
Structural formula based on thirty two oxygens																			
Si	9.386	9.688	9.650	9.638	9.633	10.140	9.913	9.768	9.728	9.677	9.713	10.387	9.634	9.074	10.311	8.943	9.710	9.928	9.908
Al	6.476	6.185	6.208	6.249	6.256	5.738	5.968	6.121	6.149	6.211	6.177	5.460	6.325	6.830	5.530	6.980	6.235	5.933	5.941
Fe	0.090	0.097	0.093	0.085	0.079	0.110	0.091	0.074	0.071	0.077	0.072	0.124	0.092	0.090	0.124	0.077	0.099	0.111	0.096
Ca	2.760	2.502	2.563	2.551	2.575	2.018	2.238	2.404	2.470	2.498	2.456	1.815	2.407	3.084	1.904	3.164	2.359	2.178	2.213
Na	1.261	1.454	1.426	1.392	1.359	1.904	1.736	1.574	1.519	1.477	1.525	2.105	1.451	0.849	2.030	0.793	1.498	1.838	1.860
K	0.065	0.039	0.037	0.037	0.032	0.065	0.048	0.037	0.037	0.030	0.035	0.090	0.040	0.019	0.083	0.014	0.042	0.074	0.065
TOTAL	20.039	19.966	19.978	19.952	19.935	19.975	19.995	19.977	19.975	19.971	19.978	19.980	19.948	19.945	19.981	19.971	19.943	20.062	20.084
Mol% An	67.54	62.62	63.66	64.09	64.91	50.61	55.64	59.88	61.35	62.36	61.16	45.26	61.76	78.04	47.40	79.67	60.50	53.24	53.47
Mol% Ab	30.86	36.40	35.42	34.98	34.27	47.77	43.16	39.20	37.73	36.89	37.97	52.50	37.22	21.48	50.54	19.98	38.43	44.94	44.95
Mol% Or	1.60	0.98	0.92	0.93	0.82	1.62	1.20	0.92	0.92	0.75	0.87	2.24	1.02	0.48	2.06	0.36	1.07	1.81	1.58

Sample #	20	21	22	23	24	25	26	27	28	29	30	31	32	33	34	35	36	37	38
SiO_2	52.15	54.52	54.60	54.31	56.64	49.66	50.29	51.84	50.90	51.06	51.77	52.00	52.03	55.04	54.50	54.28	54.80	54.83	52.81
Al_2O_3	28.92	27.37	27.21	27.48	26.34	30.94	30.37	29.67	30.52	30.31	29.88	29.71	29.62	27.78	28.23	28.06	27.70	27.75	29.30
FeO	0.55	0.65	0.66	0.47	0.70	0.38	0.40	0.49	0.48	0.48	0.50	0.51	0.48	0.70	0.73	0.68	0.61	0.68	0.47
CaO	13.14	11.23	11.01	11.15	9.38	14.77	14.39	13.87	14.69	14.64	13.90	13.93	13.80	11.39	11.79	12.03	11.47	11.43	13.39
Na_2O	4.13	5.28	5.50	5.05	6.15	3.03	3.32	3.74	3.24	3.33	3.63	3.72	3.83	5.06	4.92	4.81	5.03	5.07	4.34
K_2O	0.15	0.26	0.28	0.20	0.35	0.08	0.09	0.19	0.14	0.16	0.17	0.20	0.18	0.32	0.30	0.29	0.31	0.32	0.18
TOTAL	99.04	99.31	99.26	98.66	99.56	98.86	98.86	99.80	99.97	99.98	99.85	100.07	99.94	100.29	100.47	100.15	99.92	100.08	100.49
Structural formula based on thirty two oxygens																			
Si	9.584	9.950	9.972	9.953	10.256	9.175	9.283	9.468	9.298	9.327	9.447	9.472	9.487	9.943	9.844	9.840	9.936	9.929	9.573
Al	6.271	5.894	5.864	5.942	5.628	6.745	6.615	6.394	6.578	6.533	6.434	6.386	6.373	5.921	6.016	6.002	5.926	5.929	6.267
Fe	0.085	0.099	0.101	0.072	0.106	0.059	0.062	0.075	0.073	0.073	0.076	0.078	0.073	0.106	0.110	0.103	0.092	0.103	0.071
Ca	2.587	2.196	2.154	2.189	1.820	2.923	2.846	2.714	2.875	2.865	2.717	2.719	2.696	2.204	2.281	2.336	2.228	2.218	2.600
Na	1.471	1.868	1.947	1.794	2.159	1.085	1.188	1.324	1.147	1.179	1.284	1.314	1.354	1.772	1.723	1.690	1.768	1.780	1.525
K	0.035	0.061	0.065	0.047	0.081	0.019	0.021	0.044	0.033	0.037	0.040	0.046	0.042	0.074	0.069	0.067	0.072	0.074	0.042
TOTAL	20.034	20.067	20.103	19.997	20.050	20.005	20.014	20.019	20.003	20.015	19.998	20.015	20.024	20.020	20.044	20.038	20.021	20.033	20.077
Mol% An	63.20	53.24	51.70	54.32	44.83	72.59	70.18	66.48	70.90	70.19	67.24	66.65	65.89	54.43	56.01	57.07	54.77	54.47	62.40
Mol% Ab	35.94	45.30	46.74	44.52	53.18	26.95	29.30	32.44	28.30	28.89	31.78	32.21	33.09	43.75	42.29	41.29	43.47	43.72	36.60
Mol% Or	0.86	1.47	1.57	1.16	1.99	0.47	0.52	1.08	0.80	0.91	0.98	1.14	1.02	1.82	1.70	1.64	1.76	1.82	1.00

Sample 1 : plagioclase 1, phenocryst (D20)
Sample 2 to 5 : plagioclase 2, margin–core, phenocryst (D20)
Sample 6 to 11 : plagioclase 3, margin–core, phenocryst (D20)
Sample 12 to 13 : various small grains (D20)
Sample 14 : phenocryst (D20)
Sample 15 : small grain (D20)
Sample 16 : phenocryst (D20)
Sample 17 : small grain (D20)
Sample 18 to 24 : various small groundmass grains (GC380)
Sample 25 to 26 : plagioclases 7 & 8, core, phenocrysts (GC380)
Sample 27 to 32 : core – margin, phenocryst (AV50)
Sample 33 to 37 : various small grains (AV50)
Sample 38 : plagioclase 1, medium phenocryst (AV90)

Table 5.3 Electron microprobe analyses of plagioclase feldspar

Sample#	39	40	41	42	43	44	45	46	47	48	49	50	51	52	53	54	55	56
SiO_2	50.92	57.73	51.18	52.62	52.39	52.61	54.16	55.39	57.08	55.19	53.29	52.62	48.06	53.09	51.03	52.21	50.86	47.79
Al_2O_3	29.73	25.28	28.71	29.48	29.53	29.16	28.12	28.41	26.47	27.64	28.69	28.88	32.10	28.84	30.17	29.35	30.36	32.50
FeO	0.77	0.57	1.45	0.60	0.60	0.83	0.69	0.77	0.96	0.91	0.62	0.55	0.43	0.84	0.45	0.83	0.46	0.43
CaO	13.99	8.34	13.50	14.05	14.24	13.37	11.39	11.31	10.65	11.50	13.07	13.49	16.77	13.06	14.69	13.65	14.92	16.77
Na_2O	3.82	6.96	3.88	3.67	3.52	3.70	4.27	4.37	5.41	5.01	4.14	3.91	2.00	4.06	3.20	3.87	3.15	2.01
K_2O	0.17	0.52	0.19	0.15	0.19	0.35	0.89	0.67	0.40	0.35	0.18	0.16	0.06	0.20	0.12	0.18	0.10	0.07
TOTAL	99.40	99.42	98.91	100.57	100.47	100.02	99.52	100.92	100.97	100.60	99.99	99.61	99.42	100.09	99.66	100.09	99.85	99.57
Structural formula based on thirty two oxygens																		
Si	9.370	10.454	9.482	9.534	9.507	9.584	9.871	9.931	10.220	9.952	9.689	9.613	8.878	9.654	9.345	9.517	9.303	8.818
Al	6.455	5.402	6.276	6.302	6.323	6.268	6.047	6.010	5.592	5.881	6.155	6.225	6.996	6.188	6.519	6.313	6.553	7.076
Fe	0.118	0.086	0.225	0.091	0.091	0.126	0.105	0.115	0.144	0.137	0.094	0.084	0.066	0.128	0.069	0.127	0.070	0.066
Ca	2.758	1.618	2.679	2.727	2.769	2.609	2.224	2.172	2.043	2.222	2.546	2.640	3.319	2.544	2.882	2.666	2.924	3.315
Na	1.363	2.450	1.394	1.289	1.238	1.307	1.509	1.519	1.878	1.751	1.459	1.385	0.716	1.431	1.136	1.368	1.117	0.719
K	0.040	0.120	0.045	0.035	0.044	0.081	0.207	0.153	0.091	0.080	0.042	0.037	0.014	0.046	0.028	0.042	0.023	0.016
TOTAL	20.104	20.130	20.100	19.977	19.972	19.976	19.963	19.900	19.968	20.024	19.984	19.985	19.989	19.991	19.978	20.031	19.991	20.011
Mol% An	66.29	38.63	65.07	67.32	68.34	65.28	56.45	56.51	50.92	54.81	62.91	64.99	81.96	63.26	71.23	65.41	71.94	81.84
Mol% Ab	32.75	58.50	33.84	31.82	30.57	32.69	38.30	39.51	46.81	43.21	36.06	34.09	17.69	35.59	28.08	33.56	27.49	17.75
Mol% Or	0.96	2.87	1.09	0.86	1.09	2.03	5.25	3.98	2.28	1.99	1.03	0.92	0.35	1.15	0.69	1.03	0.57	0.41

Sample#	57	58	59	60	61	62	63	64	65	66	67	68	69	70	71	72	73	74
SiO_2	50.82	51.67	51.51	52.81	50.83	51.27	51.96	47.96	50.96	50.26	50.11	54.44	53.78	51.31	51.49	55.03	54.78	55.2
Al_2O_3	30.63	30.58	30.42	29.56	30.97	30.43	29.87	32.7	29.62	30.89	31.32	27.47	27.76	29.13	29.08	27.1	26.89	26.98
FeO	0.62	0.42	0.41	0.65	0.64	0.45	0.53	0.37	1.05	0.47	0.47	0.66	0.61	0.6	0.63	0.74	0.74	0.73
CaO	14.66	14.43	14.4	13.1	14.89	14.43	14.16	17	14.47	15.35	15.58	11.44	11.62	13.46	13.33	10.38	10.66	10.51
Na_2O	3.50	3.57	3.6	4.23	3.24	3.52	3.54	2.05	3.39	2.95	2.83	5.34	5.14	4.16	4.23	5.64	5.77	5.82
K_2O	0.13	0.12	0.12	0.23	0.14	0.13	0.14	0.06	0.15	0.1	0.07	0.28	0.26	0.17	0.17	0.38	0.38	0.38
TOTAL	100.36	100.79	100.46	100.58	100.71	100.23	100.20	100.14	99.64	100.02	100.38	99.63	99.17	98.83	98.93	99.27	99.22	99.62
Structural formula based on thirty two oxygens																		
Si	9.264	9.351	9.355	9.560	9.232	9.336	9.452	8.803	9.366	9.193	9.136	9.917	9.845	9.478	9.499	10.036	10.015	10.042
Al	6.588	6.530	6.519	6.314	6.637	6.538	6.411	7.082	6.424	6.667	6.737	5.905	5.996	6.349	6.330	5.831	5.801	5.791
Fe	0.094	0.064	0.062	0.098	0.097	0.069	0.081	0.057	0.161	0.072	0.072	0.101	0.093	0.093	0.097	0.113	0.113	0.111
Ca	2.863	2.798	2.802	2.541	2.897	2.815	2.759	3.343	2.849	3.008	3.043	2.233	2.279	2.664	2.634	2.028	2.088	2.048
Na	1.237	1.253	1.268	1.485	1.141	1.243	1.248	0.729	1.208	1.046	1.000	1.886	1.824	1.490	1.513	1.994	2.045	2.053
K	0.030	0.028	0.028	0.053	0.032	0.030	0.032	0.014	0.035	0.023	0.016	0.065	0.061	0.040	0.040	0.088	0.089	0.088
TOTAL	20.076	20.024	20.033	20.051	20.036	20.031	19.983	20.028	20.044	20.009	20.004	20.106	20.099	20.113	20.113	20.090	20.151	20.133
Mol% An	69.32	68.61	68.38	62.30	71.18	68.86	68.30	81.81	69.62	73.77	74.96	53.37	54.73	63.52	62.92	49.34	49.46	48.90
Mol% Ab	29.95	30.71	30.94	36.40	28.03	30.40	30.90	17.85	29.52	25.66	24.64	45.08	43.81	35.53	36.13	48.51	48.44	49.00
Mol% Or	0.73	0.68	0.68	1.30	0.80	0.74	0.80	0.34	0.86	0.57	0.40	1.55	1.46	0.96	0.96	2.15	2.10	2.10

Sample 36 : plagioclase 2, medium phenocryst (AV90)
Sample 37 : plagioclase 3, groundmass (AV90)
Sample 38 : plagioclase 4, medium phenocryst (AV90)
Sample 42 to 46 : plagioclase 1, margin – core (AV90)
Sample 47 to 51 : macrophenocryst, margin – core (S120)
Sample 52 to 54 : medium phenocrysts (S120)
Sample 55 : plagioclase 3, phenocryst, core (S120)
Sample 56 : plagioclase 4, core, phenocryst (S120)
Sample 57 to 62 : various subophitic plagioclase (P180)
Sample 63 to 67 : various subophitic plagioclase (P184)
Sample 68 to 71 : subophitic plagioclase 1, margin – core (P187)
Sample 72 to 74 : subophitic plagioclase 2, core – margin (P187)

Table 5.3 Electron microprobe analyses of plagioclase feldspar

Sample#	75	76	77	78	79	80	81	82	83	84	85	86	87	88	89	90	91	92
SiO_2	55.11	55.05	56.94	56.49	55.74	55.04	55.47	55.09	53.47	51.84	51.94	53.00	50.21	49.25	53.13	54.11	51.07	51.06
Al_2O_3	27.03	26.73	26.50	26.69	26.99	27.36	27.53	27.53	28.58	29.65	29.72	29.37	30.41	31.05	28.83	28.18	30.36	30.54
FeO	0.62	0.83	0.61	0.64	0.57	0.56	0.58	0.62	0.57	0.76	0.59	0.54	0.97	0.54	0.62	0.78	0.63	0.57
CaO	10.51	10.42	9.64	10.02	10.43	10.66	10.78	10.96	12.16	13.41	13.46	13.01	14.53	15.13	12.55	11.51	14.19	14.54
Na_2O	5.89	5.77	5.95	5.82	5.53	5.37	5.46	5.27	4.73	3.95	3.90	4.20	3.29	2.97	4.47	5.05	3.65	3.44
K_2O	0.37	0.38	0.41	0.43	0.39	0.37	0.37	0.33	0.26	0.23	0.21	0.22	0.15	0.12	0.27	0.28	0.15	0.12
TOTAL	99.53	99.18	100.05	100.09	99.65	99.36	100.19	99.80	99.77	99.84	99.82	100.34	99.58	99.06	99.87	99.91	100.05	100.27
Structural formula based on thirty two oxygens																		
Si	10.032	10.060	10.257	10.190	10.105	10.017	10.016	9.989	9.734	9.472	9.481	9.605	9.239	9.106	9.673	9.830	9.326	9.303
Al	5.806	5.764	5.632	5.681	5.774	5.875	5.865	5.890	6.139	6.392	6.401	6.280	6.603	6.774	6.194	6.040	6.542	6.565
Fe	0.094	0.127	0.092	0.097	0.086	0.085	0.088	0.094	0.087	0.116	0.090	0.082	0.149	0.083	0.094	0.118	0.096	0.087
Ca	2.050	2.040	1.860	1.936	2.026	2.078	2.085	2.129	2.372	2.625	2.632	2.526	2.864	2.997	2.448	2.240	2.776	2.838
Na	2.079	2.044	2.078	2.035	1.944	1.895	1.911	1.853	1.669	1.399	1.380	1.476	1.174	1.065	1.578	1.779	1.292	1.215
K	0.086	0.089	0.094	0.099	0.090	0.086	0.085	0.076	0.060	0.054	0.049	0.051	0.035	0.028	0.063	0.065	0.035	0.028
TOTAL	20.147	20.124	20.013	20.037	20.025	20.036	20.050	20.031	20.061	20.058	20.033	20.019	20.064	20.053	20.050	20.072	20.067	20.036
Mol% An	48.64	48.89	46.14	47.57	49.90	51.21	51.09	52.47	57.83	64.37	64.81	62.33	70.32	73.28	59.88	54.86	67.66	69.54
Mol% Ab	49.32	48.99	51.53	50.00	47.88	46.68	46.82	45.65	40.70	34.31	33.98	36.41	28.81	26.03	38.59	43.55	31.49	29.77
Mol% Or	2.04	2.12	2.34	2.43	2.22	2.12	2.09	1.88	1.47	1.31	1.20	1.25	0.86	0.69	1.53	1.59	0.85	0.68

Sample#	93	94	95	96	97	98	99	100	101	102	103	104	105	106	107	108	109	110
SiO_2	50.33	50.15	51.48	51.81	52.19	48.63	50.25	50.88	52.6	51.27	51.04	51.21	50.65	50.38	50.27	54.21	50.78	50.06
Al_2O_3	30.50	30.92	29.61	29.7	29.37	31.98	30.48	30.14	28.91	30.04	30.2	30.08	30.16	29.99	30.04	27.18	30.01	30.1
FeO	0.56	0.55	0.68	0.66	0.71	0.4	0.66	0.73	0.54	0.55	0.5	0.48	0.43	0.43	0.59	0.97	0.63	0.83
CaO	14.69	14.76	13.44	13.44	13.25	16.38	14.66	14.14	12.66	14.19	14.41	14.36	14.48	14.52	14.4	11.03	14.26	14.74
Na_2O	3.39	3.26	3.51	3.74	3.87	2.33	3.05	3.39	4.63	3.87	3.71	3.76	3.71	3.65	3.42	5.31	3.61	3.37
K_2O	0.11	0.11	0.16	0.15	0.17	0.07	0.12	0.16	0.19	0.16	0.13	0.12	0.13	0.11	0.12	0.31	0.12	0.12
TOTAL	99.58	99.75	98.88	99.50	99.56	99.79	99.22	99.44	99.53	100.08	99.99	100.01	99.56	99.08	98.84	99.01	99.41	99.22
Structural formula based on thirty two oxygens																		
Si	9.245	9.195	9.476	9.482	9.543	8.941	9.255	9.344	9.619	9.363	9.330	9.355	9.303	9.299	9.297	9.941	9.336	9.248
Al	6.611	6.689	6.431	6.413	6.336	6.938	6.624	6.531	6.238	6.473	6.513	6.484	6.536	6.532	6.556	5.881	6.510	6.561
Fe	0.086	0.084	0.105	0.101	0.109	0.061	0.102	0.112	0.083	0.084	0.076	0.073	0.066	0.066	0.091	0.149	0.097	0.128
Ca	2.891	2.899	2.651	2.635	2.596	3.226	2.893	2.782	2.480	2.776	2.822	2.810	2.849	2.871	2.853	2.167	2.809	2.917
Na	1.207	1.159	1.253	1.327	1.372	0.831	1.089	1.207	1.641	1.370	1.315	1.332	1.321	1.306	1.226	1.888	1.287	1.207
K	0.026	0.026	0.038	0.035	0.040	0.016	0.028	0.037	0.044	0.037	0.030	0.028	0.030	0.026	0.028	0.073	0.028	0.028
TOTAL	20.066	20.053	19.953	19.993	19.995	20.014	19.991	20.013	20.105	20.104	20.086	20.083	20.105	20.101	20.052	20.098	20.066	20.089
Mol% An	70.10	70.99	67.26	65.93	64.77	79.21	72.14	69.09	59.54	66.36	67.72	67.40	67.83	68.31	69.46	52.50	68.11	70.25
Mol% Ab	29.27	28.38	31.79	33.20	34.24	20.39	27.16	29.98	39.40	32.75	31.55	31.93	31.45	31.07	29.85	45.74	31.20	29.07
Mol% Or	0.62	0.63	0.95	0.88	0.99	0.40	0.70	0.93	1.06	0.89	0.73	0.67	0.72	0.62	0.69	1.76	0.68	0.68

Sample 75 to 76 : plagioclase 2, core – margin, subophitic (P187)
Sample 77 to 82 : medium plagioclase 1, subophitic (P205)
Sample 84 : small plagioclase 2, core, subophitic (P205)
Sample 85 to 86 : subophitic medium plagioclase 3, core – margin (P205)
Sample 87 to 88 : large plagioclase 4, margin – core, subophitic (P205)
Sample 89 : large plagioclase 5, subophitic (P205)
Sample 90 to 92 : plagioclase 1, margin – core, subophitic (P200)
Sample 95 : plagioclase 2, core, subophitic (P200)
Sample 96 to 97 : plagioclase 3, core – margin, subophitic (P200)
Sample 98 : plagioclase 4, core, subophitic (P200)
Sample 99 to 100 : plagioclase 5, core – margin, subophitic (P200)
Sample 101 to 106 : large plagioclase 1, margin – core, subophitic (P223)
Sample 107 to 108 : medium plagioclase 2, core – margin, subophitic (P223)
Sample 109 : small plagioclase 3, core, subophitic (P223)
Sample 110 : Large plagioclase 4, core, subophitic (P223)

Table 5.3 Electron microprobe analyses of plagioclase feldspar

Sample#	111	112	113	114	115	116	117	118	119	120	121	122	123	124	125	126	127	128
SiO_2	50.50	50.24	55.82	52.97	52.18	52.79	57.63	53.11	51.31	57.16	57.38	52.27	57.04	51.00	51.24	51.28	49.62	49.23
Al_2O_3	30.22	29.97	26.41	28.60	29.74	29.02	25.55	29.00	29.98	26.33	25.66	29.26	26.59	30.26	30.77	30.63	31.87	31.78
FeO	0.63	0.56	0.84	0.79	0.58	0.63	0.63	0.63	0.60	0.80	0.64	0.71	0.73	0.60	0.44	0.42	0.42	0.44
CaO	14.60	14.53	9.86	12.41	13.50	12.54	8.49	12.55	13.96	9.25	8.77	13.06	9.68	14.30	15.03	14.80	16.10	16.08
Na_2O	3.37	3.43	6.02	4.41	3.96	4.43	6.63	4.50	3.80	6.57	6.52	4.23	5.94	3.53	3.23	3.22	2.59	2.53
K_2O	0.12	0.11	0.43	0.21	0.19	0.23	0.62	0.24	0.04	0.33	0.59	0.19	0.48	0.15	0.11	0.12	0.09	0.09
TOTAL	99.44	98.84	99.38	99.39	100.15	99.64	99.55	100.03	99.69	100.44	99.56	99.72	100.44	99.84	100.82	100.47	100.69	100.15
Structural formula based on thirty two oxygens																		
Si	9.267	9.295	10.163	9.690	9.492	9.634	10.423	9.655	9.391	10.271	10.385	9.551	10.245	9.331	9.284	9.314	9.031	9.012
Al	6.558	6.543	5.674	6.173	6.384	6.249	5.453	6.220	6.474	5.583	5.480	6.308	5.635	6.533	6.578	6.565	6.844	6.864
Fe	0.097	0.087	0.128	0.121	0.088	0.096	0.095	0.096	0.092	0.120	0.097	0.108	0.110	0.092	0.067	0.064	0.064	0.067
Ca	2.877	2.880	1.923	2.432	2.631	2.452	1.645	2.444	2.737	1.781	1.701	2.557	1.859	2.803	2.918	2.880	3.139	3.153
Na	1.202	1.230	2.125	1.564	1.397	1.567	2.325	1.586	1.348	2.289	2.288	1.498	2.068	1.252	1.135	1.134	0.914	0.898
K	0.028	0.026	0.100	0.049	0.044	0.054	0.143	0.056	0.009	0.076	0.136	0.044	0.110	0.035	0.025	0.028	0.021	0.021
TOTAL	20.048	20.061	20.113	20.030	20.036	20.052	20.084	20.056	20.051	20.119	20.087	20.067	20.027	20.046	20.007	19.984	20.014	20.016
Mol% An	70.05	69.63	46.37	60.13	64.62	60.20	40.00	59.82	66.85	42.96	41.23	62.37	46.04	68.53	71.55	71.26	77.06	77.44
Mol% Ab	29.26	29.74	51.23	38.66	34.30	38.48	56.52	38.82	32.93	55.22	55.47	36.55	51.23	30.61	27.83	28.05	22.43	22.05
Mol% Or	0.69	0.63	2.41	1.21	1.06	1.31	3.48	1.36	0.23	1.82	3.30	1.08	2.72	0.86	0.62	0.69	0.51	0.52

Sample#	129	130	131	132	133	134	135	136	137	138	139	140	141	142	143	144	145
SiO_2	50.83	49.87	50.64	50.71	50.23	48.6	55.5	49.33	48.7	50.74	54.26	52.7	60.4	52.02	51.89	52.37	52.19
Al_2O_3	30.82	31.1	29.31	29.48	28.67	31.35	26.09	31.58	32	30.48	27.96	29.44	24.65	29.76	29.96	29.41	29.71
FeO	0.40	0.47	1.12	1.03	1.62	0.5	2.02	0.4	0.4	0.37	0.71	0.72	0.71	0.74	0.59	0.71	0.64
CaO	14.93	15.19	13.23	13.24	12.83	15.33	9.86	15.76	16.26	14.64	11.97	13.42	7.29	13.8	13.85	13.08	13.57
Na_2O	3.15	2.96	3.89	3.85	4.08	2.67	5.94	2.73	2.48	3.27	4.59	4	6.97	3.75	3.75	4.08	3.8
K_2O	0.13	0.1	0.24	0.22	0.23	0.07	0.37	0.08	0.07	0.1	0.24	0.2	0.75	0.19	0.14	0.22	0.16
TOTAL	100.26	99.69	98.43	98.53	97.66	98.52	99.78	99.88	99.91	99.60	99.73	100.48	100.77	100.26	100.18	99.87	100.07
Structural formula based on thirty two oxygens																	
Si	9.259	9.151	9.411	9.406	9.433	9.033	10.124	9.048	8.944	9.297	9.864	9.555	10.734	9.465	9.442	9.549	9.499
Al	6.624	6.734	6.427	6.452	6.353	6.876	5.616	6.834	6.934	6.589	5.997	6.298	5.169	6.389	6.432	6.328	6.380
Fe	0.061	0.072	0.174	0.160	0.254	0.078	0.308	0.061	0.061	0.057	0.108	0.109	0.106	0.113	0.090	0.108	0.097
Ca	2.914	2.986	2.634	2.631	2.581	3.053	1.927	3.097	3.199	2.874	2.331	2.607	1.388	2.690	2.700	2.555	2.646
Na	1.112	1.053	1.402	1.384	1.485	0.962	2.101	0.971	0.883	1.162	1.618	1.406	2.401	1.323	1.323	1.442	1.341
K	0.030	0.023	0.057	0.052	0.055	0.017	0.086	0.019	0.016	0.023	0.056	0.046	0.170	0.044	0.032	0.051	0.037
TOTAL	20.000	20.020	20.105	20.086	20.161	20.018	20.161	20.030	20.038	20.001	19.974	20.022	19.967	20.024	20.019	20.034	20.000
Mol% An	71.83	73.50	64.36	64.68	62.63	75.72	46.84	75.79	78.06	70.81	58.22	64.22	35.06	66.31	66.58	63.11	65.76
Mol% Ab	27.42	25.92	34.25	34.04	36.04	23.87	51.07	23.76	21.54	28.62	40.40	34.64	60.65	32.61	32.62	35.62	33.32
Mol% Or	0.74	0.58	1.39	1.28	1.34	0.41	2.09	0.46	0.40	0.58	1.39	1.14	4.29	1.09	0.80	1.26	0.92

Sample 111 to 114 : small plagioclase 6–8, core, subophitic (P223)
Sample 116 to 117 : medium plagioclase 2, core–margin, subophitic (P227)
Sample 119 : medium plagioclase 4, core, subophitic (P227)
Sample 121 : groundmass plagioclase, glomeroporphyritic (P259)
Sample 123 : plagioclase 2, margin (P271)
Sample 125 : plagioclase 4, core (P271)
Sample 130 : plagioclase 1, core, phenocryst (P273)
Sample 135 to 138 : plagioclase 2, margin–core, phenocryst (P273)
Sample 142 : plagioclase 2, margin (P278)
Sample 143 : plagioclase 4, core (P278)
Sample 145 : plagioclase 5, core (P278)

Sample 118 : small plagioclase 1, core, subophitic (P227)
Sample 118 : small plagioclase 3,core, subophitic (P227)
Sample 120 : small plagioclase 1, groundmass (P259)
Sample 122 : plagioclase 1, core (P271)
Sample 124 : plagioclase 3,core (P271)
Sample 125 to 129 : glomeroporphyritic plagioclase (P276)
Sample 131 to 134 : plagioclase 2 to 5, phenocrysts (P276)
Sample 139 to 140 : plagioclase 1, margin–core (P278)
Sample 142 : plagioclase 3, core (P278)
Sample 144 : plagioclase 5, core (P278)

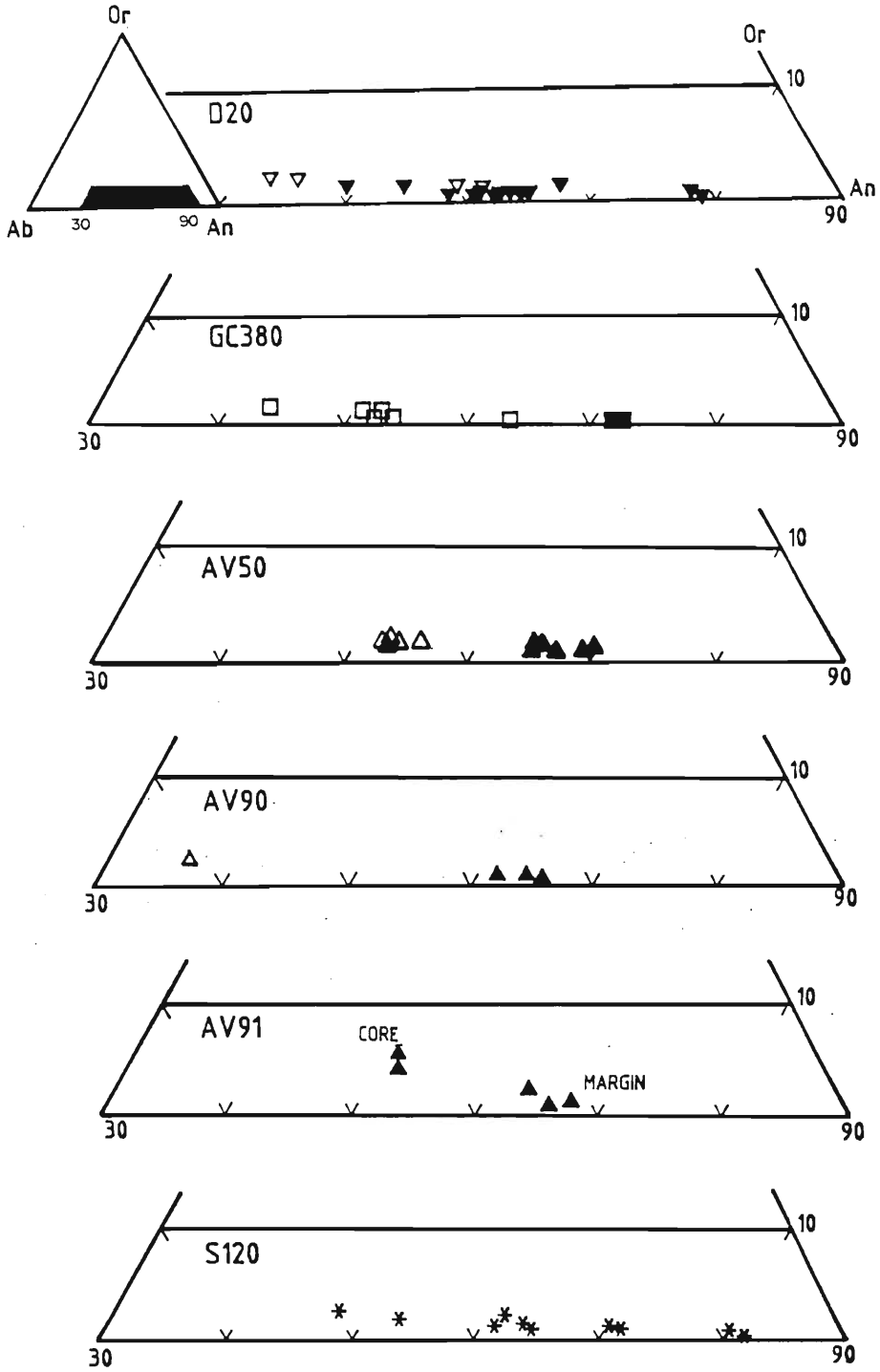

Fig. 5.9a Feldspar compositions in terms of anorthite (An), albite (Ab) and orthoclase (Or) endmembers for the dolerite and the pre- Phinong basalts. Note the lower An compositional range for the groundmass plagioclase. The groundmass plagioclase is indicated by open symbols, and shaded symbols represent phenocryst compositions. For samples S120 and AV91 only phenocryst compositions are represented.

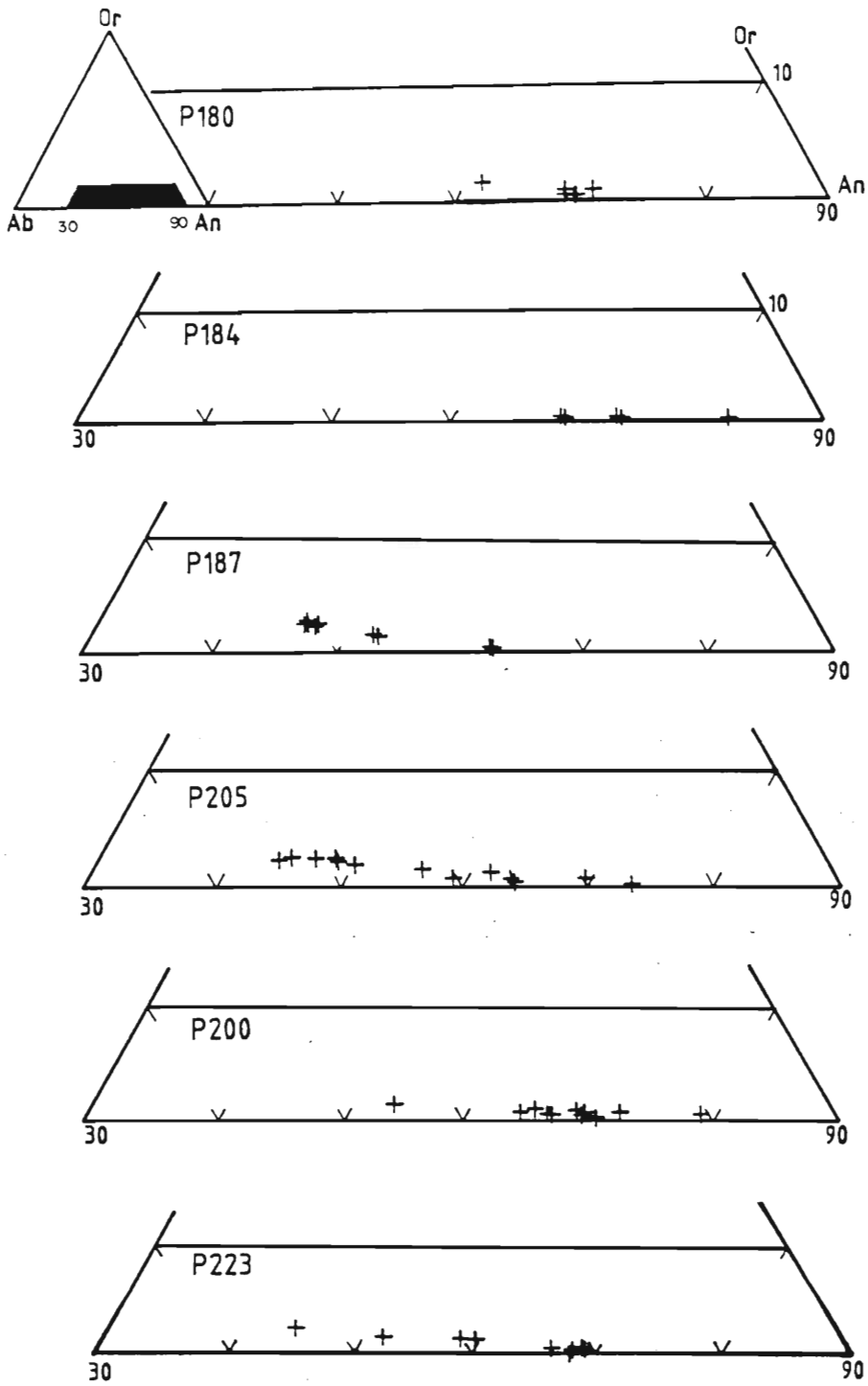

Fig. 5.9b Feldspar compositions in terms of anorthite (An), albite (Ab) and orthoclase (Or) endmembers for the Phinong basalts. All samples represented on this figure are subophitic.

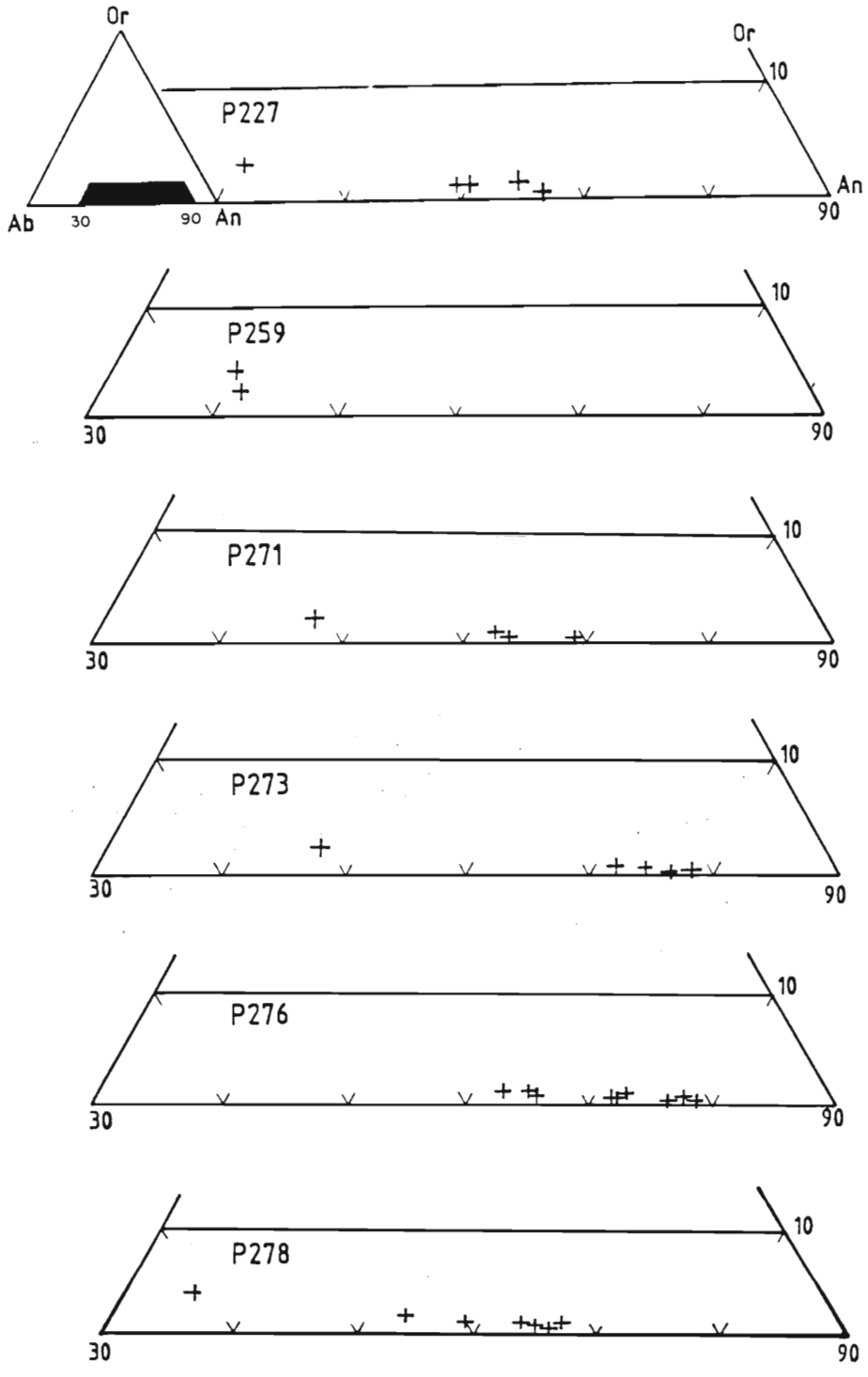

Fig. 5.9c Feldspar compositions in terms of anorthite (An), albite (Ab) and orthoclase (Or) endmembers for the Phinong basalts. All samples are porphyritic, except sample P227 which is subophitic.

1.58 and molecular percent anorthite = 67.57) the plagioclases from the dolerite as well as the Giant's Cup basalts have a consistently lower inverse ratio of Or to An than plagioclases from the Phinong, Sakeng and Agate Vale basalts. This relates directly to bulk-rock geochemistry, where the average K_2O content of the dolerites and the Giant's Cup basalts is lower than that for the Phinong and Agate Vale basalts. The Sakeng basalts, however, have a slightly lower average K_2O content than the dolerites and the Giant's Cup basalts. Plagioclase from the Phinong, Sakeng and Agate Vale basalts have orthoclase compositional ranges similar to one another, and therefore cannot be adequately separated on this basis. A dividing line at An_{59} effectively separates the groundmass compositions from the phenocryst compositions for the Giant's Cup and Agate Vale plagioclases. For plagioclases belonging to the Phinong basalts, this separation in terms of anorthite composition is masked by phenocryst rim compositions which are lower in anorthite than An_{59} and therefore overlap somewhat with groundmass anorthite compositions. Rim compositions, for plagioclases from the dolerite sample and Sakeng basalt also show anorthite contents less than An_{59}. However, in all samples the core analyses for the phenocrysts are greater than An_{59}.

5.5. Summary

The mineral chemistry of the major silicates plagioclase, pyroxene and olivine has been determined for the Sani Pass basaltic rocks.

Although olivines from only a single sample (P227) were probed, the range of measured forsterite (Fo_{66} to Fo_{75}) is within the range of olivines from other Karoo-age lavas (Fo_{11} to Fo_{86}) reported by Marsh and Eales, (1984). However, the high whole-rock MgO content of sample P227 is not within the range for normal Lesotho-type basalts of 5.0 to 8.0 weight percent MgO (Eales and Marsh, 1979). A calculated forsterite content (using Roeder and Emslie's (1970) method) for sample P227, having MgO=12.09 weight percent, yields a value of Fo_{86}. This deviation of calculated forsterite content from the measured value (Fo_{66} to Fo_{75}) implies a proportion of cumulus olivine in sample P227. This is supported by evidence provided by the Ni/Mg relationships (Figs. 5.2). Cumulus olivine enrichment of

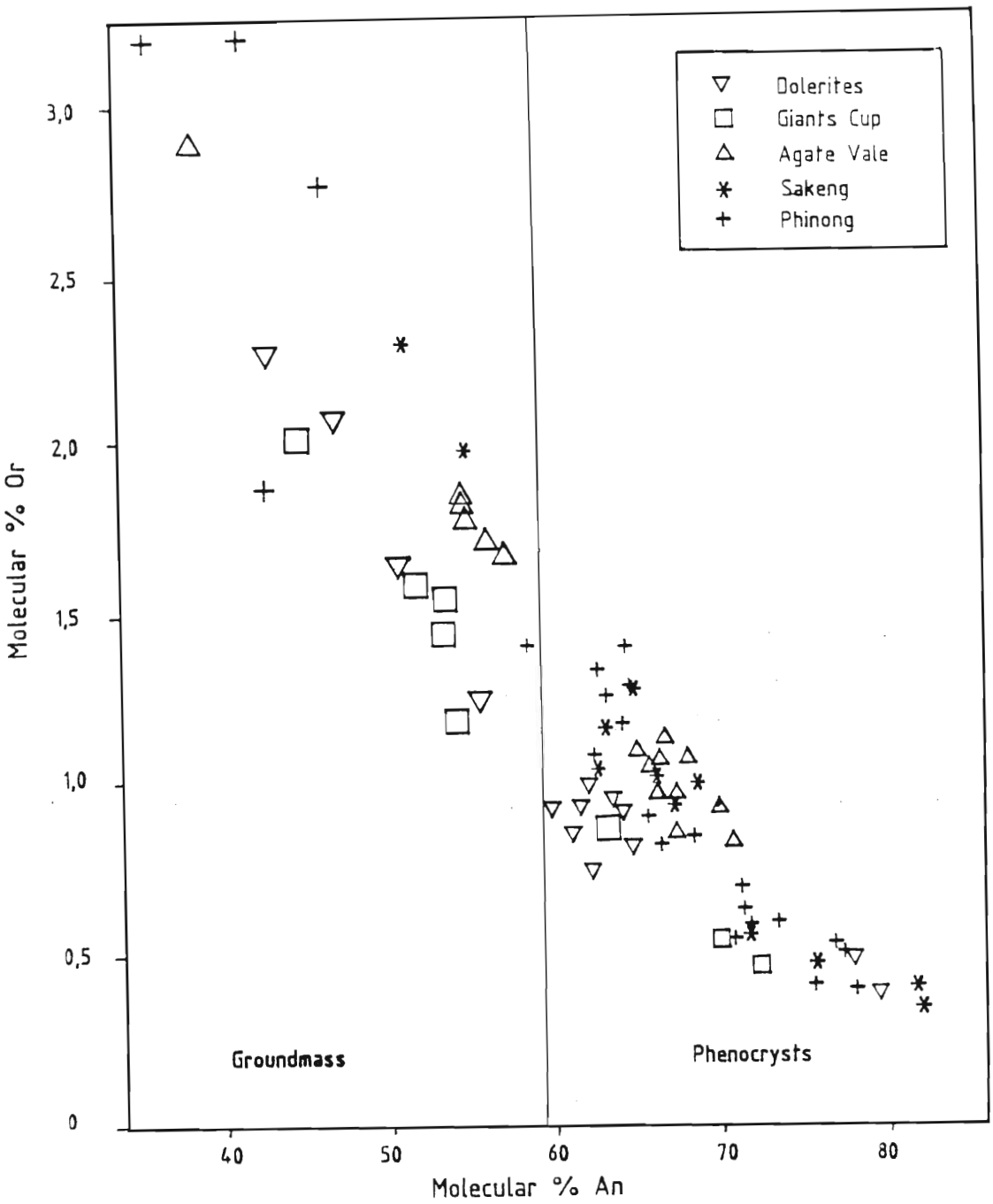

Fig. 5.10 Diagram showing the variation of molecular % orthoclase (Or) with molecular % anorthite (An) for the Sani Pass basalts and dolerite. Molecular Or increases with increasing An content, and most of the groundmass compositions are enriched in Or and poorer in An, than their corresponding phenocryst compositions. The dolerite and the Giant's Cup basalt have the lowest Or/An ratio. The larger symbols indicate groundmass compositions.

a normal Lesotho-type magma, may have been caused by flowage differentiation (Bhattercharji, 1967).

Microprobe data for pyroxenes from the Agate Vale and Phinong-type basalts indicate predominantly augite and subordinate pigeonite compositions. Compositional ranges for the augite and pigeonite of the Agate Vale magma type are $Wo_{39}En_{51}Fs_{10}$ to $Wo_{31}En_{29}Fs_{40}$ and $Wo_{9}En_{64}Fe_{27}$ respectively, and equivalent ranges in the Phinong-type basalts are: $Wo_{27}En_{52}Fs_{21}$ to $Wo_{42}En_{49}Fs_{9}$ and $Wo_{10}En_{44}Fs_{46}$ to $Wo_{8}En_{63}Fs_{29}$. Augites from the Agate Vale magma, display a tholeiitic trend similar to that at Skaergaard (Brown and Vincent, 1963) and Bird's River (Eales and Booth, 1974). This trend is characterized by decreasing calcium content as the iron content increases. A similar trend is not developed in the augites from the Phinong basalts, which instead indicate composite analyses of pigeonite and augite.

The distribution of the minor elements Ti^{4+}, Al^{3+}, Cr^{3+} and Mn^{2+} relative to Mg^{2+} is broadly consistent with whole-rock geochemistry for both the Agate Vale and Phinong magma types. The groundmass pyroxenes from the Agate Vale magma type have experienced depletion in Mg and Cr, and enrichment in Mn and Ti, relative to the earlier-formed phenocrystic augite. The groundmass augites also have low Al, possibly due to the presence of plagioclase on the liquidus during their formation.

Plagioclase is mainly in the labradorite-bytownite range. Phenocrysts are slightly more enriched in anorthite than the groundmass. A similar compositional pattern is observed between margin and core, the latter being anorthite enriched. Reverse zoning in sample AV91 (Agate Vale magma) suggests that a proportion of the feldspar might be xenocrystic. Plagioclase from the dolerites and the Giant's Cup basalts is lower in terms of the Or/An ratio, than for plagioclase from the Phinong, Sakeng and Agate Vale basalts.

CHAPTER 6

6. ZEOLITES AND OTHER SECONDARY MINERALS

6.1. Introduction

In many flood basalt sequences, such as those in Iceland, India, Antrim and the Parana Basin of Brazil, the secondary minerals display a distinct vertical zonal relationship (Walker, 1960; Mehegen *et al.*, 1982; Sukheswala *et al.*, 1974; Murata *et al.*, 1987). Although Wheelock (1978) demonstrated the presence of some zonation in the secondary minerals of the southern Lebombo volcanics, the work of Anderson (1975) suggested that a zonation was not present at Naude's Nek in the Drakensberg massif.

Secondary minerals are common in rocks of the Sani Pass, as in most basaltic lava sequences. In addition to there being several different amygdale morphologies (Section 3.2), with each type being composed of several secondary minerals, secondary minerals also occur as vein fillings and pod-like masses. This variety in the mode of occurrence indicates that the formation of secondary minerals was a complex process with several distinct phases.

Field observations clearly indicated that, in the Sani Pass succession, quartz (agate) and calcite are the dominant amygdale minerals in the lower lavas (basal 170m) while zeolite minerals dominated in the upper lavas (Table 6.2). Therefore a systematic sampling of the secondary minerals was undertaken to establish details of the zonation. A total of 58 secondary mineral samples were collected, and for each the altitude and mode of occurrence was noted. Only the most abundant amygdale mineral from each lava flow was sampled. The mineral species were identified using X-ray diffraction powder methods and the JCPD data file (Appendix 4).

6.2. Morphology of the Secondary Minerals

The secondary minerals in the basalts of the Sani Pass occur in three distinct forms, amygdales, veins and pod-like masses.

Amygdales are the commonest form of secondary minerals and are present throughout the sequence. Almost all the amygdales are composite in that a thin layer of chlorite (less than 0.30mm thick) coats the outer surface and forms a layer between the mineral filling the amygdale and the lava. However, apart from this coating, the amygdales are mostly monomineralic. Although the amygdale morphology and formation can be related to the conditions prevailing during eruption (Section 3.2) the mineral filling is the result of post-eruptive solidification reactions, and the monomineralic nature of most amygdales implies equilibrium with the chemicophysical environment.

The vast majority of veins are less than 20mm wide, but in some places the veins cementing broken rock fragments combine to produce features up to 400mm wide. The veins of secondary minerals lack the chlorite sheath, and occasionally contain more than one secondary mineral species. In the cases where calcite and a zeolite were observed to co-exist in a single vein, there was clear evidence of disruption of primary calcite, and the later deposition of the zeolite mineral. The field evidence of displacement across some of the calcite/zeolite veins and the cleavage-rhomb shaped nature of the calcite clearly indicates that there were several distinct episodes in the formation of these veins. The brecciated rock and mineral fragments present in the larger veins are considered to be evidence of minor tectonic disruption of the lava.

The pods or lens-like masses of zeolites were only found in the very top part of the basaltic sequence in Lesotho. These bodies occur in highly altered rock, and normally contain chlorite in addition to two, or more, other secondary minerals. The intimate mixture and large size of these secondary mineral masses suggests that their formation may have been related to late-stage fumarole activity or the circulation of heated water through the lavas.

6.3. Mineralogy

Of the 9 different secondary minerals identified (Table 6.1) all but three are members of the zeolite group. Quartz in the form of agate and crystalline material is more common than calcite, although the latter often occurs as vein filling and can be present in masses up to 200mm in width. Chlorite, the other non-zeolite mineral, forms a "skin" between virtually all amygdale infillings and the rock as well as forming very thin, less than 2mm wide, veins.

Table 6.1 Secondary Minerals of the Sani Pass.

Mineral	Chemical Composition	Crystal Structure
Quartz	SiO_2	Trigonal
Chlorite	$(Mg,Fe)_{10}Al_2(Si,Al)_8O_{20}(OH,F)_{16}$	Monoclinic
Calcite	$CaCO_3$	Trigonal
Laumonite	$Ca(Al_2Si_4O_{12}).4H_2O$	Monoclinic
Mordenite	$(CaNa_2K_2)Al_2Si_{10}O_{24}.7H_2O$	Orthorhombic
Mesolite	$Na_2Ca_2(Al_2Si_3O_{10})_3.8H_2O$	Monoclinic
Heulandite	$(Ca,Na_2)(Al_2Si_7O_{18}).6H_2O$	Monoclinic
Stellerite	$CaAl_2Si_7O_{18}.7H_2O$	Orthorhombic
Stilbite	$(Ca,Na_2K_2)(Al_2Si_7O_{18}).7H_2O$	Monoclinic
Epistilbite	$Ca(Al_2Si_6O_{16}).5H_2O$	Monoclinic

6.4. Distribution of the Zeolites

It is apparent from the stratigraphic distribution of the amygdales (Table 6.2 and Figs. 6.1 and 6.2), that the amygdale minerals define two distinct zones within the Sani Pass volcanic succession. The lower 170m of the volcanic sequence is completely zeolite-free and characterized by quartz and calcite. The overlying lavas, which constitute the major bulk of the succession contain, in addition to quartz and calcite, a variety of zeolite-filled amygdales. This latter zone may be further subdivided on the basis of the zeolite species

TABLE 6.2 Distribution of Zeolites with Stratigraphy

ALTITUDE (METERS)	SAMPLE	Quartz	Calcite	Laumontite	Mordenite	Heulandite	Epistilbite	Stilbite	Mesolite	Stellerite
797	278a	X								
796	278b				X		X			
795	278c					X				
789	277a								X	
780	275a								X	
777	274a								X	
770	272c								X	
770	272b									+
770	272a								X	
765	271b									+
746	267a								X	
728	263a								X	
721	262a							X		
697	259a								X	
691	257a					X				
676	255a					X			X	
594	251a									
590	250b			+						
564	248c								X	
557	246b				X		X			
557	246a	X			X					
554	245a								X	
550	243a						X			
545	242a					X				
540	240a	X			X		X			
536	238a								X	
527	233	X			X					
522	230a					X				
422	204a	X	X							
420	203a			X						
414	201a	X			X					
403	222a	X		X						
304	188a			X						
259	180a			X						
213	177a	X	X							
171	160a			X						
170	150a	X	X							
150	133a		X							
118	120a	X								
82	112b	X								
82	112a		X							
62	110a		X							
38	90a		X							
0	350a	X	X							

X = Mineral present in vesicle

+ = Mineral along fractures, joints or faults

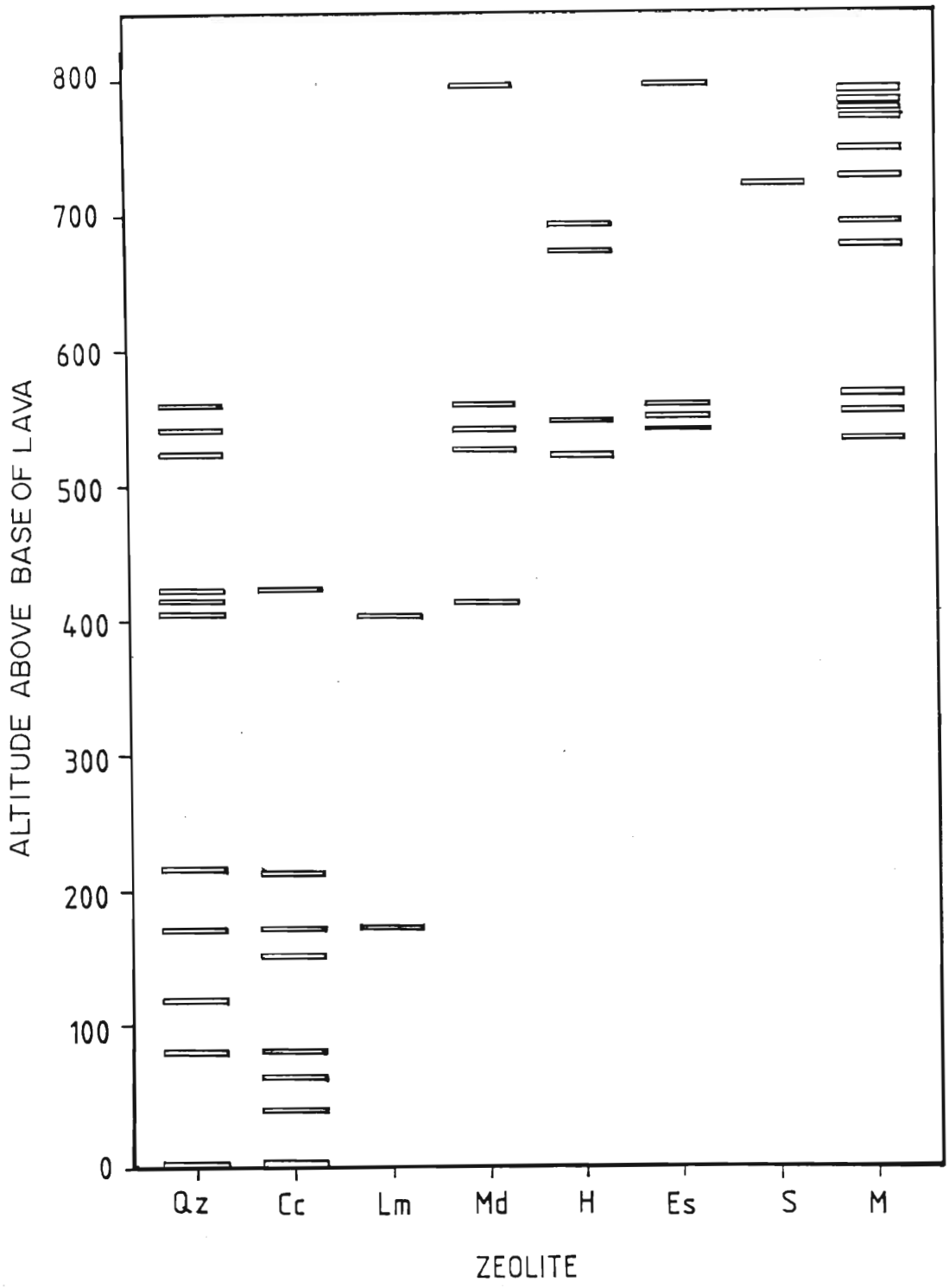

Fig. 6.1 Distribution of amygdales in the Sani Pass indicating a lowermost zeolite-free zone, succeeded by a laumontite zone, which is overlain by a mesolite-dominated zone. Altitude is in meters above the sandstone/basalt contact. (Qz = quartz, Cc = calcite, Lm = laumontite, Md = mordenite, H = heulandite, Es = epistilbite, St = stilbite and M = mesolite).

into a lower laumontite zone and an upper mesolite dominated zone (Fig. 6.2). The zeolite assemblages of these two zones are as follows:

1. laumontite zone: laumontite
2. mesolite zone: mesolite with lesser amounts of heulandite, mordenite, epistilbite and stilbite

Quartz and calcite are well developed throughout these two zones, both as individual amygdales and as intergrowths associated with the zeolites. Chlorite is also widespread and commonly occurs as a rim between the lava and the amygdale infilling. The chlorite is the variety clinochlore.

The laumontite zone occurs immediately above the quartz-calcite zone and extends for 249m (Fig. 6.1). Calcite and quartz are still common amygdale minerals within this zone and occur both as individual amygdale fillings and intergrowths. One anomalous occurrence of mordenite and quartz occurs in flow P201. Laumontite occurs most commonly as a radiating aggregate of coarse prismatic crystals that fill vesicles.

Zeolite mineralization is best developed within the mesolite zone (Fig. 6.2), which extends for over 400m and persists into the highlands of Lesotho. Mesolite is the most widespread zeolite and is best developed in the upper portion of this zone. It is characterised by different shades of cream, pink and green, and occurs as well-developed radiating acicular aggregates. Heulandite occurs throughout this zone and is present as thick tabular crystals, often associated with stilbite. Stilbite, which occurs on its own, has only been documented in one flow (P262), as platy, sheaf-like crystals, and together with heulandite, epistilbite and mordenite occurs in the lower to middle parts of the mesolite zone (Fig. 6.1).

Six pipe amygdale samples 250p; 253p; 259p; 269p; 271p; 274p from the mesolite zone were also analysed and all of these contain epistilbite, mordenite and quartz. Quartz is the most abundant pipe amygdale mineral and occurs on its own, as well as in association with the zeolites. Within individual flows, there appears to be little, if any, relationship between the composition of the pipe amygdales and the spherical amygdales.

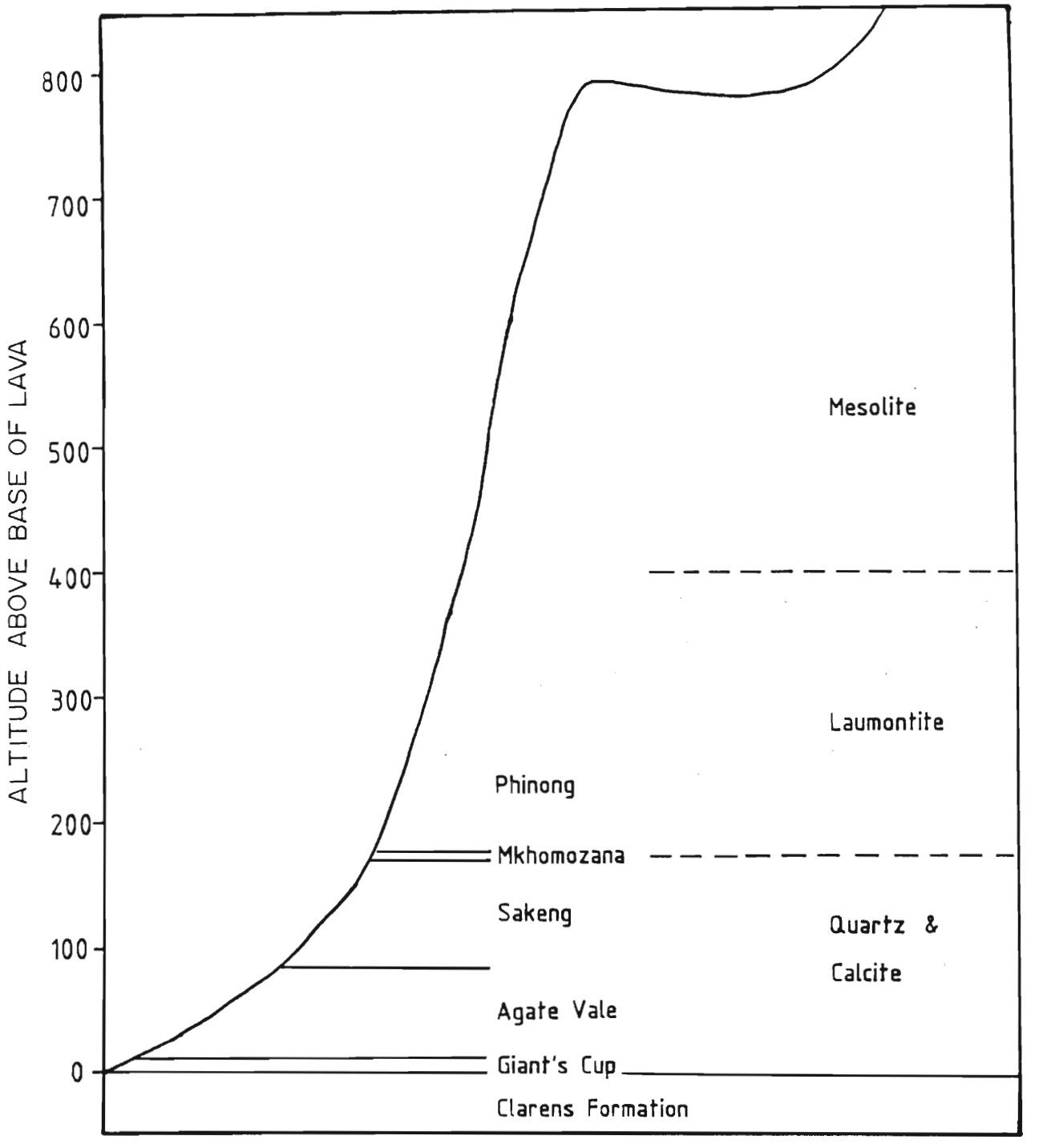

Fig. 6.2 The distribution of the amygdale zones in the Sani Pass, in relation to the geochemically defined magma types. Attitude is in meters above the basalt/sandstone contact.

The post-eruptive veins and fractures in the upper part of the succession are filled by calcite, stellerite and laumonite. Clearly, these zeolites must be ascribed to a later period of formation.

6.5. Causes of Zeolite Zonation

The distribution of zeolites into specific zones similar to those found in the Sani Pass lavas has been noted in the volcanic piles in Eastern Iceland (Walker, 1960; Mehegen *et al.*, 1982), Deccan Traps (Sukheswala *et al.*, 1974) and the Parana lavas (Murata *et al.*, 1987). These volcanic sequences are characterized by a basal laumontite zone and an immediately overlying scolecite-mesolite zone. Above the scolecite-mesolite zone differences exist in zeolite composition amongst the different volcanic provinces. Murata *et al.*, (1987) suggested that the vertical flow of earth heat, which causes a temperature gradient within the volcanic pile, was the main factor that controlled the nature and extent of zonation.

Microprobe and fluid inclusion studies of zeolites within basalts of currently active geothermal fields in various parts of Iceland (Kristmannsdottir and Tomasson, 1978; Kristmannsdottir, 1982; Mehegen *et al.*, 1982), have yielded approximate temperature ranges for the successive zeolite zones (Table 6.3). These temperatures are considered indicative of prevailing temperature regimes during zeolitization of the Icelandic lavas, and are based on the assumption that the authigenic minerals are in equilibrium with prevailing physicochemical conditions. The data in Table 6.3, suggests that the presence of laumontite in the Sani Pass basalts, indicates a temperature of 100 to 230°C for the lower part of the volcanic succession. The heulandite-mordenite assemblage, which occurs directly above the laumontite zone, is seldom stable in systems above temperatures of 100 to 120°C (Palmasson *et al.*, 1979; Kristmannsdottir, 1978) and indicates a vertical drop in temperature. The existance of lower temperatures in the higher part of the succession is supported by the widespread occurrence of mesolite, which is stable in the range 60 to 100°C. Subsequent to overall cooling of the lava flows, a rejuvenation in temperature occurred during the formation of the late stage laumontite-filled veins.

Table 6.3 Approximate bounding temperatures of geothermal fields of Iceland

Zone	Bounding temp. (°C)
Chabazite	50 to 70
Mesolite-scolecite	60 to 100
Heulandite-stilbite-mordenite	60 to 170
Laumonite	100 to 230
Epidote	>230

After Kristmannsdottir and Tomasson (1978) and Kristmannsdottir (1982).

In Iceland the lava sequence is cross-cut by four regionally extensive and flat-lying amygdale zones (Walker, 1960; Gibson *et al.*, 1966). In addition, the highest stratigraphic zone is characterised by numerous amygdale-free lava flows that are considered to be near the top of the original lava succession (Mehegen *et al.*, 1982). The Icelandic lava pile is exposed for 1 500m above sea-level and has an unexposed extent of an additional 1 900m, totalling at least 3 400m (Robinson *et al.*, 1982). The upper 1 200m of the unexposed lavas are still in the laumontite zone, below which is a higher grade zone characterized by abundant prehnite and epidote (Mehegen *et al.*, 1982). The basalts of the Parana volcanic succession are up to 1500m thick, with laumonite developed in the lower 300m; similarly in the zeolite zoned basaltic sequence of Antrim (Walker, 1960) laumontite occurs at depths of 1200 to 1400m below the ancient lava surface.

These depths of 1200 to 1400m for the formation of the laumoontite zone can be used to provide an estimate of the total thickness of the lava sequence in the Sani Pass area. The upper surface of the laumontite zone is 420m above the base of the lava sequence, indicating that the total thickness of the lavas was between 1620 and 1820m. These values are compatible with the 2000m estimated by Potgieter *et al.*, (1982) from studies of laumontite at the base of the Drakensberg Formation on the farm Bamboes Kloof (north-eastern Cape).

The implication of the zeolite data is that, since the extrusion of the lavas, some 213 to 413m of lava has been removed from above the summit of Thabana Ntlenyana (3 482m

above sea level), the highest peak in Lesotho. In the Karoo-age Lebombo mountains the basaltic lavas are overlain by a thick succession of felsic extrusive rocks (SACS, 1980). In view of the proximity of the preserved basalt outliers in Lesotho to the estimated upper surface of the volcanic sequence, it is concluded that rhyolitic units equivalent to those found in the Lebombo monocline (Fig. 6.3) were never present in the Lesotho portion of the Central igneous province.

Besides providing evidence for inferring the thickness of the original basaltic pile, the presence of laumontite in the Sani Pass volcanics can be used to infer the approximate fossil geothermal gradient. Assuming a maximum temperature range of 100 to 230°C for the laumontite zone, which would have been approximately 1 649 to 1 200m below the top of the original lava pile (deepest possible base and shallowest upper surface), the maximum fossil geothermal gradient for the Sani Pass volcanics would have been 139°C/km, while a minimum fossil gradient would have been 83°C/km. Thus, the average fossil geothermal gradient for the Sani Pass volcanics is 111°C/km. This value is twice the present day temperature for basalts in northern Lesotho, which is about 55°C/km (Jones, 1990). In Iceland, fossil geothermal gradients of 60°C/km to 90°C/km have been calculated for areas that today show regional gradients of 50°C/km to 65°C/km (Kristmannsdottir, 1982). Although fundamental differences existed in the mode of production of magmas in Iceland (oceanic) and the Sani Pass (continental), Murata *et al.*, (1987) noted that these differences in igneous activity were of little consequence in the post eruption development of zeolite zones.

Laumontite and the other lower temperature zeolites have a large proportion of calcium in their composition, and are therefore considered to have precipitated from solutions with high calcium activities and low partial pressures of carbon dioxide (Mehegen *et al.*, 1982). Calcium-rich solutions having high partial pressures of carbon dioxide would precipitate calcite rather than calcium-rich zeolites (Thompson, 1971). Therefore the sequence of calcite, quartz and laumontite in the lower section of the Sani Pass volcanic succession may reflect not only an increase in temperature, but also a decrease in the partial pressure of carbon dioxide. Boles and Coombs (1977), suggested that laumontite may form by the

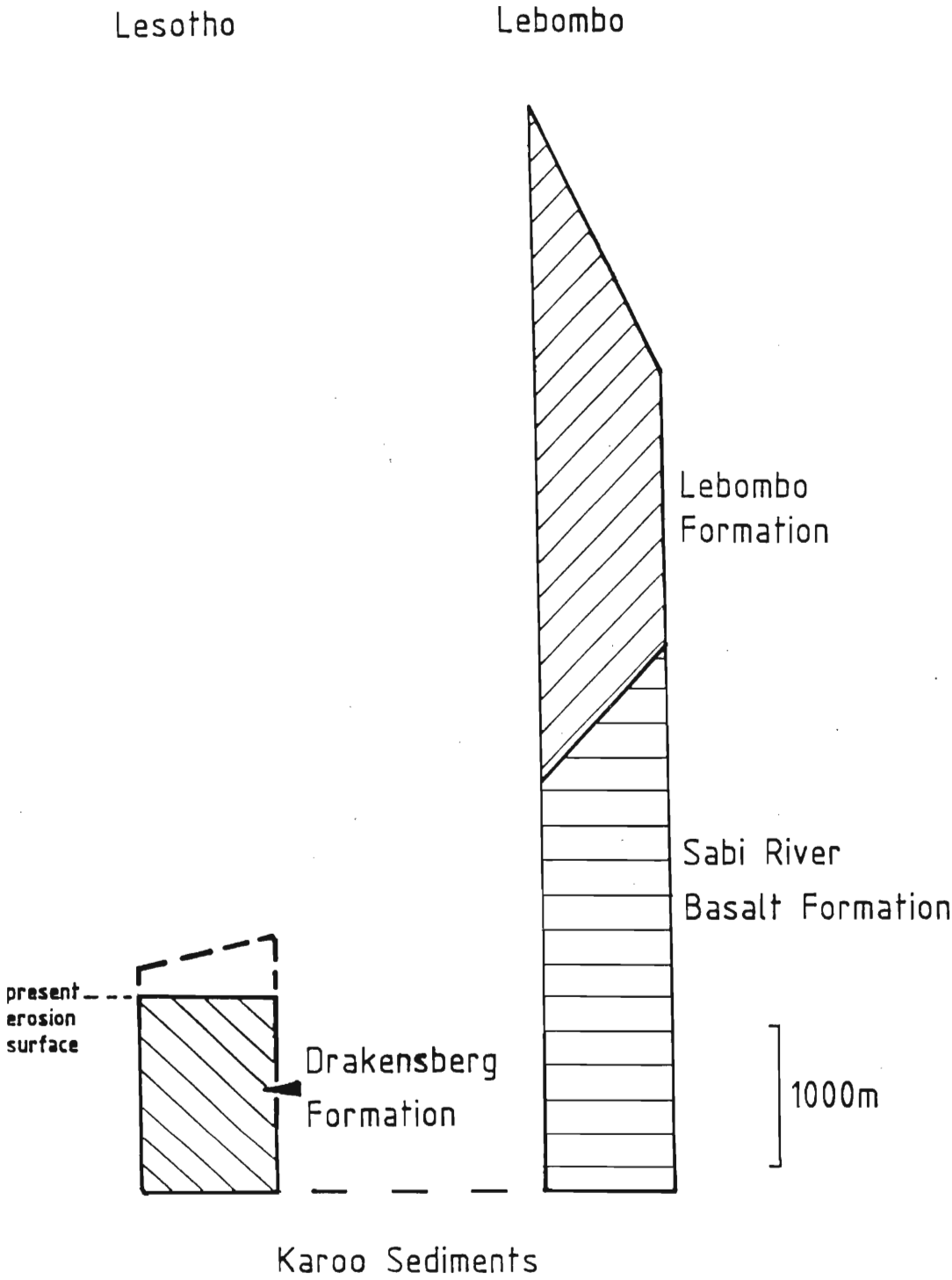

Fig. 6.3 The Lebombo volcanic succession in relation to volcanics preserved in Lesotho. The rhyolitic Lebombo Formation is unlikely to have extended to the Lesotho, as indicated by the amount of volcanics calculated to have been removed in the Sani Pass (shown in broken lines). Thickness for the Lebombo and Sabie River Basalt Formations have been obtained from Bristow (1976).

replacement of heulandite by a simple dehydration-desilicification reaction. In the Icelandic lavas, laumontite also occurs as a replacement product of calcic plagioclase (Mehegen *et al.*, 1982). A similar process may have occurred in sample M160 in which calcic plagioclase is albitized and laumontite occurs as the zeolite. This process requires the addition of Na^+ from the hydrothermal solutions and the release of Ca^{2+}, for the formation of laumontite. However, the geothermal fluids in most of Iceland's active systems are of meteoric origin with low salinities (Palmasson *et al.*, 1979). The presence of intergrown calcite and laumontite in late stage veins suggests equilibrium precipitation from the same fluid. This would require initial precipitation of calcite, thus lowering the partial pressure of CO_2 so laumontite can form (Thompson, 1971).

The control of zeolite mineralogy by the composition of the host lava has been documented in the Icelandic and Parana basalts (Mehegen *et al.*, 1982; Murata *et al.*, 1987). The limited range in the whole-rock chemistry of the Sani Pass lavas suggests that secondary mineral development was controlled by ambient temperatures rather than host rock chemistry. Although mordenite in the previously documented zeolite studies occurs principally in the high silicic rocks (SiO_2=65 to 70 weight percent), within the Sani Pass lavas it occurs in rocks with silica content of 50.50 to 52.73 weight percent. Coombs *et al.*, (1959) have shown that mordenite can crystallize outside its stability range in the presence of amorphous silica in the hydrothermal solutions, however, the stability and post crystallisation reaction are as yet unclear.

6.6. Summary

The Sani Pass lavas are diagenetically altered into a zeolite-free zone, a laumontite zone and a mesolite dominated zone (Fig. 6.1). The laumontite zone is restricted to the bottom portion of the zeolite succession. The stratigraphically higher mesolite dominated zone comprises mordenite, heulandite, epistilbite and stilbite, but no laumontite. The virtual restriction of laumontite to the lower lavas of the zeolite zone reflects the high temperature (100 to 230°C) required for its formation and thereby exemplifies the control of zeolite

mineralogy by temperature conditions. The presence of silica-rich zeolites in the mesolite zone may be due to an increase in silica activity of the hydrothermal solution.

Using the high-temperature geothermal Icelandic province as a model of geothermal activity, an original maximum thickness of 1 820m has been inferred for the Sani Pass basalts and an average fossil temperature gradient of 111°C/km has been calculated. This is much higher than the present day average and is in keeping with elevated temperatures during igneous activity. The inferred original thickness for the Sani Pass basaltic succession indicates that felsic extrusives, equivalent to those preserved in the Lebombo Mountains (Fig. 6.3), could not have been erupted in the Lesotho portion of the Central igneous province.

CHAPTER 7

7. BASALT CLASSIFICATION

7.1. Introduction

This chapter describes briefly various classifications of basalts, with emphasis on the major element-based classifications. The Sani Pass basalts and dolerites are characterized in terms of these classifications, including tectonic discriminant diagrams that utilize trace and minor elements.

Although alteration can affect the classification of these rocks all samples have been used in the classifications. Notwithstanding a detailed assessment of alteration in Section 10.2, altered samples are mentioned where relevant in this chapter.

7.2. Review of Basalt Nomenclature

Bailey *et al.*, (1924), in their Memoir on the Scottish Isle of Mull recognised two main basaltic magma types namely: (1) a plateau-basalt magma type, and (2) a central non-porphyritic magma type. They recognised two further minor rock types being intermediate to felsic in composition. These four rock types they believed to be genetically related, with the voluminous plateau magma types as the probable parent. Subsequent basalt classifications have been based on the parental status of basaltic magmas.

The plateau and central magma types can be equated with Kennedy's (1933) two primary basalt magma types, namely: (1) the olivine-basalt magma type, and (2) the tholeiitic magma type, respectively. Kennedy (1933) reiterated that the composition of late differentiates of basaltic magmas "depends primarily on the nature and composition of the parent basalt magma," and that the olivine-basalt magma type is parental to an alkaline line of magmatic

descent, whereas the tholeiitic magma type leads to a more siliceous association. Further refinements on the same theme were made by Tilley (1950), who recognised the critically higher alkali content of Kennedy's (1933) olivine-basalt magma type and renamed it and its associated series "alkali-olivine basalt."

Nockolds and Allen (1954) divided the basaltic rocks into tholeiitic basalts, alkali basalts and central basalts, while Nockolds and Le Bas (1977) subsequently recommended that the term central basalt be abandoned in place of the more commonly used calc-alkali basalt. Kuno (1960) postulated a third type of primary magma, namely the "high alumina basalt," which is chemically intermediate between the tholeiite and the alkali basalt and similar to the calc-alkali basalt which Tilley (1950) considered to be a tholeiitic derivative. Yoder and Tilley (1962) adopted a simple scheme of basalt classification, based on normative mineralogy. These latter authors demonstrated that basaltic compositions of the alkaline and tholeiitic basalts could be conceived of as lying within the basalt tetrahedron and separated compositionally by a critical thermal divide at low pressures. Further, the presence of orthopyroxene in a basalt immediately identifies it as a tholeiite, and subdivision of the tholeiite field into quartz tholeiite or olivine tholeiite is based simply on which of these two minerals is present in the norm.

Chayes (1966) argued that the term "tholeiite" should be abandoned and recommended "subalkaline basalt" as an alternative. Wilkinson (1968) and Irvine and Baragar (1971) subsequently used "subalkaline" as a more general name for rocks of both the tholeiitic basalt and calc-alkali series.

The uncertain status of magma series is well illustrated in Turner's (1970) remarks, "... the basaltic magma-types cover a broad spectrum. Probably more than one type is primitive. Others may be derivative. On a more refined but still legible scale each has its unique character; the magma-types are not just two or three but are infinite in number."

7.3. Normative Mineralogy

7.3.1. Norm calculation and the Fe_2O_3/FeO ratio

Igneous rocks are prone to oxidation by secondary alteration (weathering, zeolitization etc.); the degree of oxidation commonly being expressed as the ratio Fe_2O_3/FeO. Oxidation elevates the Fe_2O_3/FeO ratio of the altered rock, thereby influencing the normative mineral composition in a rather complex fashion (Middlemost, 1989, Chayes, 1990). The oxidized rock will contain more normative magnetite, thus less FeO will be available to form silicate minerals such as diopside, hypersthene, and olivine. This causes an excess of silica to appear in the norm. In order to overcome this problem, a number of methods of standardizing the ferric iron content of magmatic rocks have been proposed (Irvine and Baragar, 1971; Le Maitre, 1976).

In order to reduce the effects of oxidation in the interpretation of geochemical data, Cox and Hornung (1966), used a standard oxidation ratio expressed as $Fe_2O_3/FeO = 0.1$, in calculating their norms. This value is close to their average oxidation value for the Karoo dolerites. The justification for using this ratio depends on the acceptance of the equivalence of the basalts and dolerites and the lower degree of oxidation of the latter. From a survey of the literature Brooks (1976) suggested an average Fe_2O_3/FeO value of 0.15. This value represents the Fe_2O_3/FeO ratio suggested for pristine ocean floor basalts. Workers involved in the National Geodynamics Project (Duncan *et al.*, 1984) have also used a Fe_2O_3/FeO ratio of 0.15 in the compilation of the geochemical database for Karoo volcanics. In work more directly correlatable with the present study (Pemberton, 1978; Mitchell, 1980) on volcanics of the Naude's Nek Pass, and Molteno and Jamestown respectively, a Fe_2O_3/FeO ratio of 0.2 has been used. This is in keeping with other work on the volcanics of the north-eastern Cape by Robey (1976) and Rumble (1979), as well as the Fe_2O_3/FeO ratio of 0.2 recommended for basalts by Middlemost (1989). A direct comparison between the volcanics of the north-eastern Cape and those of the study area is envisaged, thus a Fe_2O_3/FeO ratio of 0.2 has been used in the norm calculations.

FeO values determined using wet chemical analysis by the Geological Survey have been obtained (Appendix 2, Tables A2.2 and A2.3). The use of these values in the oxidation ratio, yields a range of values with an average of 0.56. Due to the range in the Fe_2O_3/FeO ratios, (0.07 to 5.74) this average value of 0.56 is not a good reflection of the overall oxidizing conditions in the Sani Pass. The high oxidation ratio of some samples yields substantially more quartz-normative results and elevated magnetite values.

Also in the norm, analyzed CO_2 content (determined by Geological Survey) has made possible the calculation of normative calcite, meaning anorthite values are not inflated (Appendix 2, Tables A2.2 and A2.3). Primary calcite has not been identified petrographically, and therefore the proportion of normative calcite indicates the amount of calcite due to alteration as well as calcite contained in amygdales, even though the samples were selected to contain the minimum quantity of amygdale material.

7.3.2. Basalt Tetrahedron

The basalt tetrahedron offers an easy conceptual analogy to natural basalt groups, and was introduced by Yoder and Tilley (1962) as a means of classifying basaltic rocks. The end members of this pseudo-quaternary system are forsterite (Fo), diopside (Di), nepheline (Ne) and quartz (Qz), with intermediate enstatite (En) and albite (Ab) on the Fo-Qz and Ne-Qz tie lines respectively. This experimental system approximates many aspects of the composition of natural basaltic rocks. In the basalt tetrahedron the plane Di-Ab-Fo, termed the critical plane of silica undersaturation, coincides with a low pressure liquidus thermal divide, which separates the differentiation trends of tholeiitic and alkaline magmas. The empirical line on the alkali-silica diagram (Fig. 7.2), which is used to separate the alkali from the sub-alkali rocks, is the trace of the critical plane of silica undersaturation (De Long and Hoffman, 1975).

Using the critical plane of silica undersaturation and the plane of silica saturation, Yoder and Tilley (1962) divided the basaltic rocks into the following groups:

1. tholeiite (oversaturated), contains normative quartz and hypersthene,
2. tholeiite (saturated), contains normative hypersthene,
3. olivine tholeiite (undersaturated), contains normative hypersthene and olivine,
4. olivine basalt, contains normative olivine, and no normative hyperstene, and
5. alkali basalt, contains normative olivine and nepheline.

Based on Yoder and Tilley's (1962) classification scheme, the majority of the basalts and dolerites of the Sani Pass are classified as oversaturated tholeiites, while twelve samples are olivine tholeiites (Appendix 2, Tables A2.6 and A2.7). The norm calculations also indicate that samples GC350, GC360 and AV400 are corundum normative. These samples also have a high proportion of calcite in the norm (22.33, 11.73 and 13.63 weight percent respectively) and are extensively altered, as noted petrographically. The presence of corundum prevents diopside from appearing in the norm. In view of the high degree of alteration of these samples, the olivine normative classification of AV400 must remain suspect. The presence of olivine in the norms of the Mkhomazana basalts (samples M150, M160 and M170) might be attributed to the deficiency of CaO in these samples, which allows an excess of MgO (after forming diopside) to appear as normative olivine. Factors that might be responsible for the low CaO content in the Mkhomazana basalts are examined in Section 10.2. The olivine normative character of sample P227 can be ascribed to the presence of cumulus olivine (section 5.2).

Fig. 7.1 displays the Sani Pass basalt and dolerite analyses plotted on the Ol-Di-Qz plane of the normative basalt tetrahedron Ol-Pl-Di-Qz, which coincides with the experimental quaternary system Fo-An-Di-Qz. The end-members of this system were recalculated from the CIPW norms (Appendix 2, Tables A2.6 and A2.7) by the method of Cox and Hornung (1966) and projected from the plagioclase apex as outlined by Cox *et al.*, (1979). Experimental phase boundaries used in this diagram have been derived from Cox *et al.*, (1979).

Compositional differences within the Sani Pass basalts and dolerites are reflected in their normative mineralogy (Fig. 7.1). The Di-En-An join (plane of silica saturation) forms an effective boundary between the Giant's Cup, Agate Vale and Sakeng magma types on the

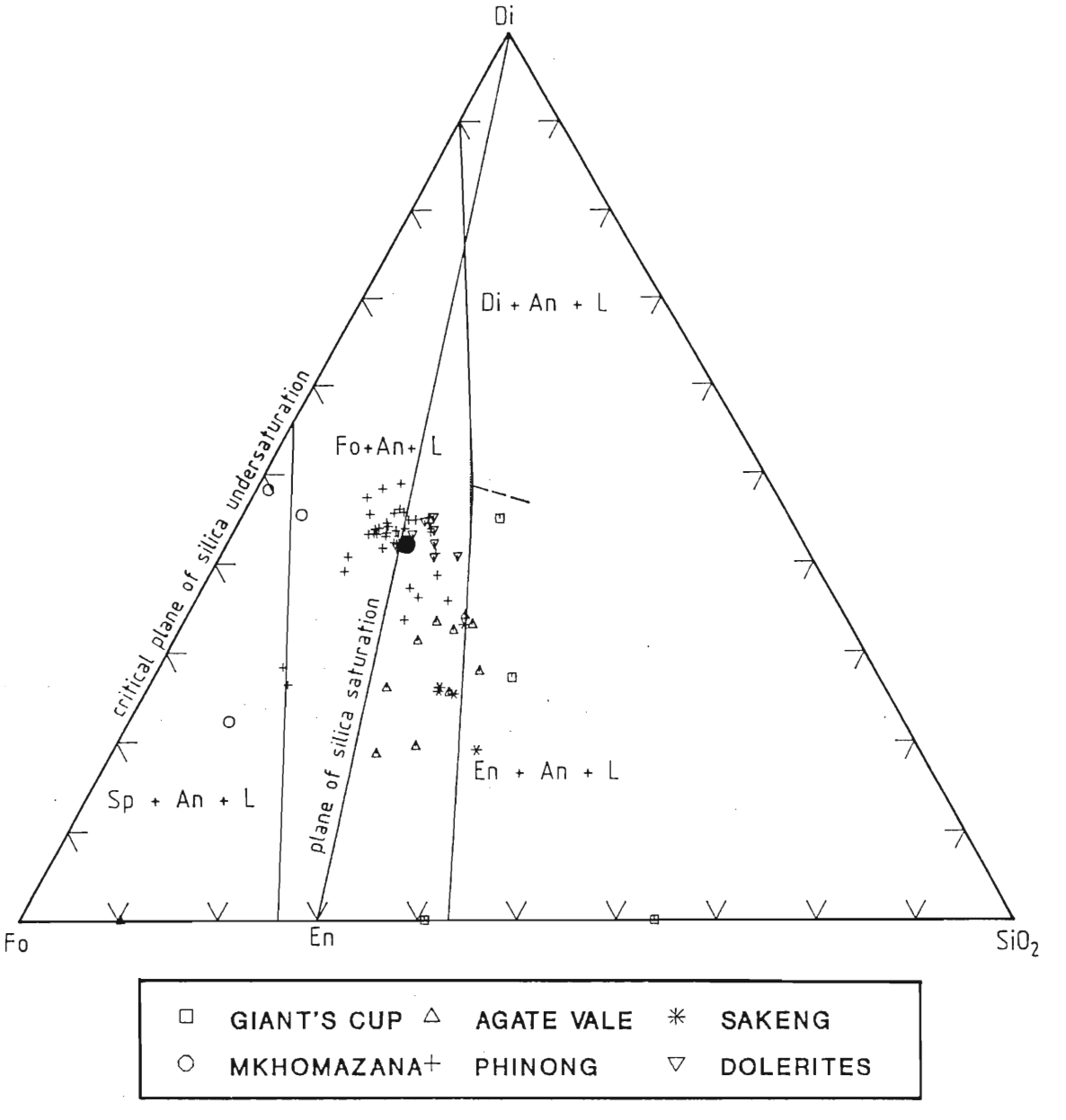

Fig. 7.1 The Sani Pass basalt and dolerite data displayed on the normative basalt tetrahedron. Note that the En-Di-An join forms an effective boundary between the Phinong and Mkhomazana basalts and the other pre-Phinong basalts and dolerites. Normative data for the average Lesotho basalt is represented by the shaded dot. Major element data for the average Lesotho basalt are from Duncan *et al.*, (1984b). Sp = Spinel, An = Anorthite, Di = Diopside, En = Enstatite, FO = Fosterite, L = Liquid.

quartz oversaturated side, and the Mkhomazana basalts on the olivine side. The Phinong type basalts straddle the Di-En-An join with most of the samples plotting on the olivine-enriched side of the Di-En-An join. The slightly more silica oversaturated nature of the pre-Phinong basalts (except the Mkhomazana basalts) is reflected in their slightly higher SiO_2 major element content than the Phinong basalts. The Mkhomazana basalts plot strongly on the olivine side of the Di-En-An join and very close to the critical plane of undersaturation. The average Lesotho type basalt plots in the field of the Phinong basalts (Fig. 7.1).

Samples GC370, GC380, AV100, AV110 and S120 plot in the En-An-Lq field, supposedly with the appearance of orthopyroxene on the liquidus. No orthopyroxene has been identified in these thin sections, although some pigeonite has been recognized in sample AV100. The position in the basalt tetrahedron of the remaining samples might be due to excess silica in the analyses, due to the presence of quartz-filled amygdales. The slightly lower Ca content in the Agate Vale basalts is reflected by their position in the basalt tetrahedron, being furthest from the diopside apex. The three corundum normative samples (GC350, GC360 and AV400) plot on the Fo-SiO_2 plane, because of insufficient Ca available for diopside formation.

It has been shown previously (section 5.2) that sample P227 is enriched in cumulus olivine and its MgO content is not a reflection of its original liquid composition. The chemical relationship indicated in Fig. 7.1 indicates that samples P180 and P227 plot near a tie-line joining the Phinong cluster of normal basalts with the olivine composition point of the tetrahedron. This demonstrates that the bulk composition of the normal Phinong basalts and samples P180 and P227 could be related to each other essentially by the addition or subtraction of the chemical components of olivine only. Interestingly, sample M160 falls on this tie-line as well.

7.4. Alkali-Silica Diagram

The alkali-silica diagram (Fig. 7.2) is an effective means of distinguishing alkaline from subalkaline igneous rocks and has been extensively used (Tilley, 1950; MacDonald and Katsura, 1964; MacDonald, 1968; Irvine and Baragar, 1971).

When plotted on the alkali-silica diagram, using Irvine and Baragar's (1971) subdivision, the Sani Pass basalts and associated dolerites plot in the subalkaline field, except sample AV400, which is strongly alkaline (Fig. 7.2). If MacDonald's (1968) dividing line is used, then samples GC350, M150, M160 and AV400 are classified as alkaline. The alkaline affinity of samples M150 and M160 is attributed to their high whole-rock Na_2O content (4.14 and 4.27 weight percent, respectively). Sample GC350 also shows an elevated Na_2O content (3.10 weight percent) and a low SiO_2 content (43.26 weight percent) which contributes to its alkaline classification. Sample AV400 is classified as alkaline due to its extreme enrichment in K_2O (6.90 weight percent).

7.5. Anorthite-Alumina Diagram

Irvine and Baragar (1971) believed that the most prominent chemical difference between the more basic members of the calc-alkali and tholeiitic series is in their alumina content. Based on the normative plagioclase (anorthite) versus alumina contents, the Sani Pass basalts are predominantly tholeiitic, except samples GC350, P178, M150, M160 and M170, which plot in the calc-alkaline field (Fig. 7.3). Samples GC350 and P178 comprise a large proportion of normative calcite, testifying to extensive alteration. Consequently, sample GC350 has a larger proportion of normative albite to normative anorthite, while sample P178 has almost equal proportions of normative albite and anorthite (27.33 and 27.48 weight percent). Nonetheless the slight enrichment in Al_2O_3 (16.55 weight percent)in sample P178 gives it a calc-alkaline characteristic. Samples M150, M160 and M170 have a high proportion of normative albite (35.03 to 37.99 weight percent), due to their high Na_2O content, thus imparting a calc-alkaline characteristic to these rocks. The typically tholeiitic character of

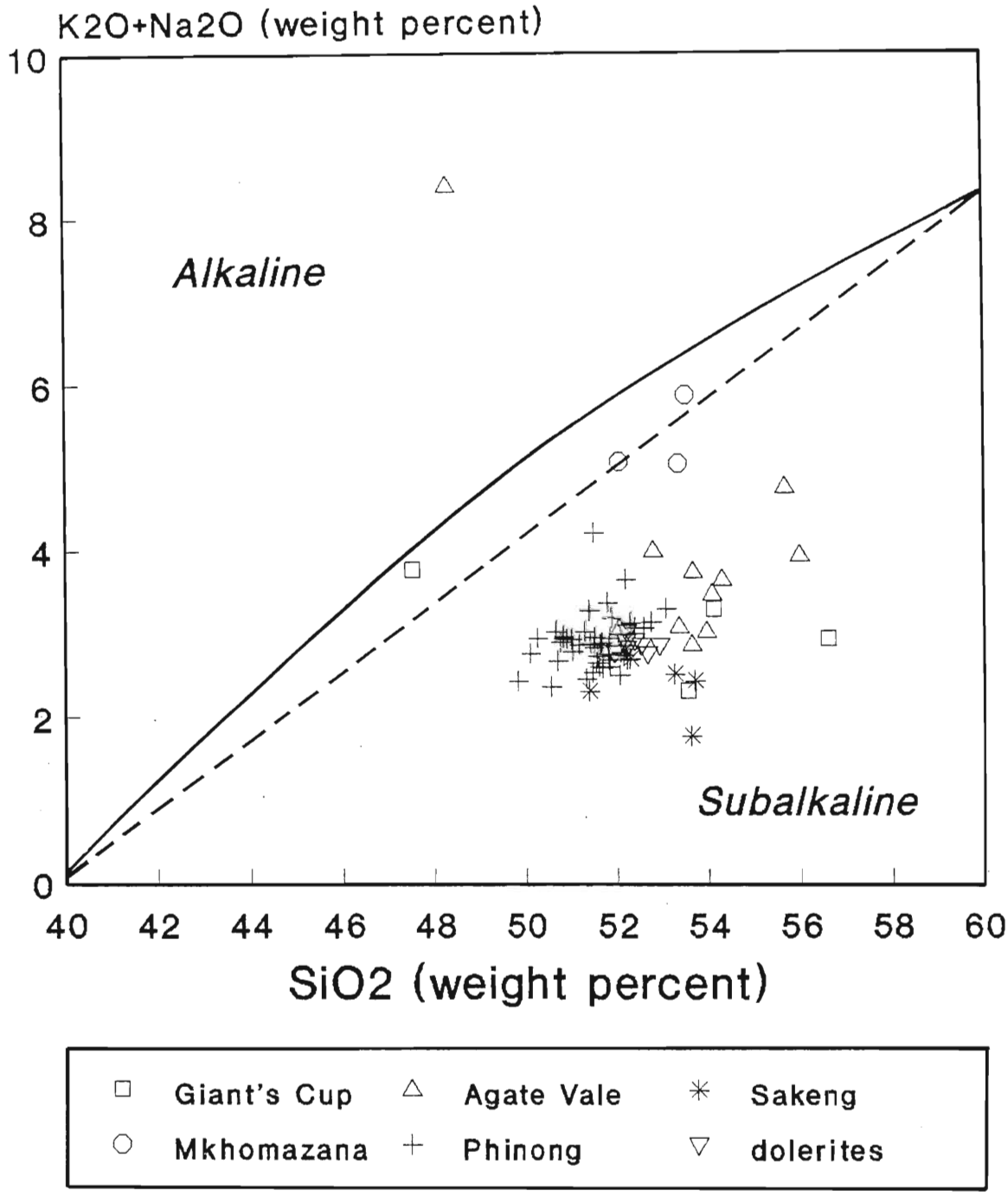

Fig. 7.2 SiO_2 versus total alkalies variation diagram. The dashed line represents the dividing line between alkaline and subalkaline basalts according to McDonald (1968). Solid line represents the equivalent dividing line according to Irvine and Baragar (1971). Except for sample AV400 all basalt samples from the Sani Pass are subalkaline according to Irvine and Baragar's (1971) subdivision, whilst samples GC350, M150, M160 are marginally alkaline according to the field delimination of McDonald (1968).

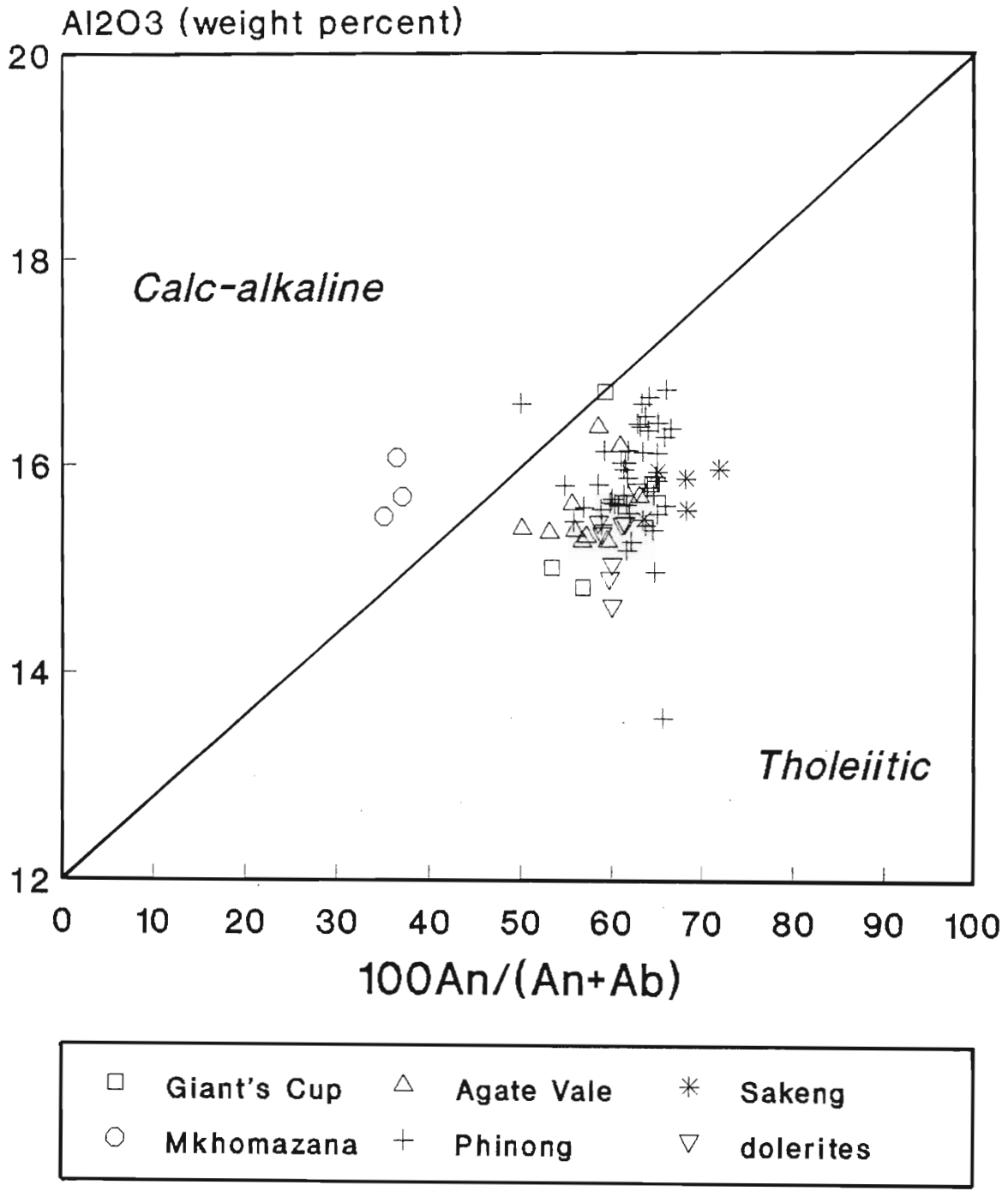

Fig. 7.3 Anorthite versus alumina variation diagram showing the division of calc-alkaline and tholeiitic rocks (Irvine and Baragar, 1971). Except for the Mkhomazana type basalts and samples G350 and P178 all the Sani Pass basalts are tholeiitic.

the Karoo basic magmas has been well established (Walker and Poldervaart, 1949; Cox and Hornung, 1966; Marsh and Eales, 1984).

7.6. AFM Diagram

The AFM variation diagram uses a triangular representation to show the relative proportions of alkalis ($Na_2O + K_2O$), iron oxides ($FeO + Fe_2O_3$) and magnesia (MgO). This diagram illustrates well the marked iron enrichment at low levels of ($K_2O + Na_2O$), followed by rapid alkali-enrichment, characteristic of tholeiitic and alkaline suites. The calc-alkaline trend shows more marked alkali-enrichment, with only gradual enrichment in iron.

Nockolds and Allen (1956) recognised three AFM trends in the Karoo dolerites (Fig. 7.4):

1. the Main trend, which is characteristic of the majority of the rocks, is marked by slight iron enrichment.
2. considerable iron-enrichment, as seen in the rocks of Elephant's Head and New Amalfi, and,
3. a third trend, which shows no absolute iron-enrichment.

Trends 1 and 2 have been identified in the basic volcanics of southern Lebombo (Bristow, 1976).

In Fig. 7.4, the Sani Pass basalts and dolerites do not show any trends identified by Nockolds and Allen (1956). All the Sani Pass samples plot in the tholeiitic field, except the Mkhomazana basalts and 2 samples (AV60 and AV70) from the Agate Vale magma type, which plot in the calc-alkaline field. The Mkhomazana basalts and samples AV60 and AV70 plot in the calc-alkaline field on the AFM diagram because of the high Na_2O content in the Mkhomazana basalts and the high K_2O content in samples AV60 and AV70. In the tholeiitic field, slight iron enrichment is shown by the Giant's Cup basalts and most of the dolerites.

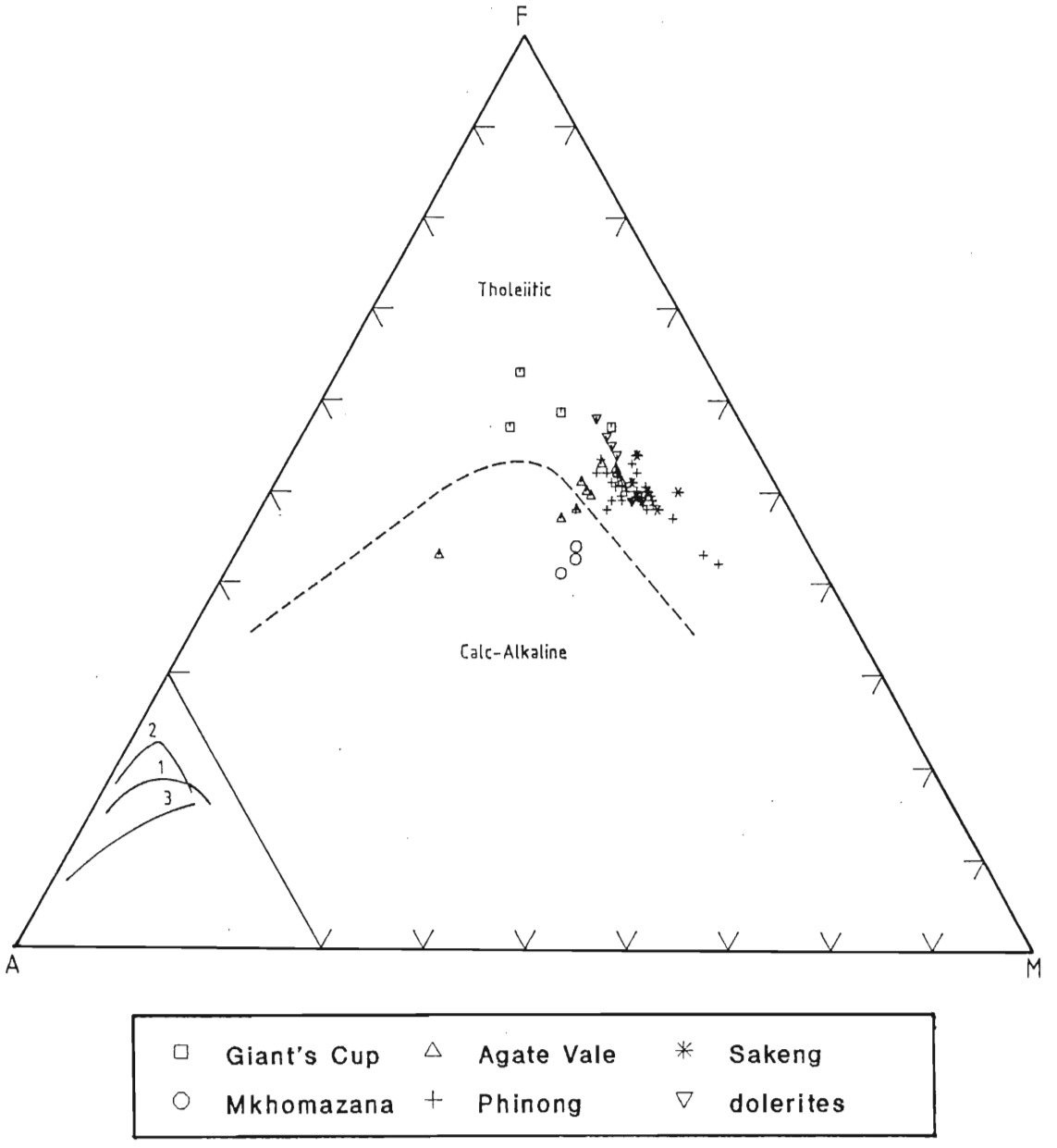

Fig. 7.4 AFM diagram showing an incipient tholeiitic trend of iron enrichment at low alkali concentrations of the Phinong, Sakeng and most of the Agate Vale basalts. Greater iron enrichment is indicated by the Giant's Cup basalts and some of the dolerites. Samples AV400, AV70, AV91, P178 and the Mkhomazana basalts plot in the calc-alkaline field and do not show the characteristic trend of no iron-enrichment with increasing alkali concentrations. The three trends marked 1, 2 and 3 in the inset are the AFM trends recognised by Nockolds and Allen (1956). The dashed line indicates the boundary between the tholeiitic and calc-alkaline fields, after Irvine and Baragar (1971).

7.7. Tectonic Discrimination

Magmatism associated with the Mesozoic-age volcanic rocks in southern Africa occurred in different tectonic settings, for example, the Etendeka volcanics are associated with rifting during opening of the south Atlantic; the southern Lebombo volcanics were erupted during rifting and lithospheric thinning associated with monoclinal warping, and central Karoo volcanics were erupted on a within-plate continental environment, termed a-tectonic (Marsh, 1987). Thus, in order to identify the original tectonic setting for a succession of basic volcanic rocks, numerous geochemical discriminant diagrams have been devised. The discriminant diagrams utilize high field strength (HFS) trace and minor elements (Pearce and Cann, 1973; Wood *et al.*, 1974; Pearce, 1982) and/or major and minor element discriminant analysis (Pearce, 1976).

When geochemical data for the southern Karoo basalts are plotted on many of the tectonic discriminant diagrams, essentially all of these rocks would be classified mainly as calc-alkali basalts (CABs), low-K-tholeiites (LKT) or ocean floor basalts (OFB) on a Ti-Zr-Y diagram (Cox, 1983; Duncan, 1987), and mainly as CABs on a Ti-Zr-Sr diagram (Duncan, 1987). (Cox, 1983; Duncan, 1987). The Sani Pass geochemical data, which have been screened according to the requirements of Pearce and Cann (1973), plot essentially in the CAB, LKT and OFB field on the Ti-Zr-Y discriminant diagram (Fig. 7.5). Two samples (S131 and AV60) plot in the within-plate basalt field (WPB), whilst a few pre-Phinong samples straddle the WPB/CAB field divide. All of these latter samples are marked by low Y contents, in the range of 14 to 18 ppm. Sample M150 does not plot in any of the demarcated fields because of enrichment in Y (43 ppm). The Agate Vale magma type, which is characterized by higher Zr content than the other magma types, expectedly plots closer to the Zr apex in the CAB field, and away from the field of the other Sani Pass magma types.

As an alternative discriminant, Pearce and Cann (1973) suggested a Ti-Zr-Sr diagram for "fresh" basalts which do not plot in the field characteristic of WPB on the Ti-Zr-Y diagram. Ti-Zr-Sr data for the Sani Pass basalts are represented in Fig. 7.6 and in terms of this diagram most of the Sani Pass basalts plot in the CAB field, except 6 samples which plot

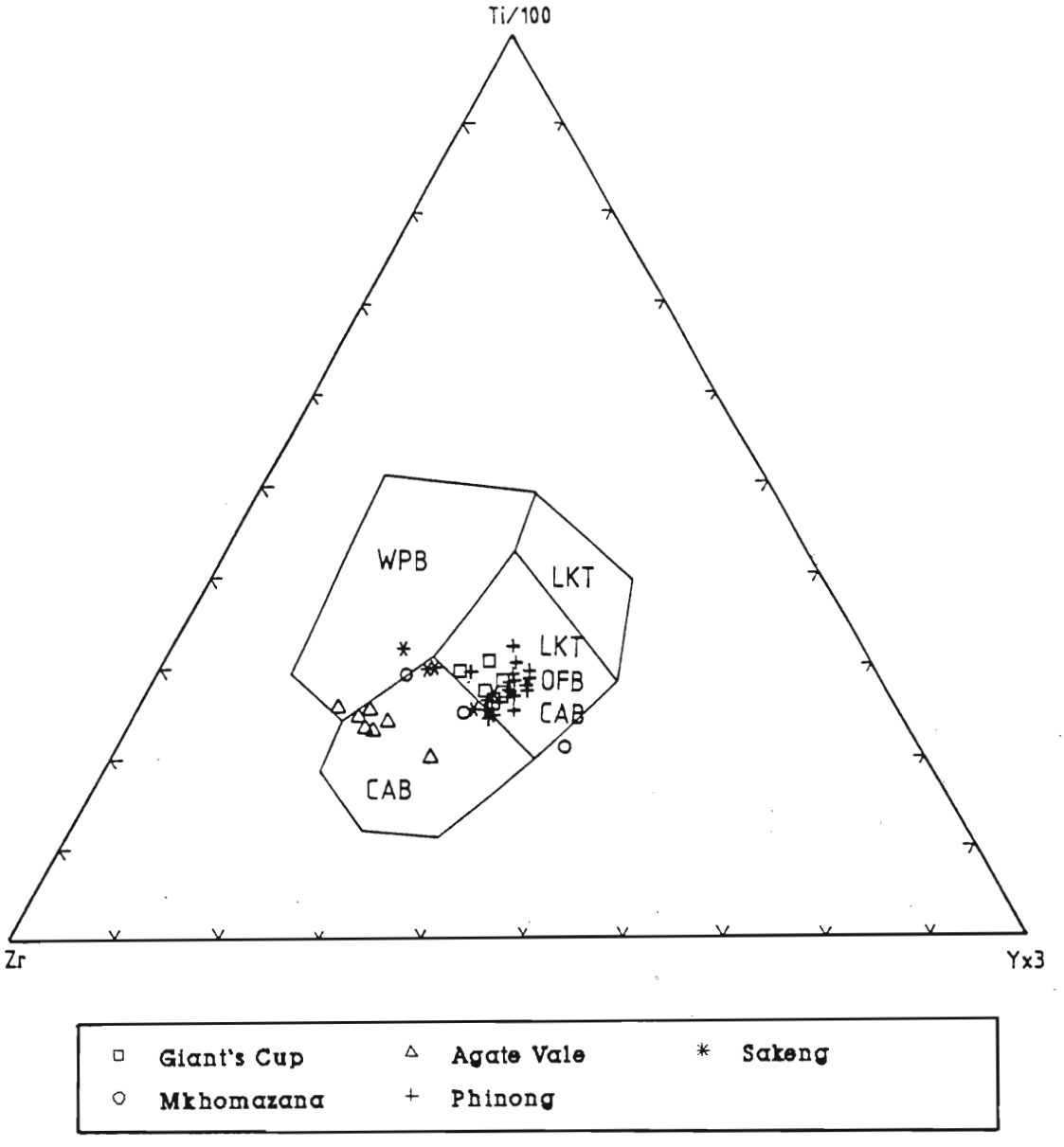

Fig. 7.5 Ti-Zr-Y discriminant diagram for the Sani Pass volcanic rocks. Only 2 samples plots in the WPB field, whilst the rest plot in the fields of CAB, OFB and LKT. Diagram after Pearce and Cann (1973). WPB = Within-plate basalts, LKT = low-potassium tholeiites, OFB = Ocean floor basalts, CAB = calc-alkali basalts.

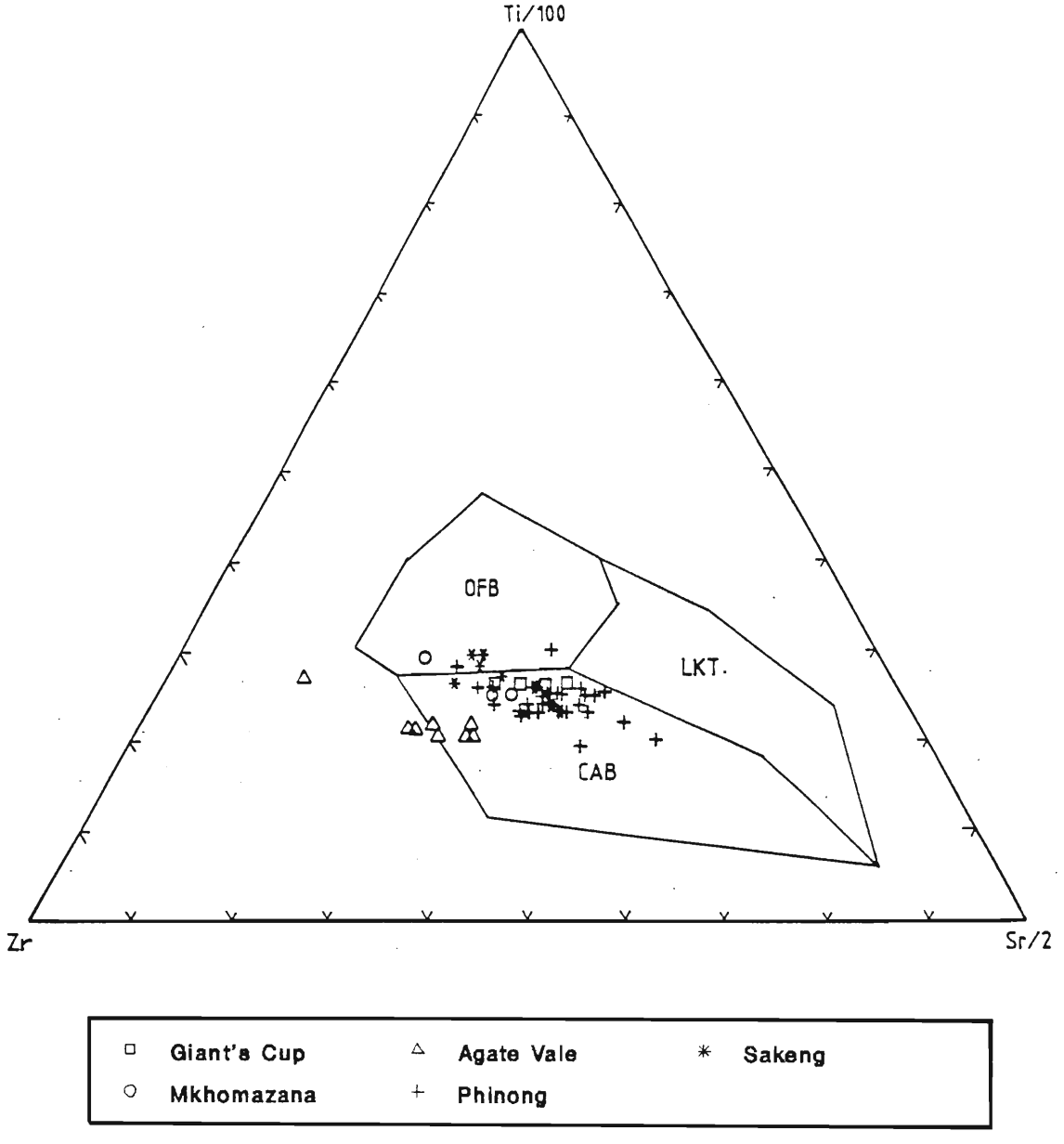

Fig. 7.6 Ti-Zr-Sr discriminant diagram for the Sani Pass volcanic rocks. The Sani Pass basalts plot predominantly in the CAB field and a few only marginally in the OFB field. This diagram is generally used for "fresh" basalts. Diagram after Pearce and Cann (1973). OFB = oceanic floor basalts, LKT = low-potassium tholeiites, CAB = calc-alkali basalts.

in the OFB field. The low Sr content in sample AV400 (70 ppm) does not permit it to plot in any of the tectonic fields delineated by Pearce and Cann's (1973) Ti-Zr-Sr diagram. Most of the Agate Vale samples, however, occupy a unique position within the CAB field.

Although Figs. 7.5 and 7.6 indicate strong similarities between the tectonic setting of CAB and the Sani Pass basalts, a more realistic comparison is achieved through the use of spidergrams that compare a more comprehensive suite of elements. Average data for the Sani Pass magma types are represented on the spidergram in Fig. 7.7 and have been normalised to an average CAB (data from Pearce, 1982). The overall pattern of these spidergrams does not indicate any distinct positive or negative trends. Instead, there is a broad compositional overlap for some elements, the Sani Pass magmas being notably enriched in the incompatible elements Nb, Zr and depleted in P and Sr. A similar comparision by Duncan (1987) indicated a strong compositional overlap between the Lesotho-type basalts and an average CAB. Also, using a similar approach Marsh (1987) concluded that the rift-related basalts of the Lebombo and Etendeka areas are somewhat enriched over the Lesotho-type, but lack any consistent and distinctive anomalies which would serve to distinguish them from the "a-tectonic" Lesotho basalts. Therefore the similarity between the Sani Pass basalts and the calc-alkali basalts indicates that the source areas for these basalts must be compositionally similar in certain aspects and have been produced by partial melting under similar physical conditions. The various possibilities that can account for these similarities have been examined in detail by Duncan (1987). The first possibility is that of subduction beneath southern Africa at the time of eruption of the southern Karoo basalts, models for which have been proposed by Elliot (1975), Cox (1978) and Froidevaux and Nataf (1981). However, on the basis of geological relationships, isotope characteristics and fractionation trends, Duncan (1987) showed that the Karoo basalts were not directly related to active subduction processes. Marsh (1987) indicated that basalts erupted in an arc environment are geochemically distinct with regard to negative Nb, Hf, and Zr and positive Sr anomalies compared to the average Lesotho basalt. Other models that were examined dealt with the addition of a subduction component to the subcontinental lithosphere by accretion (Cox, 1983; Hawksworth *et al.*, 1984) convective roll (Froidevaux

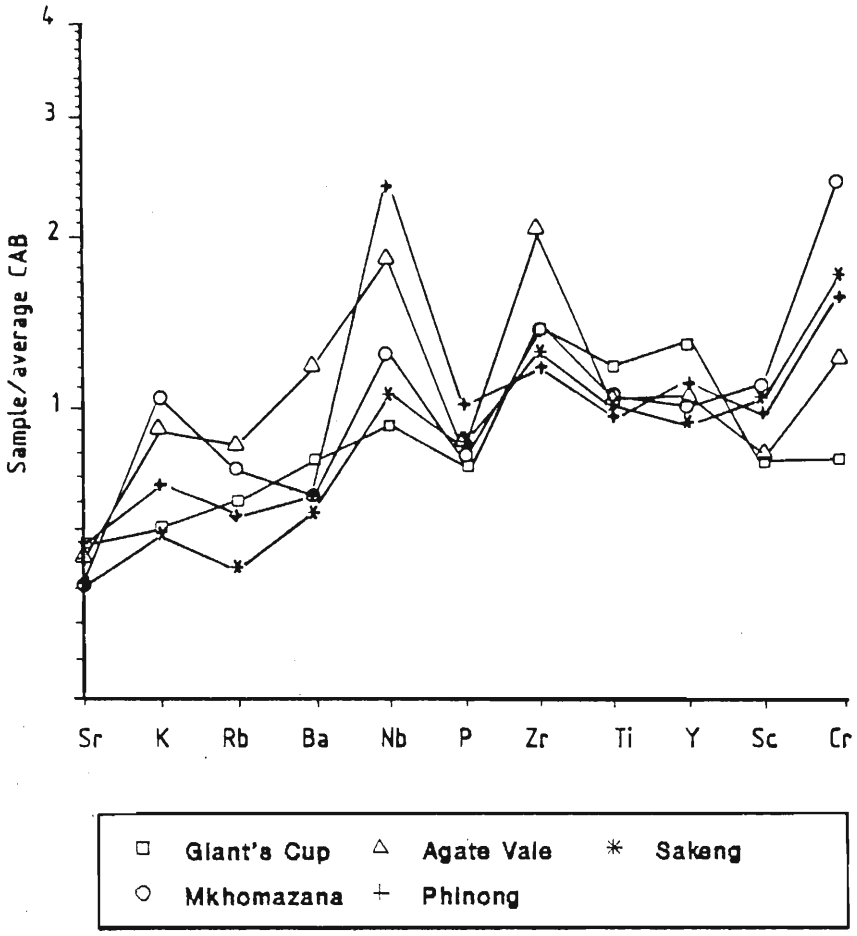

Fig. 7.7 Spidergram illustrating average Sani Pass magma compositions normalised to a calc-alkali basalt composition (normalizing data from Pearce, 1982).

and Nataf, 1981) and buoyancy contrasts of Ringwood's (1982) CAB megaliths stored at the 650 km discontinuity. As a third possibility Duncan (1987) suggested that "mantle metasomatism" (Duncan *et al.*, 1984b; Hawksworth *et al.*, 1984; Erlank *et al.*, 1984) produced the CAB character of the source areas which produced the southern Karoo basalts.

Both Duncan (1987) and Marsh (1987) concluded that the geochemistry of flood basalts reflects the composition of their sources and to quote Marsh (1987) "The influence of tectonics lies in the way volcanism is given access to the sources". The use of the empirically derived tectonomagmatic geochemical discriminant diagrams is, in essence, a better indicator of source characteristics, rather than tectonic environment, unless a specific source area is exclusive to a particular tectonic environment. Therefore an assessment of tectonic environment in which basalts were erupted cannot be done purely on the basis of geochemistry. It is therefore pertinent to conclude that application of the Ti-Zr-Y and Ti-Zr-Sr diagrams to basalts from the Sani Pass succession, in order to determine their tectonic environment in which they were erupted is erroneous.

7.8. Summary

The basalts and the dolerites of the Sani Pass basaltic successions are characterized in terms of various chemically-based classification diagrams.

The basalt tetrahedron, based on normative mineralogy, classifies the majority of the Sani Pass basalts and dolerites as oversaturated tholeiites and twelve samples as olivine tholeiites (Fig. 7.1). The compositional differences of the various magma types are reflected in the basalt tetrahedron, with the plane of silica saturation forming an effective boundary between the Giant's Cup, Agate Vale and Sakeng magma types and dolerites on the quartz-oversatursated side, and the more alkali-enriched Mkhomazana magma type on the olivine side. The Phinong magma type with its larger compositional variability straddles the plane of silica saturation, and shows a good correlation with the average Lesotho-type basalts.

The predominantly subalkaline character of the Sani Pass basalts is reflected in the alkali-silica diagram (Fig. 7.2). Using Irvine and Baragar's (1971) subdivision only sample

AV400 is alkaline, however, samples GC350, M150, M160 and AV400 become alkaline using MacDonald's (1968) subdivision.

In terms of the alumina-anorthite discriminant diagram (Fig. 7.3), samples GC350 and P178 and the Mkhomazana type basalts plot in the calc-alkaline field, while the remaining samples are characterized as tholeiitic.

The calc-alkaline affinity of the Mkhomazana magma type is further shown on the AFM diagram (Fig. 7.4), while the tholeiitic nature of the other magma types is also indicated. The Phinong and most of the Agate Vale type basalts follow a trend of slight iron enrichment, the Main trend of Nockolds and Allen (1956), while greater iron enrichment is indicated by the Giant's Cup type basalts and the dolerites.

The geochemically-based tectonic discriminant diagrams, namely, Ti-Zr-Y and Ti-Zr-Sr diagrams (Figs. 7.5, 7.6 and 7.7), indicate that the Sani Pass basalts were erupted in a CAB environment, whilst a Sani Pass data-based spidergram normalised to CAB, reflects the similarity between the CAB and Sani Pass basalts. However, the fact that no conclusive evidence exists to suggest a CAB or subduction environment, during eruption of the Sani Pass volcanics, renders these geochemically-based discriminant diagrams unreliable for classifying tectonic environment during eruption of these basalts.

CHAPTER 8

8. WHOLE-ROCK MAJOR AND TRACE ELEMENT GEOCHEMISTRY

8.1. Introduction

Major and trace element variations in the Sani Pass basalts and dolerites are illustrated by means of oxide variation diagrams in Figs. 8.2a-i; 8.3a-n. The various magma types are discriminated on the basis of major and trace element geochemistry, and any significant trends associated with differentiation are elucidated. In addition, selected major and trace elements are plotted against stratigraphic height. Samples suspected to be altered have been deliberately included in this discussion, in order to evaluate the elemental effects of alteration.

New major and trace element data are presented for 67 basalts (Appendix 2, Table A2.4) and 8 dolerites (Appendix 2, Table A2.5) from the Sani Pass area. The analyses were performed by X-ray fluorescence spectrometry, analytical techniques and spectrometer readings for which are described in Appendix 2. FeO and CO_2 concentrations have been determined by wet chemical methods (Appendix 2, Tables A2.2 and A2.3). All major element data used in the following discussion are anhydrous values, normalised to 100%, unless otherwise stated, and are tabulated in Appendix 2, Tables A2.4 and A2.5. A Fe_2O_3/FeO ratio of 0.2 has been used in calculating these normalised data.

8.2. Major Element Geochemistry

8.2.1. Introduction

In the following discussion, the Sani Pass magma types are characterized in terms of the major element geochemistry, using SiO_2 as the abscissa, an approach adopted by Mitchell

(1980). In contrast, numerous previous workers have used MgO as an index of differentiation (for example: Cox *et al.*, 1967; Robey, 1976; Pemberton, 1978; Bristow, 1980; Sweeney, 1988).

8.2.2. SiO_2

The reasons for using SiO_2 as a variable against which other major oxides of the Sani Pass are plotted are:

(1) Marsh and Eales (1984) indicated that silica is relatively stable and little affected by alteration,

(2) assuming then that silica is immobile during alteration, its use as the abscissa in the succeeding diagrams serves as an index of differentiation, and

(3) a histogram of silica frequency indicates two peaks, one for the pre-Phinong basalts at 54 weight percent and the other for the Phinong basalts at 52 weight percent (Fig. 8.1).

The frequency distribution of SiO_2 (Fig. 8.1), as well as the variation diagrams depicted in Figs. 8.2a-i and 8.3a-n, indicate that the majority of the Phinong basalts are less silicic (49.81 to 53.08 weight percent) than the pre-Phinong basalts (47.51 to 56.59 weight percent). The large range in the silica content exhibited by the pre-Phinong basalts is due, in part, to the variability of the Giant's Cup samples that have silica ranging from 47.51 to 56.59 weight percent.

The variability of silica in the Giant's Cup basalts might be related to the presence of amygdales. Sample GC360, which has SiO_2 = 56.59 weight percent has a large proportion of quartz-filled amygdales, while sample GC350, similarly, has a large proportion of calcite amygdales. In the latter sample, the large amount of calcite which is reflected by the amount of CO_2 (8.95 weight percent), is causing the low SiO_2 (47.51 weight percent) in this sample. Sample AV400, which is the basal flow of the Agate Vale magma type, and overlies sediments, also has a low SiO_2 content (48.29 weight percent). Like sample GC350, this sample has a large proportion of calcite (CO_2 = 5.65 weight percent) which

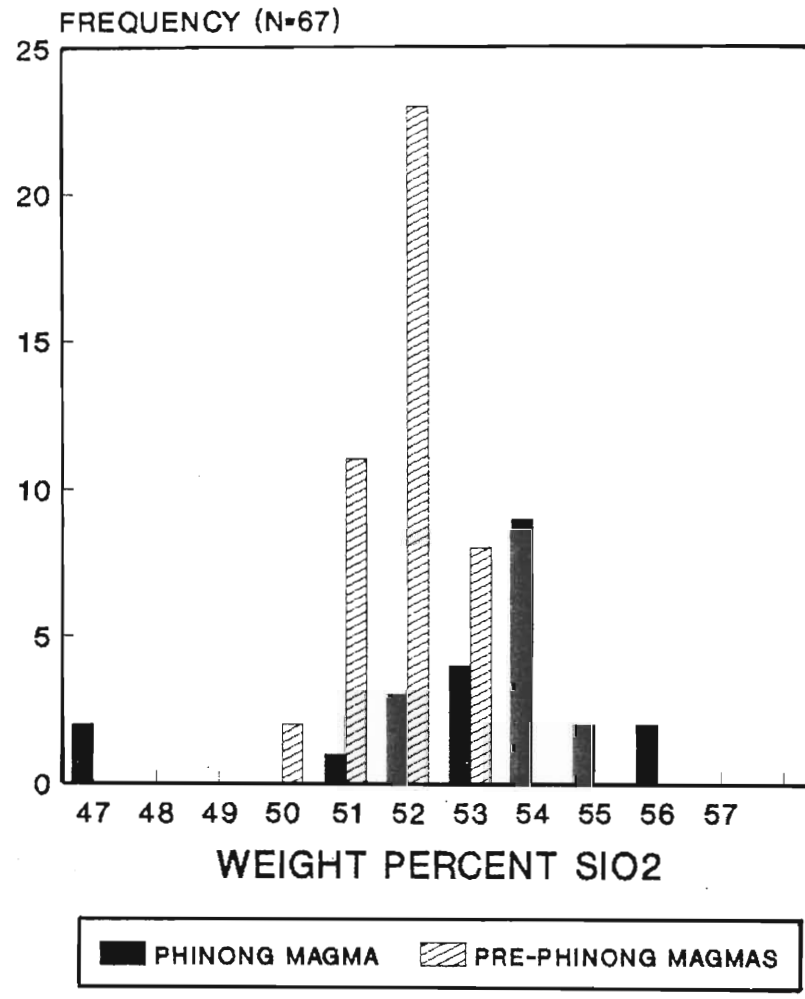

Fig. 8.1 A histogram of silica frequency, indicating two peaks, namely, one for the Phinong basalts and the other for the pre-Phinong basalts. The Phinong basalt peak occurs at 52 weight percent and that for the pre-Phinong basalts at 54 weight percent.

is responsible for its low silica content. Although the higher silica in the pre-Phinong basalts might be a reflection of the presence of quartz-filled amygdales, quartz has been detected, albeit sparsely, as a groundmass constituent. This feature is totally absent in the Phinong samples.

Sample P174, which is the basal flow of the Phinong basalts also has a low SiO_2 content (49.49 weight percent), which is accompanied by a slightly higher CO_2 content, compared to the remaining Phinong basalts. Although sample P180 is characterized by a low silica content (49.76 weight percent), this sample is suspected to have experienced cumulus enrichment of ferromagnesian minerals, which would account for its depleted silica content.

8.2.3. TiO_2

TiO_2 content in the Sani Pass basalts and dolerites ranges between 0.68 and 1.32 weight percent, with most of the samples occurring in the range 0.8 to 1.2 weight percent (Fig. 8.2a). Enrichment/depletion trends between and within magma types are lacking.

The Giant's Cup magma type has the highest TiO_2 content (1.04 to 1.32 weight percent) compared to all other magma types in the Sani Pass. The highest concentration of TiO_2 is in samples GC350 (1.26 weight percent) and GC380 (1.32 weight percent). In both these samples, the TiO_2 enrichment is indicated by high modal ilmenite laths in sample GC350, and a combination of ilmenite laths and exsolved ilmenite in sample GC380. The ilmenite laths in sample GC380 might be due to the presence of microxenoliths derived from the underlying flows.

Slight TiO_2 enrichment is present in the basal sample of the Agate Vale magma type (AV400, TiO_2 = 1.14 weight percent), compared to the underlying flows constituting this magma type. These flows are rather restricted in terms of TiO_2 concentrations, in the range 0.96 to 1.09 weight percent. TiO_2 in sample AV400, like sample GC350, occurs in the abundant ilmenite laths.

TiO_2 within the Sakeng basalts is present mainly in the form of ilmenite exsolutions, and varies in its concentration from 0.85 weight percent in the lowest flow (S120) to 1.09 weight

percent in sample S131. The low TiO_2 content in sample S120 is accompanied by a slightly higher MgO content (7.30 weight percent) and lower P_2O_5 (0.10 weight percent) and alkalies (1.75 weight percent) than the remaining basalts belonging to this magma type.

The Mkhomazana basalts are marked by TiO_2 contents restricted in the range 0.98 to 1.04 weight percent. This magma type shows the least variation in TiO_2 content compared to the other Sani Pass magma types.

Except for sample P180, the TiO_2 contents for the Phinong basalts varies between 0.84 and 1.12 weight percent. Sample P180 has the lowest TiO_2 content (0.68 weight percent) and cumulus enrichment of olivine is suspected in this sample. Sample P227 which has experienced cumulus enrichment of olivine also has a low TiO_2 content (0.89 weight percent). Most of the Phinong basalts have TiO_2 concentrations marginally less than 1.0 weight percent, but those exceeding 1.0 weight percent include the five uppermost flows of this unit. Generally, ilmenite exsolutions in the Phinong basalts account for the TiO_2 concentration.

Four dolerite samples have TiO_2 contents less than 1.0 weight percent (0.97 to 0.99 weight percent) and therefore plot in the range for most of the Phinong basalts. The remaining four dolerite samples are marginally more enriched in TiO_2, varying between 1.09 and 1.17 weight percent.

8.2.4. Al_2O_3

Depletion/enrichment trends are lacking in terms of Al_2O_3 concentrations in the Sani Pass basalts and dolerites (Fig. 8.2b). In the Giant's Cup basalts Al_2O_3 contents vary from 14.81 to 16.51 weight percent, the highest content being in sample GC350 which rests directly on the Clarens Formation sandstones. Similarly, a high Al_2O_3 content is seen in sample AV400, the basal Agate Vale basalt (Al_2O_3 = 16.70 weight percent). Al_2O_3 contents for this magma type varies from 15.26 to 16.70 weight percent. Al_2O_3 in the Sakeng basalts is rather constrained, in the range 15.47 to 15.97 weight percent. Similarly, Al_2O_3 in the Mkhomazana basalts is restricted in the range 15.50 to 16.07 weight percent. In terms of

Al_2O_3 contents, the Phinong basalts show the largest variability, from 13.55 to 16.73 weight percent. This variability reflects, in part, a modal effect. For example, sample P227 is enriched in cumulus olivine and therefore has less plagioclase, which accounts for its low Al_2O_3 content (13.54 weight percent).

The dolerites vary in Al_2O_3 contents from 14.62 to 15.75 weight percent, this variation being over a restricted SiO_2 content (51.96 to 52.94 weight percent). These intrusives have a lower Al_2O_3 content than most of the Phinong basalts.

8.2.5. Total iron

Total iron content for the Sani Pass magma types shown in Fig. 8.2c is represented as $Fe_2O_3(t)$. The $Fe_2O_3(t)$ content for the different Sani Pass magma types, in general, is highly variable and does not indicate any distinct enrichment/depletion trends.

Total iron content in the Giant's Cup basalts increases from 10.25 weight percent in the basal flow (GC350) to 12.33 weight percent in the uppermost flow (GC380). This trend of increasing iron content with time, is due to similar trends in the Fe_2O_3 and FeO contents for these flows.

The Agate Vale basalts exhibit a trend of decreasing $Fe_2O_3(t)$ with increasing SiO_2 content. However, sample AV400 falls off this trend due to its low silica content. Consecutive flows do not show increasing iron content. The Agate Vale basalts vary in their total iron content, from 10.10 to 12.01 weight percent.

Basalts belonging to the Sakeng geochemical unit contain very variable $Fe_2O_3(t)$, ranging from 9.74 to 11.42 weight percent. Less variation, however, is shown by the Mkhomazana basalts, which contain 10.10 to 10.71 weight percent total iron.

The Phinong basalts occupy a compositional field, ranging from 10.17 to 12.45 weight percent. Sample P227 has the highest total iron content because of its enrichment in ferromagnesian minerals, and consequently its high FeO content (9.49 weight percent). Other samples that show a slight enrichment in $Fe_2O_3(t)$, compared to the remaining basalts, are four samples that occur in the upper part of the stratigraphic succession. These are P272

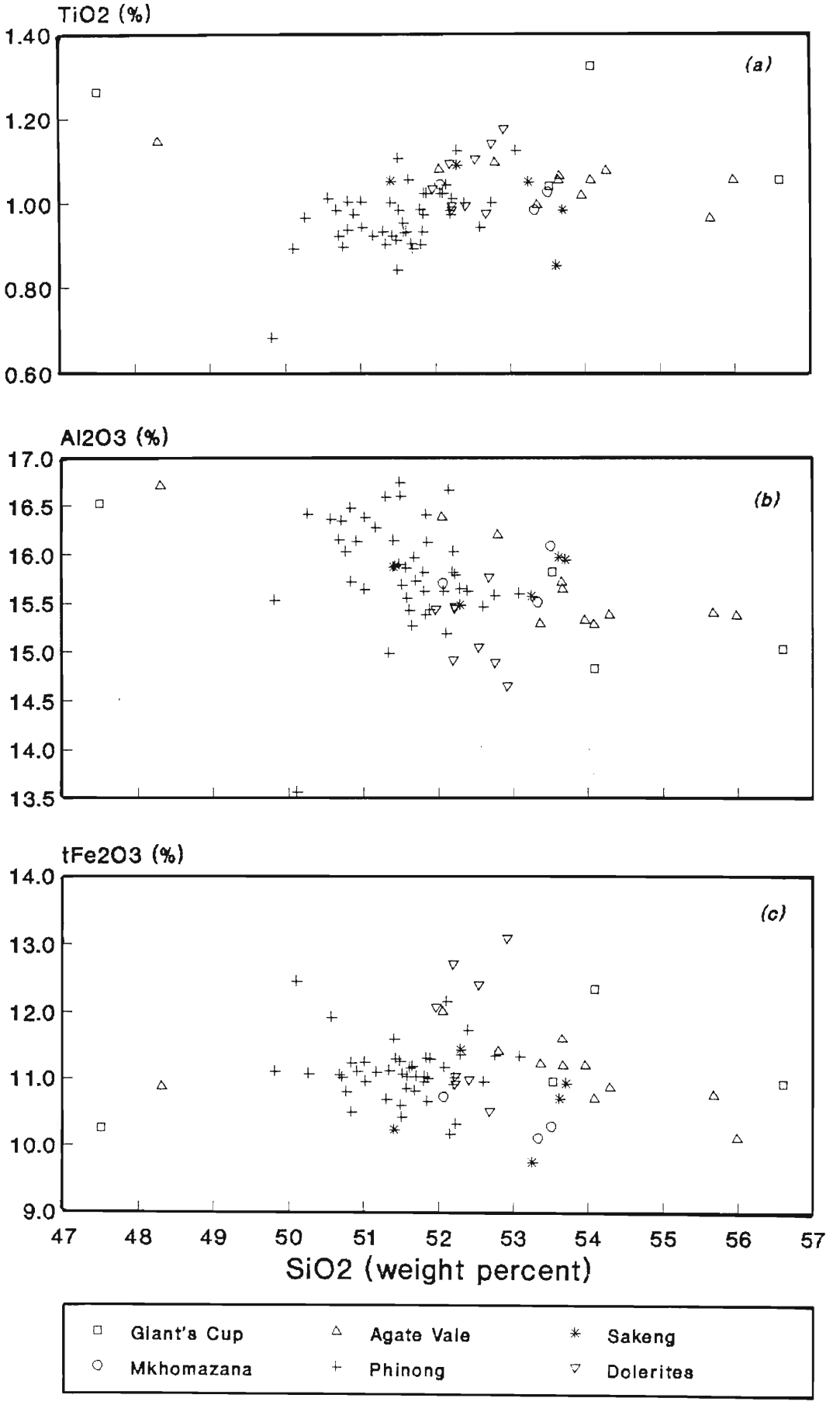

Fig. 8.2a-c SiO_2 variation diagrams for TiO_2, Al_2O_3, and $Fe_2O_3(t)$ in the Sani Pass basalts and dolerites.

(12.15 weight percent), P273 (11.72 weight percent), P276 (11.58 weight percent) and P277 (11.92 weight percent).

The dolerites show a slightly larger variation in Fe_2O_3(t) contents (10.49 to 13.06 weight percent) than the basalts from the Sani Pass. Four dolerite samples (D10, D30, D41 and D80) are more iron enriched (12.68, 13.06, 12.38 and 12.05 weight percent, respectively) than most of the Sani Pass basalts. The remaining four dolerite samples, however, plot in the range 10.49 to 11.01 weight percent and within the compositional field of the Phinong basalts.

8.2.6. MnO

Compositional diversity in the Sani Pass magma types is rather restricted in terms of MnO contents and they do not show any enrichment or depletion trends (Fig. 8.2d). An exception, however, is the Giants Cup magma type which shows a trend of decreasing MnO contents with increasing SiO_2 contents. The MnO content in these basalts varies from 0.13 to 0.21 weight percent. The basal flow (GC350) has the highest concentration of MnO (0.21 weight percent), compared to the overlying flows.

The Agate Vale basalts show the largest variation in MnO content, compared to the other Sani Pass magma types, ranging from 0.12 to 0.25 weight percent. Like the basal flow of the Giant's Cup magma type, the lower most flow of the Agate Vale (AV400) has the highest MnO content (0.25 weight percent), compared to the later flows.

The Sakeng basalts have variable MnO, in the range 0.12 to 0.18 weight percent. Less variation is indicated by the Mkhomazana basalts which contain 0.15 to 0.18 weight percent MnO.

Except for samples P174 and P183, MnO contents in the Phinong basalts is rather restricted (0.15 to 0.19 weight percent). Samples P174 and P183 contain 0.22 and 0.20 weight percent MnO, respectively with P174 being the basal flow to the Phinong basalts.

The dolerites do not show any enrichment or depletion patterns, having MnO contents

between 0.16 and 0.20 weight percent. Marginal enrichment in MnO is shown by samples D10 (0.19 weight percent), D30 (0.20 weight percent), D41 (0.20 weight percent), and D80 (0.20 weight percent).

8.2.7. MgO

There is a subdued overall trend of decreasing MgO with increasing SiO_2 content in the basalts of the Sani Pass succession (Fig. 8.2e). Two major exceptions to this trend are GC350, the basal flow of the Giant's Cup magma type (SiO_2 = 47.46 weight percent; MgO = 3.15 weight percent), and AV400, the basal flow of the Agate Vale magma type (SiO_2= 48.12; MgO = 4.58 weight percent). In both these samples, MgO contents are extremely low relative to particularly low SiO_2 contents. Notably, GC350 is from a flow extruded directly onto the Clarens Formation sediments. Similarly AV400, at the base of the Agate Vale sequence, was extruded onto sediments deposited in a period of quiescence between the Giant's Cup and Agate Vale eruptive periods.

Excluding GC350, the remaining three samples of the basal Giant's Cup magma type fall on the general MgO depletion trend. They are, however, extremely SiO_2-enriched and MgO-depleted relative to the overlying magma types. They all contain more than 53.5 weight percent SiO_2 and, with the exception of GC370, contain less than 5 weight percent MgO. They therefore fall outside the range (5 to 8 weight percent MgO) that Eales and Marsh (1979) regarded as characteristic of non-fractionated Karoo Central Province basalts.

With the exception of the basal sample (AV400), the Agate Vale basalts fall within less than one standard deviation of their mean MgO content of 6.22 weight percent. Overlying the Agate Vale flows, the Sakeng basalts are relatively MgO-rich (all in excess of 6.5 weight percent MgO). Above the Sakeng basalts, the three flows of the Mkhomazana type are even more magnesian, all exceeding 7.1 weight percent MgO.

The Phinong lavas are broadly more MgO-rich, and less SiO_2-rich, than the underlying lavas. Occasional excessively high MgO contents in the Phinong lavas (e.g. in samples

P180 and P227, where MgO is in excess of 11.0 weight percent) are accompanied by high nickel contents, indicating cumulus olivine enrichment, as suggested by Eales and Marsh (1979), rather than primary Mg-rich magmas, as postulated by Cawthorn (1980) and Cawthorn *et al.* (1988) for parts of the Insizwa intrusion. A quantitive assessment of cumulus olivine enrichment in sample P227 is given in section 5.2.

8.2.8. CaO

CaO contents in the Sani Pass basalts and dolerites do not show any systematic variation with the SiO_2 contents (Fig. 8.2f), and are generally scattered. Most of the samples plot in the range 8.0 to 12.0 weight percent CaO. The earliest flow of the Giant's Cup magma type (sample GC350) shows extreme enrichment in CaO (18.06 weight percent), which is due to calcite preserved in the amygdales. The remaining three samples contain 10.23 to 11.80 weight percent CaO. They also contain correspondingly low CO_2 (4.91 to 0.03 weight percent), compared to sample GC350 (CO_2 = 8.95 weight percent).

The Agate Vale basalts occupy a CaO compositional field (6.85 to 10.51 weight percent) lower than that for the Giant's Cup, Sakeng, and Phinong magma types and dolerites. Within this magma type, sample AV400 has the highest CaO content (10.51 weight percent), a proportion of which indicates secondary calcite contained in the amygdales, since the high CaO content is accompanied by a high CO_2 content (5.65 weight percent). Samples AV60 and AV91, on the other hand show the lowest CaO content (6.85 and 8.84 weight percent, respectively), accompanied by the highest SiO_2 content (55.67 and 55.99 weight percent, respectively), within the Agate Vale magma type.

The Sakeng basalts show a rather poorly developed negative trend, and less variability in their CaO content than the remaining pre-Phinong basalts. Their CaO content varies between 10.44 and 12.04 weight percent, accompanied by a CO_2 content of 0.24 to 1.90 weight percent.

The Mkhomazana magma type is relatively depleted in CaO compared to the remaining magma types in the Sani Pass. Only samples AV60 and AV91 fall in the CaO range of the

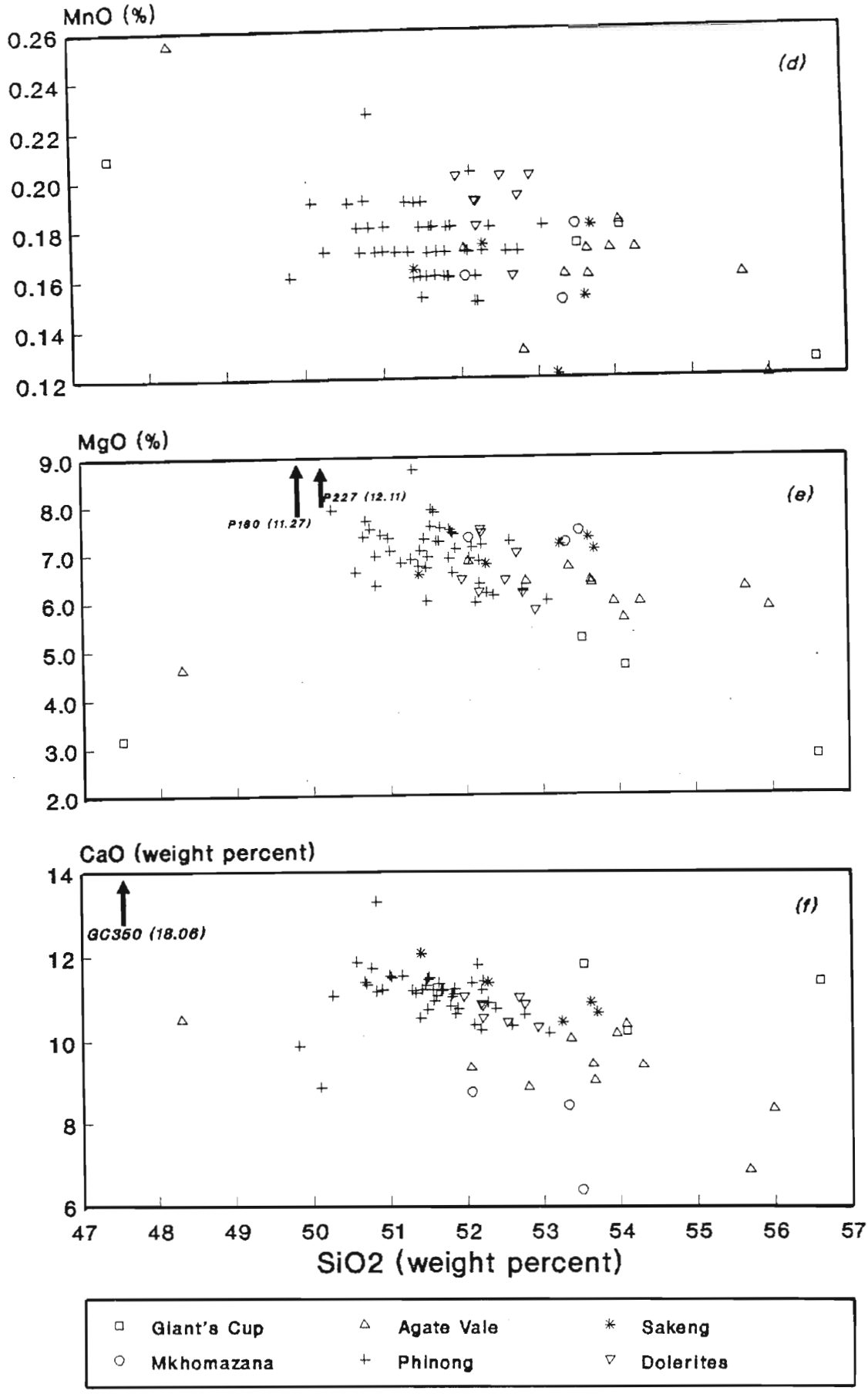

Fig. 8.2d-f SiO_2 variation diagrams for MnO, MgO and CaO in the Sani Pass basalts and dolerites.

Mkhomazana basalts, which is 6.36 to 8.73 weight percent.

Most of the Phinong basalts have a CaO content ranging from 10.19 to 11.86 weight percent. Plotting out of this range are three samples, namely P174, P180 and P227. Sample P174, which is the basal flow of the Phinong basalts has CaO = 13.29 weight percent, accompanied by CO_2 = 2.68 weight percent. The high CaO content of this sample is, therefore due to a proportion of calcite being present in the amygdales. Samples P180 and P227, which are suspected to have experienced cumulus enrichment of ferromagnesian minerals and which could reduce the CaO contents, accordingly yield the lowest CaO concentrations (9.87 and 8.84 weight percent, respectively).

The dolerite samples show the least variability in their CaO content, ranging from 10.30 to 11.04 weight percent. They occupy a coherent field within the compositional range of most of the Phinong basalts.

8.2.9. Na_2O

There are no obvious trends of enrichment or depletion of Na_2O (Fig. 8.2g). With the exception of the basal flow GC350 (Na_2O = 3.40 weight percent), the Giant's Cup lavas have Na_2O contents tightly grouped in the range 2.16 to 2.46 weight percent.

At the base of the succeeding Agate Vale basalt succession, sample AV400 displays an uncommonly low Na_2O content (1.07 weight percent). The remainder of the Agate Vale basalts group in the range 2.15 to 2.91 weight percent Na_2O.

The five Sakeng basalt samples group in the range 1.66 to 2.11 weight percent Na_2O, making them the least sodic of any of the pre-Phinong basalt types, with the exception of AV400. The three samples of the uppermost pre-Phinong basalt type, the Mkhomazana, are notable for their exceptionally high Na_2O contents, in the range 4.15 to 4.51 weight percent.

With the exception of sample P178, near the base of the sequence, the Phinong basalts occupy a relatively limited range of compositions, from 1.63 to 2.74 weight percent Na_2O. Occurring in this compositional field, but having a more restricted range are the dolerite samples from the Sani Pass which contain 2.20 to 2.46 weight percent Na_2O.

8.2.10. K_2O

The K_2O contents of the basalts of the Sani Pass do not behave in sympathy with the Na_2O contents. Although no linear trends are present, there are certain significant features in the behaviour of K_2O.

The Giant's Cup basalts all have extremely low K_2O contents (less than 0.54 weight percent), with the exception of the uppermost sample (GC380: 0.84 weight percent K_2O). Even the basal flow, GC350, contains only 0.35 weight percent K_2O, which contrasts with its high Na_2O content (3.40 weight percent).

The Agate Vale basalts indicate a large compositional range in terms of K_2O concentrations, varying from 0.40 to 7.32 weight percent. The basal Agate Vale flow shows extreme enrichment in K_2O contents (7.32 weight percent) which is accompanied by similarly high Rb (109 ppm) and Ba (868 ppm) concentrations. Enrichment in these LILEs is compatible with the presence of biotite, none of which could be identified petrographically. Seven Agate Vale samples are enriched in K_2O (0.99 to 7.32 weight percent) relative to the remaining basalts (except P227 and M150) and dolerites in the Sani Pass.

The Sakeng basalts group in the range 0.10 to 0.74 weight percent K_2O. The basal flow of this geochemical unit has an extremely low K_2O content of 0.10 weight percent, accompanied by virtually no Rb and very little Ba (51 ppm). In contrast, the basal flow of the succeeding Mkhomazana basalts is enriched in K_2O (1.70 weight percent), Rb (43 ppm) and Ba (468 ppm). The remaining two flows in this magma type have K_2O = 0.53 and 0.78 weight percent.

The Phinong basalts generally contain more than 0.30 weight percent K_2O, but generally not exceeding 1.00 weight percent. An exception, however, is sample P227 which contains 1.13 weight percent K_2O, and also contains the least Na_2O (1.63 weight percent) amongst the Phinong basalts. K_2O contents are least variable in the dolerite samples, occupying a rather restricted compositional range of 0.47 to 0.62 weight percent K_2O.

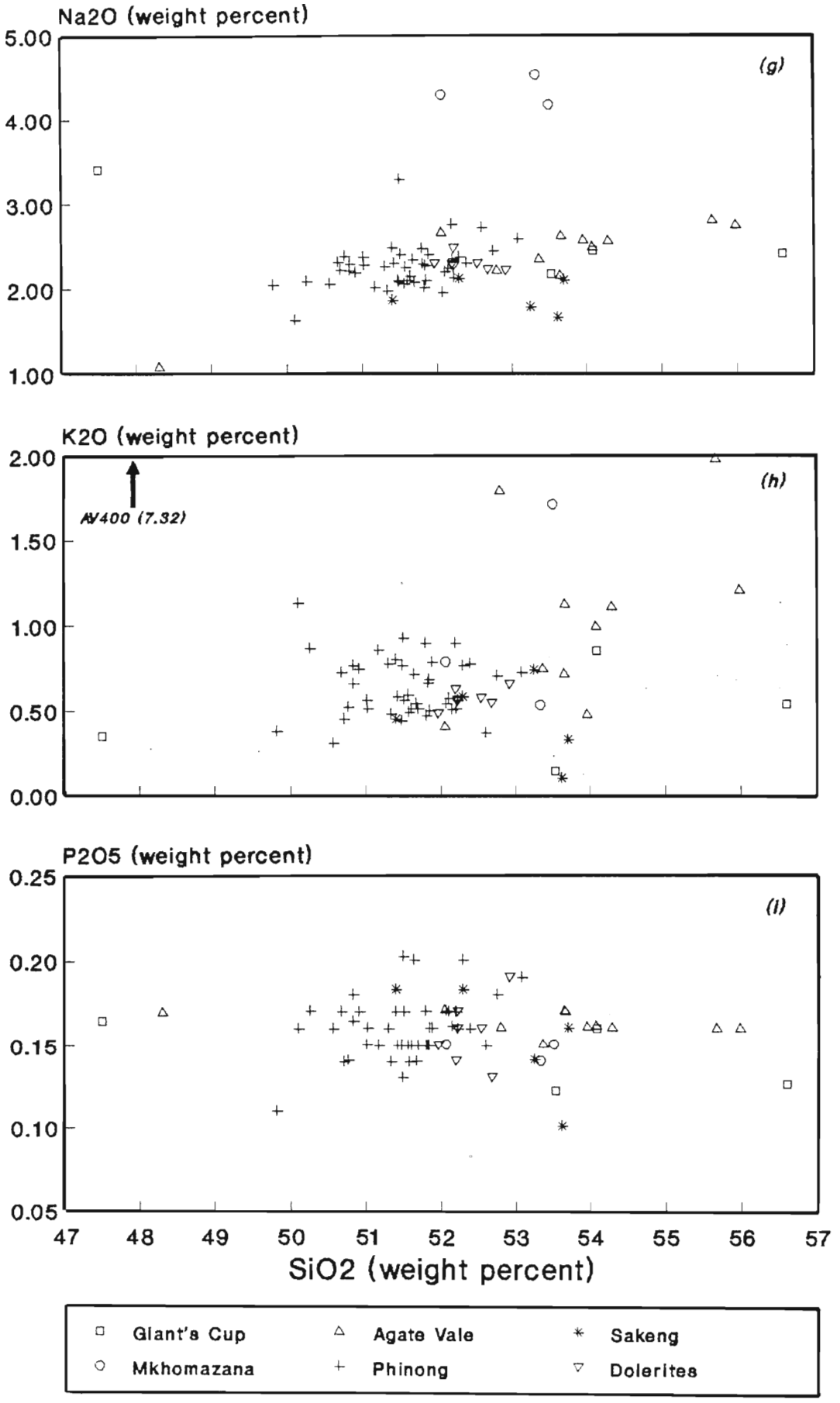

Fig. 8.2g-i SiO_2 variation diagrams for Na_2O, K_2O and P_2O_5 (weight percents) in the Sani Pass basalts and dolerites.

8.2.11. P_2O_5

P_2O_5 contents in the Sani Pass basalts are generally scattered, and consequently do not show any linear trends (Fig. 8.21). The intermediate flows in the Giant's Cup geochemical unit (GC360 and GC370) contain less P_2O_5 (0.12 weight percent), than the flows above (GC380, P_2O_5 = 0.16) and below (GC350, P_2O_5 = 0.16).

The Agate Vale basalts are tightly grouped in terms of their P_2O_5 content, which ranges from 0.15 to 0.17 weight percent. The succeeding Sakeng basalts, however, show greater variation in P_2O_5, ranging from 0.10 to 0.18 weight percent. The least P_2O_5 is contained within the basal Sakeng flow. The Mkhomazana basalts show the least variability in P_2O_5 contents, and are restricted in the range 0.14 to 0.15 weight percent.

Except for the Sakeng magma type, the remaining pre-Phinong basalts are generally restricted in their P_2O_5 contents, compared to the Phinong basalts. These latter basalts contain P_2O_5 varying from 0.10 to 0.20 weight percent, the least P_2O_5 being contained in sample P180. In terms of P_2O_5 contents, the dolerites range from 0.13 to 0.19 weight percent, and plot in the compositional field of the Phinong basalts.

8.3. Trace Element Geochemistry

8.3.1. Introduction

Trace element variations are represented diagrammatically in a similar manner to the major elements, using SiO_2 as the abscissa on the variation diagrams (Figs. 8.3a-n). Unnormalised trace element data for the Sani Pass basalts and dolerites are presented in Tables A2.4 and A2.5, respectively (Appendix 2). Since this chapter is purely descriptive, the theoretical aspects of trace element modelling are discussed in Section 10.3. However, factors controlling the distribution of various trace elements are discussed where relevant.

8.3.2. Strontium (Sr)

Strontium is divalent and has an ionic radius (1.18Å) intermediate between Ca (0.99 Å) and K (1.33 Å). It is, therefore, mainly distributed in Ca-rich minerals such as plagioclase, clinopyroxene and apatite, and high-temperature K-bearing minerals, such as K-feldspar and feldspathoids. In the basaltic assemblage Sr would readily distribute into plagioclase (Table A5.1, Appendix 5). Thus, Sr contents would enrich in a differentiating system, only as long as plagioclase is not a fractionating phase.

Generally, the Sr data for the Sani Pass basalts and dolerites display a scatter of values (Fig. 8.3a). In detail, however, the Giant's Cup basalts indicate a very diffuse negative correlation, in the range 175 to 238 ppm. In contrast to the basal flow of the Giant's Cup magma type, which has the highest Sr content in this unit (238 ppm), the basal Agate Vale flow (AV400) has the lowest Sr content (70 ppm). The remaining flows within the Agate Vale unit are grouped in the range 164 to 214 ppm. The overlying Sakeng basalts contain much less Sr than the Agate Vale basalts, in the range 109 to 150 ppm. The Sakeng magma type is also depleted in Sr relative to the remaining magma types, except samples M170, P247, P257, P267 and P277. The Mkhomazana basalts have very variable Sr contents, ranging from 96 to 190 ppm, whilst in the overlying Phinong magma type, Sr contents range from 112 to 248 ppm. The dolerites plot in the compositional field of the Phinong basalts, but group in a more restricted range of 166 to 214 ppm Sr.

8.3.3. Rubidium (Rb)

Rubidium is very similar to K in terms of electronegativity, ionization potential and ionic size; it therefore substitutes for K in feldspar. Rb shows a preference for substituting in K-feldspar rather than plagioclases. The low distribution co-efficient (D_{Rb}) for Rb (Table A5.1, Appendix 5), therefore indicates that Rb does not behave as a compatible element for the basaltic assemblage, and therefore, will enrich progressively in a differentiating system, if K-feldspar is not a major fractionating phase. It is noteworthy that

the total depletion of Rb in sample S12O (Sakeng magma) is reflected in its very low K_2O content of 0.1 weight percent and similarly the extremely high Rb content in sample AV400 (109 ppm) is mirrored by its high K_2O content, which is 7.29 weight percent. Although the high K_2O and Rb content in sample AV400 might be due to the presence of alkali feldspar, this effect could very well be achieved by the presence of biotite. However, neither of these minerals could be confirmed petrographically.

A comparison of Rb versus SiO_2 with K_2O versus SiO_2 (Fig. 8.2h) indicates similar patterns for the different magma types. Generally the Rb data are scattered and linear trends are lacking.

The three earliest flows in the Giant's Cup magma type contain low Rb (4 to 12 ppm), but the overlying flow (GC380) shows a slight enrichment in the Rb (24 ppm), which is also accompanied by a slightly elevated K_2O content (0.84 weight percent). Extreme enrichment in Rb (109 ppm) and K_2O (7.32 weight percent) is shown by the basal Agate Vale flow (AV400). Flows GC380 and AV400 are separated by a metasedimentary lens. Most of the succeeding Agate Vale flows are also enriched in Rb, although less so than the basal flow, compared to the remaining magma types in the Sani Pass. Sample AV80 from the Agate Vale geochemical unit is depleted in Rb (5 ppm) relative to the remainder of the Agate Vale basalts. This sample also has the lowest K_2O content (0.40 weight percent) within the Agate Vale magma type.

The Sakeng magma type is generally lower in Rb content, compared to the Agate Vale and Mkhomazana magma types. The Sakeng basalts contain Rb, in the range 0 to 16 ppm, the basal flow being completely devoid of Rb and the uppermost flow being enriched (16 ppm). The basal flow of this magma type overlies a tuffaceous lens, while the uppermost flow is succeeded by the Mkhomazana basalts, the basal flow of which shows extreme enrichment in Rb (43 ppm). The remaining two flows in the Mkhomazana magma type contain 13 and 20 ppm Rb. Rb content in the Phinong basalts does not vary systematically with SiO_2, and ranges between 6 and 28 ppm. The dolerites, however, are more constrained in terms of Rb contents varying from 12 to 15 ppm.

8.3.4. Barium (Ba)

The higher charge and similar ionic size to K makes Ba a viable substitute in potash feldspar and biotite. Ba enrichment occurs in the early-formed potassium minerals and only very limited substitution occurs in the plagioclases.

Ba content in Sani Pass basalts (Fig. 8.3c) seems to mimic the patterns shown for K_2O and Rb. The Giant's Cup basalts contain low Ba (130 to 196 ppm), except the topmost flow (GC380) which is slightly enriched (268 ppm). Similarly, the basal flow of the Agate Vale basalts is enriched in Ba (868 ppm), but two other flows (AV60 and AV70) contain more than 600 ppm Ba (670 and 751 ppm, respectively). The remaining Agate Vale flows contain 254 to 386 ppm Ba, and are all enriched relative to the remaining magma types (except samples M150, D90, P227).

The Sakeng basalts have generally, relatively low Ba (51 to 224 ppm), and there is no correlation with SiO_2 content. The lowermost sample, S120, has the lowest Ba (51 ppm), and the topmost sample (S136) has the highest (224 ppm) Ba content. However, S136 at the top of the Sakeng has significantly higher Ba than the other Sakeng samples, which is possibly due to the fact that it underlies the basal flow of the Mkhomazana magma type (M150), which has a relatively high Ba content of 468 ppm. The remaining two flows in the Mkhomazana magma type have less than half the Ba content of the basal flow (122 and 197 ppm).

The Phinong basalts do not show any correlation between Ba and SiO_2 and contain 81 to 282 ppm Ba. Generally most of the samples have below 250 ppm Ba, sample P227 (Ba = 282 ppm), being an exception. This sample is enriched in cumulus olivine (MgO = 12.13 weight percent, Ni = 188 ppm), but is also unusually rich in K_2O (1.13 weight percent), and Rb (22 ppm). The intrusives from the Sani Pass are generally constrained in the range 186 to 219 ppm Ba, except sample D90 (Ba = 377 ppm). This sample does not show a corresponding increase in K_2O (0.55 weight percent) and Rb (13 ppm).

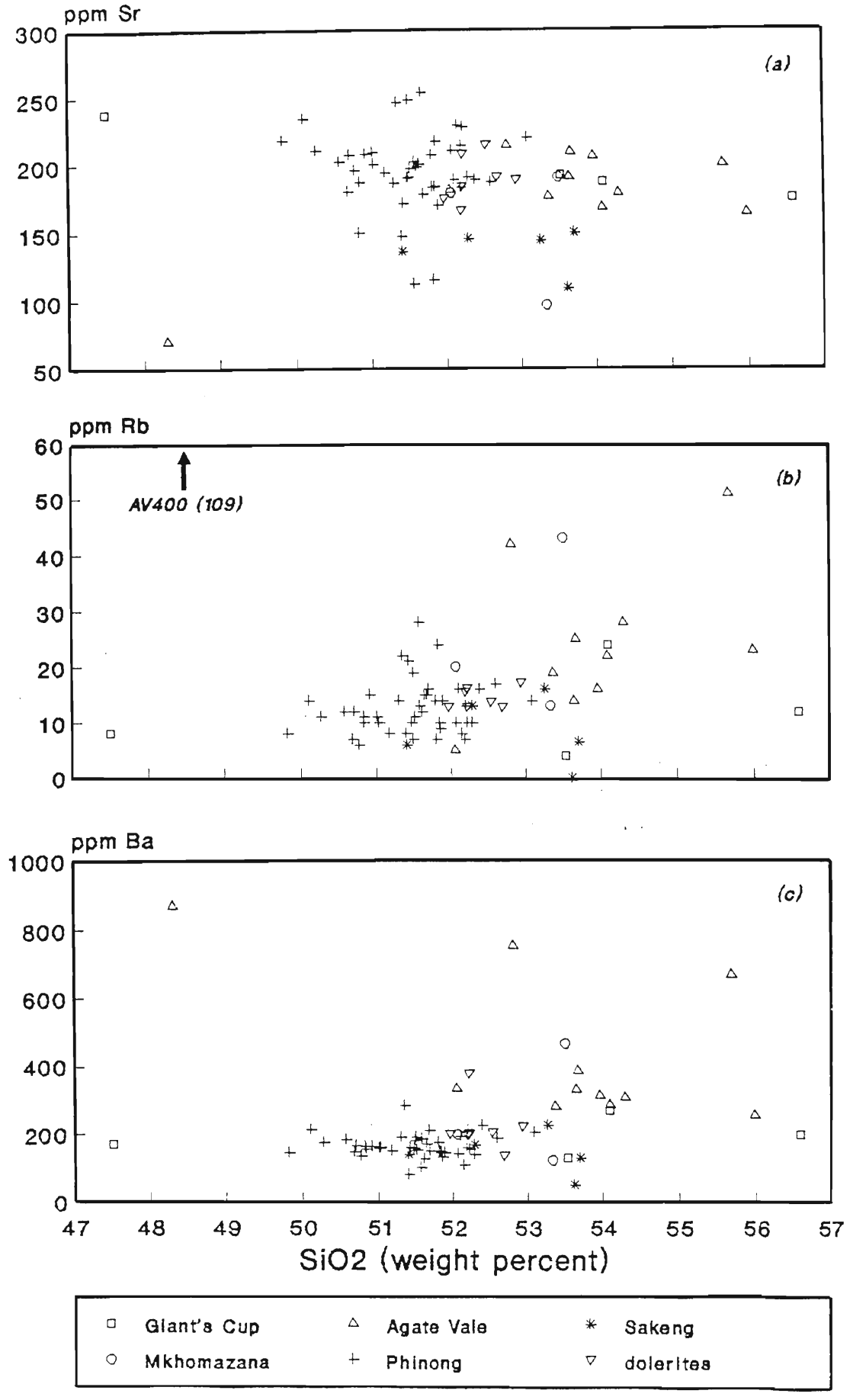

Fig. 8.3a-c SiO_2 variation diagrams for Sr, Rb, Ba (ppm)

8.3.5. Yttrium (Y)

Distribution coefficients for the basaltic assemblage indicate that yttrium is highly unlikely to distribute into any of the major fractionating phases (Table A5.1, Appendix 5). Yttrium is generally abundant in minerals of the late-fractionation stage, and since it is rejected by the early-crystallizing minerals, yttrium concentrations should increase in a progressively fractionating melt.

Yttrium data for the Sani Pass basalts and dolerites are generally scattered and do not indicate any coherent linear trends (Fig. 8.3d). Yttrium in the Giant's Cup basalts varies from 22 ppm in flow GC360 to 32 ppm in the uppermost flow (GC380). In general, most of the Agate Vale basalts contain less yttrium than the Giant's Cup basalts, in the range 16 to 24 ppm. Yttrium enrichment, however, is present in sample AV91 (32 ppm) which is a sample of pillow lava. The three lowermost flows in the Sakeng magma type, have lower yttrium (14 to 18 ppm) than the two overlying flows (25 to 27 ppm). The Mkhomazana basalts have extremely variable yttrium contents, decreasing from 43 ppm in the lowermost flow (M150) to 16 ppm in the uppermost flow (M170). The voluminous Phinong lavas show the least variation in yttrium, varying from 23 to 29 ppm (excluding sample P180). Sample P180 is depleted in yttrium containing only 19 ppm. The dolerites show a slight depletion trend, in the range 25 to 29 ppm. Plotting off this trend is sample D30, which contains 32 ppm yttrium.

8.3.6. Zirconium (Zr)

The combination of high charge and comparatively large radius (0.79Å) precludes Zr from substituting for major elements in igneous rocks. In a differentiating suite, therefore, Zr would enriched in the residual melt. It might, however, appear in a specific phase, usually zircon, which is normally a late differentiate in the crystallizing series. In the Sani Pass basalt no zircon has been identified and therefore, the concentration of Zr is inferred to be a good indicator of fractionation.

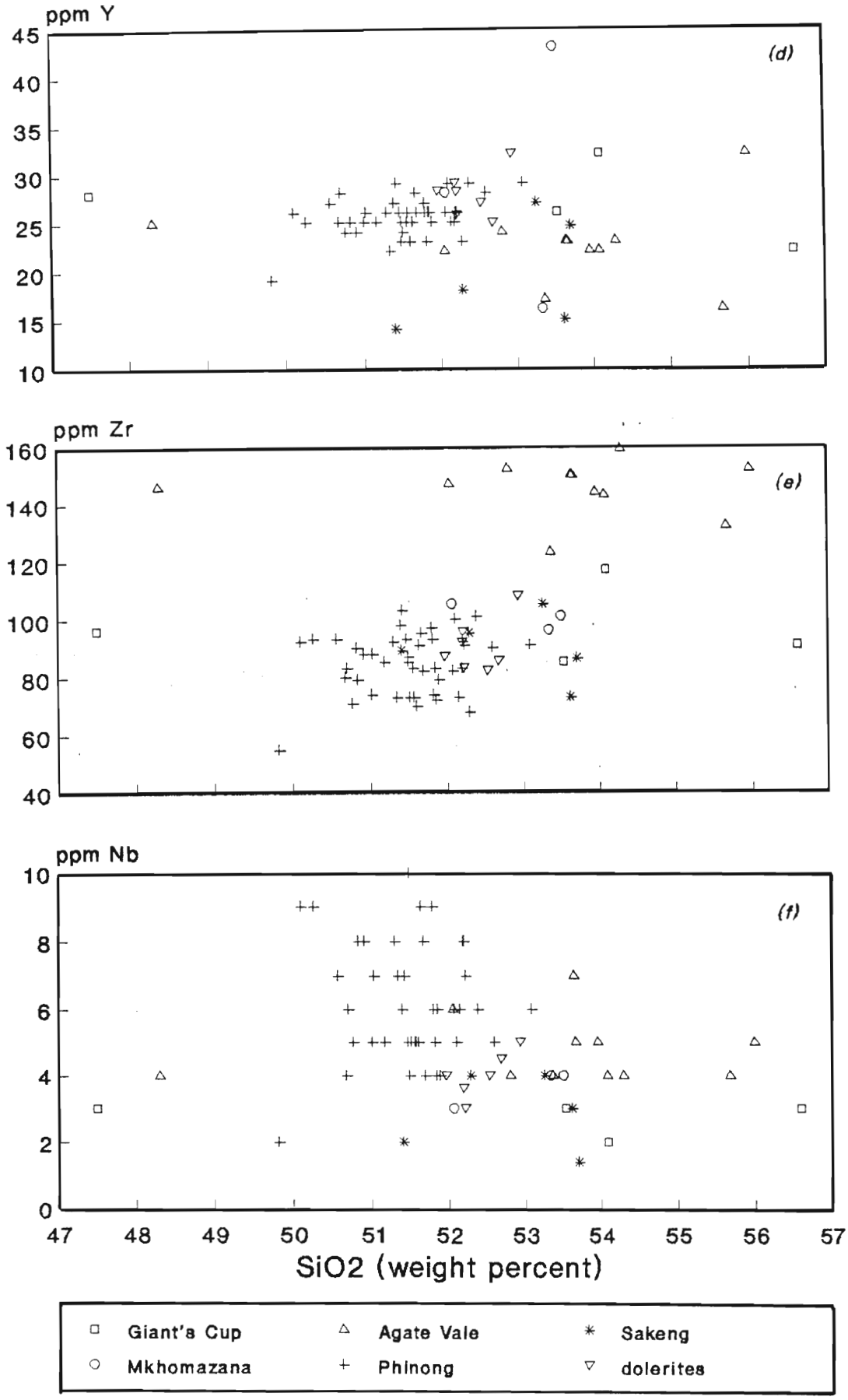

Fig. 8.3d-f SiO_2 variation diagrams for Y, Zr and Nb (ppm).

Zr in the Sani Pass basalts and dolerites is generally scattered, but two compositional fields are apparent (Fig. 8.3e). The Agate Vale basalts are clearly enriched in Zr (123 ppm to 159 ppm) relative to the other magma types which contain less than 120 ppm Zr. The Giant's Cup basalts are generally restricted, in terms of Zr (85 to 96 ppm), but again, the uppermost flow is enriched (117 ppm) and plots only marginally off the field occupied by the Agate Vale basalts. The Sakeng basalts, on the other hand, are variable, with the lowest flow containing the least Zr (73 ppm) and the uppermost flow being relatively enriched (105 ppm). The Mkhomazana basalts maintain some coherency, in the range 96 to 105 ppm. The Phinong basalts are generally scattered, in their Zr content, (55 to 103 ppm) and do not show any linear trends. Sample P180, which is suspected to have experienced cumulus olivine enrichment contains the least Zr (55 ppm). Zr in the dolerites is restricted in the range 85 to 96 ppm, except sample D30 which contains 108 ppm Zr.

8.3.7. Niobium (Nb)

Niobium data for the Sani Pass volcanic rocks show a rather diffuse depletion trend. Falling off this trend are the low-silica basal samples of the Giant's Cup (GC350) and Agate Vale (AV400) magma types and samples P180 and S130. Samples having SiO_2 larger than 55 weight percent also do not plot on this trend (AV60, AV91 and GC360). The Giant's Cup, Sakeng and Mkhomazana magma types plot in a compositional field of 1 to 14 ppm Nb, whilst slight Nb enrichment is shown by the Phinong (except sample P180) and Agate Vale basalts which have Nb varying from 4 to 10 ppm. The dolerites, however, occupy an intermediate field, having Nb = 3 to 5 ppm.

8.3.8. Lanthanum (La)

Lanthanum is a LREE and its comparatively large radius (1.06Å) precludes it from replacing major elements during magmatic crystallization. However, some replacement of Ca^{2+} can take place in apatite. In general, therefore, La should increase during differentiation of a

basaltic assemblage.

Lanthanum contents for the Sani Pass basalts and dolerites are scattered, in the range 3 to 20 ppm, and do not show any linear trends characteristic of differentiation (Fig. 8.3g). In the Giant's Cup basalts La varies from 9 to 17 ppm, the uppermost flow being enriched (17 ppm) compared to the lower flows. On average, the Agate Vale basalts contain slightly more La (10 to 20 ppm) than the remaining Sani Pass magma types. An exception, however, is sample AV90 (La = 3 ppm) which has the lowest La content. The Sakeng basalts do not show any systematic variation in La, varying from 7 to 15 ppm. The Mkhomazana basalts indicate a depletion trend, which however, is not consistent with the stratigraphic succession of the flows, the highest La content being in flow M160 (18 ppm) and the lowest in flow M150 (6 ppm). La in the Phinong basalts is generally scattered, in the range 6 to 19 ppm. The dolerites show increasing La (5 to 20 ppm) over a very restricted SiO_2 range (52.00 to 53.09 weight percent).

8.3.9. Cobalt (Co)

The Co^{2+} ion is almost equivalent in size (0.74Å) to the ferrous ion (0.77Å), and therefore Co should concentrate mainly in ferrous compounds. However, the Co:Fe ratio decreases during progressive fractionation, being greatest in the early-formed minerals (Mason and Moore, 1982). This is due to the effect of the crystal field stabilization, which effectively reduces the radius of the Co^{2+} ion, making its radius almost identical to that of Mg. Thus, most of the cobalt in a magma is substituted in the early-formed magnesian minerals, especially olivine. McDougal and Lovering (1963) showed that Co enters the same minerals as Ni, but in lesser amounts and with more constant values.

Co data for the Sani Pass basalts and dolerites show a spread on the Co-SiO_2 diagram (Fig. 8.3h) and lack any enrichment or depletion trends. In accordance with their low MgO content the Giant's Cup basalts are depleted in Co (28 to 38 ppm) compared to the pre-Phinong basalts (except sample S133) and most of the Phinong basalts (exceptions being samples P174, P185, P254 and P273). The Agate Vale basalts have a restricted Co content

(40 to 51 ppm) over a rather variable SiO_2 content (48.13 to 55.86 weight percent). In contrast to the comparatively restricted Co range shown by the Giant's Cup, Agate Vale and Mkhomazana basalts, the Sakeng basalts are very variable (33 to 51 ppm). The Mkhomazana basalts plot in the range 40 to 47 ppm.

Large variation is also shown by the Phinong basalts, which vary from 22 to 64 ppm. However, most of the basalts group in the range 35 to 50 ppm. Plotting above 50 ppm are the olivine-enriched samples (P180, Co = 62 ppm and P227, Co = 64 ppm), and their high Co content reflects the high distribution coefficient of Co for olivine (Table A5.1, Appendix 5). The two samples (P268 and P185) having less Co than 35 ppm, however, do not show correspondingly low MgO contents (7.42 and 6.88 weight percent, respectively).

Four dolerite samples (D51, D41, D80 and D90) contain marginally less Co (31 to 36 ppm) than most of the Phinong basalts, but the remaining four dolerite samples plot well within the compositional field of the Phinong basalts, in the range 39 to 44 ppm.

8.3.10. Nickel (Ni)

The distribution coefficient for Ni indicates that it will partition with ease into the mafic phases of the basaltic assemblage (Table A5.1, Appendix 5). The nickel ion has essentially the same radius and the same charge as magnesium and therefore, concentrates in magnesium minerals. The Ni/Mg ratio should, therefore, show a steady decline with differentiation in rocks that have not experienced cumulus enrichment of olivine.

Fig. 8.7i, which is a plot of Ni versus SiO_2 for the Sani Pass basalts and dolerites does not show the depletion trend expected from normal fractionation, instead the data are very scattered. The variation in Ni of the Sani Pass basalts and dolerites is broadly similar to that shown by Co (Fig. 8.3h). The Giant's Cup basalts contain less Ni (53 to 69 ppm) than the other pre-Phinong basalts (except samples AV400: Ni = 66 ppm and AV50: Ni = 66 ppm), and most of the Phinong basalts, except some of the uppermost flows. The overlying Agate Vale basalts contain 66 to 141 ppm Ni. Two samples, AV60 (141 ppm) and AV70 (96 ppm), have high Ni accompanied by a high SiO_2 content (55.67 and

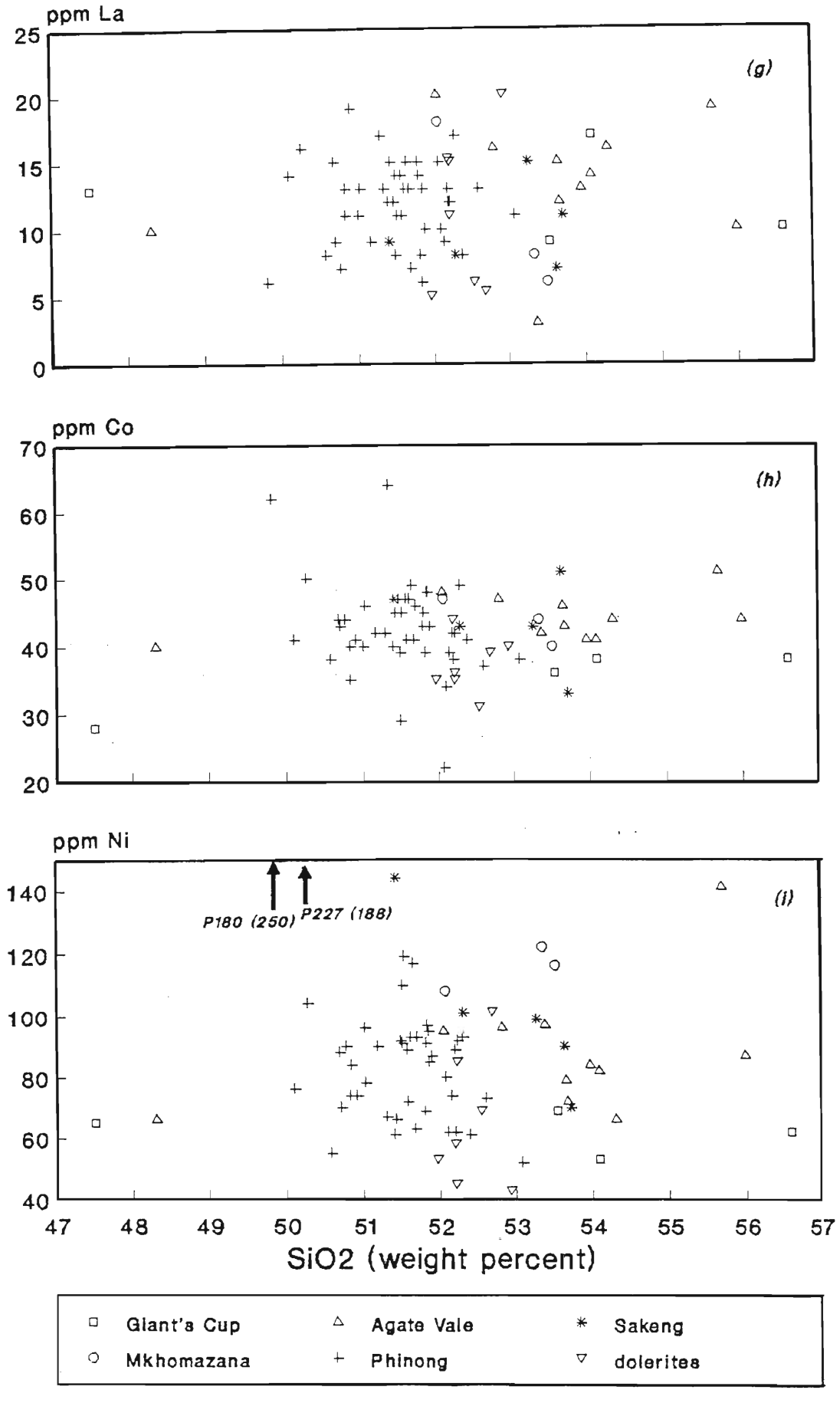

Fig. 8.3g-i SiO_2 variation diagrams for La, Co and Ni (ppm).

52.79 weight percent, respectively) and moderate MgO content (6.24 and 6.37 weight percent, respectively). This variation is not consistent with Ni distribution during normal fractionation. Large variation is again shown by the Sakeng basalts with Ni ranging from 70 to 144 ppm. The high Ni content in sample S130 (144 ppm) is unaccompanied by elevated MgO (6.54 weight percent). The Mkhomazana basalts are enriched in Ni (108 to 122 ppm) compared to the pre-Phinong magma types, except samples S130 (144 ppm) and AV60 (141 pm).

The high distribution coefficient of Ni for olivine is shown by samples P180 and P227, which have high MgO contents, (11.27 and 12.11 weight percent, respectively), and also show extreme Ni enrichment (250 and 188 ppm, respectively). The remaining Phinong basalts group in the range 55 to 120 ppm Ni. Ni concentrations in the dolerites are variable, ranging from 43 to 101 ppm. Samples D10, D30, D41 and D80 contain less than 60 ppm Ni, and therefore fall out of the compositional range for the Phinong basalts (except samples P181 and P278). The remaining four dolerites, however, plot between 76 and 101 ppm Ni, and well within the compositional range of the Phinong basalts.

8.3.11. Chromium (Cr)

Chromium occurs in magmas as the Cr^{3+} ion. Although the ionic radius of Cr is similar to that of Fe, its strong crystal field stabilization energy enhances its concentration relative to Fe. Cr is therefore largely removed during the early stages of crystallization as chromite, but the distribution coefficients (Table A5.1, Appendix 5) indicate that Cr will also enrich in early pyroxene and later magnetite.

The Cr-SiO_2 plot (Fig. 8.3i) displays a spread of data for the Sani Pass basalts and dolerites and no distinct enrichment/depletion trends are apparent. Compared to all the Sani Pass magma types, the Giant's Cup type shows the lowest Cr content (89 to 127 ppm). The overlying Agate Vale basalts have Cr in the range 167 to 407 ppm. No Cr-bearing spinels were detected in sample AV70, which has the highest Cr content (407 ppm). Cr in the Sakeng basalts varies from 211 to 333 ppm. The basal flow of the Mkhomazana basalts has

less Cr (259 ppm) compared to the two overlying flows (M160: Cr = 368 ppm and M170 = 390 ppm). Cr data for the Phinong basalts are generally scattered, with most of the basalts having Cr in the range 133 to 336 ppm. Two exceptions are samples P180 and P223, which are enriched in Cr, containing 477 to 400 ppm, respectively. In both these samples remnant spinel minerals occur as inclusions in the olivines (see Section 4.2.6). The dolerite samples occupy two distinct fields on the Cr-SiO_2 diagram. These are a low Cr field (93 to 412 ppm) comprising samples D10, D30, D41 and D80, and a slightly Cr enriched field (248 to 272 ppm) occupied by the remaining four samples. The latter field plots well within the compositional range of the Phinong basalts.

8.3.12. Vanadium (V)

Vanadium occurs as the V^{3+} ion, and due to its similarities to Fe^{3+} in ionic radius, electronegativity and crystal field stabilization energy, it generally substitutes for this element. V is most abundant during the middle stage of fractionation and decreases during the late-fractionation stage. V, therefore, readily enters the magnetite lattice, and to a lesser extent that of the pyroxenes (Mason and Moore, 1982).

Vanadium content in the Sani Pass basalts and dolerites is highly scattered and defines large compositional ranges for the various magma types (Fig. 8.3k). No clear-cut depletion/enrichment trends are present. The Giant's Cup basalts show the least variability in V, compared to the other Sani Pass magma types. These earliest flows vary in their V content from 242 to 279 ppm. The succeeding Agate Vale flows contain 214 to 274 ppm V. A similar range is exhibited by the Sakeng basalts (211 to 262 ppm). The overlying Mkhomazana basalts are grouped in the range 246 to 285 ppm. The largest variation in V is shown by the voluminous Phinong basalts. Most of these basalts plot in the compositional field 191 to 276 ppm, except sample P180 which contains the least vanadium (163 ppm). This is due to the general lack of magnetite in this sample. Most of the dolerites plot in the Phinong magma type compositional field, but two samples (D10 and D30) show slight vanadium enrichment (280 and 266 ppm).

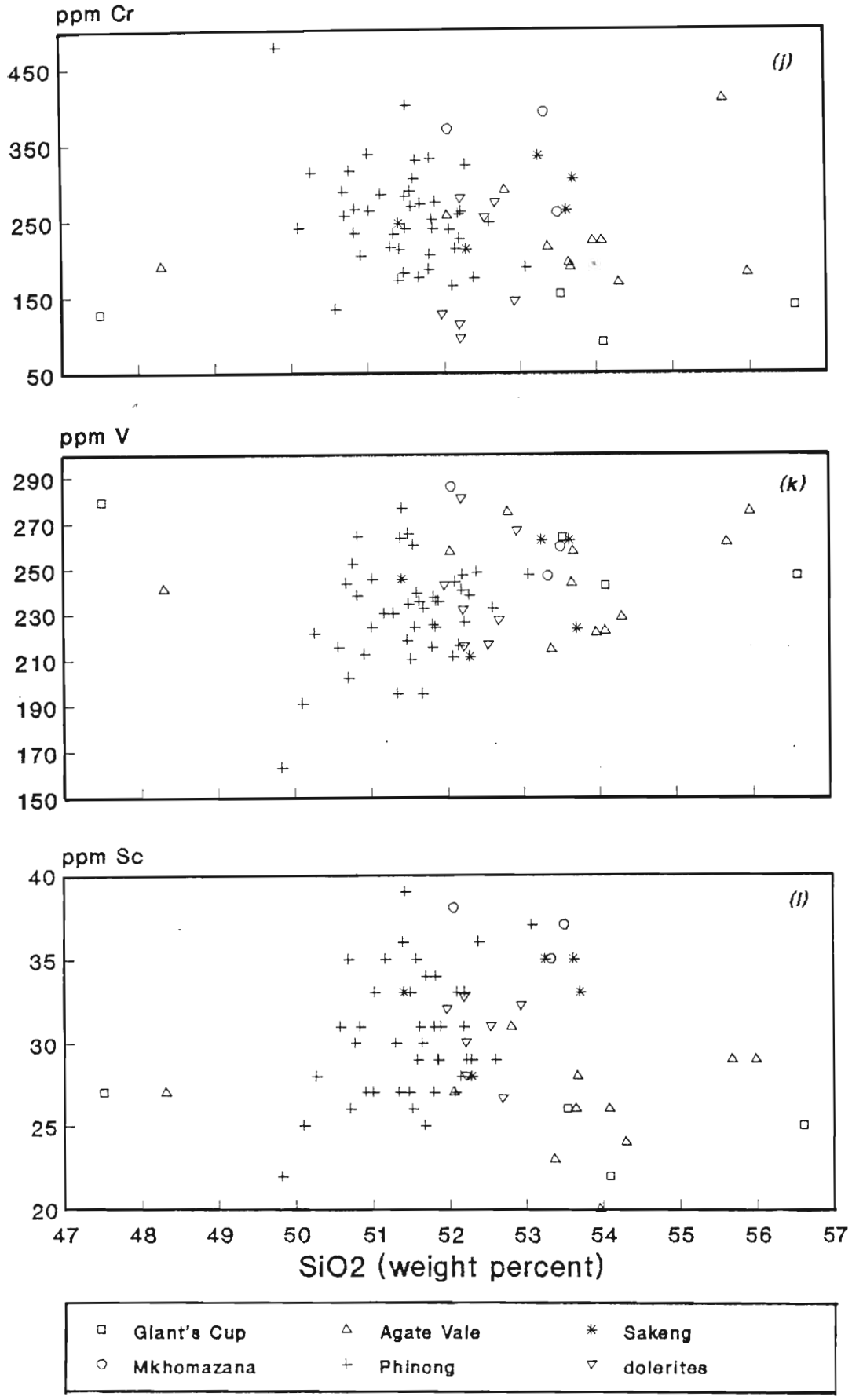

Fig. 8.7 j-l SiO_2 variation diagrams for Cr, V and Sc (ppm).

8.3.13. Scandium (Sc)

Scandium has a radius very similar to that of ferrous iron, and is frequently incorporated into the ferromagnesian minerals. Sc, therefore, concentrates in pyroxenes, amphiboles and to a lesser extent, biotites. In the basaltic assemblage it would, therefore, concentrate only in the pyroxenes, and not the earlier-formed olivines.

No differentiation trends are discernable in the Sc content of the Sani Pass basalts and dolerites (Fig. 8.3e). The Giant's Cup magma type, in general contains less Sc than the other Sani Pass magma types. The Sc content in the Giant's Cup basalts varies from 22 to 27 ppm. The overlying Agate Vale basalts contain Sc in range 20 to 31 ppm, and similarly, are slightly depleted in Sc compared to the Mkhomazana, and most of the Sakeng and Phinong basalts. Sample AV60, AV70 and AV91 contain highest Sc (29, 31 and 29 ppm, respectively). Sc in the Sakeng basalts varies between 28 and 35 ppm. The Mkhomazana basalts are clearly enriched in Sc (35 to 38 ppm) compared to the pre-Phinong basalts and most of the Phinong basalts. The Phinong basalts (except P180) plot in the range 25 to 36 ppm Sc. Sample P180, which is suspected to have experienced cumulus olivine enrichment, contains much lower Sc (22 ppm). The dolerites plot in the Phinong magma type compositional field and contain 27 to 33 ppm Sc.

8.3.14. Zinc (Zn)

Partition coefficient data for Zn are extremely scarce. Nevertheless, Ahrens (1964) noted that Zn displays some characteristics of compatible elements, which he attributed to the relatively covalent nature of the Zn-O bond.

Zn data for the Sani Pass basalts and dolerites do not show any differentiation trends (Fig. 8.3m). Variable Zn is contained in the Giant's Cup basalts, their concentrations ranging from 66 to 98 ppm. The Agate Vale lavas, except samples AV60 and AV90, contain 97 to 130 ppm Zn, which is slightly higher than the range characteristic of the remaining magma types. The Zn content in the Sakeng basalts decreases from 80 ppm in

the basal flow to 51 ppm in the penultimate flow (S133), and then increases to 85 ppm in the uppermost flow. The Mkhomazana basalts show the most constrained Zn concentrations, grouping in the range 83 to 87 ppm. The Phinong basalts are characterized by a rather uniform distribution of Zn, restricted in the range 58 to 89 ppm. Six dolerite samples plot in this compositional field, although in a more restricted range of 65 to 79 ppm. The remaining two dolerite samples are more enriched (93 to 138 ppm) in Zn.

8.3.15. Copper (Cu)

Cu has very low distribution coefficients for silicate minerals, but this increases considerably for sulphides (Naldrett and Barnes, 1986). It therefore behaves somewhat like an incompatible element (in the absence of sulphides) and is commonly used as a pathfinder for sulphides and associated platinum group elements. Sulphur concentrations have been obtained for the Sani Pass basalts and dolerites (Tables A2.2 and A2.3, Appendix 2) and when plotted against Cu concentrations the pattern obtained is generally scattered.

Cu in the Sani Pass basalts and dolerites does not show any systematic variation with SiO_2 (Fig. 8.3n). Generally the Giant's Cup basalts contain marginally less Cu (53 to 72 ppm) than most of the Sakeng and Phinong basalts and all of the Mkhomazana basalts. The Agate Vale basalts are variable in their Cu content, ranging from 53 ppm in flow AV60 to 140 ppm in flow AV100. Although the sulphur content in AV100 (S = 0.05 weight percent) is not the largest in the Agate Vale unit, it is slightly higher than the sulphur content of AV60 (S = 0.01 weight percent). Cu concentrations in the Sakeng basalts vary from 60 to 133 ppm. Here again, the highest sulphur content (0.76 weight percent in S136) is not accompanied by the highest Cu content (99 ppm in flow S136). Cu enrichment is present in the uppermost flow of the Mkhomazana basalts (135 ppm), the two lower flows both containing 79 ppm copper. Most of the Phinong basalts cluster in the range 64 to 92 ppm copper. Samples P180 and P227 plot out of this range and contain 52 and 55 ppm Cu, respectively. Slight Cu enrichment is shown by four samples (P181, P268, P272 and P273) which plot in the range 99 to 104 ppm, and greater enrichment is shown by samples

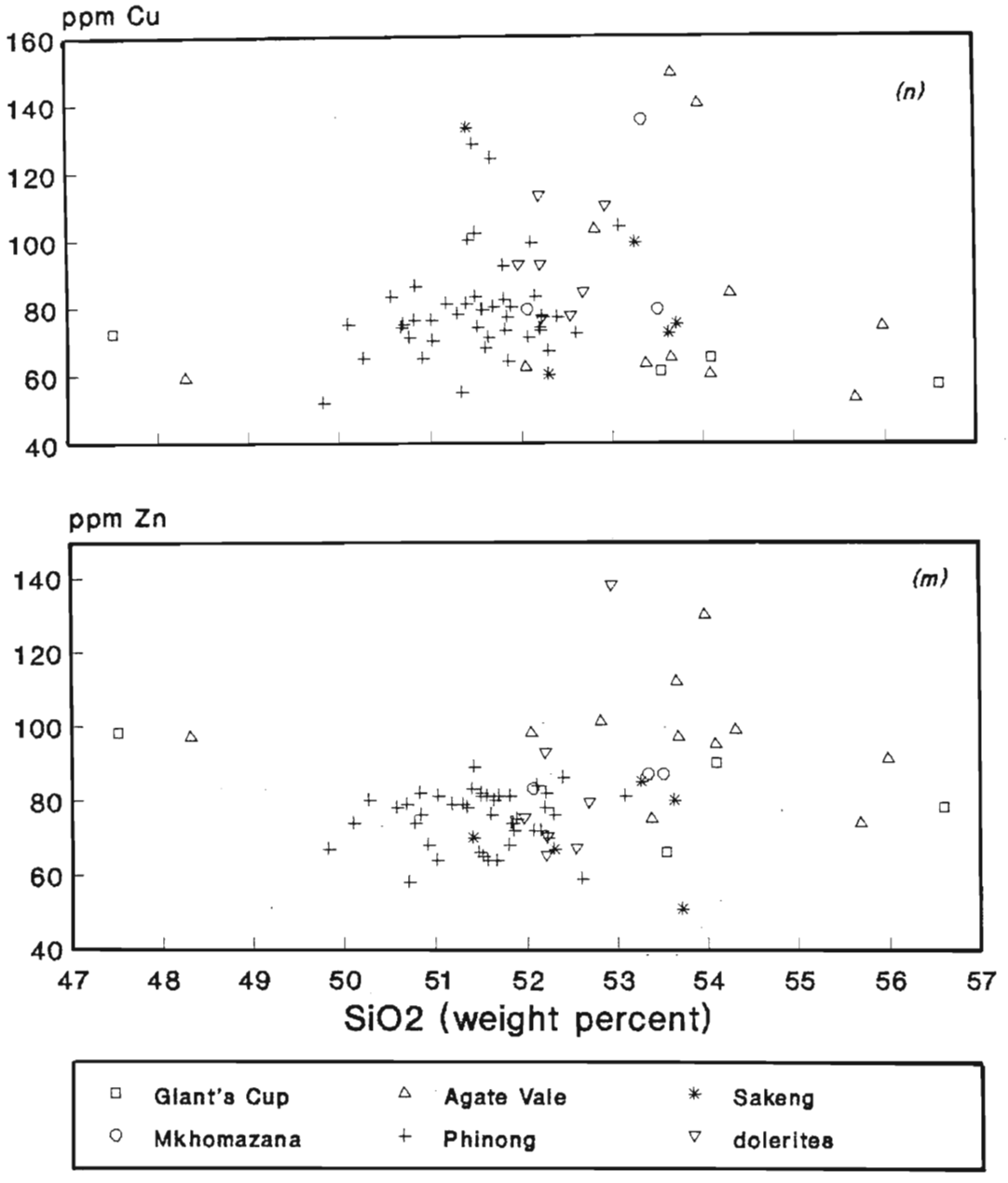

Fig. 8.3m-n SiO_2 variation diagrams for Zn and Cu (ppm).

P271 and P205, having 128 and 124 ppm copper, respectively. None of these Cu-enriched samples contain any sulphur (Table A2.2, Appendix 2). Cu in the dolerites varies from 76 to 113 ppm.

8.4. Dolerites: Comparison with lavas

Within the Sani Pass volcanic succession different magma types are recognizable in terms of major and trace element geochemistry. However, in the immediate vicinity of the volcanics, and intrusive in the underlying Karoo sediments, is a network of dolerite dykes (Fig. A1.1). It is pertinent to consider whether the magma types identified in the volcanic succession can be recognized in the intrusive suite. Walker and Poldervaart (1949) identified several different dolerite types based on petrography. These petrographic types, however, could not be sustained on the basis of chemistry, except the Hangnest type. Pemberton (1978) and Marsh and Eales (1984) have subsequently indicated that within the dolerite suite several magma types could be established on the basis of lava chemistry, despite any in-situ differentiation.

A comparison of the major and trace element chemistry of the Sani Pass basalts with the dolerites reveals strong similarities (Figs. 8.2a-i, Figs. 8.3a-n). In detail however, the dolerites seem to show two groups, one comprising samples D20, D51, D90 and D91, and which plot in the compositional field for the Phinong basalts for most elements, and a second group comprising samples D10, D20, D41 and D80 which are slightly different in terms of specific elements.

The latter group, termed the low-MgO dolerites, contains 5.77 to 6.41 weight percent MgO, whilst the second group, termed the normal-MgO dolerites, contains 6.95 to 7.46 weight percent MgO. Consequently, the low-MgO dolerites contain less Cr and Ni, and more Cu, Ti and tFe_2O_3, than the normal-MgO dolerites. Also, the low-MgO dolerites (except sample D80) contain less Al_2O_3 (14.62 to 15.03 weight percent) than the normal-MgO dolerites. Therefore, the low-MgO dolerites do not plot in the compositional range for *most* of the Phinong basalts for TiO_2 (Fig. 8.2a), Al_2O_3 (Fig. 8.2b), tFe_2O_2 (Fig. 8.2c),

Ni (Fig. 8.3i), Cr (Fig. 8.3j) and Cu (Fig. 8.3n). For all other major and trace elements, the two dolerite groups plot within the Phinong basalts compositional field, and in most cases show a very restricted compositional range.

The foregoing discussion has illustrated the geochemical similarities between the Phinong magma type and the dolerites, for *most* elements. In terms of specific elements, however, samples D10, D20, D41 and D80 differ from the Phinong basalts and the remaining dolerites.

8.5. Stratigraphic Variations

Since the five magma types in the Sani Pass display variable major and trace element contents, any consistent variation with stratigraphy must be assessed. This section is purely descriptive and any petrogenetic implications are discussed in Chapter 10. Only elements that show some trend with stratigraphy have been plotted. Normalised major element analyses and unnormalised trace element data for each sample are given in Table A2.4 (Appendix 2). Each data point on Figs. 8.4a-i represents a single lava flow, except samples AV20, AV40 and AV50, and samples AV60 and AV70 which are from two consecutive flows in the Agate Vale geochemical unit.

Studies based on geochemical stratigraphic variations of the Lesotho Formation have indicated consistent patterns. In their study of the Lesotho Formation basalts exposed in the Letele Pass, Cox and Hornung (1966) noted that the Fe/Mg index increased with height in the volcanic succession and concluded "there is a slight tendency for more fractionated rocks to be found stratigraphically higher." Pemberton's (1978) study of the Lesotho Formation basalts in the Naude's Nek succession (north-eastern Cape) indicated a similar trend of increasing Fe/Mg with height. His study also concluded that the uppermost basalts in the Naude's Nek Pass are enriched in Fe_2O_3, P_2O_5, Ce, La and Zr, and have a lower Ni, Cr and Mg-number (Mg#).

The variation of Mg# in the Sani Pass is indicated in Fig. 8.4a, and has been computed as molecular MgO/(MgO+FeO), where FeO has been calculated assuming $Fe_2O_3/FeO=0.2$.

Mg# in the Giant's Cup basalts is generally low compared to the overlying magma types, varying from 37 to 53. Except for the basal flow (AV400), the Agate Vale basalts show a slight increase in Mg#, ranging from 55 to 58. The increase in Mg# is further evident in the Sakeng basalts, grouping in the range 57 to 63. The overlying Mkhomazana basalts also reflect a trend of increasing Mg#, having Mg# restricted in the range 61 to 63. A lower Mg# is observed in the lowermost flow of the Phinong basalts (Mg#=58). Within the Phinong magma type, Mg# is maintained in the range 57 to 62, except samples P180 (Mg#=70) and P227 (Mg#=69), both samples which might have experienced cumulus olivine enrichment, and therefore show elevated Mg#'s. A slight trend of decreasing Mg# with stratigraphic height is evident in the uppermost 100m of the Sani Pass. This trend is preceded by a less well developed trend, starting at a height of 525m and which is marked by initially high Mg# (62), followed by a decrease to 57 at a height of 540m. Above this height the Mg# again increases, to 61 in flow P247, after which it decreases somewhat.

It is therefore apparent that no overall trend of decreasing Mg# with stratigraphic height is present in the Sani Pass volcanic succession. Instead, there is a hint of increasing Mg# from the Giant's Cup basalts through the Agate Vale and Sakeng magma types, to the Mkhomazana type basalts, while a slight decrease in Mg# is evident in the uppermost 100m of the Sani Pass volcanic succession.

Although the silica content of the pre-Phinong basalts is somewhat variable, in the range 47.50 to 55.59 weight percent, these basalts generally have higher silica contents than the Phinong basalts (Fig. 8.4b) which contain between 49.82 and 53.08 weight percent SiO_2. In addition, the pre-Phinong basalts indicate an overall, albeit rather diffuse, trend of decreasing SiO_2 with stratigraphic height. However, the basal flows of the Giant's Cup and Agate Vale magma types contain extremely loe SiO_2 (47.51 and 48.29 weight percent, respectively), and therefore plot out of the range of this trend. Trends are generally lacking in terms of silica variation within the Phinong unit. However, silica increases from 51.83 weight percent in sample P263 to 52.76 weight percent in the uppermost flow (P278). Two flows (P276 and P277) plot out of this trend because of their slightly lower silica content.

TiO_2 content within the Giant's Cup basalts ranges from 1.04 to 1.32 weight percent and

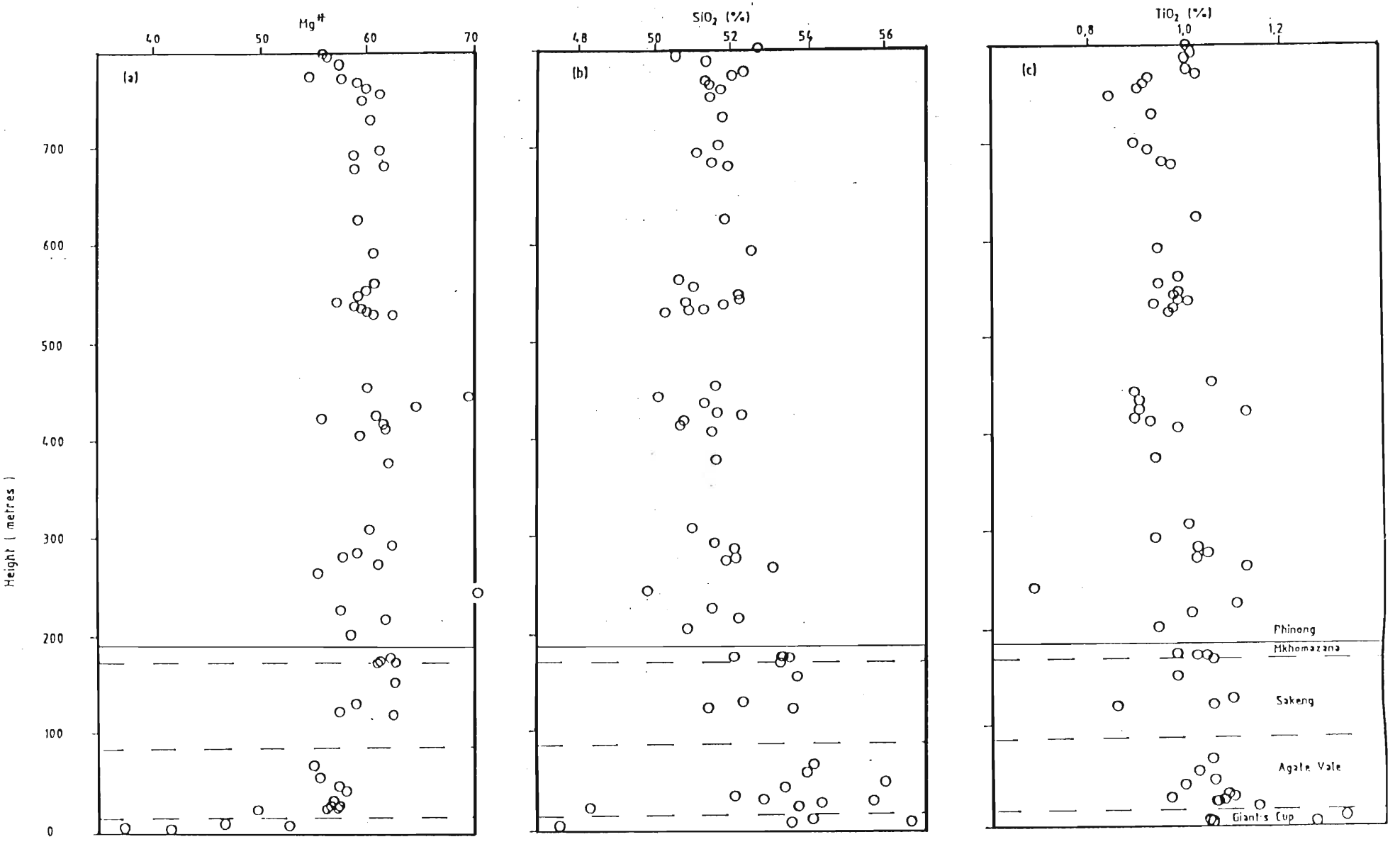

Fig. 8.4a-c Variation of Mg#, SiO_2, and TiO2 (weight percent) with stratigraphic height in the Sani Pass.

in the Agate Vale succession, from 0.98 to 1.08 weight percent (Fig. 8.4c). A low TiO_2 content of 0.85 weight percent is present at the base of the Sakeng magma type which increases in the overlying Sakeng lava flows in a restricted range of 0.98 to 1.09 weight percent. Overlying the Sakeng basalts, in the Mkhomazana magma type, TiO_2 contents are more consistent ranging from 0.98 to 1.04 weight percent. Thus, within the pre-Phinong basalts TiO_2 is generally constrained in the range 0.95 to 1.09 weight percent (excluding samples GC350, GC360, AV400 and S120) and does not show any distinct trend. At the base of the Phinong magma type, TiO_2 contents decrease slightly to 0.94 weight percent and then fluctuate throughout this succession in the range 0.89 to 1.12 weight percent. Sample P180 shows an extremely low TiO_2 content (0.68 weight percent). The seven uppermost lava flows within the Phinong unit show a slight trend of increasing TiO_2 content, from 0.84 weight percent in flow P267 to a maximum of 1.02 weight percent in flow P272, and then decreases marginally to 1.00 and 1.01 weight percent in the overlying flows.

The stratigraphic variation of the compatible elements Ni (Fig. 8.4d) and Cr (Fig. 8.4e) is broadly similar to that of Mg# (Fig. 8.4a) in the Sani Pass volcanic succession. Ni increases from 65ppm in the basal Giant's Cup flow (GC350) to 122ppm in the uppermost Mkhomazana flow (M170). Falling off this general trend of increasing Ni content in the pre-Phinong basalts are two samples that show Ni enrichment (AV60: Ni=141ppm and S130: Ni=144ppm), and sample S133 which is slightly depleted (Ni=70ppm). Ni content in the lowermost flow of the Phinong succession drops to 84ppm. Above this and up to a height of 746m, the Ni content is variable, in the range 52 to 119ppm. Extreme Ni enrichment is present in samples P227 (Ni=188ppm) and P180 (Ni=250ppm), this enrichment being due to accumulation of cumulus olivine. There is a hint of increasing Ni content in the uppermost portion of this stratigraphic range. Above 746m, and within the uppermost 50m of the Sani Pass succession, Ni decreases from 97 to 55ppm.

Chromium contents in the Giant's Cup basalts varies from 89 to 152ppm (Fig. 8.4e). In the overlying Agate Vale basalts Cr content is slightly larger, in the range 167 to 407ppm. Slight Cr enrichment is shown by samples AV70 (Cr=256ppm) and AV90 (Cr=214ppm), while extreme Cr enrichment is shown by sample AV60 (Cr=407ppm). A general increase

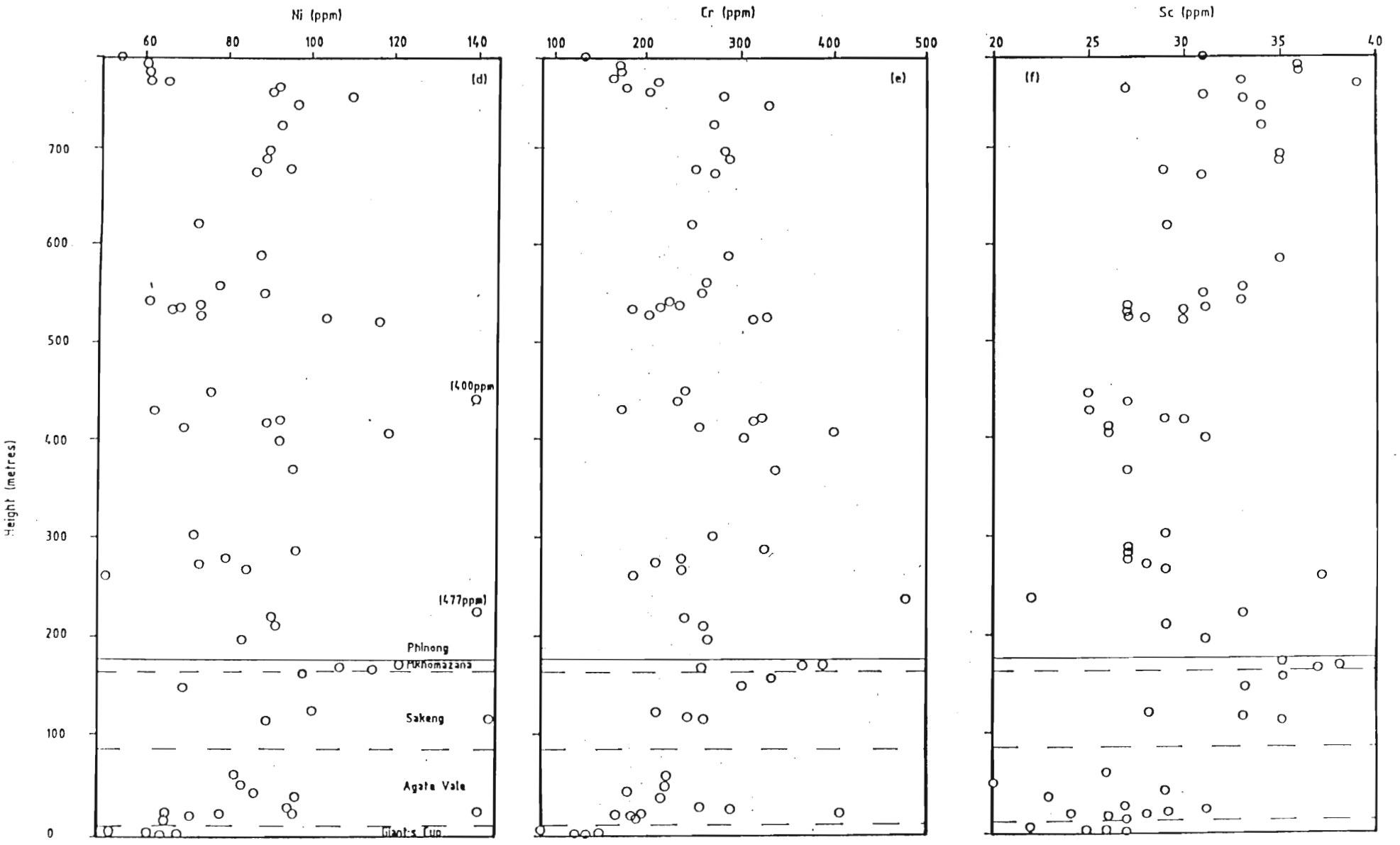

Fig. 8.4d-f Variation of Ni, Cr and Sc (ppm) with stratigraphic height in the Sani Pass.

in Cr is present in the Sakeng basalts which contain 211 to 333ppm chromium. High Cr contents are also shown by the Mkhomazana basalts which increase from 259ppm in the lowermost flow to 390ppm in the uppermost flow. In the lowermost Phinong flow Cr content drops to 265ppm, but is maintained in the range 175 to 336ppm, up to a height of about 750m within this magma type. Two flows, P180 and P223 show high Cr concentrations (477 and 400ppm, respectively). Between lava flows P234 (at 530m) and P267 (at 746m), Cr shows a slight trend of increasing concentration from 203 to 330ppm. In the uppermost 50m of the stratigraphic succession Cr contents reduce rapidly from 330ppm to 133ppm.

The variation of Sc contents with stratigraphic height in the Sani Pass is depicted in Fig. 8.4f. The trends shown by the other compatible elements, Ni and Cr, are less well developed in terms of Sc. Nevertheless, within the pre-Phinong magma types Sc shows an overall increase, from a range of 22 to 27ppm in the Giant's Cup, 20 to 31ppm in the overlying Agate Vale basalts, 28 to 35ppm in the Sakeng basalts, and 35 to 38ppm in the succeeding Mkhomazana basalts. Within the Phinong magma type, Sc concentrations are variable, ranging from 22 to 39ppm. However, there is a slight indication of increasing Sc content from about 525m to the uppermost flows.

The variation of the incompatible elements Y, Zr and Nb with the Sani Pass stratigraphy is shown in Figs. 8.4g-i. Y contents in the Giant's Cup and Agate Vale basalts varies from 22 to 32 ppm, being slightly lower (16 and 17ppm) in flows AV60 and AV90 of the Agate Vale basalts, respectively (Fig.8.4g). At the base of the Sakeng magma type, Y content decreases further to 15ppm, whence it increases to 27ppm in the uppermost flow of this unit. A substantial increase to 43ppm is observed at the base of the Mkhomazana magma type. Within this unit Y content decreases consistently to 16ppm at the top. At the base of the Phinong magma type Y is slightly elevated to 25ppm. In the Phinong basalts Y content is very consistent, and displays the least variation, in the range 22 to 29ppm. An exception, however, is sample P180, which has Y = 19ppm. Y in the uppermost 50m of the volcanic succession increases slightly from 23ppm in flow P267 to 29ppm in flow P276. The two uppermost flows both contain 27ppm yttrium.

The slightly Zr- enriched nature of the Agate Vale basalts is shown in Fig. 8.4h. These basalts have a Zr content ranging from 123 to 159ppm, in contrast to the underlying Giant's Cup basalts (85 to 117ppm) and the overlying Sakeng basalts (73 to 105ppm), Mkhomazana basalts (96 to 105ppm) and the Phinong basalts (55 to 103ppm). Zr content within the individual pre-Phinong magma types is reasonably consistent showing only very little variation with stratigraphic height. The Phinong magma type, although a very large volcanic package, also shows some consistency in Zr content, varying from 68 to 103ppm (excluding P180, Zr = 55ppm). However, the uppermost 50m of this unit shows a slight increase in Zr from 80ppm in flow P267 to a maximum of 103ppm in flow P272 at 770m.

Figure 8.4i, which is a plot of the variation of Nb with stratigraphic height, displays pronounced trends of increasing and decreasing Nb content within the Phinong magma type. Although cognizance must be taken of the very low level of detection for Nb, these trends are present in the range 4 to 9ppm Nb, which should be reasonably reliable. Fig. 8.4i also shows the distinct geochemical break between the pre-Phinong and Phinong magma types, where the Nb content increases from 4ppm in the uppermost Mkhomazana flow to 8ppm in the basal Phinong flow. Within the pre-Phinong volcanic package a very subtle decrease in Nb content is apparent, mainly from the Agate Vale basalts to the Mkhomazana basalts. The Nb content in the Phinong basalts decreases to 4ppm (at 422m) and then increases again to 9ppm at 536m. At about this height the Nb content varies very little (8 to 9ppm) after which it begins to decrease again to 4ppm at 590m. Within the uppermost 70m the Nb content increases consistently to a maximum of 7ppm at 797m.

The preceding discussion has therefore indicated a trend of increasing Mg#, Ni, Cr and Sc, and slightly decreasing SiO_2 and Nb from the Giant's Cup basalts, up to and including the Mkhomazana basalts. This trend, however, cannot be sustained for the incompatible elements TiO_2, Y and Zr. Mg# is generally used as an indication of the degree of fractionation and its variation in the pre-Phinong basalts indicates that the less fractionated rocks occur higher up in the stratigraphy. In the Phinong succession there is a tendency for the more fractionated rocks to be found in the uppermost 50m. These samples describe a trend marked by decreasing Mg#, Ni and Cr, and increasing SiO_2, TiO_2, Y, Zr, Nb and

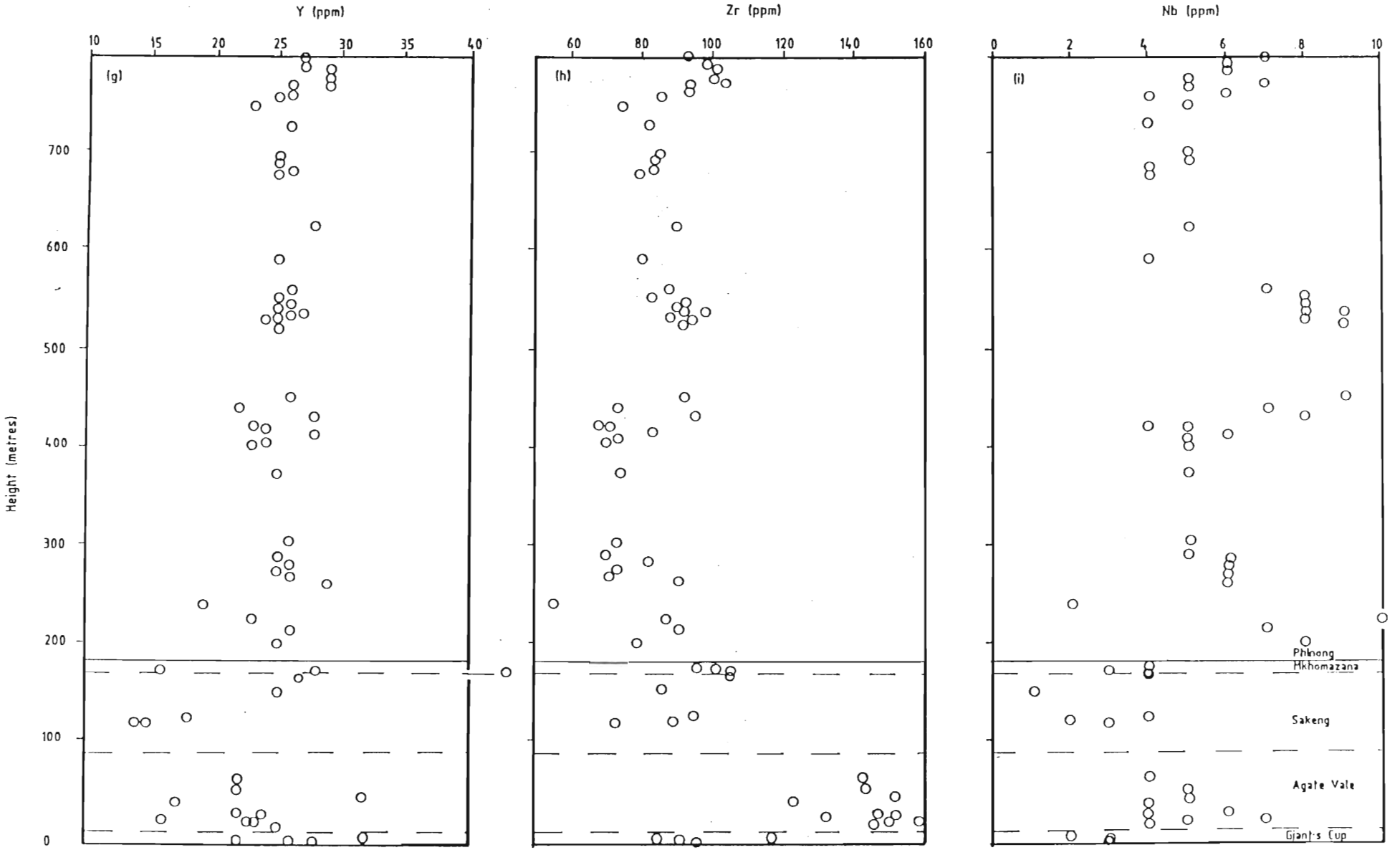

Fig. 8.4g-i Variation of Y, Zr and Nb (ppm) with stratigraphic height in the Sani Pass.

possibly Sc. This trend might indicate the waning phase of volcanism in the Sani Pass. .

8.6. Summary of Whole-Rock Geochemistry

Major and trace element geochemistry for 67 basalts and 8 dolerites have been presented. Whole-rock geochemistry for the Sani Pass basalts is variable for the five different magma types. The Giant's Cup magma type is depleted in MgO, Cr, Ni and Co content and shows slight enrichment in TiO_2, relative to the overlying magma types. The Agate Vale basalts are enriched in the alkalies and Rb, Sr, Ba and Zr, and depleted in CaO. The Sakeng basalts which overlie the Agate Vale basalts are depleted in the alkalies relative to the Agate Vale magma. The Mkhomazana basalts show extreme enrichment in Na_2O, and relatively depleted CaO and slight enrichment in MgO, Ni, Cr and Sc, relative to the underlying pre-Phinong basalts. Within the pre-Phinong magma succession there is a tendency for the less fractionated rocks to be found higher up in the stratigraphy. The Phinong basalts are generally uniform in their composition and are relatively depleted in Zr content compared to the pre-Phinong basalts. Also, the Phinong basalts show a poorly developed depletion trend in MgO with increasing SiO_2 content. In the Phinong succession there is a tendency for the more fractionated rocks to be found in the uppermost 50m.

The dolerites are very similar in composition to the Phinong magma type for most elements. In terms of specific elements, however, four dolerite samples have slightly differing compositions, compared to the basalts and remaining dolerites.

CHAPTER 9

9. DISCRIMINATION AND CHARACTERIZATION OF THE DIFFERENT MAGMA TYPES

9.1. Introduction

From the preceding discussion it is evident that the Sani Pass volcanic succession cannot be successfully subdivided on the basis of lithology or mineralogy. However, the major and trace element analyses indicate five different magma types, namely, the Giant's Cup, Agate Vale, Sakeng, Mkhomazana and Phinong types. This chapter, therefore, attempts to clearly elucidate the chemical differences amongst the magma types using discriminant function analysis and relative concentrations and ratios of incompatible elements.

9.2. Canonical Discrimination Function Analyses

Statistical comparison techniques have thus far been successfully used by Rhodes and Kröhn (1972) and Duncan *et al.*, (1984b) to elucidate regional variations in the geochemistry of the Karoo volcanics from different geographical regions. Rhodes and Kröhn (1972) performed a regional geochemical comparison using the Mann-Whitney U-test, which is a non-parametric analogue to the two-sample t-test, while Duncan *et al.*, (1984b), who had a much larger database to contend with, opted for discriminant function analysis. Discriminant function analysis (DFA) is not a "primary" classification tool and its purpose is to find a function which is a linear combination of some or all element and oxide abundances such that values of this function produce the maximum differences between the defined groups of samples. The best linear combinations of the discriminant variables are expressed as canonical variables.

Discriminant function analysis has been used to compare the overall composition of the Sani Pass basalts, using the Central area magma types as the training groups or "knowns". The resulting DFA diagram is shown in Fig. 9.1. Using the DFA technique, only two of the magma types are clearly separated, namely, the Agate Vale and the Phinong magma types. The Giant's Cup, Sakeng and the Mkhomazana magma types do not maintain any coherency and plot in and about the field occupied by the Phinong type basalts. These magma types do, however, seem to be different from the Agate Vale magma type.

Duncan *et al.*, (1984b) carried out discriminant analysis for their entire geochemical database on Central area basalts, and the fields occupied by their various volcanic units are shown in Fig. 9.1. (see overlay). It is important that the discriminant analyses for the Sani Pass basalts be compared with those of Duncan *et al.*, (1984b) for other Central area basalts, since the two groups of data are from two different geographic areas. However, it must be emphasised that this comparison is only a preliminary effort, since the Sani Pass data do not form part of Duncan *et al's.*, (1984b) database, and thus the plots are statistically invalid. Nevertheless, this exercise does indicate that the majority of the Phinong basalts fall in the field delineated by the Lesotho type basalts. Only a single sample from the Giant's Cup and Mkhomazana magma types, and 3 samples from the Sakeng magma, fall in this field. The Agate Vale magma type does not plot within any of the fields delineated for the magmas from the central areas; thus indicating a unique magma type in the Central area.

It seems that the DFA, which utilizes both major and trace elements is not very successful in discriminating amongst the different magma types in the Sani Pass succession, but rather separates the Agate Vale magma type from the Phinong, Giant's Cup, Sakeng and Mkomazana magma types.

9.3. Incompatible Interelement Ratios

Incompatible interelement ratios have been successfully used by previous workers on the Central area (Pemberton, 1978; Mitchell, 1980; Marsh and Eales, 1984) to distinguish between different basaltic units.

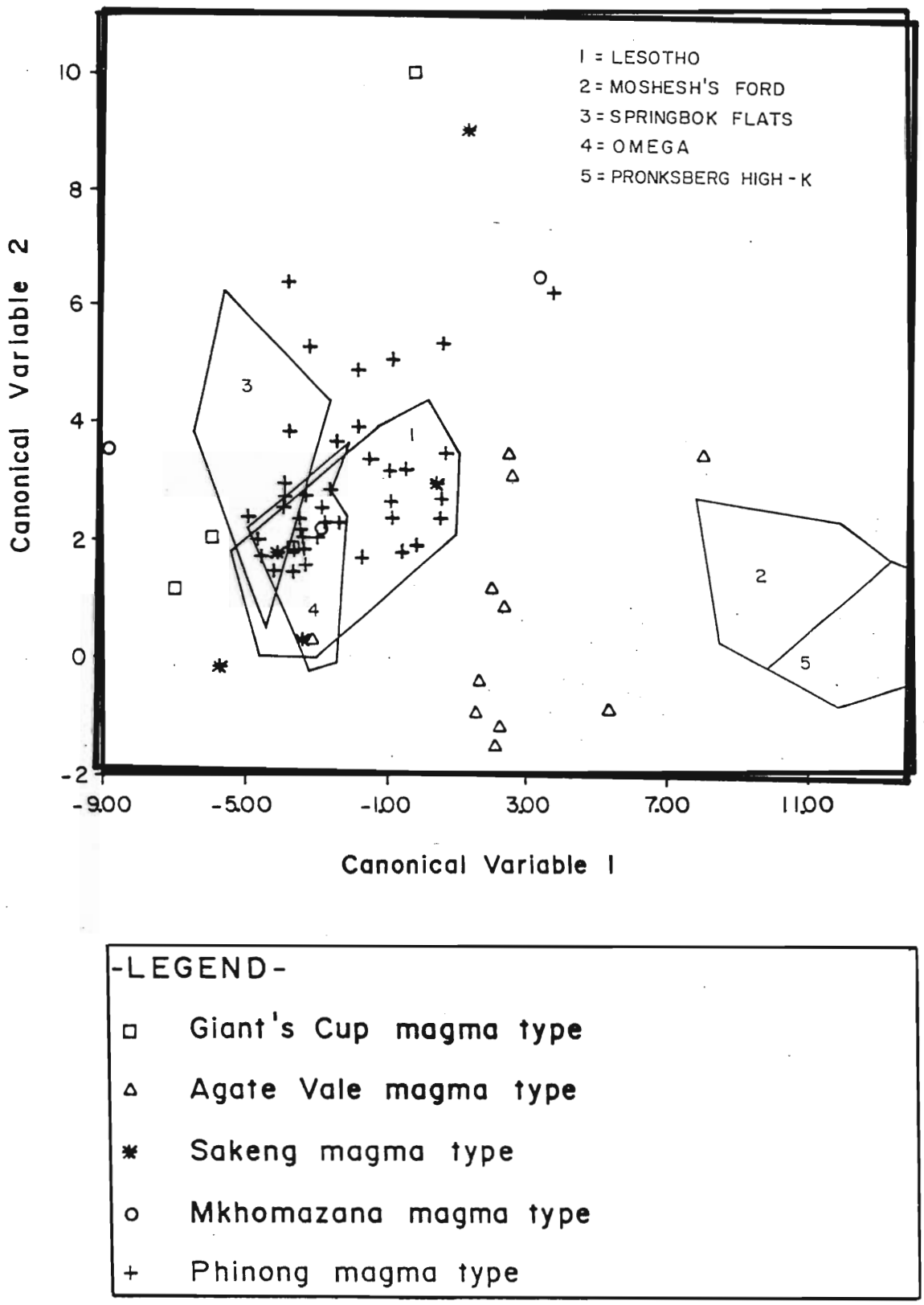

Fig. 9.1 Discriminant function analysis (DFA) diagram for basalts in the Sani Pass volcanic succession.

$$CV1 = +(1.17633*TiO_2) + (6.62942*MnO) + (0.46443*CaO) + (1.07646*Na_2O) + (1.51120*K_2O) + (10.29664*P_2O_5) - (0.00681*Sr) + (0.06093*Zr) + (0.65640*Nb) + (0.00550*Cr) + (0.01315*Ni) - (0.06638*Co) + (0.00906*Cu) - (0.51329*Y) - 12.45877$$

$$CV2 = +(5.08668*TiO_2) - (10.40098*MnO) + (0.81252*CaO) + (1.08935*Na_2O) + (0.99413*K_2O) - (4.03409*P_2O_5) - (0.00257*Sr) - (0.03961*Zr) + (0.21604*Nb) - (0.01053*Cr) + (0.06997*Ni) - (0.08437*Co) + (0.05305*Cu) + (0.01098*Y) - 13.39369$$

During magma genesis individual incompatible elements are rejected by the crystalline phases and preferentially portion into the melt phase and are therefore good indicators of pristine magma compositions and fractional crystallization. Also, except for the more mobile or low field strength elements (LFSE) (eg: K, Rb, Ba), the incompatible elements are unlikely to be significantly affected by alteration and thus represent the least variability between lava flows. A ratio of two incompatible elements should therefore remain constant.

Therefore the incompatible elements, Zr, Nb, Y, Ti and P have been chosen to illustrate between-magma type compositional differences. The petrogenesis of the different magma types in terms of trace element differentiation models is discussed in a subsequent section. Selected interelement plots are represented in Figs. 9.2a-c.

Zr/Y ratios effectively distinguish between the Phinong and Agate Vale magma types (Fig. 9.2a). The Agate Vale basalts are relatively enriched in Zr and somewhat depleted in Y, and consequently have higher Zr/Y ratios. The basalts of this magma type straddle the line designated Zr/Y=6, except sample AV91 which has Zr/Y=4.5. The Phinong basalts fall within the field delineated by Zr/Y ratios of 2 and 4. Within the Giant's Cup, Sakeng and Mkhomazana magma types less uniformity is exhibited; the Giant's Cup magma type plots in the field of the Phinong basalts, except sample GC360 (Zr/Y = 4.1) which falls marginally above Zr/Y=4. The Sakeng basalts (Zr/Y=3.89 to 4.87) are intermediate, plotting in both fields and the Mkhomazana type shows a continuum in values ranging from Zr/Y=2.35 to Zr/Y=6.

Nb plotted against Zr clearly illustrates two compositional fields, one occupied by the Phinong type basalts, and the other by the pre-Phinong magma types, in which Nb content is lower (Fig. 9.2b). The line Zr/Nb=20 effectively separates these two groups, except for a few basalts from the Phinong type which exceed this ratio marginally. Sample P180, which plots in the field of the lower group and has a Zr/Nb=27.5 is an exception. Zr/Nb ratios in the Phinong basalts (except sample P180) range from 8.70 to 21.25, whilst higher Zr/Nb ratios (21.43 to 86.00) are characteristic of the Giant's Cup, Sakeng and the Mkhomazana magma types. High Zr/Nb ratios (21.40 to 39.75) also characterize the Agate Vale basalts which have a similar Nb compositional range to the Phinong basalts (4 to

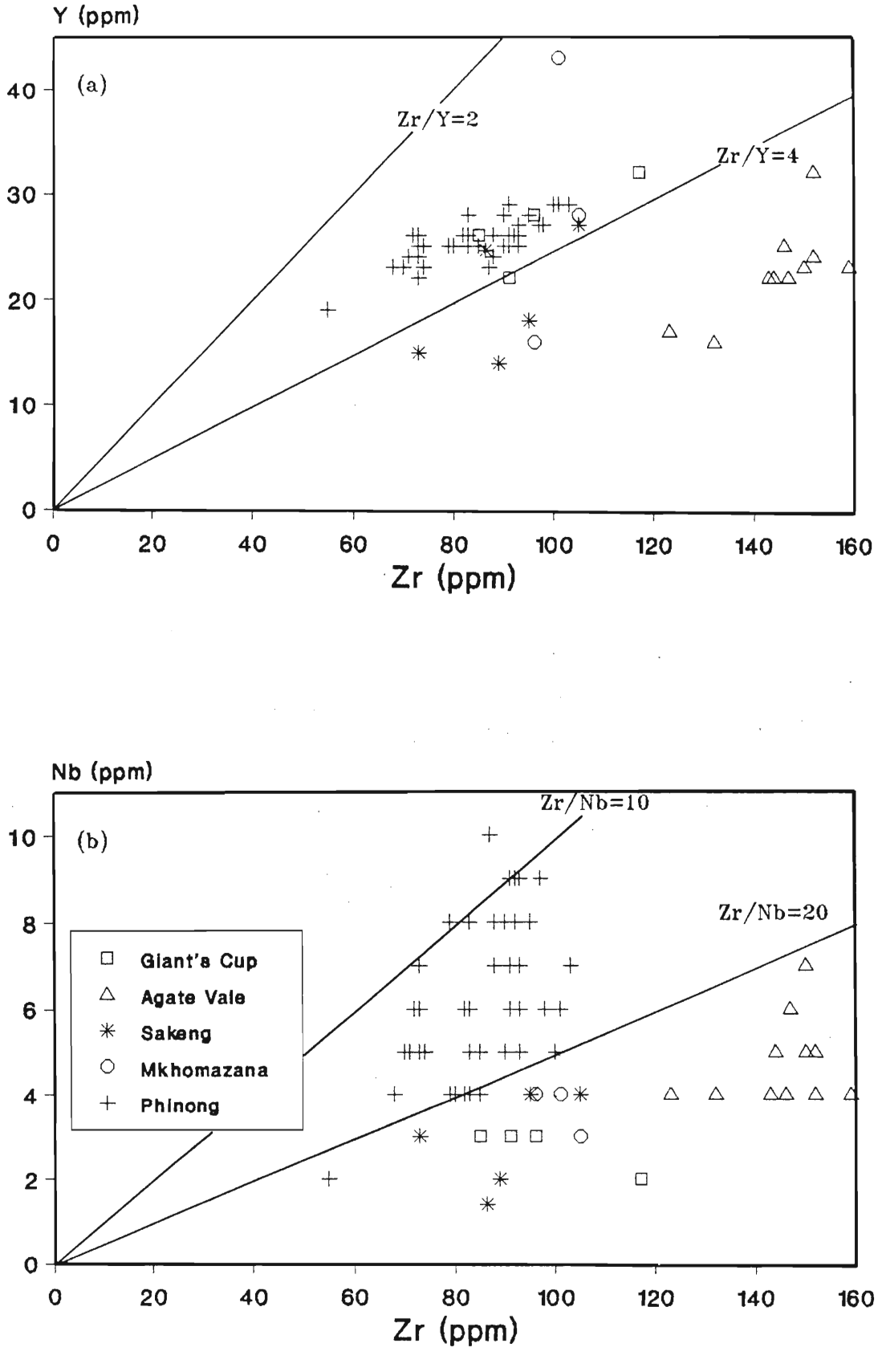

Fig. 9.2a-b Y-Zr and Nb-Zr discrimination diagrams for the Sani Pass magma types. For both ratios the Phinong basalts are clearly separated from the Agate Vale compositions, whilst the Giant's Cup, Sakeng and Mkhomazana basalts show incompatible element ratios akin to both the Phinong and Agate Vale magma types.

7 ppm) but higher Zr concentrations than all other magma types.

Ti/Zr ratios between 50 and 57 form an effective compositional gap between the Agate Vale and the Phinong basalts (Fig. 9.2c). The Giant's Cup, Sakeng and the Mkhomazana type basalts plot in the field of the Phinong basalts, and together have a compositional range of 57 to 100, whilst the Agate Vale type basalts range from 36 to 50 in Ti/Zr ratios.

P/Zr = 7 effectively separates the Phinong basalts (except sample P205) from the Agate Vale, Mkhomazana and the Giant's Cup (except sample GC350) basalts (Fig. 9.2d). The Sakeng basalts are variable in terms of P/Zr ratios, plotting in both these compositional fields. A further subdivision is present at P/Zr=5.5, which separates the Agate Vale basalts from the remaining magma types.

In their study of the Witwatersrand Triad lavas T B Bowen (1984) and M P Bowen (1984) found that the incompatible elements Zr, Ti and P best discriminated between the various lava types. Hence, the Ti/P and Ti/Zr ratios, which when plotted against one another, yield a useful discrimination diagram. A similar plot for the Sani Pass basalts effectively separates the Giant's Cup, Agate Vale, Mkhomazana and Phinong basalts (Fig. 9.3). The Sakeng basalts, however, show compositional characteristics in terms of Ti, P and Zr similar to the Giant's Cup, Mkhomazana and Phinong basalts.

Figs. 9.2a-d serve to illustrate the uniqueness of the Phinong and Agate Vale magma types. In terms of these diagrams the more variable Giant's Cup, Sakeng, and Mkhomazana magmas share geochemical characteristics of both the Phinong and Agate Vale type basalts. A more successful discrimination is obtained using Zr/Ti and Ti/P ratios which effectively separate the Giant's Cup, Agate Vale, Mkhomazana and Phinong basalts (Fig. 9.3).

9.4. Relative Abundance of Incompatible Elements

"Spidergrams" have been successfully used as a tool to infer source area characteristics and relative abundances and petrogenesis of incompatible elements. The discussion that follows is purely descriptive and aims specifically at comparing the relative abundances of incompatible elements amongst the various magma types in the Sani Pass. Inferences drawn

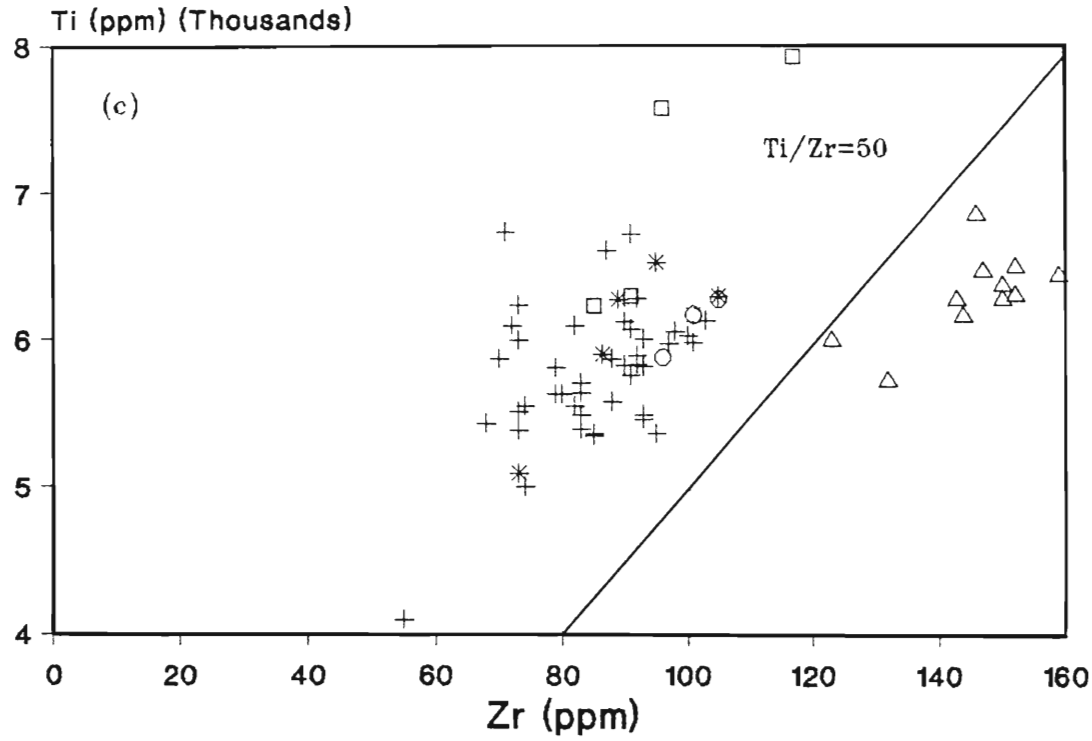

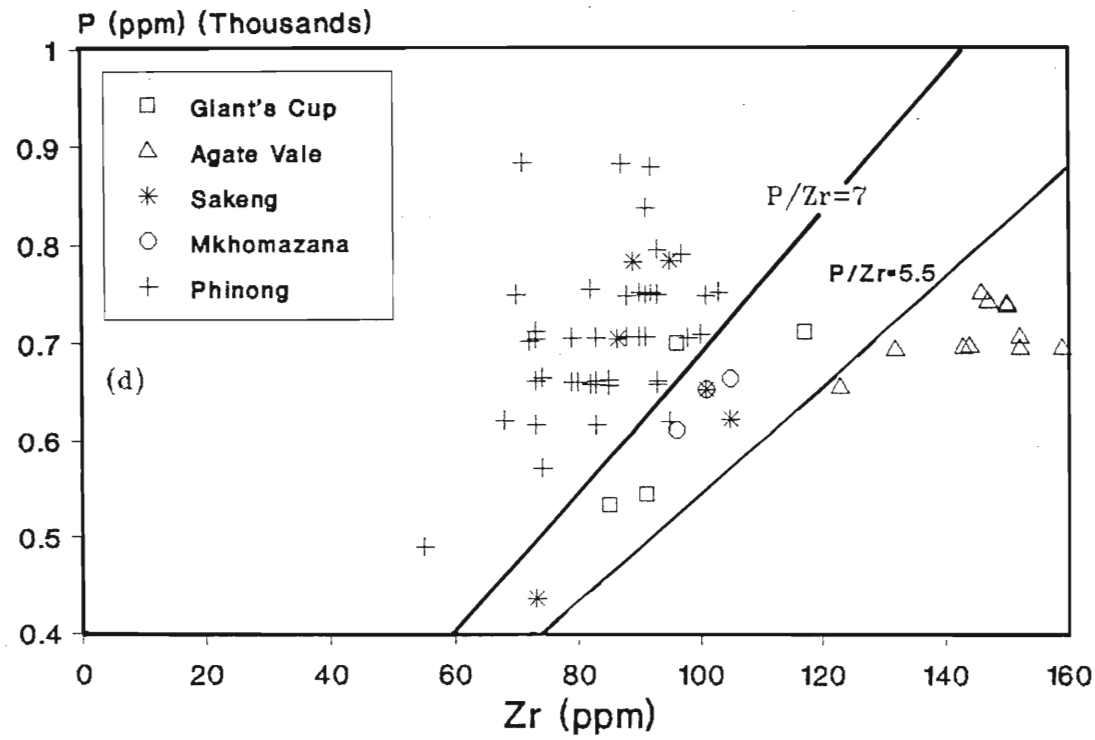

Fig. 9.2c-d Ti-Zr and P-Zr discrimination diagrams for the Sani Pass magma types. The Ti-Zr diagram effectively separates the Agate Vale basalts from the other Sani Pass basalts, while the P-Zr diagram separates most of the pre-Phinong basalts from the Phinong basalts.

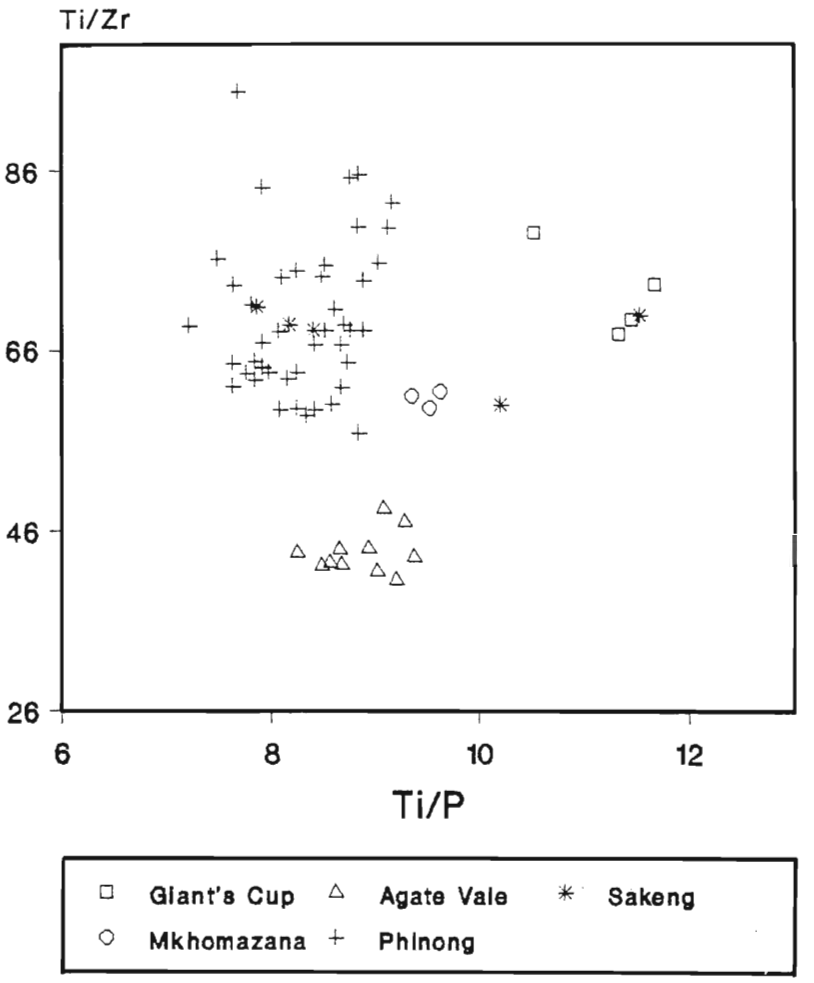

Fig. 9.3 Ti-P-Zr discrimination diagram for the Sani Pass basalts. This diagram effectively separates the Giant's Cup, Agate Vale, Mkomazana and Phinong basalts into different compositional fields. The Sakeng basalts, however, are less restricted and plot in the compostional fields of the Phinong, Mkhomazana and Giant's Cup magma types.

regarding source area characteristics and petrogenesis are discussed in Chapter 10.

The rationale behind the ordering of the elements in the "spidergrams" (Fig. 9.4) is based on two parameters, namely, ionic potential and the bulk distribution coefficient for the elements between garnet lherzolite and melt. The first parameter is a measure of the mobility of an element, and the mobile elements Sr, K, Rb and Ba have been placed on the left of the pattern. The second parameter is a measure of the incompatibility of an element, and in this regard, the incompatibilities of both the mobile and immobile elements increase from the outside to the centre of the pattern. In constructing "spidergrams" for the Sani Pass magma types, average incompatible element concentrations for the different magma types have been plotted. Although the more mobile elements show large within-type variability due to superimposed processes (section 10.2), the average concentrations of these elements are assumed to be good approximations of their pristine values. The relative abundances of incompatible elements for the five magma types in the Sani Pass are displayed in Fig. 9.4. Wood *et al.*, (1979) noted that compositional variation amongst basic lavas is best described using a reference composition to which all lavas are compared. In this study, the Sani Pass basalts have been normalised to the average Lesotho-type basalt (data from Duncan *et al.*, 1984b), since this allows a direct comparison with other Central Area basalts (e.g. Marsh and Eales, 1984) rather than via a third composition as when MORB, chondrite or primordial mantle are used as normalizing compositions. Relative to the average Lesotho basalt the Giant's Cup basalts are depleted in K and Nb and show slight enrichment in Ti and Y. The Agate Vale basalts show slight enrichment in Sr, Rb, Ba and Zr. In terms of the other incompatible elements these basalts are very similar to the average Lesotho basalt. The Sakeng basalts show a relatively flat spidergram, but are depleted in Sr, K, Rb, Ba, Nb and Y relative to the other Sani Pass magmas, as well as the average Lesotho basalt. The Mkhomazana basalts show enrichment anomalies similar to that of the Agate Vale but are also enriched in Y contents and depleted in Nb. Only the Phinong basalts show enrichement in Nb relative to the average Lesotho basalt. For all other elements this magma type shows compositional similarities to the average Lesotho basalt.

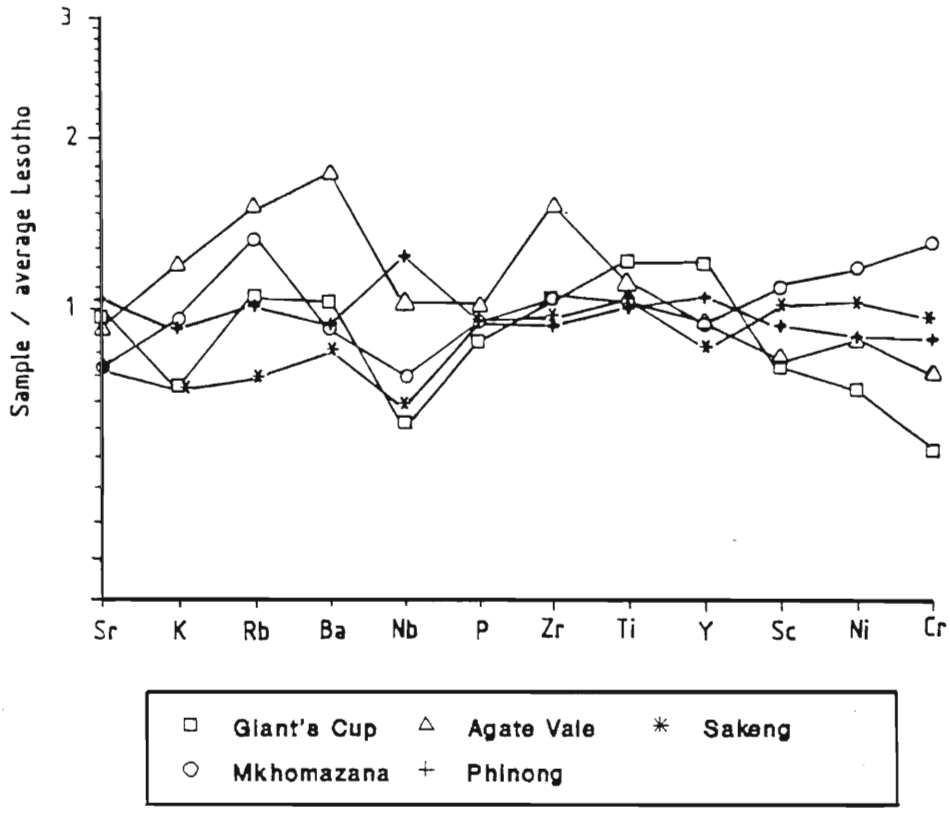

Fig. 9.4 Spidergram of average Sani Pass magma compositions normalized to an average Lesotho-type basalt (normalizing data from Duncan *et al.* 1984b).

9.5. Summary

Although the discussion in chapter 8 has indicated that the Sani Pass basalts can be clearly discriminated on the basis of simple binary major and trace element variation diagrams, this chapter has attempted to better elucidate the individual magma types in the Sani Pass, using a combination of elements. Three techniques have been used, namely, discriminant function analysis (DFA), which utilizes a combination of trace and major elements, incompatible trace element ratios, which make use of high field strength elements, and "spidergrams," using a combination of incompatible and compatible trace elements.

The DFA technique clearly discriminates between the Agate Vale and a combination of Phinong, Sakeng, Mkhomazana and Giant's Cup magma types. Although the Phinong basalts plot in a somewhat coherent field, the Giant's Cup, Mkhomazana and Sakeng magma types are rather erratic, plotting in and about the field for the Phinong basalts. Better discrimination is achieved using incompatible element ratios. The Zr/Nb ratio clearly separates the pre-Phinong basalts from the Phinong basalts. The Zr/Nb, Zr/Y and Zr/Ti, like the DFA, clearly discriminate between the Agate Vale and the remaining lava types in the study area. Zr/Y and Zr/Ti ratios for the Giant's Cup, Sakeng and Mkhomazana basalts are in the range of the Phinong basalts. A combination of Zr/Ti and Ti/P clearly discriminates between the Giant's Cup, Agate Vale, Mkhomazana and Phinong basalts. For all the incompatible element diagrams (except Zr/Nb, Fig. 9.2b) the Sakeng basalts show compositional similarities to the Phinong and other pre-Phinong basalts, (except for the Agate Vale), a feature which in itself makes this magma type some what different. A combination of incompatible elements displayed as "spidergrams" clearly indicates the relative abundance of these elements for each of the magma types in the Sani Pass. The relatively flat pattern displayed by the Phinong basalts indicates compositional similarities with the average Lesotho-type basalt, which has been used as a normalising composition. However, relative to the average Lesotho basalt and the pre-Phinong basalts, the Phinong magma type shows enrichment in Nb. The Agate Vale and Mkhomazana basalts are characterized by enrichment in K, Rb and Ba relative to the other magma types, and in

addition, the Agate Vale has marked Zr enrichment. The Sakeng magma types is depleted in Sr, K, Rb, Ba, Nb and Y, whilst the Giant's Cup is slightly enriched in Ti and Y concentrations.

It is apparent therefore that the combined use of DFA, incompatible element ratios and relative abundances discriminates amongst the different magma types in the Sani Pass.

CHAPTER 10

10. PETROGENESIS OF THE KAROO BASALTS OF THE SANI PASS

10.1. Introduction

The preceding discussion has illustrated the distinctive chemical compositions of the various magma types in the Sani Pass. In a recent publication on the Jurassic Kirwan basalts of Antarctica, Harris *et al.*, (1990) enumerated the factors likely to be responsible for chemical variations in a sequence of lavas. These are:

a) alteration,

b) crystal fractionation with or without crustal assimilation,

c) variation in the degree of partial melting of the source during melt extraction,

d) a heterogeneous source.

These various possibilities will be considered for the Sani Pass basalts.

10.2. Alteration and its effect on whole-rock geochemistry

10.2.1. Introduction

It is important that any geochemical variation due to post-extrusion alteration of the basalts be evaluated, as this can affect further interpretation of the genesis and evolution of these rocks. A range of parameters might be employed to establish evidence of alteration, and several of these are evaluated in respect of the Sani Pass basalts.

10.2.2. Petrographic and field evidence

Petrographic and field evidence might be useful in identifying alteration. As pointed out by Harris *et al.*,(1990), the presence of amygdales, sericitization of plagioclase phenocrysts and alteration of groundmass are all pointers to possible alteration. Most of the pre-Phinong lavas in the Sani Pass succession display ample evidence of alteration, including substantial sericitization of groundmass and phenocryst plagioclase, alteration of groundmass, and the presence of amygdales (Chapter 4). These petrographic features, in particular the amygdales, should be reflected in the whole-rock chemistry.

All the samples in this study have been analyzed for CO_2 (Table A2.2, Appendix 2), enabling normative calcite to be calculated (Table A2.6, Appendix 2). Excessive normative calcite in a rock is an indicator of possible concentrations of amygdales. Abnormally high normative quartz might similarly indicate the presence of amygdales. Zeolite minerals as amygdale infillings are rather more difficult to identify geochemically, although zeolites, chlorite and other hydrated minerals will be reflected in high H_2O^+ values. H_2O^-, on the other hand, is an indication of surface weathering.

In general, the pre-Phinong basalts all have more than 4 weight percent normative quartz, with the exception of AV40, AV70 and AV80 in the Agate Vale unit and the three flows in the Mkhomazana unit. This contrasts with the Phinong basalts, of which only two (P181 and P183) contain more than 4% normative quartz. Similarly, more than 50% of the pre-Phinong basalts (excluding the Mkhomazana unit) contain more than one percent normative calcite, whereas only 4 (P174, P178, P183, P201) out of 44 Phinong samples contain more than one percent normative calcite.

The most noticeably amygdaloidal flows in the Sani Pass basalt succession are GC350 and GC360, at the base of the Giant's Cup unit, and AV400, at the base of the Agate Vale unit. The amygdales in these samples are filled with calcite and, particularly in the case of GC360, quartz. This is clearly reflected in the chemistry, as these are the only three samples in the entire succession containing more than two percent CO_2 (GC350 = 9.74%; GC360 = 5.11%; AV400 = 5.93%). The high CO_2 content of these samples means, in

turn, that they each contain more than 10% normative calcite (Table A2.6, Appendix 2). The high proportion of calcite means that the amount of CaO remaining to form feldspar is low compared to the amount of available Al_2O_3. The excess Al_2O_3 is therefore reflected as normative corundum in these samples. Although crustal contamination can also account for normative corundum, this process is unlikely to be responsible for the normative corundum in samples GC350, GC360 and AV400 (see Section 10.3). The abnormally high normative quartz content of GC360 (19.81 weight percent) reflects the significant amount of quartz present in the rock as amygdale infilling. An important point that should be emphasized, however, is that, in some of the pre-Phinong basalts, calcite and quartz are clearly part of the groundmass, rather than amygdaloidal minerals.

Except for samples P174, P178 and P183, near the base of the succession, the Phinong lavas are uniformly relatively amygdale-free throughout. This feature is reflected in the CO_2 content, which does not exceed 0.4%, except in the aforementioned three samples.

Amygdales should not, however, be taken in isolation as indicators of alteration, as they may represent volatiles exsolved from the magma on the release of pressure. H_2O^+, which represents water bound up in hydrous minerals, and H_2O^-, which represents non-constitional water in the rock, normally behave in tandem. This is because hydrous minerals like zeolites and chlorite (represented by H_2O^+) are often concentrated in amygdales. An amygdaloidal rock is, in turn, porous, and can absorb significant amounts of non-constitional water. Three samples which contrast noticeably in their H_2O^+ and H_2O^- concentrations are M150, M160 and M170 (the Mkhomazana unit).

10.2.3. Oxidation Ratio

The breakdown or decomposition of high-temperature primary minerals and glass to more stable temperature minerals is common in basaltic rocks (Best, 1982) and commonly involves the oxidation of Fe^{2+}, since most of the iron in magmas in the mantle is in the reduced ferrous state, Fe^{2+} (Wood *et al.*, 1990), residing either in the melt or in ferrous silicates. Primary magmas generated from the upper mantle are generally considered to

have low oxidation ratios, but there is much debate about the state of oxidation in the upper mantle (Arculus, 1985). Upon eruption of the basaltic magmas ferrous silicates are unstable, due to a larger concentration of oxygen, and break down to ferric-ferrous oxides, which can be described by the experimental system Fe-Si-O (Ernst, 1976). The increased oxygen may come from the atmosphere or dissociation of H_2O dissolved in the melt, where hydrogen readily diffuses out of the system, leaving the less mobile oxygen molecules to participate in oxidation reactions (Sato, 1978; Mathez, 1984). Although the lithosperic mantle is thought of as a reduced environment (Richardson *et al.*, 1984), oxidizing conditions may be introduced via subduction of altered oceanic crust deep into the mantle (Ballhaus, *et al.*, 1990, Wood *et al.*, 1990).

The degree of oxidation can affect the Fe_2O_3 content of basalts considerably. In order to correct for this secondary or 'accidental' oxidation, numerous oxidation ratios, i.e., Fe_2O_3/FeO, have been proposed which supposedly reflect pristine compositions (Brooks, 1976; Hughes, 1979; Hughes and Hussey, 1976; Middlemost, 1989). In this study, actual FeO concentrations have been determined by wet chemical methods (Appendix 2, Tables A2.2 and A2.3) as well as total iron as Fe_2O_3 (by XRF), making it possible to assess the degree of oxidation of the Sani Pass basalts and dolerites, compared to a pristine basalt, having a ferric to ferrous ratio in the proportion 2:10.

Figure 10.1 displays the actual FeO concentrations and Fe_2O_3 (recalculated from tFe_2O_3) for the Sani Pass basalts and dolerites. These data show a negative trend of increasing Fe_2O_3 with a corresponding decrease in the FeO content. Fe_2O_3/FeO varies from 0.07 to 5.20, but most of the basalt analyses plot in a field having $Fe_2O_3/FeO > 0.2$, implying that these rocks have undergone variable degrees of oxidation and do not reflect the pristine iron composition. Four samples (S120, M150, P204 and P227) have $Fe_2O_3/Fe < 0.2$ and of these, sample P227 has been shown to have experienced cumulus enrichment of ferromagnesian minerals which would have increased its FeO content (9.62 weight percent), giving it a low Fe_2O_3/FeO ratio. The three remaining samples that have $Fe_2O_3/FeO < 0.2$ also have high FeO concentrations, in the range 7.97 to 8.92 weight percent (Table A2.2, Appendix 2). Sample P180 is the only basalt sample with a Fe_2O_3/FeO ratio of 0.2.

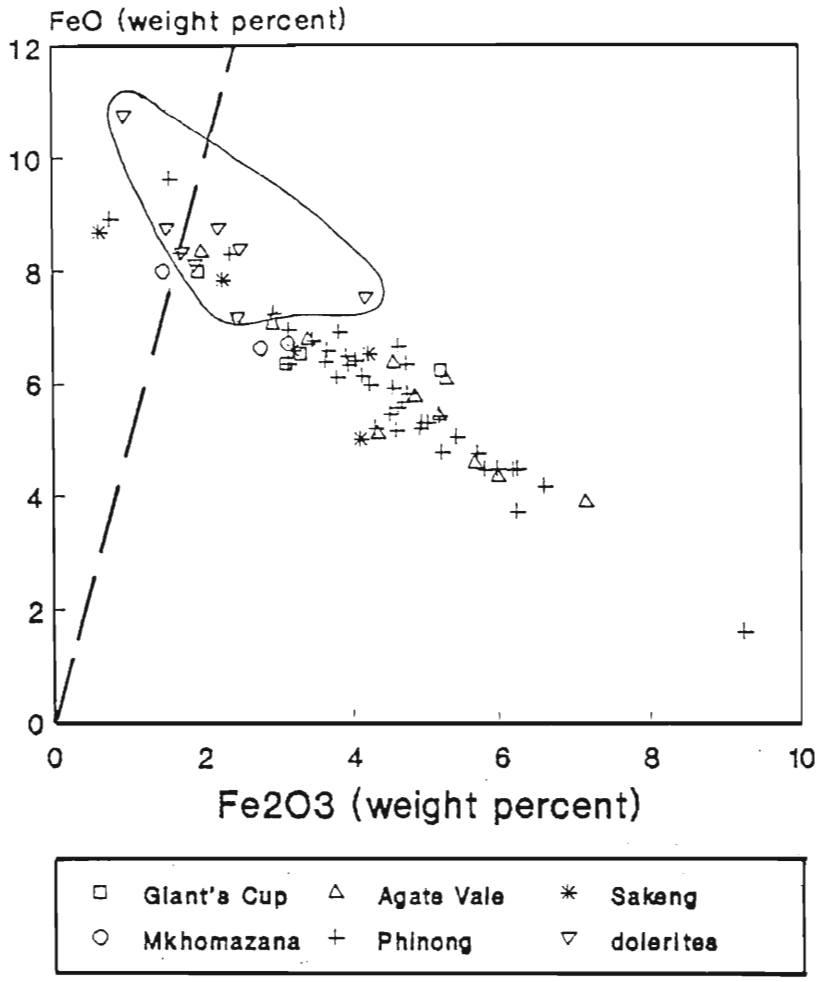

Fig. 10.1 The variation of measured FeO and Fe_2O_3 concentrations in the Sani Pass basalts and dolerites. The broken line represents an oxidation ratio (Fe_2O_3/FeO) of 0.2. The field delineated by the solid line is that for the dolerites.

Unlike the basalts in the Sani Pass, the dolerites in the immediate vicinity show less variability, but more interestingly, most are located close to $Fe_2O_3/FeO = 0.2$. Cox and Hornung (1966) used an oxidation ratio of 0.1 in their study of the Lesotho basalts, on the basis that this value approximated the oxidation ratio of the dolerites which had been less altered than the basalts and therefore approximated pristine compositions very closely. Petrographic evidence does indicate that the dolerites are much fresher than most of the basalts in the Sani Pass. The use of an oxidation ratio of 0.2 in this study, therefore seems justifiable. The higher oxidation ratio of the Sani Pass basalts compared to the dolerites is possibly a consequence of weathering or alteration during zeolitization of the lava pile. The variation in the oxidation ratio of the Sani Pass basalts and dolerites is therefore not an artifact of the source region characteristics, which Carmichael (1991) proposed for the redox conditions of basic and silicic magmas.

Using actual measured FeO concentrations in the oxidation ratio, average Fe_2O_3/FeO values for the Sani Pass magmas are:

Dolerites = 0.27

Phinong = 0.89

Mkhomazana = 0.35

Sakeng = 0.46

Agate Vale = 0.89

Giant's Cup = 0.52

Although the average Fe_2O_3/FeO ratios for all the magma types exceed $Fe_2O_3/FeO = 0.2$, there is considerable variation from flow to flow (Fig. 10.1), with some being more than 0.2 and others less.

The Giant's Cup basalts vary in their Fe_2O_3/FeO ratio from 0.24 to 0.83. The comparatively low oxidation ratio of sample GC370 is due to its high FeO content (7.97 weight percent, unnormalised), while sample GC380 has a high tFe_2O_3 content (12.11 weight percent, unnormalised), giving it the highest oxidation ratio in this magma type.

Oxidation ratios for the Agate Vale basalts are highly variable, ranging from 0.24 to 1.83

and are essentially due to the range in FeO concentrations (3.88 to 8.33 weight percent, unnormalized). In samples AV400, AV60 and AV70 the Fe_2O_3/FeO ratio exceeds 1, meaning that these samples contain more oxidized iron than FeO. Middlemost (1989) noted that the Fe^{3+} is generally accommodated by the oxide minerals, in addition to Fe^{2+}.

The basal flow of the Sakeng basalts is marked by an extremely low oxidation ratio of 0.07, whilst the overlying basalts from this magma type range in oxidation ratio from 0.29 to 0.65. The low oxidation ratio of sample S120 is due to a high FeO content (8.68 weight percent, unnormalized), this oxide being contained in the ferromagnesian minerals.

The Mkhomazana basalts, which show petrographic evidence for alteration, show a somewhat restricted range of oxidation ratios, from 0.18 to 0.46. The basal flow of this magma type is also characterized by a low oxidation ratio (0.18) and high FeO content (7.97 weight percent, unnormalized).

The Phinong basalts are variable in their Fe_2O_3/FeO ratios, ranging from 0.08 to 5.74. Sample P228 has an extremely low FeO content (1.61 weight percent, unnormalized), and consequently a very high oxidation ratio. Petrographically, however, the ferromagnesian minerals in this sample do not show the extreme decomposition expected from such a high oxidation ratio. Nine other samples have Fe_2O_3 > FeO and oxidation ratios larger than 1. Two samples (P204 and P227) have Fe_2O_3/FeO < 0.2, but P227 has been shown to be enriched in cumulus olivine (and possibly, pyroxene), which could account for the high FeO (9.62 weight percent, unnormalized) in this sample. Samples P204 and P180 also have a high FeO content of 8.92 and 8.30 weight percent (unnormalized), respectively; the latter sample having an oxidation ratio of 0.20. Sample P204 is altered, whilst P180 is much fresher in handsample and thin section.

The dolerites have the lowest range of oxidation ratios, ranging from 0.09 to 0.56, their average therefore approximates the theoretical oxidation ratio of 0.2 most closely compared to the Sani Pass volcanics. The suite of samples is also petrographically the freshest.

An assessment of oxidation indicates that most of the Sani Pass basalts have experienced post-eruptive oxidation. The degree of oxidation in the Sani Pass has been variable and individual magma types do not indicate specific oxidation ratios. However, the dolerites are

broadly, less oxidized than the basalts, as reflected petrographically , as well as by their low oxidation ratios.

10.2.4. Chemical Index of Alteration

Nesbitt and Young (1982) employed a formula, known as the 'chemical index of alteration' (CIA) to evaluate alteration in terms of chemical effects. This formula which utilizes molecular proportions is represented as:

$$CIA = [Al_2O_3/(Al_2O_3+CaO+Na_2O+K_2O)] \times 100$$

where CaO is the amount of CaO incorporated in the silicate fraction of the rock. Hence, it is necessary to correct for the CaO content of the apatite and carbonate, as outlined by Nesbitt and Young (1982). The resultant value is therefore a measure of the proportion of Al_2O_3 versus the labile oxides in the analysed sample. CIA values for unaltered plagioclase, augite and magnetite/ilmenite are approximately 50, 6 and 100 respectively; consequently fresh basalts have values between 30 to 45.

Figure 10.2, which is plot of CIA against stratigraphy, indicates that all the basalt analyses obtained in this study fall within the range 38 to 49. Although most of the samples fall within the CIA range for fresh basalts (30 to 45), petrographic evidence indicates that alteration has affected the Sani Pass rocks to varying degrees. Rocks that appear petrographically to be the freshest, generally have a CIA range of about 38 to 41.

It is evident in Fig. 10.2 that the two lowermost flows of the Giant's Cup unit (GC350 and GC360), and the basal flow of the Agate Vale magma type (AV400) have high CIA values (44 to 49), which reflect the proportion of calcium loss, possibly during amygdale formation, since most of the calcium now occurs as calcite in the vesicles. The CIA in the Agate Vale samples (except AV400) is an indication of their low whole-rock CaO content, ranging from 6.85 to 10.38 weight percent. The low CaO content in these basalts is accompanied by a slight enrichment in the alkalies, Sr and Zr, and a slight depletion in Mg#, suggesting that their low CaO content is more likely to be a primary effect, rather than as a result of alteration. In fact, in thin section the Agate Vale basalts (except sample

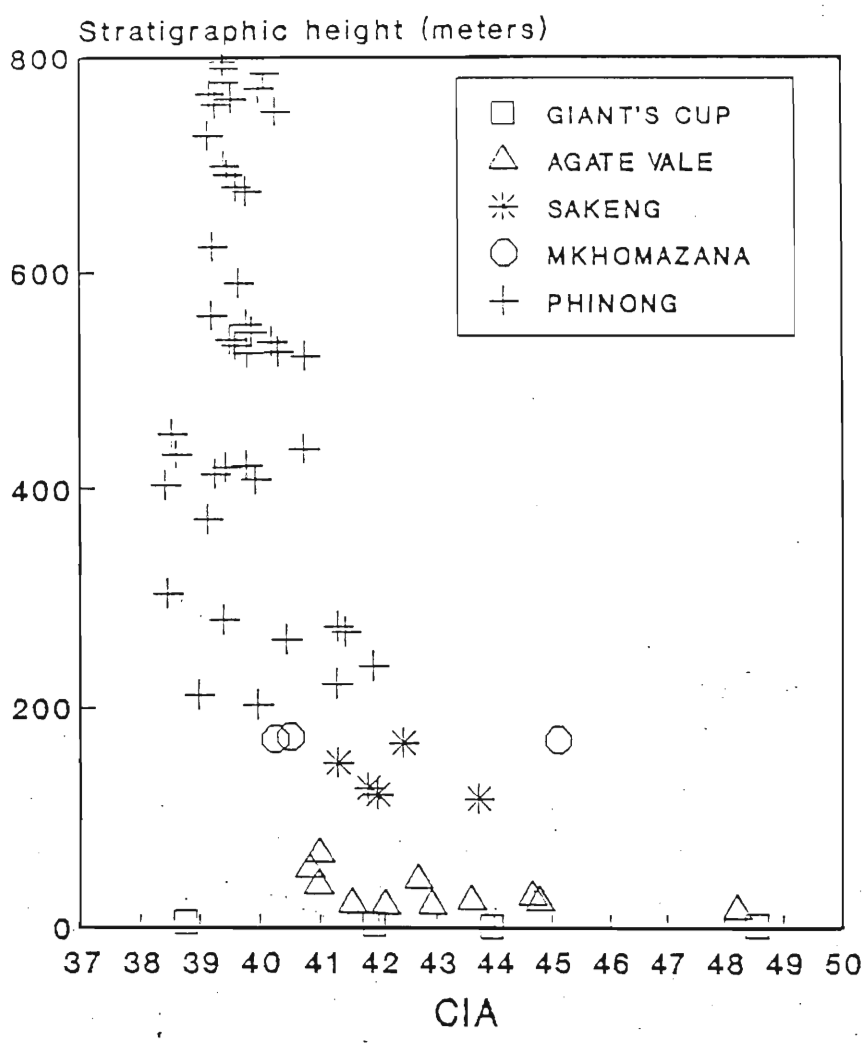

Fig. 10.2 The variation of the chemical index of alteration (CIA) in the Sani Pass volcanic succession.

AV400) are moderately fresh, and in most cases are just as fresh as the Phinong basalts. All of the Sakeng basalts fall out of the CIA range of 38 to 41 for the petrographically fresh rocks, their CIA varying from 41 to 44. This slightly larger CIA for the Sakeng basalts is attributed to a slight depletion in Na_2O content (1.65 to 2.11 weight percent). No supporting evidence exists to suggest that the lower Na_2O content in these rocks might be a primary effect. In fact, the low Na_2O contents in the Sakeng basalts are accompanied by a slight depletion in Sr contents; both of these elements being very mobile (Marsh and Eales, 1984; Noack *et al.*, 1990; Prudencio *et al.*, 1990; Marsh, 1991). The low Na_2O and Sr content in these basalts might therefore be a consequence of alteration.

The use of the CIA in quantifying alteration breaks down when applied to the Mkhomazana basalts. These rocks show the strongest petrographic evidence for alteration, but only the basal flow (M150) has a correspondingly high CIA (45), while the overlying flows (M160 and M170) have CIA values in the range of petrographically fresher rocks (38 to 41). The Mkhomazana basalts are depleted in CaO contents (6.36 to 8.73 weight percent) and enriched in Na_2O contents (4.16 to 4.51 weight percent) compared to the other Sani Pass basalts. It seems that this gain and loss in Na_2O and CaO content, respectively, is masking the true effects of any alteration. The basal flow (M150) has a high CIA because of the extremely low CaO content and slight enrichment in Al_2O_3. The Phinong basalts generally have lower CIA values than the pre-Phinong basalts and are also the least altered as a group.

The use of the CIA is limited and its application to the Sani Pass basalts has only been partially successful. A limitation of the CIA is that it reflects, in certain instances (for example, the Agate Vale basalts), primary compositional differences, and for this reason it cannot be assessed in isolation but must be viewed in conjunction with other elements not incorporated in the index. Also, it is apparent that unless a nett loss in CaO, Na_2O and K_2O, compared to Al_2O_3 content occurs, the use of the CIA is not very successful. Nevertheless, this index has indicated that the two lowermost flows of the Giant's Cup unit and the basal flow of the Agate Vale basaltic unit have experienced CaO loss from the silicate fraction, while the Sakeng basalts suffered a nett loss in Na_2O.

10.2.5. Albitisation

The Mkhomazana basalts are enriched in Na_2O contents (4.16 to 4.51 weight percent) and slightly depleted in CaO (6.37 to 8.73 weight percent) compared to all other magma types in the Sani Pass. Commonly volcanic rocks that show a similar enrichment in Na_2O include the alkaline basalts found in Hawaii (Chen *et al.*, 1991) and, particularly, the high sodic alkaline rocks from Tasmania documented by Adam (1990). However, the Mkhomazana basalts differ from these rocks in having excess silica, and therefore plot on the silica oversaturated side of the Yoder and Tilley (1962) basalt tetrahedron, in contrast to the silica undersaturated nature of the alkalic basalts.

The presence of plagioclase phenocrysts, as well as those in subophitic association with pyroxene in the Mkhomazana basalts (Chapter 4) indicate that plagioclase formed before pyroxene, or both phases crystallized more or less simultaneously. It is unlikely that Na-rich plagioclase would crystallize before or simultaneously with augite, since Na-rich plagioclase would be incapable of such development at the temperatures required by the pyroxenes. The Na-rich plagioclase in the Mkhomazana basalts, therefore must have resulted from changes in conditions imposed after consolidation of the melt, that is, they must have a secondary status.

Rocks having a similar chemistry to the Mkhomazana basalts have been well documented (e.g. Vallance, 1974; Schutte and Cornell, 1990; Erlank *et al.*, 1990a). A common feature of these rocks, however, is that they all have been erupted in a sub-marine environment, and have been altered by sea-water containing sodium, which brought about albitisation of the plagioclase feldspars. Vallance (1974) noted that the albitisation process is accompanied by an increase in Ba, Sr, Rb and K concentrations. The basal flow of the Mkhomazana magma (M150) shows extreme enrichment in these elements (K, Rb and Ba) that decrease progressively through the two overlying flows. This decrease in K, Rb and Ba content results in sample M170 attaining an almost Lesotho-type basalt composition for these specific elements. Thus, feldspar alteration for the Mkhomazana basalts by hydrothermal fluids does not hold for all three flows.

Humphris and Thomson (1978), Seyfried and Bischoff (1977), and Erlank *et al.*, (1990a), have shown that during sea-water alteration of pillow lavas MgO is commonly added during serpentinisation and chloritisation of the ferromagnesian minerals and calcium is removed. The Mkhomazana basalts do show high MgO contents relative to most of the other pre-Phinong basalts (7.19 to 7.44 weight percent). However, the slightly elevated MgO content, which gives these rocks an olivine-normative character, is also accompanied by a higher Cr and Ni content, meaning that the high MgO content of these rocks is probably primary and has not been affected by alteration.

The possibility for localised alteration by hydrothermal solutions does exist, since sediment-filled post-extrusion cracks above the Mkhomazana magma type and numerous rheomorphic dykes within the flows could have been ideal pathways for any hydrothermal solutions percolating through the flows. However, it is difficult to reconcile why only three flows, with a total thickness of 6m, were affected and not the whole pre-Phinong package. More specifically, there is a sharp cut-off at the base of the Mkhomazana unit in terms of CaO and Na_2O contents, whereas a gradual tailing off downwards would be expected of any postulated alteration. The effect of alteration cannot be conclusively resolved in the Mkhomazana basalts and therefore, other possibilities will be examined in the following sections.

10.3. Crystal Fractionation

Petrological research has documented the importance of fractional crystallization as a means of producing variation in magmas, and numerous studies have demonstrated that *in situ* crystal fractionation has operated within intrusions of Lesotho-type magmas (Eales and Robey, 1976; Le Roex and Reid, 1978; Eales, 1980). Crystal fractionation has also been invoked to explain variation of magmas in other flood basalt sequences (Cox and Mitchell, 1988; Harris *et al.*, 1990).

Crystal fractionation may occur under conditions of high or low-pressure and in an open or closed system. If material is added to or removed from a fractionating magma chamber,

then the system is regarded as "open" and if no material has been introduced into or removed from the chamber, the system is regarded as "closed." In the latter case crystalline material may be separated from the liquid in the form of cumulates. In open systems material may be introduced by assimilation of wall rocks and/or continental lithosphere, or removed by eruption.

10.3.1. Closed system low pressure fractionation

Closed system low pressure fractionation is evaluated using major element oxides and a least squares mixing technique. A problem with modelling possible crystal fractionation processes in the Sani Pass basalts is that compositional trends are not well defined for most interelement plots, and the choice of endmembers is restricted by the lack of mineral chemistry. The use of this technique is therefore only semi-quantitative.

Major element oxides are modelled using SiO_2 variation diagrams that compare basalt composition trends with mineral composition data. This technique therefore provides an indication of the path along which a liquid would evolve as particular minerals or combinations thereof are "extracted." The Sani Pass basalts are assessed in terms of TiO_2, Al_2O_3, CaO, MgO and FeO (Fig. 10.3a-e); the major constituents in plagioclase, olivine, pyroxene and magnetite, which are likely fractionating phases in a basaltic assemblage. These plots were derived from the major element variation diagrams (Fig. 8.2) discussed in Chapter 8, and microprobe data discussed in Chapter 5, and plotted according to the method of Cox *et al.*, (1979). The estimated between - magma type trend in Figs. 10.3a-e is designated by the thick arrow, whilst the less bold vectors indicate the different phenocryst phases.

Evaluation of these graphical data indicates a combination of possible fractionating phases, namely, olivine + plagioclase, olivine + plagioclase + pyroxene (either augite or pigeonite, or augite and pigeonite). Plagioclase fractionation is essential, since it promotes a depletion in Al_2O_3 and inhibits rapid depletion of MgO and FeO which are incorporated into any crystallizing mafic phases. The separation of olivine is necessary in order to

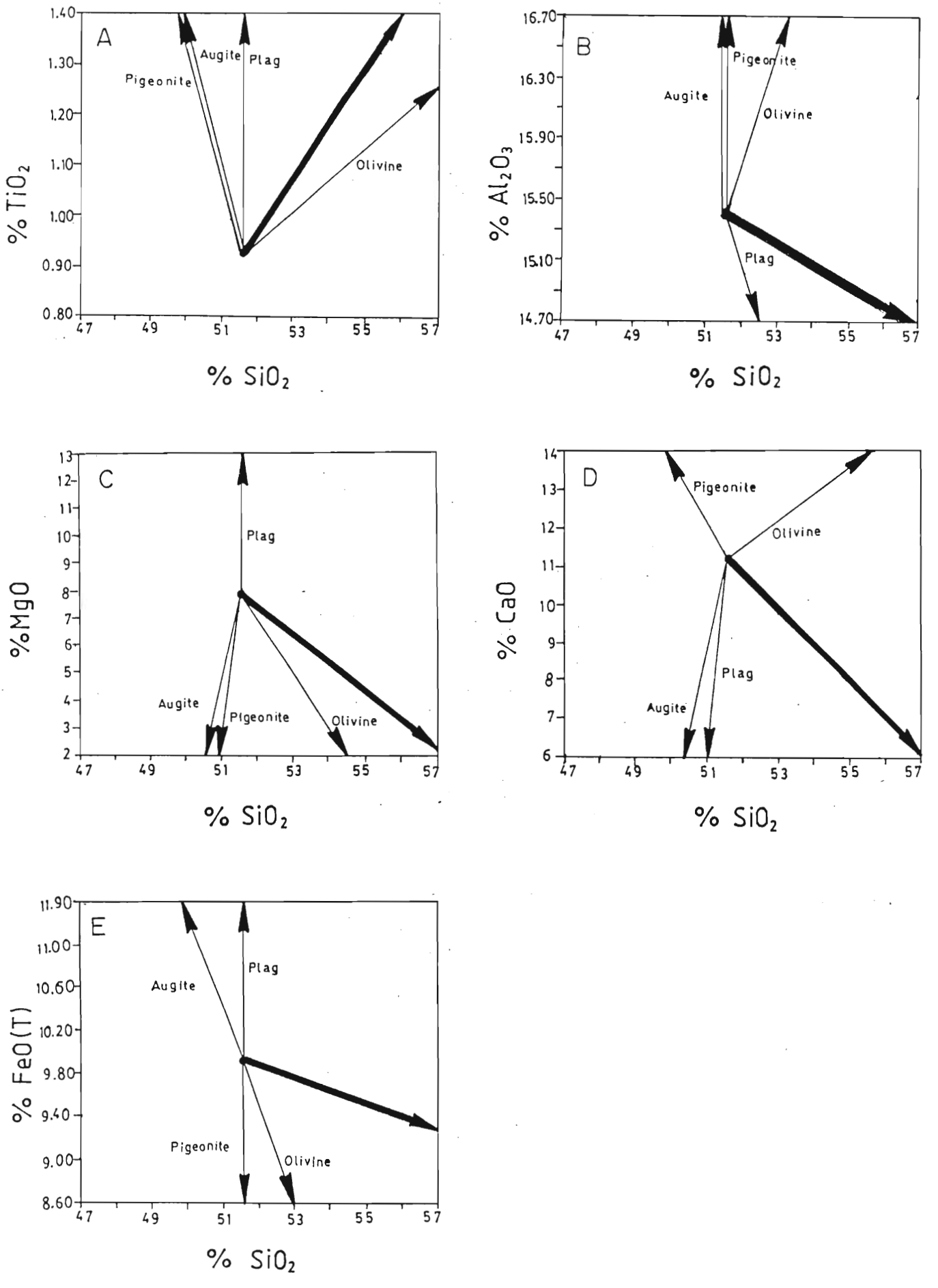

Fig. 10.3a-f Between - magma type composition trends (broad arrows) in relation to phase extract vectors (arrows). The lengths of the vectors have no significance.

maintain the balance due to the effect of plagioclase (or augite) fractionation on the rate of CaO depletion.

The Sani Pass magma types have been modelled using a least squares mixing programme of B M Eglington and R E Harmer of the CSIR, Pretoria, based on the algorithm of Bryan *et al.*, (1968). The approach used here is to use the major elements to test whether differentiation can produce the general changes observed between a hypothetical parent and the more evolved daughter composition from each magma type. The Phinong magma type, by virtue of its large relative volume and less evolved nature, compared to the other magma types in the Sani Pass, must be considered as the most likely parent to the other magma types. Samples having MgO greater than 8 weight percent have been ignored as possible parent compositions, since they are most likely to have experienced cumulus olivine enrichment, and therefore do not reflect their pristine compositions. Sample P200 which has MgO=7.84 weight percent and does not show any evidence of cumulus enrichment or significant alteration which might have affected its composition, has been chosen as the hypothetical parent.

Confident acceptance of the least squares mixing technique relies an obtaining very small residuals (Wright, 1974). When the daughter compositions for the Giant's Cup, Agate Vale, Sakeng and Mkhomazana magma types are modelled using P200 as a hypothetical parent, using olivine + plagioclase and olivine + plagioclase + pyroxene as fractionating phases, the results are statistically inconsistent. In all cases, squared residuals are in excess of 1%. It is also noteworthy that the positive P_2O_5 residual in all cases suggests that apatite may have crystallized in addition to other fractionating phases.

From the preceding discussion, it is concluded that the variation in terms of major elements between the various magma types in the Sani Pass, cannot be explained by a low pressure fractionation model that utilizes a parent composition such as P200 and olivine + plagioclase, and olivine + pyroxene + plagioclase as fractionating phases.

The Phinong magma type, which is the most abundant magma type in the study area and therefore has the most data, has been modelled using the least squares technique in order to ascertain whether fractionation within it can be used to relate the primitive compositions to

the more evolved compositions. Limited mineral chemistry data precludes any realistic modelling of variations within the other magma types. Sample P273 which occurs stratigraphically high up in the Phinong succession, and has a relatively evolved composition has been chosen as the daughter composition.

The model in Table 10.1 which depicts the Phinong magma type end-member compositions requires plagioclase + pyroxene + olivine as fractionating phases in the proportion 48%, 32% and 20% respectively, with 26% fractionation. The inclusion of ilmenite (mineral chemistry from Sweeney, 1988) in the fractionating assemblage also yields results with low squared residuals, indicating that ilmenite might have become an important fractionating phase in the advanced stage of crystallization. However, it is fortuitous to include ilmenite as a fractionating phase in the Sani Pass basalt assemblage, since the mineral chemistry data were obtained from Sweeney (1988). The phenocryst populations are much richer in plagioclase and very much less in olivine than the crystal extracts calculated for the mixing model in Table 10.1. Petrographic evidence indicates that the average phenocryst assemblage consists of plagioclase, clinopyroxene and olivine in the proportions 70%, 25%, 5% respectively. The enrichment of plagioclase relative to the expected cotectic proportions as predicted by the mixing model in Table 10.1 has been observed by Cox and Mitchell (1988) in basalts from the Deccan Traps, and Harris *et al.*, (1990) in basalts from Dronning Maud Land. Cox and Mitchell (1988) ascribed the enrichment in plagioclase phenocrysts to their neutral density in basaltic liquids and consequent selective transport to the surface. They also observed, like Harris *et al.*, (1990), that the porphyritic basalts have groundmasses which are more iron-rich and therefore denser than the groundmasses of the aphyric basalts. For the Sani Pass basalts, the presence of accumulated plagioclase does not invalidate the crystal fractionation model, because in both endmembers the phenocryst content is relatively low.

Table 10.1 Mixing calculations relating primitive basalt P200 to evolved basalt P273.

Input data: (elements concentrations recalculated to 100%)

	P273	P200oliv	P200plag	P200aug	P200
SiO2	52.56	37.01	52.29	53.40	51.70
TiO2	1.00	0.00	0.00	0.48	0.93
Al2O3	15.66	0.00	30.12	1.61	15.44
FeO*	10.45	26.34	0.71	10.09	10.03
MnO	0.18	0.00	0.00	0.29	0.18
MgO	6.12	36.36	0.00	17.05	7.85
CaO	10.80	0.29	13.79	16.93	11.09
Na2O	2.30	0.00	2.93	0.14	2.10
K2O	0.77	0.00	0.16	0.00	0.52
P2O5	0.16	0.00	0.00	0.00	0.15

Model is:

P273 + components = P200

X Y

	Y.Obs.	Y.Est.	Residuals	Component	Wt %	S.Dev.
SiO2	51.70	51.70	-0.0002	P273	74.1284	1.090
TiO2	0.93	0.78	0.1431	P200oliv	5.2687	0.277
Al2O3	15.44	15.44	0.0020	P200plag	12.2897	0.645
FeO*	10.03	10.05	-0.0163	P200aug	8.1706	0.515
MnO	0.18	0.16	0.0255			
MgO	7.85	7.84	0.0121	Total	99.8575	1.395
CaO	11.09	11.10	-0.0067			
Na2O	2.10	2.07	0.0227			
K2O	0.52	0.59	-0.0733			
P2O5	0.15	0.12	0.0337			

Squared residuals : 0.0286

CHI squared := 0.044 Limit := 3.33

10.3.2. Trace element variations

Trace element variations are used to independently evaluate the results of the major element least squares model, by utilizing published mineral/liquid distribution coefficients and the Rayleigh fractionation equation. The theoretical basis of this model is discussed below.

When a mineral is in chemical equilibrium with a liquid, elements are partitioned between the two phases according to their chemical activity in each. For trace elements this relationship can be expressed as:

$$K_D = \frac{[X] \text{ crystal}}{[X] \text{ liquid}} \qquad \text{----- (10.1)}$$

where K_D is a constant known as the distribution or partition coefficient for a given crystal-liquid equilibrium and [X] is the concentration of the trace element.

In this study trace element fractionation is modelled using the Rayleigh fractionation law given in Arth (1976):

$$C_L/C_o = F^{(D-1)} \qquad \text{----- (10.2)}$$

where C_L is the concentration of an element in the differentiated liquid, C_o is the concentration of an element in the original melt, and F is the fraction of liquid remaining. D is the bulk partition coefficient for an element and is given by:

$$D = W^aK^{a/i} + W^bK^{b/i} + \ldots \qquad \text{----- (10.3) (after Greenland, 1970)}$$

where W is the weight proportion of each mineral and K is the solid-liquid partition coefficient for each of the precipitated phases a, b, etc. The distribution coefficients used are listed in Appendix 5 and have been selected from values available in the literature.

The bulk distribution coefficient is a function of the ease of distribution of trace elements

between coexisting mineral and melt. Hence if $D < 1$, the trace elements are preferentially concentrated in the liquid phase and are incompatible with coexisting minerals, while compatible elements which have $D > 1$ are preferentially retained in the crystallizing solid phase and depleted in the residual liquids. From this it follows that incompatible elements (Rb, Zr, Y, Nb, Ti-except for magnetite) should be rejected by most early crystallizing minerals. Thus, during fractional crystallization, two incompatible elements in a comagmatic suite of liquid compositions, should maintain a constant ratio. Compatible elements, on the other hand, will be enriched or depleted relative to one another depending on the phases fractionating.

In assessing crystal fractionation within the Phinong magma type, the approach adopted is to check the trace element concentrations (calculated using the Rayleigh fractionation law, equation 10.2) against those observed in the actual daughter sample (P273).

Table 10.2 shows the predicted and actual trace element concentrations for sample P273, using plagioclase, clinopyroxene and olivine as fractionating phases in the proportions calculated by least squares mixing (Table 10.1). A reasonably good agreement between predicted and actual concentrations is achieved for the incompatible elements, Nb, Zr, Y and Rb, whilst the poor fit for Ba and Sr can be attributed to mobility of these elements during alteration. For the compatible elements poorer agreement is achieved. Ni is underestimated because of the greater proportion of olivine involved, and Cr is overestimated because of the absence of magnetite in the fractionating assemblage. In conclusion, although the incompatible elements are slightly overestimated, the major elements are consistent with 26% crystal fractionation within the Phinong magma type involving plagioclase (48%), clinopyroxene (32%), olivine (20%) and possibly small amounts of magnetite.

Table 10.2 **Comparison of observed and calculated trace element compositions for the model presented in Table 10.1**

Element	Parent (P200)	Daughter (P273)	
	Obs	Obs	Calc
Ba	158	189	213
Nb	5	5	7
Zr	74	100	98
Y	25	29	31
Sr	209	189	246
Rb	11	16	15
Ni	96	62	14
Cr	336	164	208
V	224	244	243

10.3.3. High Pressure Fractionation

Unlike low pressure fractionation, high pressure fractionation cannot be properly constrained for various reasons, namely, the lack of field or petrographic evidence for high pressure indicator minerals, the scarcity of high pressure fractional crystallization data for Karoo basaltic rocks, and the effect of pressure and bulk composition on trace element distribution coefficients is poorly constrained. This problem is compounded by the fact that the Sani Pass basalts evolved to their present compositions by low pressure fractionation. This is indicated by Fig. 10.4, which is a plagioclase projection for the Sani Pass basalts into the plagioclase-diopside-olivine-quartz system (as determined for mid-ocean ridge basalts at 1 atmosphere by Walker *et al.*, (1979). The Sani Pass basalts, therefore, contain no record of their high pressure assemblage (if any) in their erupted major element composition.

Possible mineral assemblages due to fractional crystallization at different pressures were predicted by O'Hara (1965; 1968) and O'Hara and Yoder (1967). At increasing pressures the olivine liquidus field contracts relative to the other phases in the CMAS system (O'Hara, 1968). Therefore, initial melts of an olivine-bearing mantle must become more olivine-rich

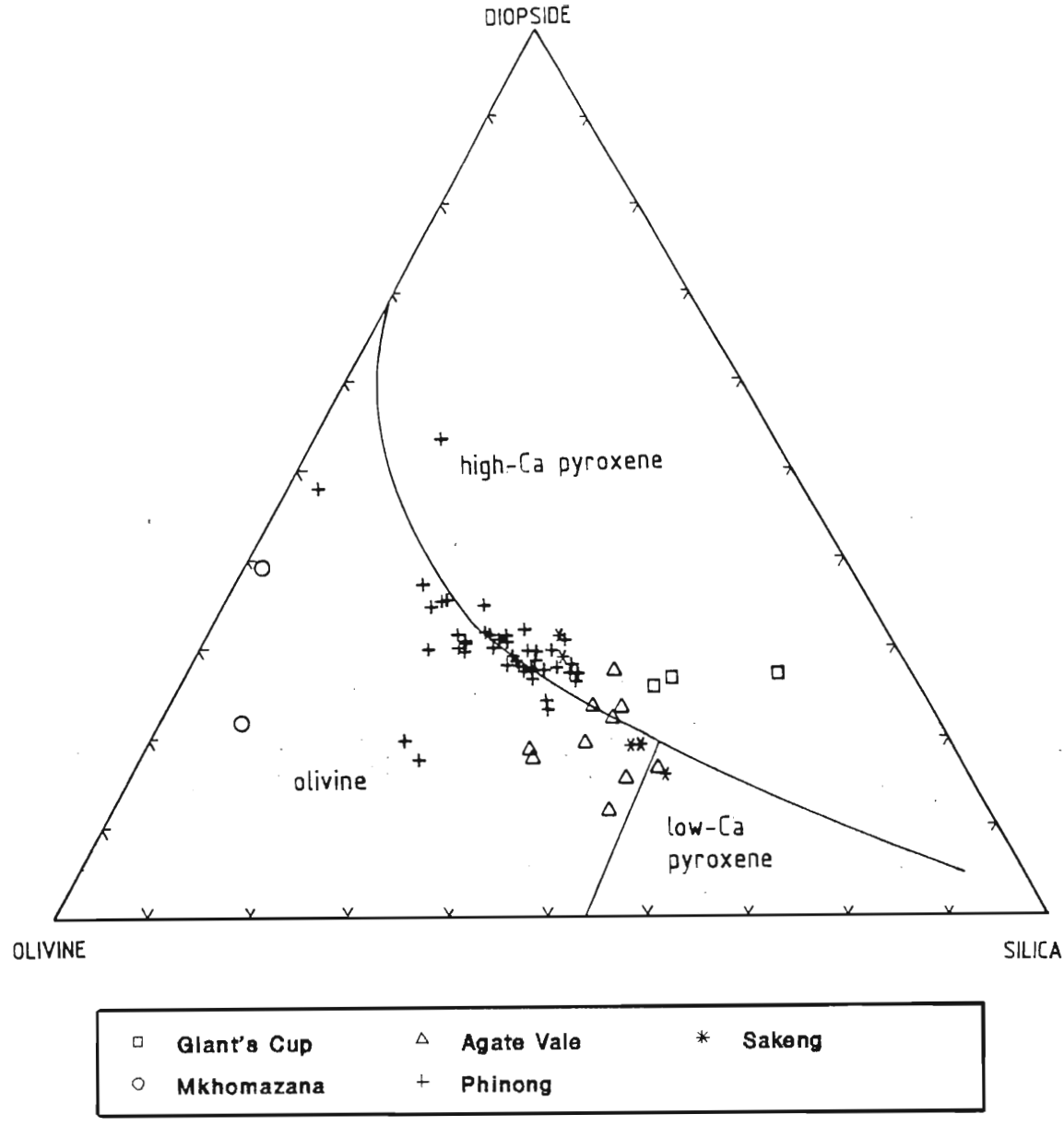

Fig. 10.4 Plagioclase projection for the Sani Pass basalts into the plagioclase - diopside - olivine - quartz system (as determined for MORB at 1 atm by Walker *et al.* (1979).

(picritic) with increasing pressure, and a melt so formed could proceed to the surface fractionating only olivine as the olivine field expanded with decompression. However, Stolper and Walker (1980) indicated that picritic melts generally "pond" in the lower continental crust because of a density contrast with the surrounding rocks. Plagioclase, which is an important fractionating phase at low pressures, is stable to only moderate pressures (9 to 13kbar) and is unlikely to be an important liquidus phase at high pressures. At moderate pressures (12 to 15kbar) orthopyroxene has a large liquidus field, and is capable of fractionating as a primary phase in tholeiitic liquids (Cox *et al.*, 1979). At higher pressures (25 to 30kbar) garnet and clinopyroxene become important liquidus phases.

Cox *et al.*, (1979) noted that trace elements are often the only means of speculating about high pressure stages of magmatic evolution, since they are most resistant to change. However, for this study a combination of trace and major elements are used to assess high pressure fractionation. For the Karoo basalts, Marsh and Eales (1984) noted that the rare earth elements (REE) offered the best means of identifying whether garnet participated in their fractionation. Garnet produces very strong relative fractionation amongst the heavy rare earth elements (HREE) which would not be obscured by later fractionation of other basaltic minerals. Therefore, garnet fractionation would produce a marked decrease in REE concentrations in residual liquids. REE data for the Sani Pass basalts is absent and therefore further constrains an assessment of garnet participation in their fractionation. Nevertheless, Cox *et al.*, (1979) have suggested that Y behaves geochemically very much like Yb. An inspection of the Y-SiO_2 variation diagram (Fig. 8.3d) does not indicate decreasing Y concentrations with increasing SiO_2, but instead shows a similar range of values between 14 and 30ppm for the different magma types. Beckinsale *et al.*, (1978) noted co-variation of K, Sr and Y with SiO_2 in a series of alkali basalts, hawaiites and mugearites from Mull, North-west Scotland, which they ascribed to differential partial melting of a garnet periotite source. Like the Y concentrations for the Sani Pass rocks, K_2O and Sr show a range of concentrations and consequently no co-variation with SiO_2 (Figs. 8.2h and 8.3a, respectively). On this basis, therefore, it can be assumed that garnet played an insignificant role (if any) in the fractionation of the Sani Pass basalts. Any assessment of high pressure

fractionation must therefore consider olivine and pyroxene as possible high pressure phases.

In the absence of appropriate experimental data to define phase proportions and compositions which would be in equilibrium with compositions of the Sani Pass basalts at high pressures, a series of models have been tested. This approach was used by Hooper (1988) to model the American Bar subgroup of the Imnaha Basalt. He showed, using the least squares technique, that compositional differences between the American Bar flows can be attributed to the fractionation of plagioclase + clinopyroxene + orthopyroxene, and that this assemblage represented a high pressure assemblage. This assemblage differs from the observed phenocryst suite of plagioclase + olivine + augite. The Sani Pass basalt data have been modelled along these lines in trying to relate the different magma types by fractionation. The use of the observed assemblage (plagioclase + olivine + augite) produced imperfect residuals for major elements and yielded decoupling between compatible and incompatible elements in terms of simple crystal fractionation (see section 10.2.1). This problem is not alleviated by the incorporation or orthopyroxene (microprobe data from Sweeny, 1988) in the fractionating assemblage. Least squares modelling therefore yields inconsistent results for any high pressure fractionating assemblage incorporating olivine and pyroxene (orthopyroxene and/or augite).

Yoder and Chayes (1986) found that a strong positive correlation existed between Na_2O and K_2O in basic alkali rocks from the Hawaiian Islands and Canary Islands. They suggested that this relationship resulted from one or a combination of 5 factors, including high pressure phase equilibria. At high pressures nepheline and kalsilite are stable and could act as buffers for K. The lack of such a linear correlation between K_2O and Na_2O in the Sani Pass basalts therefore exempts fractionation of these magma types at high pressures.

Marsh and Eales (1984) used incompatible element ratios to disprove high pressure fractionation as a means of causing the compositional variation in the Central area basalts. The validity of using incompatible element ratios is based on the assumption that if the effects of changing conditions on the partition coefficients of two elements are similar in magnitude and direction, then the effects will be largely cancelled by considering the ratio of the two elements. Thus, the higher Zr/Nb and similar Zr/Y and Ti/Zr for the pre-

Phinong basalts (except for the Agate Vale basalts) cannot be generated from magmas with incompatible element ratios characteristic of the Phinong magma by fractionation of the phases considered above. The higher Zr/Nb and Zr/Y, and lower Ti/Zr ratios of the Agate Vale also cannot be derived from the Phinong magma.

On the basis of least squares modelling, using major element compositions, and the use of incompatible elements, it is concluded that high pressure fractionation was not responsible for the compositional variation exhibited by the different magma types in the Sani Pass.

10.3.4. Open System Low-Pressure Fractional Crystallization

Models for open system fractional crystallization have been postulated by O'Hara (1977) and subsequently modified by O'Hara and Matthews (1981). This model allows enrichment of incompatible trace elements without concomitant changes in major element composition, in a continuously fractionating magma chamber that is periodically tapped and replenished. An assessment of open system fractionation is directly applicable to the Sani Pass basalts, since the different magma types exhibit discrete ranges and distinctive trace and minor element compositions. The theoretical aspects of the open system model are briefly discussed below.

A feature of the open system fractionation model is that during repeated cycles of crystallization, replenishment and mixing, the concentration of a given trace element tends towards a steady state concentration, C_{ss}, that can be calculated by the expression (after O'Hara and Matthews, 1981),

$$C_{ss} = \frac{(X + Y)(1 - X)^{D-1}C_o}{[(1-(1-X-Y)(1-X)^{D-1})]} \qquad \text{--10.4}$$

where C_o is the concentration in the undifferentiated liquid, X is the fraction of liquid that crystallizes in each cycle and Y is the fraction of liquid that erupts as lava flows.

The amount of undifferentiated liquid replenishing the chamber in each cycle, A, is given by $X + Y = A$, and thus equation 10.4 can be expressed in terms of A and F, the fraction of residual liquid after crystallization:

$$C_{ss} = \frac{C_o . AF^{D-1}}{1-(1-A)F^{D-1}} \qquad 10.5$$ (taken from Marsh and Eales, 1984)

At the end of each cycle the composition of the liquid changes and can be expressed as C_m in the form:

$$C_m = \frac{(FC_L + AC_0)}{F+A} \qquad 10.6$$ (taken from Marsh and Eales, 1984)

where C_L is the residual liquid composition in the Rayleigh fractionation equation for the crystallization step.

Marsh and Eales (1984) have examined the geological and geochemical implications of high level magma chambers fractionating under open system conditions for the Karoo-age north-eastern Cape basalts. They noted, that the absence of any evidence for magma chambers within the lava pile implied that previously erupted basalts were not digested into the chambers. Therefore, in order to attain steady state compositions, the mass of the replenishing liquid (A) must be greater than the mass of magma crystallized (X). However, if $X > A$, then steady state compositions are not achieved, since the mass of the liquid in the chamber decreases steadily. The large volume of lava in the study and adjacent areas are unlikely to have formed under such conditions of a steadily decreasing mass of liquid. For maximum fractionation of incompatible elements, the steady state system requires the cyclic process of fractionation, replenishment and eruption; the fraction of material erupted, Y, being small in relation to the degree of crystallization. A natural consequence of this, given the very large volume of erupted lavas in the study area, would be large cumulate-rich magma chambers. The discussion in the previous section has indicated that the Sani Pass basalts did not undergo high pressure fractionation, in which case magma chambers responsible for these basalts must have been shallow. No evidence exists for such large cumulate-rich magma chambers in the Sani Pass area, and surface collapse structures as one would expect from large and rapid eruptions from shallow reservoirs (Hooper, 1988) are totally absent.

Although the geological evidence is lacking for the RTF magma chambers in the Sani Pass study area, the geochemical implications of an RTF model also need to be assessed. A feature of the RTF model, and which is to some extent exhibited by the Sani Pass basalts, is a considerable change in incompatible element concentrations for small major element variations (Cox, 1988). For the RTF model to be applicable to a volcanic suite, it must have attained steady-state conditions. The Sani Pass basalts do not fit this requirement, since the successive lava flows generally display random compositional ranges in incompatible element concentrations, rather than a progressive trace element compositional variation.

10.3.5. Crustal Contamination

The preceding discussion has indicated that neither alteration nor fractional crystallization (open and closed systems, and high and low pressure) models adequately explain the range in major and trace element variation between the various magma types in the Sani Pass. Contamination has been identified in other flood basalt sequences (Carlson, *et al.*, 1981; Cox and Hawksworth, 1984; Devey and Cox, 1987; Lightfoot *et al.*, 1991) and therefore it is justifiable that the Sani Pass basalts be examined for any evidence of contamination.

Contamination is normally examined on two levels namely, bulk contamination and selective contamination. This study is concerned only with bulk contamination since selective contamination relies heavily on the systematics of a number of isotope systems (see Moorbath and Thompson, 1981). Selective contamination changes the isotope characteristics considerably without significantly altering the bulk composition of the contaminated magma. Bulk contamination may occur in magma chambers or conduits. Contamination occurring in magma chambers is accompanied by fractionation, and concomitant release of latent heat which contributes to the melting and assimilation of wall rocks. This is known as coupled-assimilation fractional crystallization (AFC), a model for which has been proposed by DePaolo (1981). Recently models developed on the same theme have been proposed by Devey and Cox (1987) and Lightfoot and Naldrett (1989). In these latter models, assimilation occurs by virtue of the temperature of the magma (that is, temperature-

controlled assimilation [TCA]), which may or may not accompany equilibrium crystallization. Conduit contamination or temperature-controlled assimilation (TCA), so-called since the more primitive magmas are more able to assimilate crustal material by virtue of their elevated temperatures compared to cooler, more evolved magmas. This type of contamination has been modelled by Huppert and Sparks (1985).

Evidence for contamination must be sought in geological and geochemical features (Bristow *et al.*, 1984; Marsh and Eales, 1984). Hall (1987) noted that xenoliths are commonly the most conspicuous evidence of contamination, although their abundance is by no means a reliable guide to the amount of contamination that has taken place. Within the Sani Pass volcanic succession there is a lack of field evidence indicating assimilation, except for a basaltic xenolith preserved in flow P232 (Plate 3.5). Field and petrographic examination of the xenolith indicate that no mixing occurred between the xenolith and the host flow. This is attributed to different liquidus temperatures between the xenolith and flow P232, with the xenolith possibly being picked up during the waning phases of magmatism.

To investigate the role of crustal contamination it is first necessary to identify possible end-member components. The Phinong magma, by virtue of its large volume and homogeneity is considered to represent uncontaminated magma. This magma type has similar geochemical characteristics to the Lesotho-type (see Chapter 11) which has been shown to be largely uncontaminated (Bristow *et al.*, 1984; Cox, 1983; Marsh and Eales, 1984) Bearing in mind the vast thickness of Karoo sediments and the Archaean basement underlying the study area (Tankard *et al.*, 1982), through which the Sani Pass basalts ascended, the most likely contaminant would probably have a silicic composition. The compositional contrast between such a contaminant and a basaltic magma is best exhibited by an increase in the elements SiO_2, K, Rb and Ba. These elements are so abundant in a contaminant such as granite, that increases consequent upon contamination much outweigh any variation induced by fractionation (if any), (Cox and Hawksworth, 1984).

An inspection of the geochemical data (Figs. 8.2h, 8.3b and 8.3c, respectively), indicates that amongst the pre-Phinong basalts the Agate Vale magma type and the basal flow of the Mkhomazana magma type show enrichment in K_2O, Rb and Ba compared to the Phinong

basalts. Although in general, the Agate Vale basalts are enriched in these elements, in detail some individual samples do not show the expected effects. Notwithstanding the fact that the two upper flows of the Mkhomazana magma type do not show enrichment in K_2O, Rb and Ba, this entire magma type would be assessed for possible contamination.

Due to the compositional contrast between SiO_2 and Mg-number in mafic magmas and possible silicic contaminations, these parameters have been used in modelling contamination (Bristow *et al.*, 1984; Cox and Hawksworth, 1984; Lightfoot *et al.*, 1991). Since Mg-number is not sensitive to contamination, while SiO_2 is insensitive to gabbro fractionation, this relationship is a good indicator of contamination with concomitant fractional crystallization. A SiO_2 versus Mg-number diagram indicates a slight scatter for the Agate Vale basalts, and a slight positive trend for the Mkhomazana basalts (Fig. 10.5), although the latter trend is based only on three points, and must be viewed with caution. This scatter of the Agate Vale basalts is inconsistent with ACF, whilst the Mkhomazana basalts indicate a trend characteristic of ACF models.

The trace elements, Cr and Ni are likewise sensitive to contamination, decreasing rapidly in contaminated magmas because of dilution by the contaminant and removal by fractionating mafic phases for which they have high distribution coefficients. In contrast, Rb and K_2O would be enriched in contaminated liquids by both the added silicic melt and fractional crystallization. Thus, Rb and K_2O plotted against Ni and Cr would yield strong negative correlations for any case of contamination accompanied by crystal fractionation. The K_2O-Ni (Fig. 10.6a) and Rb-Ni (Fig. 10.6b) relationships for the Agate Vale and Mkhomazana basalts indicate a scatter of data, due primarily to two fields of data; a high K_2O and Rb field (samples AV60, AV70 and M150) and a field of lower K_2O and Rb. The lower field, occupied by majority of the Agate Vale and Mkhomazana samples, shows a poorly developed negative correlation for both K_2O and Rb against Ni. A similar trend is observed in terms of chromium concentrations for both these magma types (Fig. 10.7a-b). These trends are unlikely to be due to crystal fractionation accompanied by contamination, since stronger trends would be expected from such a process. In addition, the similar Nb, Co, Ni and Cr, and marginally higher TiO_2 contents in these Agate Vale samples, than in most

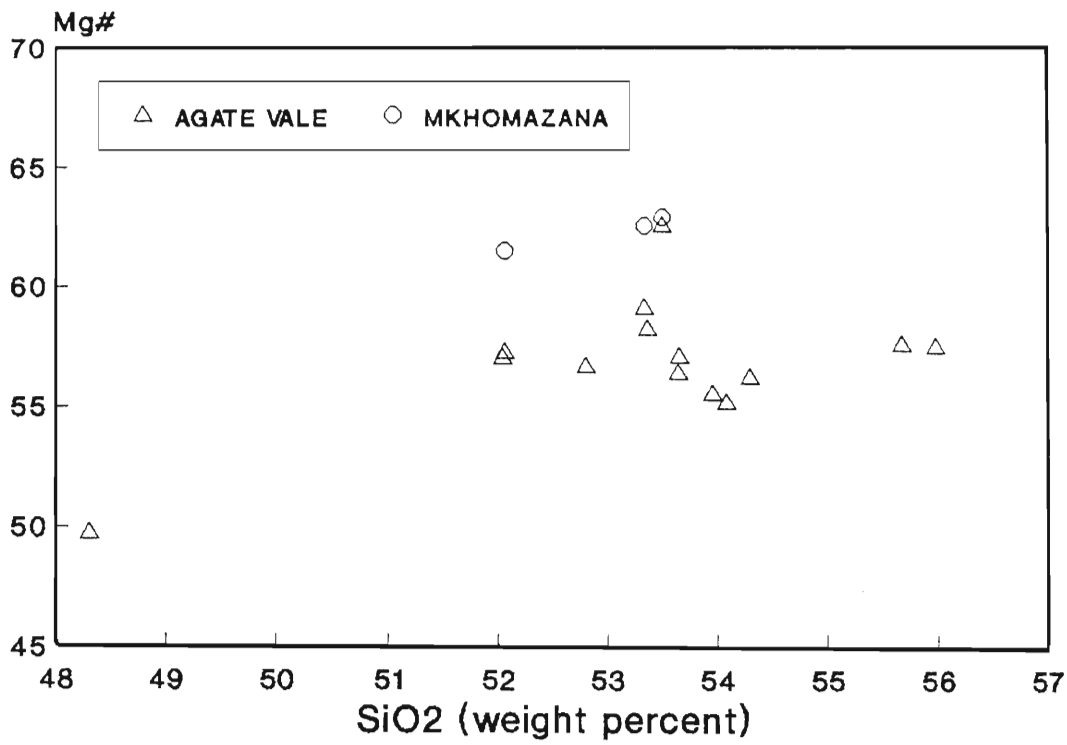

Fig. 10.5 SiO_2 versus Mg-number for the Agate Vale and Mkhomazana basalts. The Agate Vale basalts are generally scattered whilst a slight positive trend is shown by the Mkhomazana basalts.

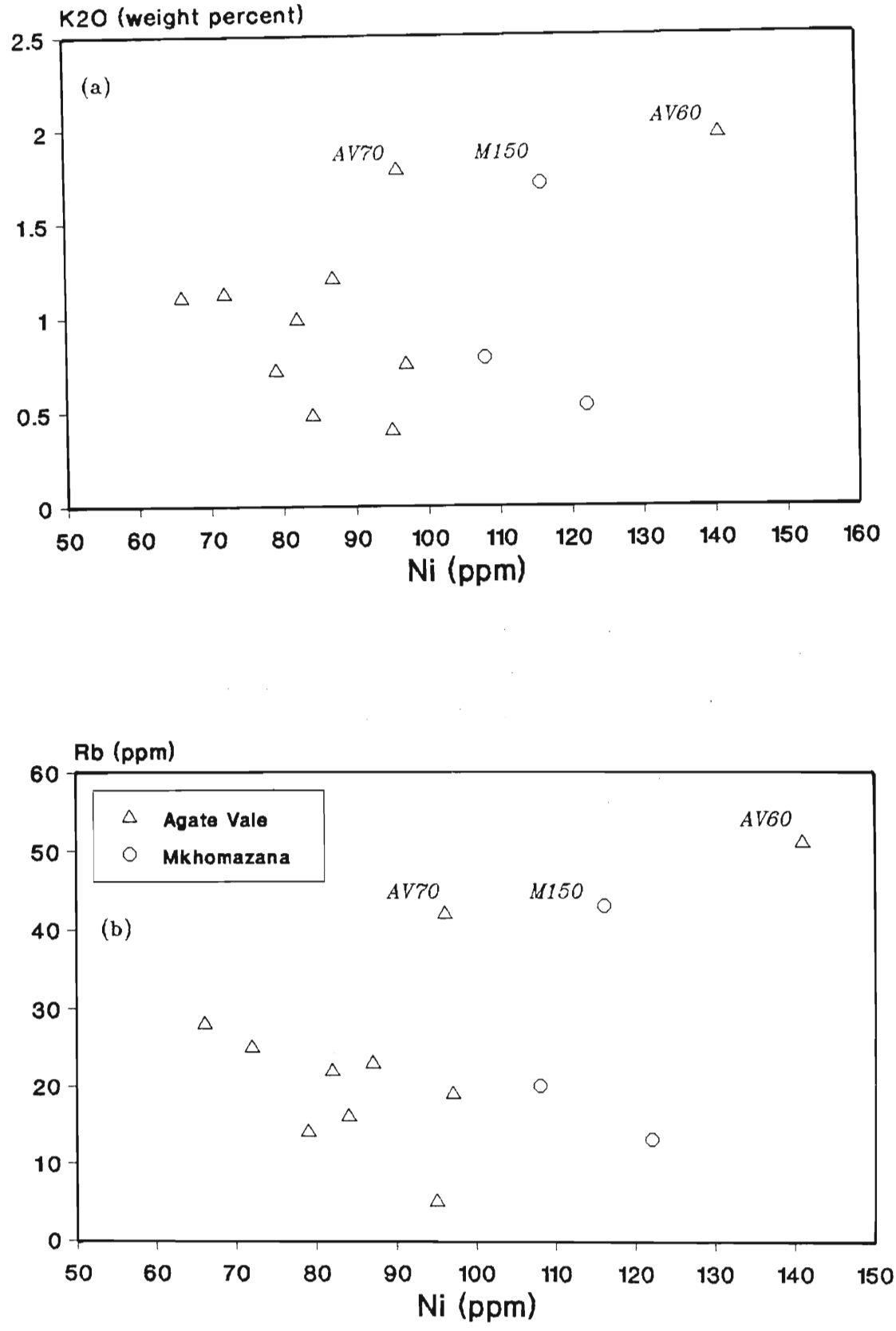

Fig. 10.6a-b An assessment of contamination in terms of (a) K_2O versus Ni, and (b) Rb versus Ni, for the Agate Vale and Mkhomazana basalts. The labelled samples indicate the high K_2O and Rb fields. Sample AV400 has not been plotted.

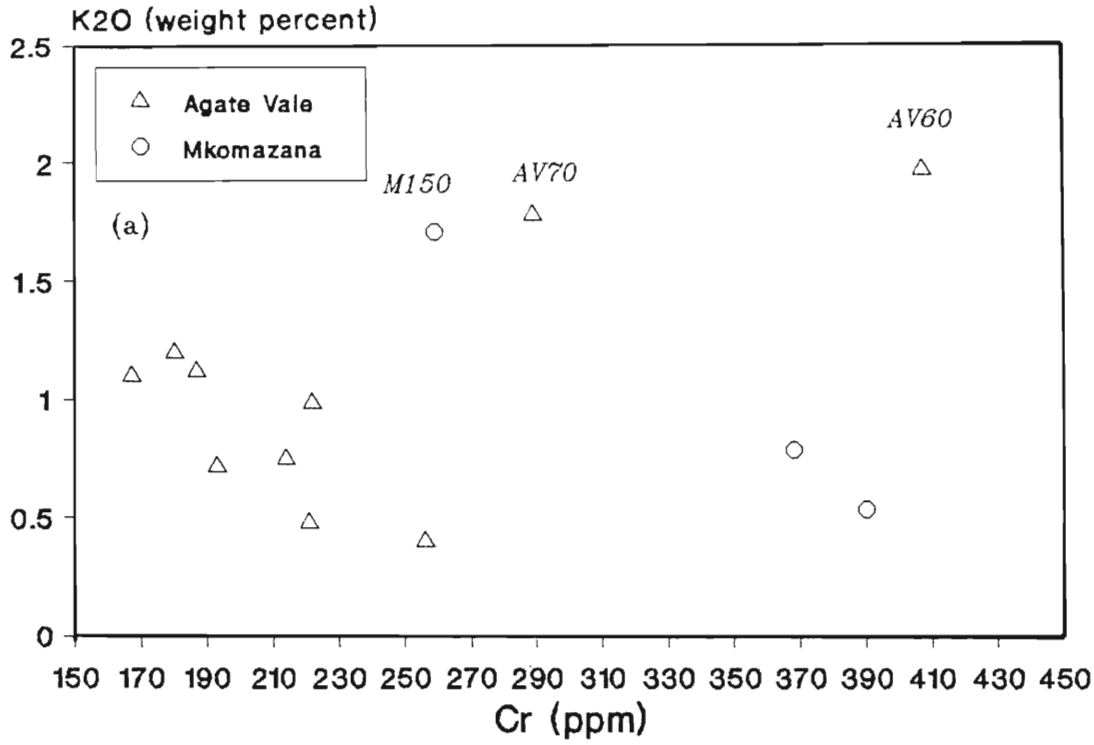

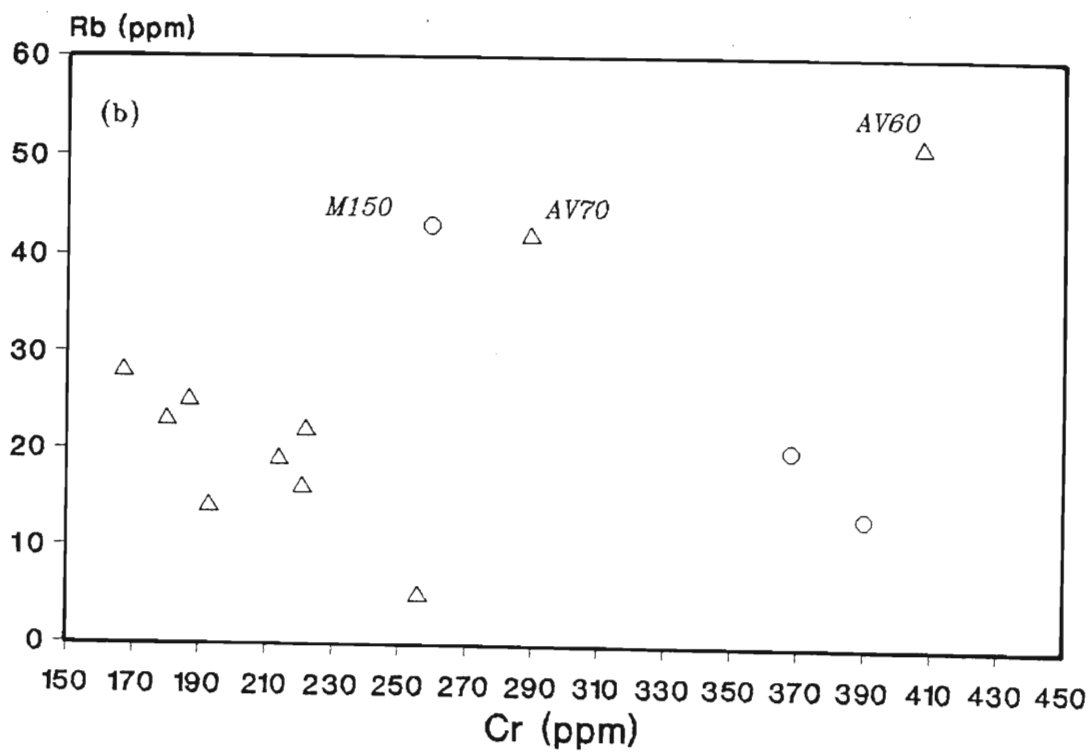

Fig. 10.7a-b An assessment of contamination in terms of (a) K_2O versus Cr, and (b) Rb versus Cr, for the Agate Vale and Mkhomazana basalts. Sample AV400 has not been plotted.

of the presumably uncontaminated Phinong basalts, is inconsistent with contamination by a silicic melt.

Two samples within the Agate Vale magma type, AV60 and AV70, have extremely high Ni contents (141 and 96 ppm, respectively) that are accompanied by high K_2O (1.96 and 1.78 weight percent respectively) and Rb (51 and 42 ppm, respectively) (Figs. 10.6a and b). The geochemistry of these 3 flows, occupying the upper field in Figs. 10.6a and b is inconsistent with an ACF model, since the move primitive flows have a higher concentration of K_2O and Rb. Such geochemical correlations have been suggested by Huppert and Sparks (1985) as a result of conduit contamination. Implicit in their model, is that the more primitive, and therefore hotter lavas would assimilate contaminants more easily, and in larger proportion, than the cooler lavas. Sample AV60 also shows enriched silica contents (SiO_2=55.67 weight percent), while the silica content in AV70 is moderate (SiO2=52.94 weight percent). The behaviour of SiO_2, however, may well be caused by analytical problems, since a relatively very high precision is required here, or by the presence of quartz-filled amygdales.

The basal Mkhomazana flow (M150) also falls in the high Rb and K_20 field in Figs. 10.6 and 10.7. However, this flow is not the most primitive in the Mkhomazana magma type, a feature which would be expected from conduit contamination. Nevertheless, the strong negative correlation depicted by the Mkhomazana basalts in Fig. 10.7a-b is more consistent with ACF, but this relationship cannot be sustained in terms of K_20, Rb and Ni concentrations (Fig. 10.6a-b). Therefore, the geochemistry of the Mkhomazana basalts must be attributed either to partial melting or a heterogeneous source.

Although sample AV400, which is the basal flow of the Agate Vale magma type, shows extreme enrichment in K_2O (7.31 weight percent) and Rb (109 ppm), its low SiO_2 (48.30 weight percent) and Ni (66 ppm) make it an unlikely candidate for conduit contamination by a silicic melt. The extremely high K_2O, Rb and Ba content in this sample would require an extremely large proportion of contaminant, richer in these elements than the average granite; a very unlikely situation. Nevertheless, enrichment in K_2O, Rb and Ba can be also as a consequence of the presence of biotite. Considering that the

metasedimentary lens below this flow is rich in biotite, it is very likely that during eruption flow AV400 may have assimilated a large proportion of sediment. However, the presence of possible contaminants in this sample could not be confirmed petrographically. An alternative scenario could have been fluids derived from the sedimentary lens, and therefore rich in K_2O, Rb and Ba, percolated through flow AV400 during eruption and subsequent solidification.

In certain instances assimilation of sedimentary country rock has resulted in a similar chemistry to that of the Mkhomazana basalts. In all of these cases incontrovertible evidence of assimilation is present, in the form of sandstone xenoliths and rheomorphic veins (Mountain, 1958, 1960). Although there is no field or petrographic evidence for sedimentary contamination in the Mkhomazana basalts, the rheomorphic veining described by Mountain (1958, 1960) is present in these flows. Also, in the streambed that cuts through the stratigraphically higher flows P174 and P178, numerous sediment-filled "desiccation cracks" are observed in the lava flows. In addition, such assimilation of sedimentary material convincingly explains the higher Na_2O content (4.16 to 4.51 weight percent) in the Mkhomazana basalts. However, this model does not satisfactorily explain the higher MgO, Ni and Cr and the range of incompatible element contents in these basalts.

From the discussion it is evident that bulk crustal contamination, although affecting only 2 flows (AV60, AV70) and possibly flow AV400, did not have a significant role in generating compositional variation in the Sani Pass basalts. Similar conclusions for the Central area basalts were achieved by Cox (1983), Marsh and Eales (1984) and Bristow *et al.* (1984), collectively utilizing geological, compatible and incompatible trace elements and isotopic evidence.

10.4. Partial Melting Models

From the preceding discussion, it is clear that the reasons for much of the trace element variability of the Sani Pass volcanic rocks must be sought either in variations in partial melting processes, or in trace element variations within the mantle source. Partial melting processes are evaluated in terms of melting models.

The simple model for the partial melting of a complex mineral assemblage is one in which the liquid remains at the site of melting, and is in chemical equilibrium with the solid residue, until mechanical conditions allow it to escape as a single "batch" of primary magma. This process is known as equilibrium or batch melting. The concentration of an element in the liquid (C_L) is related to that in the original unmelted source (C_o) by the expression:

$$C_L/C_o = 1/[D_0 + F(1-P)] \quad \text{--------- (10.7) (after Shaw, 1970)}$$

where: $D_0 = \Sigma D^i \,.\, X^i$, D^i and X^i are the individual mineral distribution coefficients and weight fraction of phases in the source respectively.

$P = \Sigma D^i \,.\, P^i$, P^i is the weight fraction of phases in the melting assemblage.

$F =$ the weight proportion of melt formed.

Fractional (Rayleigh) melting, on the other hand, involves the continuous and complete removal of small amounts of melt from solid phases. For non-modal melting the equation given by Shaw (1970) is:

$$C_l/C_o = 1/D_o(1 - PF/D_o)^{(1/P-1)} \quad \text{-----(10.8)}$$

Many variants of these two "end-member" models have been proposed. Wood *et al.* (1979) suggested that incremental batch melting involves the repeated extraction of melts from the same source, each melt increment formed by an equilibrium/batch process. A variation of Rayleigh melting is collection melting, where the fractional melts leave the source but gather elsewhere in the chamber and mix thoroughly. Langmuir *et al.* (1977) suggested that continuous melting is a more likely process in nature, in which fractions of melt are continuously but incompletely removed from the solid phase as melting proceeds.

Partial melting is difficult to constrain, particularly with regard to source compositions. The partial melting models discussed above indicate that highly incompatible elements in the source would be strongly partitioned into the liquid initially formed during melting, but their concentration in the melt would decrease with subsequent small increases in the degree of melting. Major and compatible elements have strong affinities for the restite assemblage and show little change for degrees of melting less than about 15%. In contrast, these componants are depleted in the melt by fractional crystallization. The Sani Pass magma types have similar Mg-numbers and compatible element concentrations, except the Giant's Cup basalts which have the lowest Mg-number and Ni, Co and Cr. This lack of extreme variability in major and compatible elements was also noted by Marsh and Eales (1984) in magma types from the north-eastern Cape. They attributed such a feature to the magmas having undergone "similar degrees of polybaric mafic mineral fractionation." The Cr/Ni and less so the Sc/Ni ratios are moderately high for the Sani Pass basalts (Table A2.4, Appendix 2), indicating that the mafic assemblage was dominated by olivine, rather than pyroxene fractionation. In addition, Marsh and Eales (1984) suggested that plagioclase extraction in the north-eastern Cape Karoo-age basalts was low, a feature which is directly applicable to the Sani Pass basalts.

Assuming olivine fractionation dominated the pre-eruption fractionation assemblage, Marsh and Eales (1984) modelled MgO and Ni fractionation paths, and estimated that the parent magma for the north-eastern Cape basalts was picritic with MgO contents in the range 12 to 18 weight percent. These authors also showed that polybaric fractionation of between 12 to 25% olivine from these picritic parents could account for the observed compositional

range of these magmas. Therefore, accepting that the Sani Pass magmas evolved along similar cooling paths from picritic parents, dominated by olivine fractionation, then the relative differences in the incompatible element chemistry can be regarded as reflecting their concentrations in the parental magma.

For equilibrium batch melting (>10% partial melting) of a homogeneous source, significant relative fractionation of REE's and other incompatible elements, results only if garnet and clinopyroxene remain in the residue (Pearce and Norry, 1979). This is assuming that minor phases such as mica, apatite and ilmenite have completed their melting significantly earlier. Since the presence of residual garnet has a marked effect on HREE and clinopyroxene on LREE fractionation, Marsh and Eales (1984), demonstrated utilizing REE data that garnet and clinopyroxene remained as restite phases during petrogenesis of the north-eastern Cape basalts. Assuming that garnet and clinopyroxene did remain as restite phases during evolution of the Sani Pass magma types, then the use of the incompatible element ratios Zr/Y, Zr/Nb, Zr/Ti and Ti/P, as an assessment of batch melting is most informative. This is so, since these ratios are only slightly fractionated by equilibrium partial melting (Pearce and Norry, 1979). An examination of incompatible element histograms for the Sani Pass magma types indicates a range of values between and within magma types (Fig. 10.8a - d). Most of the pre-Phinong basalts have higher Zr/Nb ratios (22 to 62) than the Phinong basalts (9 to 22) (Fig. 10.8b), whilst the Agate Vale basalts which have much higher Zr contents than the other magma types also have the highest Zr/Y ratio (5 to 9) (Fig. 10.8a). In addition, the Agate Vale magma type has Zr/Ti ratios much larger than any of the other magma types (Fig. 10.8c). In terms of Zr/Ti and Zr/Y ratios for the Giant's Cup, Sakeng and Mkhomazana magmas there is considerable compositional overlap in these ratios with the Phinong magma type, whilst being somewhat higher in Zr/Nb ratios than the Phinong basalts. The Ti/P ratio is also appropriate as an assessment of partial melting, since apatite and ilmenite are generally consumed at very low degrees of partial melting. The presence of such phases as apatite, ilmenite and rutile in the residue would be indicated by a significant depletion of Ti and P in the earliest erupted lavas. No such pattern exists, instead the Giant's Cup magma type shows slightly higher

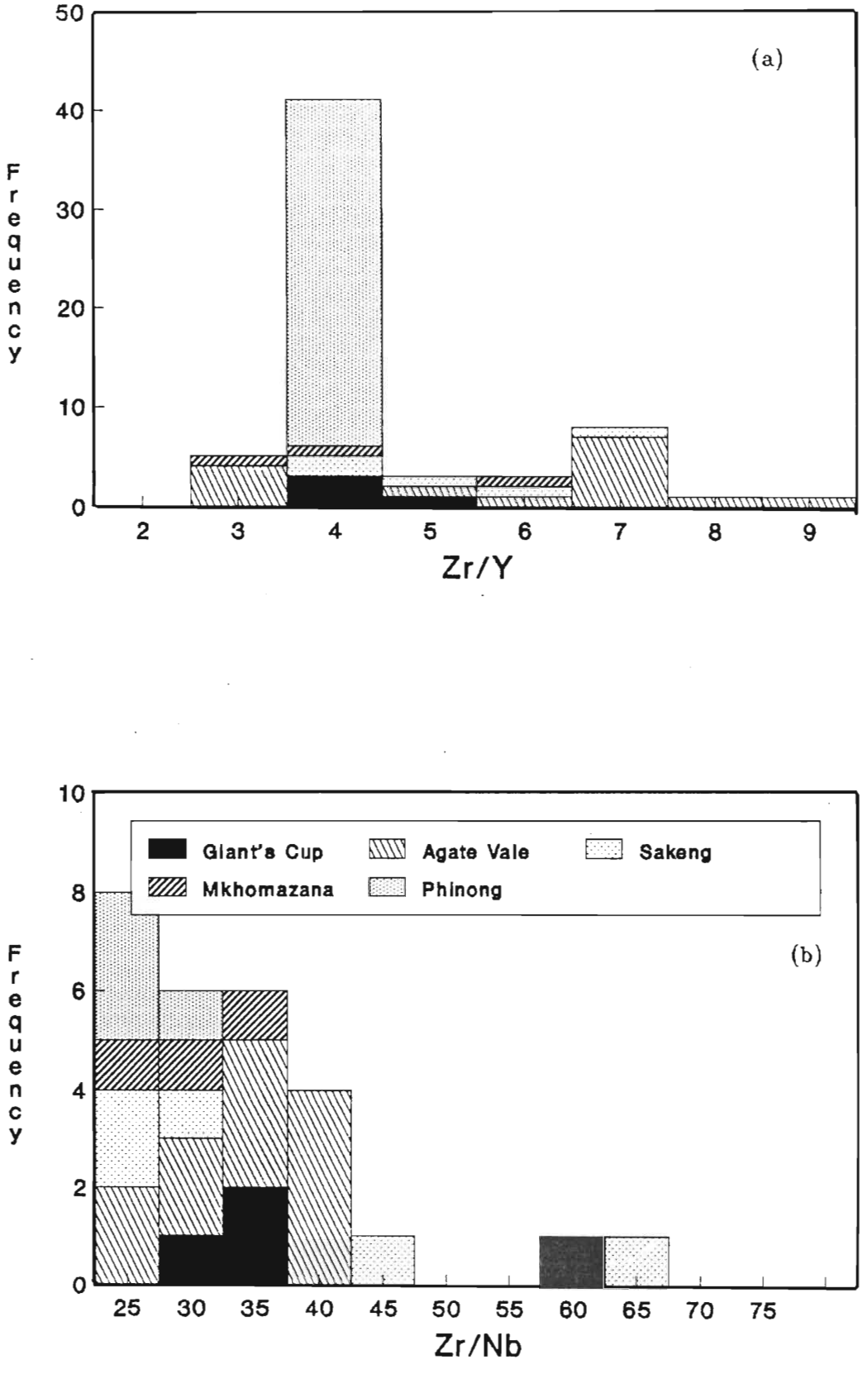

Fig. 10.8a-b Stepped histograms indicating the distribution of (a) Zr/Y and (b) Zr/Nb ratios for the Sani Pass magma types.

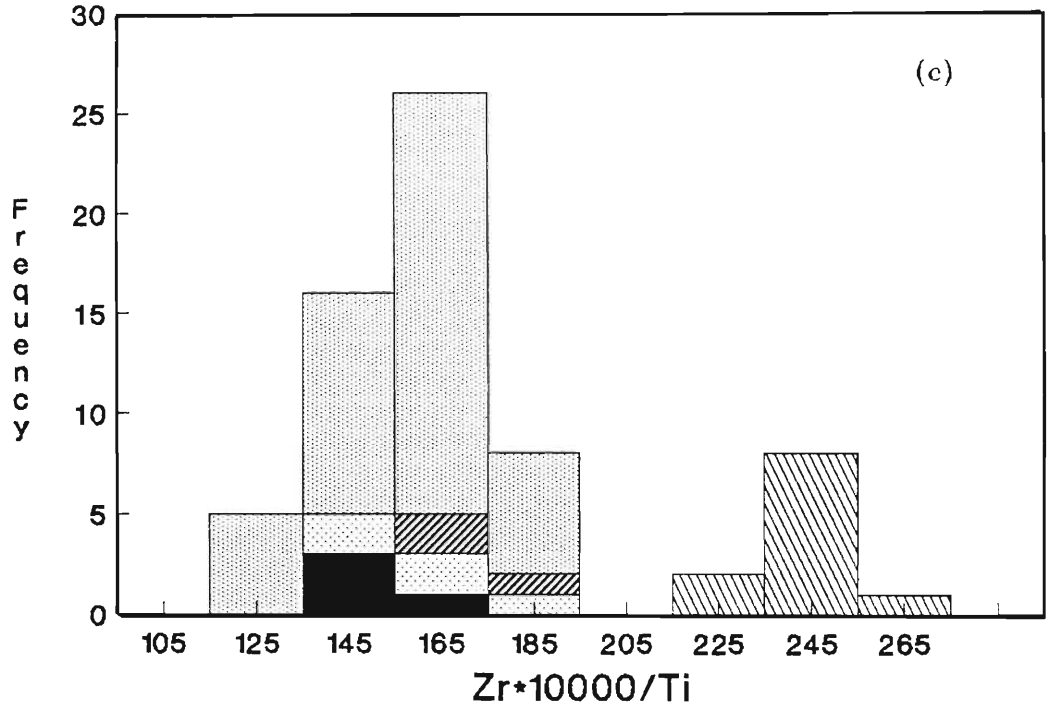

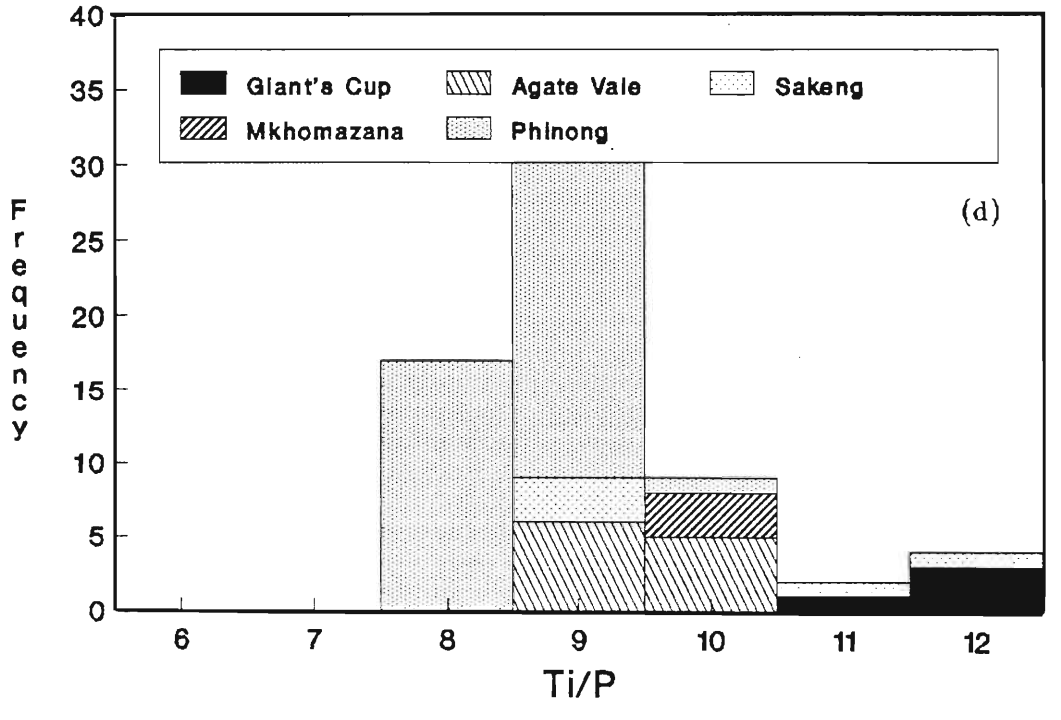

Fig. 10.8c-d Stepped histograms indicating the distribution of (c) Zr/Ti and (d) Ti/P ratios for the Sani Pass magma types.

TiO_2 than the overlying magma types. The Ti/P ratio displays the higher Ti content in the Giant's Cup basalts than most of the other basalts (Fig. 10.8d). The Mkhomazana basalts have intermediate Ti/P (10) and most of the Phinong, Sakeng and Agate Vale basalts have lower Ti/P (8-9) ratios (Fig. 10.8d). These large variations in incompatible element ratios between and within the magma types, clearly indicates that equilibrium batch melting of a homogeneous source was not responsible for the compositional variability of the Sani Pass magma types.

In reality equilibrium batch melting can rarely be envisaged as a truly likely situation, and a more realistic scenario is continuous or dynamic melting of a homogeneous source. Continuous melting can produce stronger fractionation of the incompatible element ratios than equilibrium batch melting, and the magnitude of this fractionation increases with decreasing increment size (Pearce and Norry, 1979). Thus, this model produces a range of melts where the ratio of a more incompatible to less incompatible element varies positively with the abundance of the more incompatible element. However, a pre-requisite for this relationship is that the partition coefficients of the elements being modelled must differ only slightly. Assuming the bulk distribution coefficients of Pearce and Norry (1979), and a residual source consisting of olivine + orthopyroxene + clinopyroxene (as suggested by Marsh and Eales, 1984), these distribution coefficients decrease as follows:
$D_Y > D_{Nb} \geq D_{Ti} > D_{Zr}$. Therefore, the ratios Zr/Nb, Zr/Ti and Zr/Y should decrease in the melt with continuous partial melting. Fig. 10.9a-c indicates that this positive correlation exists qualitatively essentially between the Agate Vale and Phinong basalts for Zr/Ti, Zr/Nb and Zr/Y and between the Agate Vale and the Giant's Cup, Sakeng and Mkhomazana basalts for Zr/Y, and Zr/Ti. In greater detail, however, the diagrams indicate that for the Zr/Ti ratio, Agate Vale > Phinong = Giant's Cup = Sakeng = Mkhomazana, but for the Zr/Nb ratio Phinong < Agate Vale = Giant's Cup = Sakeng = Mkhomazana. For Zr/Y ratios Agate Vale > Phinong, but overlaps most of the Giant's Cup, Sakeng and Mkhomazana samples. These patterns are inconsistent with simple continuous melting of a homogeneous source.

For a partial melting model to be applicable to the Sani Pass magma types, it must be

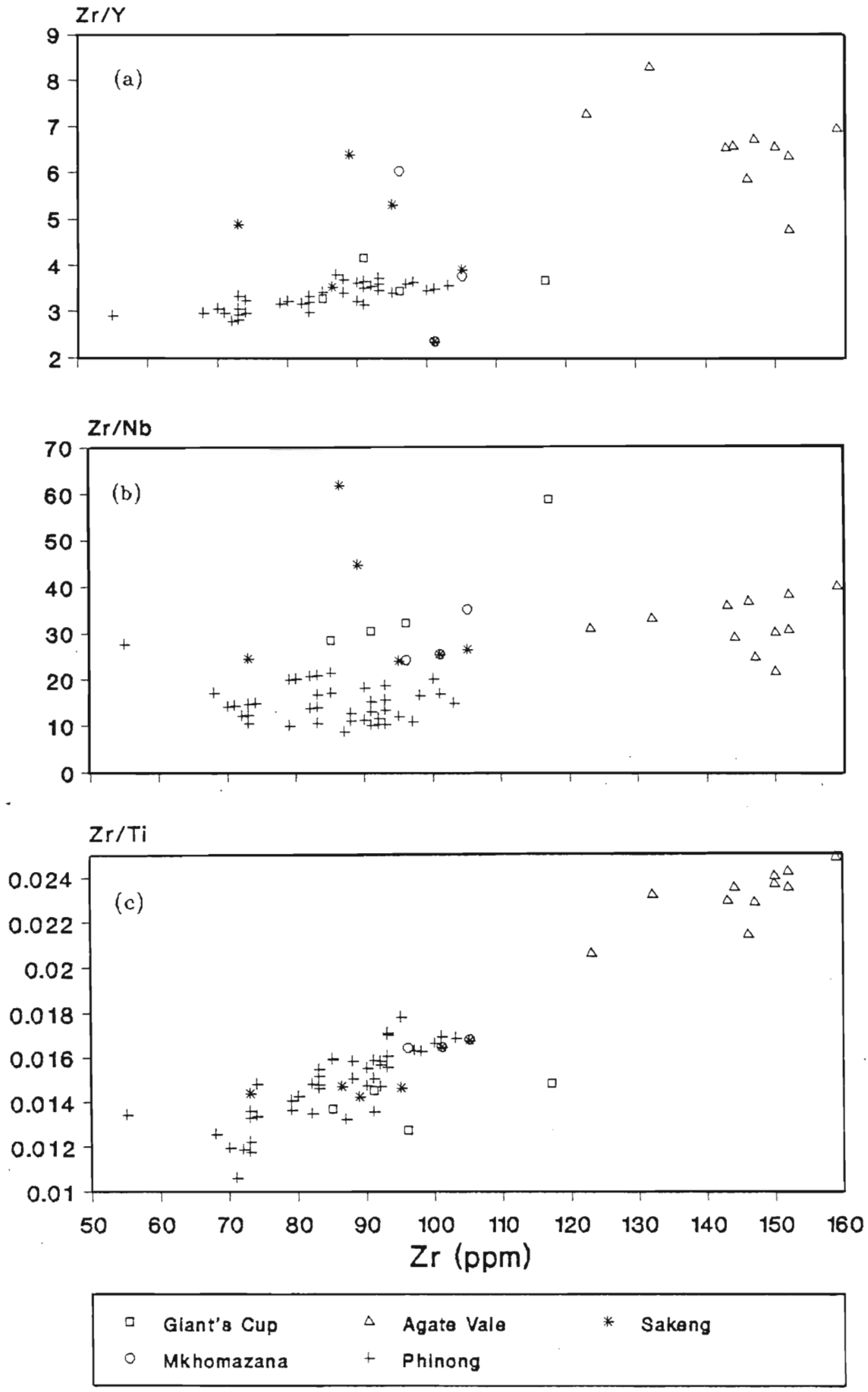

Fig. 10.9a-c The variation of the incompatible element ratios (a) Zr/Y, (b) Zr/Nb and (c) Zr/Ti, with continuous partial melting for the Sani Pass magmas.

consistent with the mechanics of melt extraction. The pre-Phinong magma types that seem to be restricted to the Sani Pass area (see Chapter 11) would, therefore, represent small amounts of magma extracted from the initial melts of the source, whereas the more extensive Phinong type would represent almost complete extraction of magma at a more progressive stage. However, the model does not explain why the products of continuous melting should be localized in a small area and not be more widespread.

The use of incompatible element ratios indicates that the Sani Pass magma types cannot be related by continuous melting of a homogeneous source, and volume relationships are also inconsistent with such a model.

10.5. Mantle Heterogeneity

Chemical heterogeneity of the earth's upper mantle is well established from evidence obtained from mantle xenoliths in alkaline lavas and kimberlites (Gurney and Harte, 1980), isotope systematics of basalts, and the theoretical consideration of trace element behaviour during melting and mantle metasomatism (Gast, 1968; Hoffman and Hart, 1978; Richardson *et al.*, 1984; Zindler and Jagoutz, 1988). Based on the compositional variability of the widespread Karoo basaltic lavas, Erlank *et al.*, (1980) concluded that the mantle beneath southern Africa shows large scale chemical inhomogeneity, a feature that has persisted since the Archaean. Other studies on the Karoo basalts by Marsh and Eales (1984) and Cox (1983) subscribed to this process as a possible cause for the geochemical variability of the north-eastern Cape basaltic rocks.

Isotope systematics and incompatible trace elements have been extensively used to assess the Central area basalts, in terms of mantle heterogeneity (Pemberton, 1978; Mitchell, 1980; Erlank *et al.*, 1980; Cox, 1983; Marsh and Eales, 1984; Duncan *et al.*, 1984b). To this end Zr/Y ratios are appropriate, since they are little altered by crystal fractionation and single stage partial melting processes (Pearce and Norry, 1979). The only processes that can **significantly** alter this ratio are progressive partial melting or mantle heterogeneity (Pearce and Norry, 1979). These authors pointed out that Zr/Y ratios are better indicators

of source heterogeneity rather than progressive melting processes. Figs. 9.2a and 10.8b indicate the Zr/Y compositional ratios for each of the magma types in the Sani Pass. It is clear that the Phinong and Agate Vale basalts are characterized by distinct Zr/Y ratios in the range 2 to 4 and 5.5 to 8 respectively. The Sakeng, Mkhomazana and Giant's Cup magmas show a continuum between these two ranges. These inter-magma type variations in Zr/Y ratios are fairly substantial, and it is believed that this range in values is due to source rock heterogeneity. Intra-magma type variations in Zr/Y ratios are relatively small for the Phinong (2.8 to 4), Agate Vale (7.2 to 6.9) and Giant's Cup basalts (3.7 to 4.1) and large for the Mkhomazana basalts (2.3 to 6). In the case of the Phinong basalts, fractional crystallization is the dominant within-unit process (section 10.3), superimposed on mantle heterogeneity.

Pearce and Norry, (1979), suggested that in modelling source heterogeneity, the Zr/Nb ratio is more informative, since it is insensitive to variations in the degree of partial melting (assuming that basaltic liquids will not be in equilibrium with minor phases). Figs. 9.2b and 10.8b indicate that the Zr/Nb ratio effectively separates most of the pre-Phinong from the Phinong magma types. Zr/Nb = 20 separates the Phinong basalts (except sample P180), which have a range of 10 to 20, from the pre-Phinong basalts, incorporating the Giant's Cup, Agate Vale, Sakeng and Mkhomazana magma types. Zr/Nb ratios within the latter group of basalts range between 20 to 58. This extremely large variation in Zr/Nb ratios, further suggests that mantle heterogeneity is a likely process for producing chemical variations within the Sani Pass volcanics.

Zr/Ti ratios, depicted in Fig. 9.2c and their abundances in Fig. 10.8c, indicate the variability of the different units in terms of this ratio, and further strengthen the hypothesis of mantle heterogeneity in explaining chemical variation within the Sani Pass basaltic rocks. The Zr/Ti ratio may be strongly affected by crystallization of magnetite. However, it has been shown that no significant magnetite (or ilmenite) fractionation has occurred within the Sani Pass volcanic rocks.

A more comprehensive analysis of composional variation within the Sani Pass magmas is indicated in Fig. 9.4, which compares a larger number of variables simultaneously.

Averages for the different magma types, normalized to an average Lesotho-type basalt (data from Marsh and Eales, 1984) have been plotted. Although Rb, Ba and K show wide intra-magma variations, the average concentrations are considered to be good approximations of their pristine values (Marsh and Eales, 1984). Marsh and Eales (1984) noted that a characteristic feature of batch partial melting and/or variable degrees of fractional crystallization, in the absence of complex melting processes and crustal contamination, is to cause parallel shifts of the incompatible element patterns for the individual magma types. Fig. 9.4, however, indicates differential depletion/enrichment of the incompatible elements for the different magma types, thus producing a complex crossed-pattern configuration. Similar patterns were found to exist in the Karoo magma types of the north-eastern Cape (Marsh and Eales, 1984) and these authors attributed such a pattern to enrichment/depletion in the underlying mantle sources. In detail Fig. 9.4 indicates the higher Nb content in the Phinong magma source relative to the other Sani Pass magma sources. A similar enrichment in Zr and Ti is present for the Agate Vale and Giant's Cup magma sources, respectively. In terms of yttrium in the source areas, the Agate Vale and Sakeng are depleted relative to the Phinong, Giant's Cup and Mkhomazana, which shows the greatest enrichment. The source areas for the Mkhomazana and Agate Vale basalts are clearly enriched in the less incompatible elements, K, Rb and Ba relative to the Phinong, Giant's Cup and Sakeng source areas.

10.6. Summary

Numerous processes have been assessed in order to explain the geochemical variation of the Sani Pass magma types. These are alteration, high and low pressure crystal fractionation in open and closed systems, partial melting and mantle heterogeneity.

Although alteration has affected the Sani Pass rocks to varying degrees, significant alteration has been restricted only to the basal flows of the Giant's Cup and Agate Vale magma types. Lower Sr concentrations in the Sakeng basalts have been attributed to leaching. Sea-water or hydrothermal alteration does not adequately explain the geochemistry

of the Mkhomazana basalts.

Low and high pressure crystal fractionation cannot account for the geochemical variability of the Sani Pass magma types. However, low pressure fractionation (26%) of olivine (20%), pyroxene (32%) and plagioclase (48%) adequately describes the geochemical variability within the Phinong basalt endmembers. RTF models cannot be sustained on geological and geochemical evidence.

Although the Agate Vale and the Mkhomazana basalts show evidence for contamination, a rigorous assessment of such a process accompanying crystal fractionation suggests that it is unlikely. Nonetheless limited conduit contamination has occurred affecting samples AV60, AV70, and possibly AV400.

Batch partial melting and continuous melting of a homogeneous source do not adequately explain the incompatible element variation within the Sani Pass magma types. The discrete ranges of some incompatible elements and considerable overlap for others in the magma types can only be attributed to a heterogeneous mantle source.

CHAPTER 11

11. THE SANI PASS VOLCANIC SUCCESSION IN RELATION TO THE KAROO IGNEOUS PROVINCE

11.1. Introduction

The Karoo igneous province in southern Africa forms a classic flood basalt province (Walker and Poldervaart, 1949; Cox, 1980) and is testimony of Gondwanaland igneous activity. Remnants of this once extensive volcanic province are found scattered throughout southern Africa (Fig. 2.1) south of latitude 15°S, the present outcrop being *ca.* 140 000 km^2 (Eales *et al.*, 1984). Older strata are host to a vast suite of Karoo-age intrusive sills and dykes, indicating that a large proportion of the southern African subcontinent was once blanketed by volcanic material.

Regional studies on the Karoo igneous province have indicated that overall it is geochemically heterogeneous (Cox *et al.*, 1967; Cox, 1972; Rhodes and Kröhn, 1972 and Duncan *et al.*, 1984b), but in detail can be subdivided into numerous subprovinces characterized by distinctive magma types. In some cases these magma types are restricted geographically, whilst others can be traced for may hundreds of kilometers (e.g. the Lesotho-type). This study is therefore, an attempt to correlate the Sani Pass magma types with others in the Karoo igneous province, primarily by comparing their geochemistry. Due to the nature of such a comparison, this work draws on published geochemical data, and all data other then for the Sani Pass rocks has been obtained from the literature.

11.2. Geochemical Provinciality of the Sani Pass Magma Types

Cox *et al.*, (1967) proposed the existence of two major geochemical provinces in the Karoo basalt outcrop area. These they termed a "northern province" comprising the outliers in Northern Lebombo, Tuli, Featherstone, Nyamandhlovu and the Victoria Falls area of Zimbabwe, and a "southern province" of Lesotho, Swaziland and the north-eastern Cape. They noted that the "northern province" basalts were markedly enriched in K, Ti, P, Ba, Sr and Zr relative to basalts of the "southern" province. Subsequent work by Sweeney (1988), Erlank *et al.* (1989; 1990b) has confirmed the existence of this geochemical boundary within the Karoo igneous province. The latter authors have demonstrated that the geochemical boundary could be well defined in the Lebombo region at *ca* 25°S and in the Etendeka area *ca* 20°S (Fig. 2.1). In these areas a transitional zone 60 to 100 km wide is present. However, this boundary could not be sustained in Botswana, suggesting some degree of discontinuity between the Lebombo and Etendeka regions (Erlank *et al.*, 1990b). However, the geochemical discontinuity between Etendeka and the Lebombo is not surprising, since they are completely different ages.

With respect to trace element concentrations Erlank *et al.* (1990b), distinguished between "enriched" basalts to the north of their geochemical boundary and "normal" basalts to the south. They suggested that the immobile elements Ti and Zr are the most reliable discriminants between "enriched" and "normal" Karoo basalts. The "enriched" basalts, termed HTZ (high Ti, Zr) contain $>2.5\%$ and >250 ppm Zr, and are also characterized by having $Zr/Y>6$, whereas the "normal" basalts, termed LTZ, (low Ti, Zr) are marked by lower concentrations of these elements.

Although in the Sani Pass succession, only the Agate Vale basalts have $Zr/Y>6$ (except samples AV400 and AV91), the individual element concentrations for an enriched magma ($TiO_2>2.5$ weight percent and $Zr > 250$ ppm) are not satisfied, since $TiO_2 = 0.95$ to 1.14 weight percent and $Zr = 123$ to 159 ppm. In fact, none of the magma types in the Sani Pass satisfy the requirements for an "enriched" magma. When the Sani Pass magmas are compared to a typical northern province HTZ basalt (Northern Lebombo basalt, data

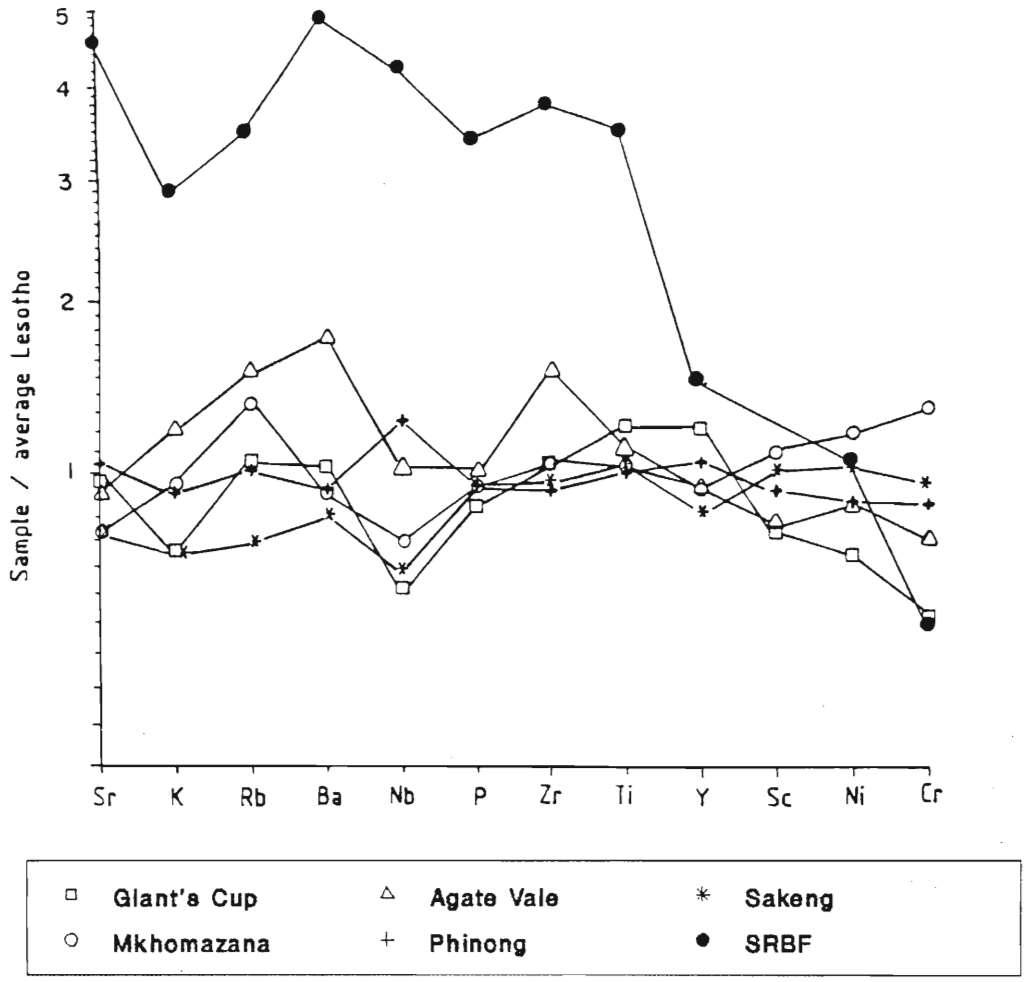

Fig. 11.1 Spidergram comparing average Sani Pass basalts with the average SRBF (northern Lebombo). The SBRF is enriched in all the incompatible elements relative to the Sani Pass basalts. Normalizing data are from Duncan *et al.*, (1984b).

from Duncan *et al.*, 1984b) on a spidergram (Fig. 11.1), they show depletion in all incompatible elements.

The Sani Pass basalts, therefore conform to Cox *et al's.* (1967) southern province basalts and Erlank *et al's.* (1990b) LTZ normal basalts.

11.3. The Sani Pass magmas compared to magma types in the southern province

Duncan and Erlank (1979) grouped the Karoo volcanics into four major magma types, namely the Atlantic type (comprising the lavas of northern Namibia - Etendeka and the Cape Cross area and equivalent basaltic lavas in Southern America), the Central Karoo (constituting the Stormberg, Drakensberg, Springbok and Mariantal lava fields and the Central Karoo dolerites), the southern Lebombo (incorporating the lavas of the southern Lebombo and Swaziland, and the northern Lebombo (incorporating the lavas in Zimbabwe). Marsh (1987), subsequently suggested that on the basis of age, association and tectonic setting, the Karoo igneous province can be divided into three subareas, namely, the Central area (made up of Lesotho, Kalkrand (in Namibia), Springbok Flats and southern Botswana), the Lebombo-Nuanetsi area and the Etendeka area on the west coast. In this subsection the Sani Pass magma types are compared to other magma types from these three areas.

Volcanic rocks *circa* 130 my old are preserved along the north-western Namibian coast between Cape Cross and the Kunene River, and comprise the Etendeka Formation/Group (see Milner *et al.*, 1990 for nomenclature) (Fig. 2.1). These volcanic rocks consist dominantly of flood basalts and voluminous quartz latites and subordinate latites (Erlank *et al.*, 1984). The Etendeka erosional remnants follow conformably on sedimentary formations of the Karoo Sequence, a feature which in the past justified correlation with the Central area basalts. However, on geochemical grounds, the Etendeka basic lavas are generally more evolved compositionally and thus have higher concentrations of TiO_2, K_2O and other incompatible trace elements than most of the Central area magma types (Erlank *et al.*, 1984), except for the Pronksberg high-K basalts, which have higher K_2O, Rb, Ba and Zr

abundances. Also, the age of the Etendeka volcanics is approximately 130 - 135 Ma, being erupted shortly prior to the opening of the South Atlantic at about 122 - 127 Ma at this latitude (Erlank *et al.*, 1984, Duncan *et al.*, 1990), thus making it slightly younger than the Central area basalts which are largely early to middle Jurassic (Fitch and Miller, 1984). Instead, the geochemical characteristics, geographic location in a pre-drift reconstruction of Gondwana and coincidence in age, make the Etendeka Formation basalts a more appropriate correlative of the Serra Geral Formation of the Paraná Basin in Brazil (Erlank *et al.*, 1984; Duncan *et al.*, 1990).

Considering the intrusive suit in the Etendeka, Erlank *et al.*, (1984) indicated that the regional dolerites have similar mineralogical and geochemical characteristics to the Lesotho Formation lavas from the Central area. However, Duncan *et al.*, (1990) concluded that the Huab dolerites are likely to be younger than the geographically associated Etendeka volcanics, thus eliminating any postulated contemporaneity with the Central area basalts.

The Lebombo area is characterized by a 700 km linear belt (Fig. 2.1) of eastward-dipping, monoclinally warped, bimodal suite of volcanics lying approximately along longitude 32°E in eastern southern Africa (Eales *et al.*, 1984). In the southern portion (south of about 20°S) of the Lebombo monocline "normal," LTZ Karoo basalts are preserved as part of the Sabie River Basalt Formation. This basaltic unit overlies Karoo sediments and is in turn overlain by rhyolites of the Jozini Formation (Cleverly and Bristow, 1979). Marsh (1987) noted that, in general, Lebombo volcanism was essentially contemporaneous with that of the Central area, with the main volcanic phase dying out by the middle of the Jurassic. However, the discussion in Chapter 6 has indicated that the acid volcanic suite of the Lebombo could not have been present in the Sani Pass area.

In terms of the basalts, Cox and Bristow (1984), indicated considerable macroscopic heterogeneity between the Sabie River Formation basalts and those of the Lesotho Formation. Utilizing a DFA technique Duncan *et al.*, (1984b) showed that the Sabie River Basalt Formation magma type from Zululand and Swaziland is clearly different from the Central area magma types. This difference they attributed to a higher content of TiO_2,

Fe_2O_3, Zr and Y, and lower content of Al_2O_3 and K_2O in the Sabie River basalts. Further evidence of the difference between the Karoo central area magma types (including those of the Sani Pass) and the low-Ti Sabie River Formation, is isotope data presented by Marsh *et al.*, (1992), which suggest separate eruptive sites and sources for the low-Ti basalts of the Central area on the one hand, and the Lebombo on the other.

The Central area incorporates basaltic remnants from the Lesotho and Stormberg mountains, those at Kalkrand (near Mariantal), Springbok Flats and southern Botswana. Basalts from all of these areas occur south of the geochemical discontinuity described previously and are low Ti, Zr basalts (except for the LTZ samples from north of this boundary in Botswana, see Erlank *et al.*, 1990). The Lesotho Formation basalts are volumetrically dominant in the Central area and their compositional coherence is persistent over laterally extensive areas, being detected in the Kalkrand basalts in Namibia and the Springbok Flats in northern Transvaal. In addition, the majority of dykes and sills which form a dense subvolcanic intrusive complex in the Central area are also representatives of this magma type (Duncan *et al.*, 1984b). Marsh and Eales (1984) expanding on work done by Robey (1976), Pemberton (1978), Rumble (1979) and Mitchell (1980) on Karoo volcanics from the north-eastern Cape, recognized numerous magma types, that underlie the Lesotho Formation basalts. These basaltic magma types are:

1. Kraai River Type
2. Vaalkop type
3. Omega type
4. Moshesh's Ford type
5. Pronksberg High - K basalt type.

In addition, to the basaltic magma types, three intermediate magma types were identified, namely Belmore andesite, Pronksberg dacite and the Roodehoek dacite. Although in general the magma types are confined to mappable stratigraphic units, Marsh and Eales' (1984) classification is based on chemical composition only.

All of these magma types, where present, occur in minor volumes below the Lesotho Formation, which in all cases comprises the major thickness of the succession. In addition, these minor magma types are the first manifestations of widespread volcanic activity in most areas, and overlie Karoo sediments. These two features are apparent in the Sani Pass volcanic succession, where the Phinong magma type comprises the major thickness of the volcanics, underlain by substantially smaller volume of the Giant's Cup, Agate Vale, Sakeng and Mkhomazana magma types. These latter magma types, comprising the pre-Phinong suite, also rest on Karoo sediments (Clarens Formation sandstone). In terms of the similarity in stratigraphic succession between the Sani Pass magma types and those from the north-eastern Cape (Fig. 11.2) a comparison and possible correlation between the magma types from the two areas is valid. Considering stratigraphical relationships, the large volume of the Phinong magma type can be correlated with the similarly voluminous Lesotho Formation, whereas the pre-Phinong magma types can be broadly correlated with the magma types listed 1 to 5 above.

Marsh and Eales (1984) noted that the major element compositional differences between the different magma types in the north-eastern Cape are not diagnostic, although some difference is observed in SiO_2 and K_2O contents. However, these magma types can be readily recognised in terms of their trace element chemistry. Accordingly, using petrographic criteria for distinguishing the different magma types is unsuccessful. In general, however, the Lesotho, Omega and Moshesh's Ford basalts are coarsely doleritic in texture (Pemberton, 1978) as are their correlatives (Perdekop Unit, Roodehoek Unit, respectively) in the Jamestown - Molteno district (Mitchell, 1980). The Kraai River and Vaalkop basalts are aphanitic, even flinty at outcrop (Marsh and Eales, 1984).

The Sani Pass magma types are compared to the other Central area basalts by means of incompatible element ratios, since these magma types are characterized by discrete ranges for incompatible elements. Figs. 11.3a-c show the compositional fields for the Sani Pass magma types, and average concentrations of the incompatible elements (Ti, Zr, Y, Nb and P) for the following magma types: Lesotho, Springbok Flats, Kraai River, Vaalkop, Omega, Moshesh's Ford and Pronksberg high - K. These average data have been taken

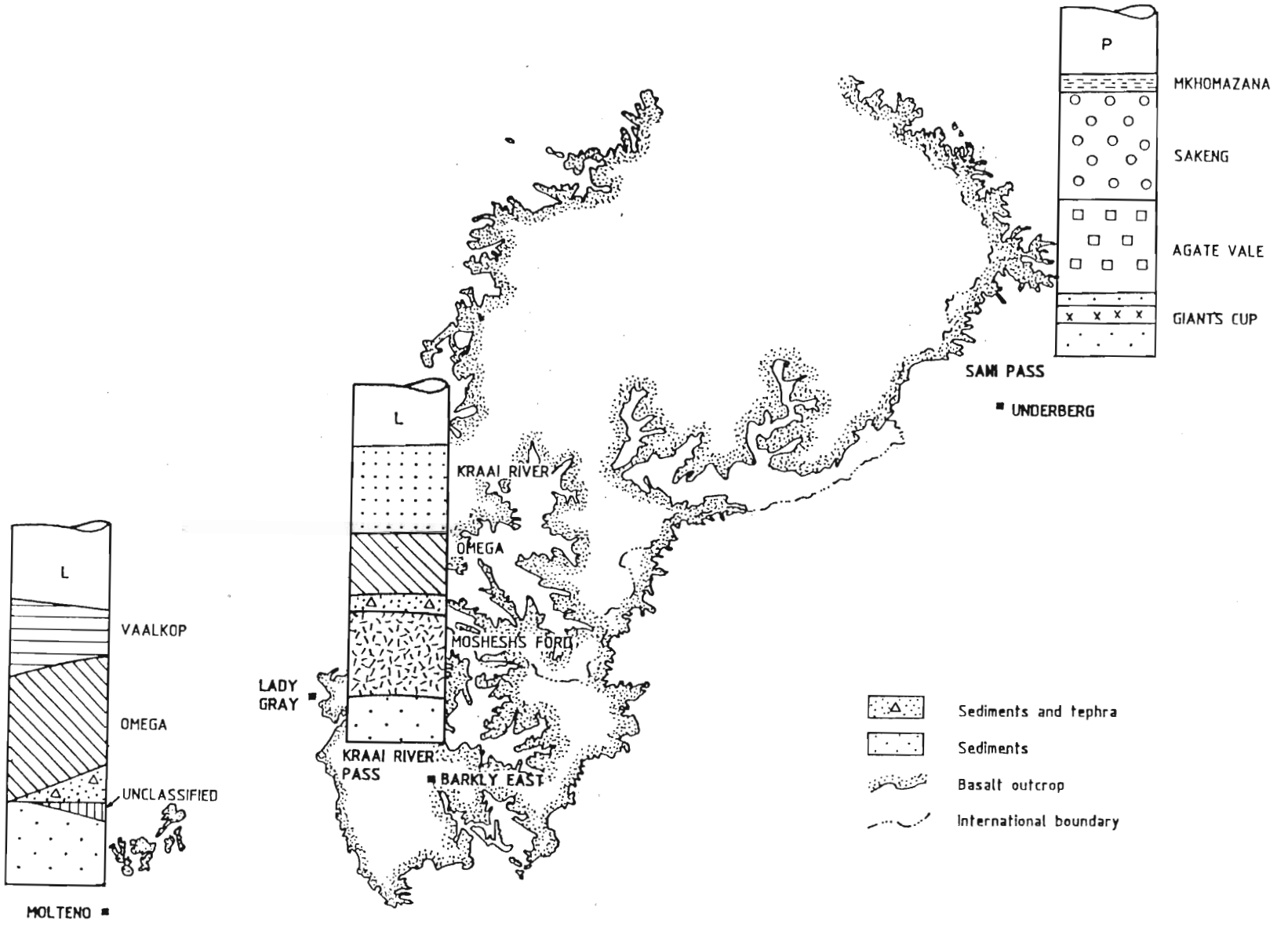

Fig. 11.2 Generalized summary of the stratigraphic relationships of the main magma types preceding the Lesotho Formation (L) in the north-eastern Cape (modified after Marsh and Eales, 1984), and at Sani Pass below the Phinong magma type (P).

from Duncan *et al.*, (1984b) and are listed in Table 11.1. Most obvious in these figures is the striking correspondence between the Lesotho and Phinong magma types, for all the incompatible elements. The Omega magma shows a similar correspondence with the Phinong type, but only in terms of P, Ti, Zr and Y. However, the average element concentrations show that the Omega type generally has lower SiO_2, TiO_2, P_2O_5, Rb, Zr and Nb and higher MgO than most of the Phinong and Lesotho type basalts (Table 11.1 and Table A2.6, Appendix 2). In terms of Ti/Zr and Zr/Y a weak correspondence is present between the Moshesh's Ford and Pronksberg high - K magmas, and the Agate Vale type. This correspondence is destroyed on the Zr/Nb plot (Fig. 11.3b) due to the higher Nb content (16 ppm) in both these north-eastern Cape magmas. The Moshesh's Ford magma type also has lower Ba, V, Ni, and SiO_2, and is somewhat enriched in MnO, CaO, P_2O_5, Y, La and Sr relative to the Agate Vale magma. The Pronksberg high - K basalts, however, are simply diagnosed by their extreme enrichment in K_2O, Sr and Ba, relative to all Central area magmas.

A discriminant functional analysis (DFA) for the Sani Pass magmas successfully classified the Phinong and Agate Vale as separate magma types. The Giant's Cup, Sakeng and Mkhomazana magmas where not classified into coherent fields and plotted in and about the field occupied by the Phinong basalts (Fig. 9.1). When these magma types are compared to those from the north-eastern Cape, using the canonical variables of Duncan *et al.*, (1984b) and fields extracted from the same reference (Fig. 8, Duncan *et al.*, 1984b), only the Lesotho and Omega magma types show any resemblance to the Sani Pass rocks (see overlay to Fig. 9.1 - this study). The former has already been correlated to the Phinong magma type, but this correlation could not be sustained for the latter on the basis of specific elements.

The problem of successfully classifying the Sakeng, Mkhomazana and less so the Giant's Cup magma types lies in their uniqueness indicated by only a limited number of major and compatible elements. Nonetheless, a comparison of average concentrations indicates that none of the north-eastern Cape magma types has low CaO and high Na_2O contents, as in the Mkhomazana magma type. Nor do any of these magmas have similarly low Rb and Sr

Table 11.1 Average compositions of some Karoo magma types (data from Duncan et al., 1984b)

	1	2	3	4	5	6	7	8	9	10	11
SiO2	51.50	52.47	54.17	52.94	51.10	50.93	53.66	53.57	52.04	52.84	51.52
TiO2	0.95	1.03	0.87	1.12	1.32	0.93	1.01	1.38	1.20	1.44	3.31
AL2O3	15.69	15.98	15.23	15.50	14.45	15.83	16.23	14.17	16.21	14.87	13.44
Fe2O3	10.96	10.21	10.07	10.47	13.36	10.97	10.21	12.61	10.97	12.32	12.91
MnO	0.16	0.18	0.20	0.22	0.18	0.24	0.23	0.18	0.16	0.17	0.16
MgO	7.01	5.94	6.58	6.40	6.30	7.10	6.45	5.25	5.92	5.51	5.40
CaO	10.69	10.36	10.05	9.55	10.61	11.00	6.75	8.59	10.10	9.27	8.40
Na2O	2.17	2.49	2.12	2.53	1.96	2.37	3.35	2.52	2.00	2.55	2.27
K2O	0.70	1.13	0.56	1.04	0.53	0.50	1.90	1.54	1.21	0.78	2.05
P2O5	0.16	0.21	0.15	0.22	0.19	0.14	0.20	0.19	0.18	0.25	0.55
Total	99.99	100.00	100.00	99.99	100.00	100.01	99.99	100.00	99.99	100.00	100.01
Rb	12	20	21	27	7.5	10	20	51	32	19	42
Ba	177	264	173	276	235	153	264	349	330	295	878
Th	1.27	3.03	3.34			0.26	3.03	5.82	5.18	2.13	4.55
Nb	4.9	16	4.8	7.1	3.7	1.39	16	10	12	5.3	21
La	9.9	18.6	13.4					24.4	28.5	15.6	52.4
Ce	23.7	42.8	31.3					55.9	63.8	33.7	123
Sr	192	309	214	279	185	217	309	229	268	316	891
Nd	13	20.3	16			3.1		27.7	31	17.4	67
Hf	2.26	3.38	2.45			0		4.53	4.38	2.65	9.69
Zr	94	146	118	117	117	80	7	165	146	134	356
Sm	3.25	4.42	3.47					6.09	5.94	4.3	13.5
Tb	0.62	0.75	0.63					1.01	0.81	0.74	1.45
Y	24	26	28	29	31	25	26	31	24	29	36
V	240	193	240	254	285	238	161	301	232	261	249
Ni	94	70	51	23	57	104	72	53	99	76	101
Cr	283	273	264	338	51	341	235	64	118	136	114

1 Lesotho Formation
2 Moshesh's Ford Formation
3 Kraai River Formation
4 Vaalkop Formation
5 Springbok Flats
6 Omega Formation
7 Pronksberg high–K
8 Etendeka Formation (Tafelberg)
9 Etendeka Formation (Albin)
10 Sabie River Basalt Formation (southern Lebombo)
11 Sabie River Basalt Formation (northern Lebombo)

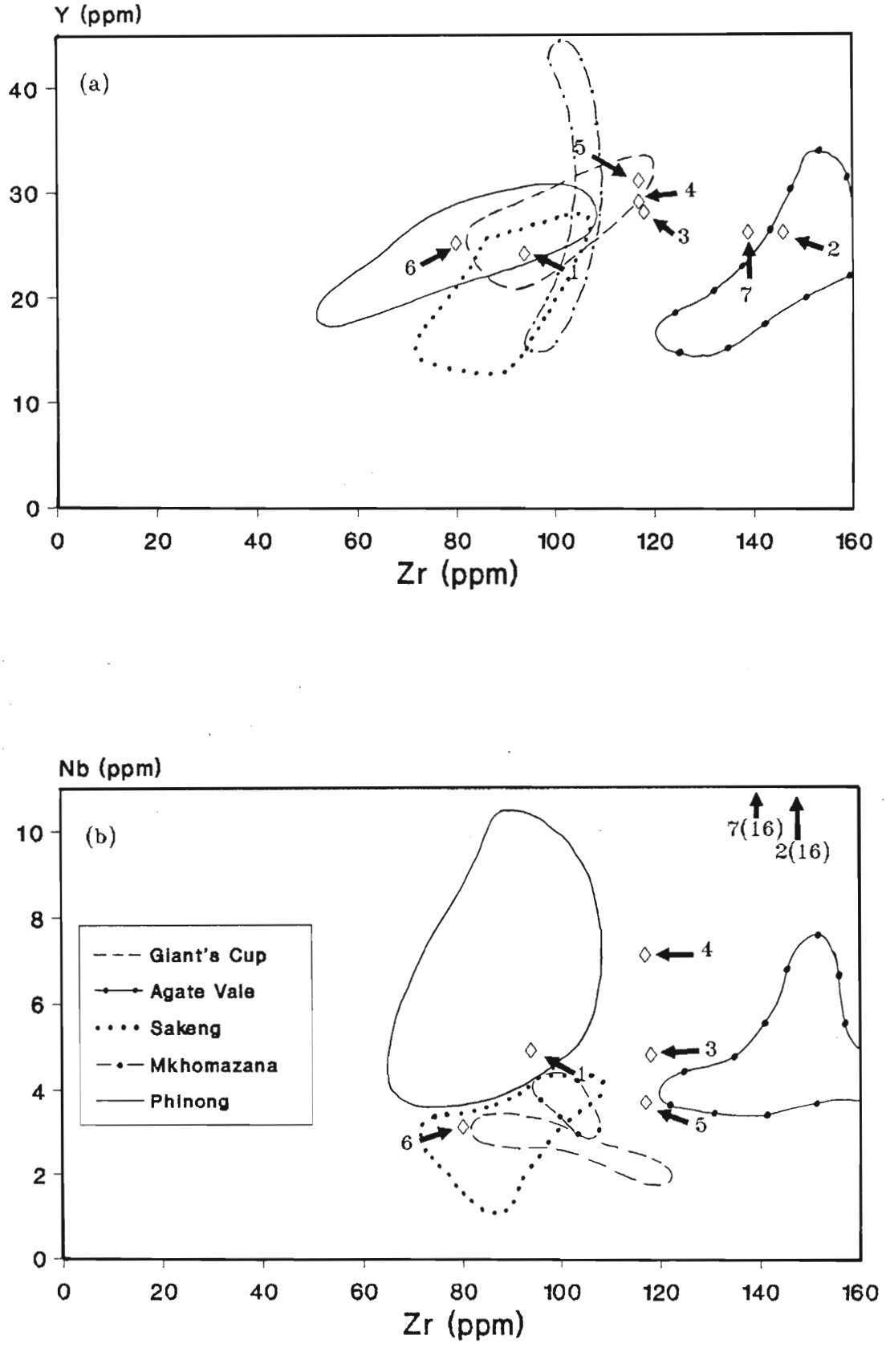

Fig. 11.3a-b Average concentrations of (a) Y and Zr, and (b) Nb and Zr, for the north-eastern Cape basalts compared to the compositional fields for the Sani Pass magmas. The numbers correspond to the numbers in Table 11.1, indicating the different north-eastern Cape magmas.

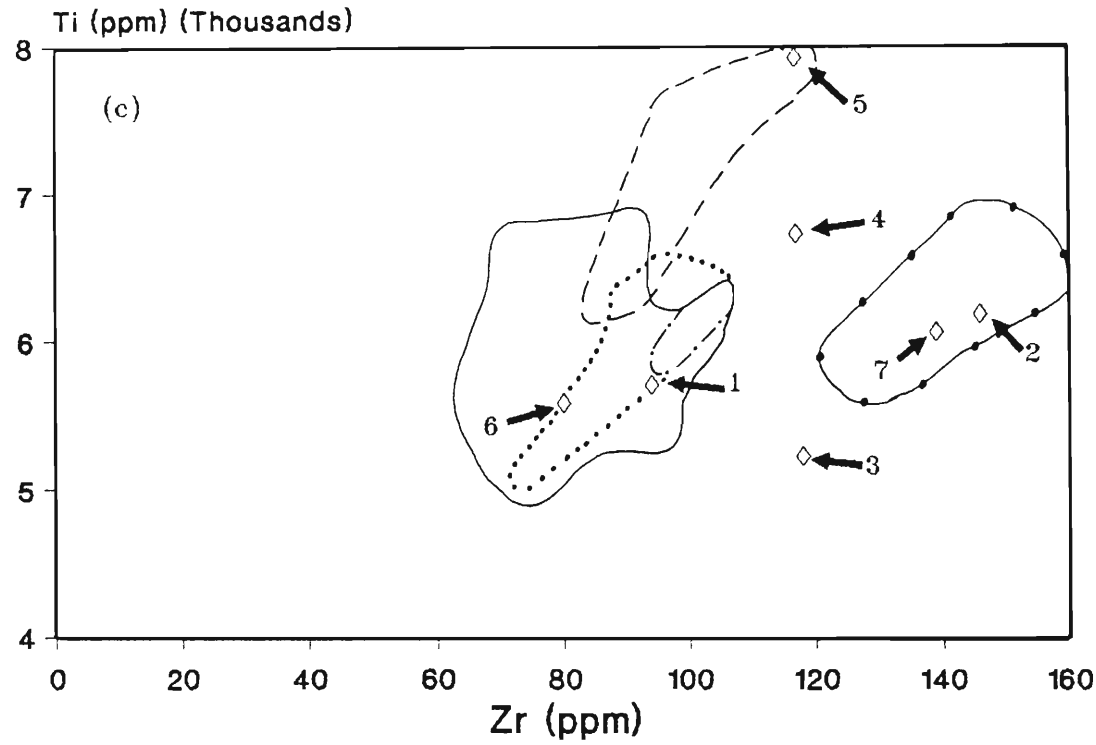

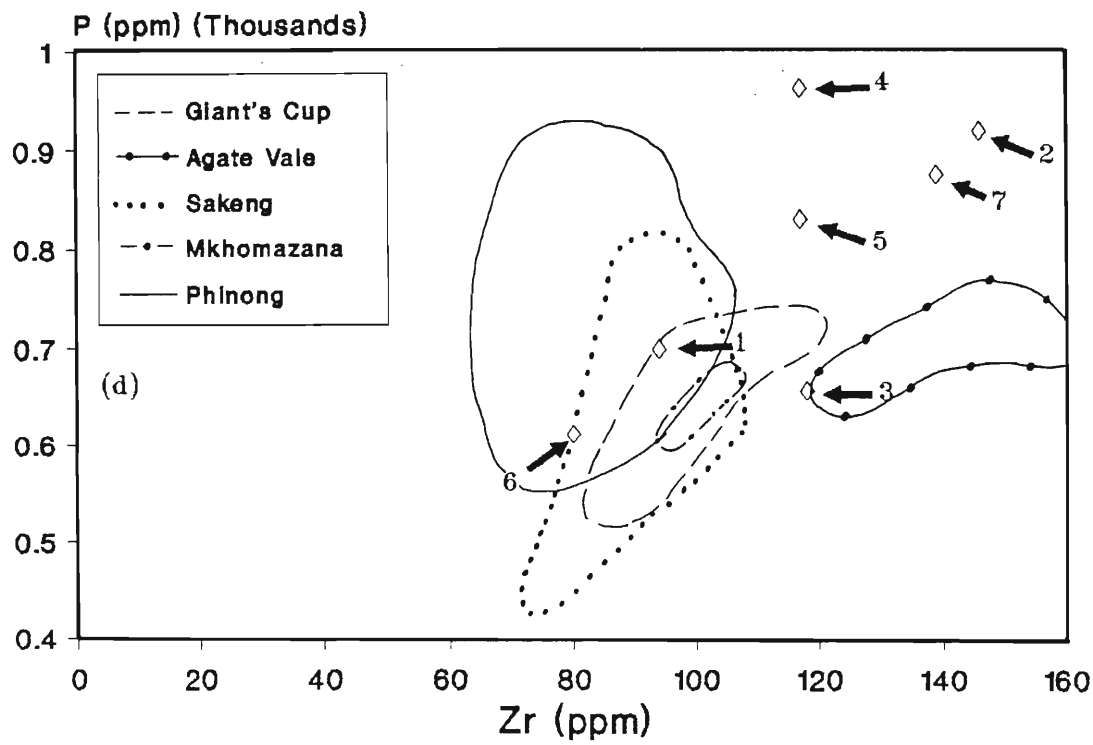

Fig. 11.3c-d Average concentration of (c) Ti and Zr, and (d) P and Zr, for the north-eastern Cape basalts compared to the compositional fields for the Sani Pass magmas. The numbers correspond to the numbers in Table 11.1, indicating the different north-eastern Cape magmas.

contents as in the Sakeng magma type, or low MgO as in the Giant's Cup basalts. This comparison, however, can only be sustained if it is assumed that the Sani Pass rocks reflect pristine concentrations (except for the Sr in the Sakeng basalts).

This exercise has adequately demonstrated that, in terms of geochemistry, the Phinong magma type can be correlated with the Lesotho-type. The minor magma types preceding the Phinong basalts are unique to the Sani Pass area, and cannot be successfully correlated with similarly localised magma types in the north-eastern Cape. In addition, this lack in correlation between the pre-Lesotho and pre-Phinong magmas in the north-eastern Cape and Natal Drakensberg respectively indicates the lateral heterogeneity of the source areas during their eruption. The eruption of Lesotho (Phinong) basalts indicates a more homogenised mantle.

11.4. Summary

The five different magma types in the Sani Pass have been compared to Central area magmas in the Karoo Igneous Province.

Incompatible elements clearly indicate that the Sani Pass magmas are normal Ti, Zr (after Erlank *et al.*, 1990b) "southern province" type (after Cox *et al.*, 1967) basalts, rather than "enriched" HTZ northern province basalts.

The Etendeka volcanics have not been compared to the Sani Pass magmas, since their Cretaceous age, and geographic location in a pre-breakup Gondwanaland make them correlations of the Paraná Basin volcanics, rather than the Central area volcanics. Similarly, the southern Lebombo basalts, namely the Sabie River Basalt Formation, were not compared to the Sani Pass magma types. This is so, since isotope data presented by Marsh *et al.*, (1992) indicate separate sources for the Sabie River Basalt Formation and for the Central area.

Nevertheless, a detailed comparison was undertaken between the Sani Pass magma types, and the following magma types from the north-eastern Cape: Lesotho, Kraai River, Vaalkop, Omega, Moshesh's Ford, Pronksberg High-K and the Springbok Flats.

Incompatible element ratios and discriminant function analysis have indicated that the Phinong magma type can be correlated with Marsh and Eales' (1984) Lesotho magma type. Although stratigraphic similarity is present between the pre-Phinong magmas in the Sani Pass and the pre-Lesotho magmas in the north-eastern Cape, their correlation cannot be sustained on a geochemical basis. Although the Giant's Cup and Sakeng magmas show compositional overlap with the Phinong magma, the Agate Vale seems to be distinctly different and indicates a unique magma type within the Central area. In terms of their Na contents the Mkhomazana basalts are also unique.

CHAPTER 12

12. COMPARISON WITH OTHER MESOZOIC BASALTS OF GONDWANALAND

12.1. Introduction

The Gondwana supercontinent comprises three magmatic provinces extending from South America, across southern Africa and Antarctica, to southern Australia (Fig. 12.1) (Hergt *et al.*, 1991). These continental flood basalt provinces are the Parana province, comprising the volcanics of Etendeka and Parana, the Karoo province, being made up of the Karoo igneous province and the Dronning Maud Land basalts, and the Ferrar Group, constituting the volcanics from south east Australia, Tasmania and the Transantarctic Mountains (Fig. 12.1) (Hergt *et al.*, 1991).

Recent reconstructions of Gondwana place Dronning Maud Land, Antarctica and the Mozambique coast of Africa into juxtaposition at *ca* 145 Ma on the basis of marine geophysical evidence (Martin and Hartnady, 1986), geological evidence (Groenewald *et al.*, 1991) and geochemical similarities (Harris *et al.*, 1986, 1990). Geochemical evidence has indicated similarities between the Kirwan basalts in Antarctica and the southern Lebombo Sabie River Basalt Formation, suggesting a common source. In this study the Sani Pass basalts are compared to those of Dronning Maud Land at Kirwan, Heimefrontfjella and Vestfjella.

12.2. Overview of basalts in Dronning Maud Land, Antarctica

Basalts of Jurassic age (Faure *et al.*, 1979) at Dronning Maud Land, Antarctica, are preserved as nunataks at Kirwanveggen, Heimefrontfjella (including the lavas at Bjounutane

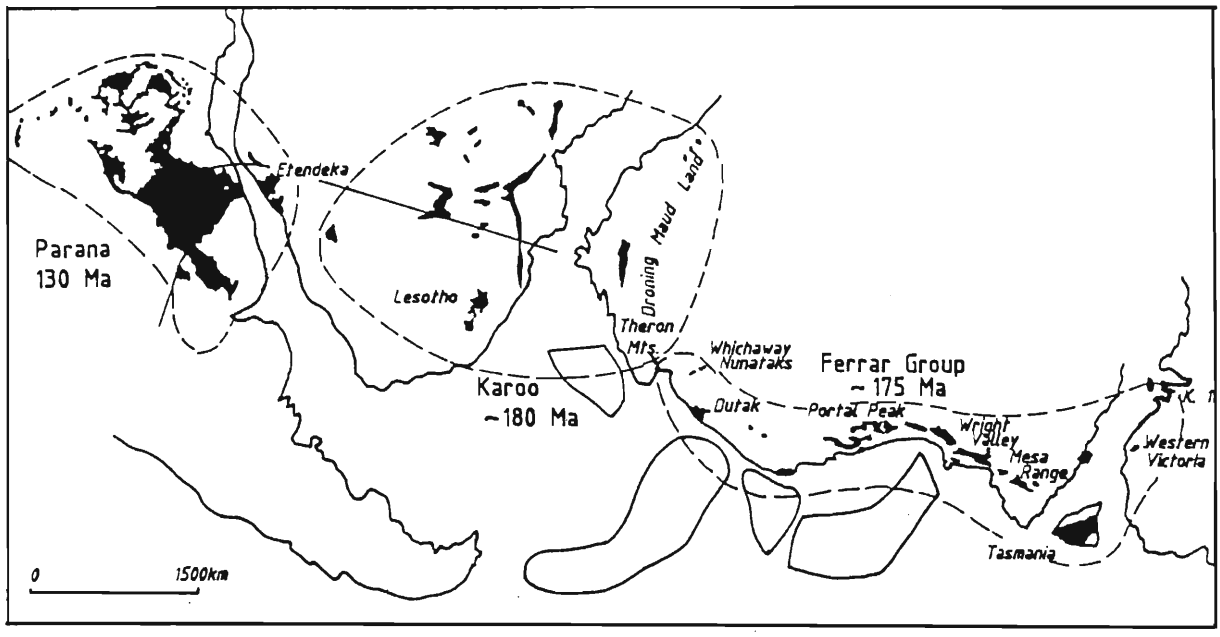

Fig. 12.1. Diagram indicating the three Karoo-age magmatic provinces in a reconstructed Gondwanaland (after Hergt et al., 1991).

and Sembberget) and Vestfjella (Fig. 12.2). The Kirwanveggen (Kirwan) basalts are preserved in the vicinity of 74°S, 6°W (Fig. 12.2), along the southernmost 50 km of the Kirwanveggen Escarpment. These basalts are preceded by sandstones of the Permian - Triassic Amelang Plateau Formation (Aucamp *et al.*, 1972), which in turn rest unconformably on a variety of Precambrian schists and gneisses and lower Palaeozoic quartzites (Harris *et al.*, 1986, 1990). West of the Kirwan basalts, in the area 75°S, 12°W and 74°S, 15°W, are the Heimefrontfjella and Vestfjella nunatak groups of basalts, respectively (Fig. 12.2). The Vestfjella basalts overlie quartzites and sandstones, with intercalated shales, and the thickness of this volcanic succession has been conservatively estimated at 1000m (Furnes et al., 1987). The Heimefrontfjella volcanics rest upon Devonian to Late Triassic sediments of the upper Beacon Supergroup (Juckes, 1972).

In the Kirwan group of nunataks the maximum thickness of basalts has been estimated to be 420m at any one section (Harris *et al.*, 1986), although the lower part of the sequence wedges out to the north-east. In the Lagfjella nunatak, where the greatest vertical section of lava is present, Harris *et al.*, (1990) measured 11 flows, where the tendency is for the lower flows to be thinner than the upper flows. In this upper flow section two flows of >90m in thickness were measured by these authors. They also noted that pipe amygdales are rare, and when present, are invariably inclined to the east, indicating the palaeoflow direction of the lavas. Intrusive rocks having a similar age to the lavas have not been documented in the Kirwan area. However, intrusive Jurassic dykes (Wolmarans and Kent, 1982; B R Watters, *pers. comm.*, 1985, cited in Harris *et al.*, 1990) of doleritic composition intrude the Precambrian rocks in the north-eastern Kirwanveggen and in the area to the north of Grunehogna. Collerson (1985) suggested that the Jurassic dolerites (dated by K - Ar method) in Western Dronning Maud Land and the Shackleton Range may be related to the southern African Karoo dolerites.

Most of the Kirwan basalts are porphyritic with plagioclase, augite and limited olivine comprising the phenocryst assemblage (Harris *et al.*, 1990). The most porphyritic samples contain 20% modal phenocrysts, but the average phenocryst content is 12%, being made up by 85% plagioclase, 11% augite and 4% olivine. Textures in the Vestfjella basalts vary

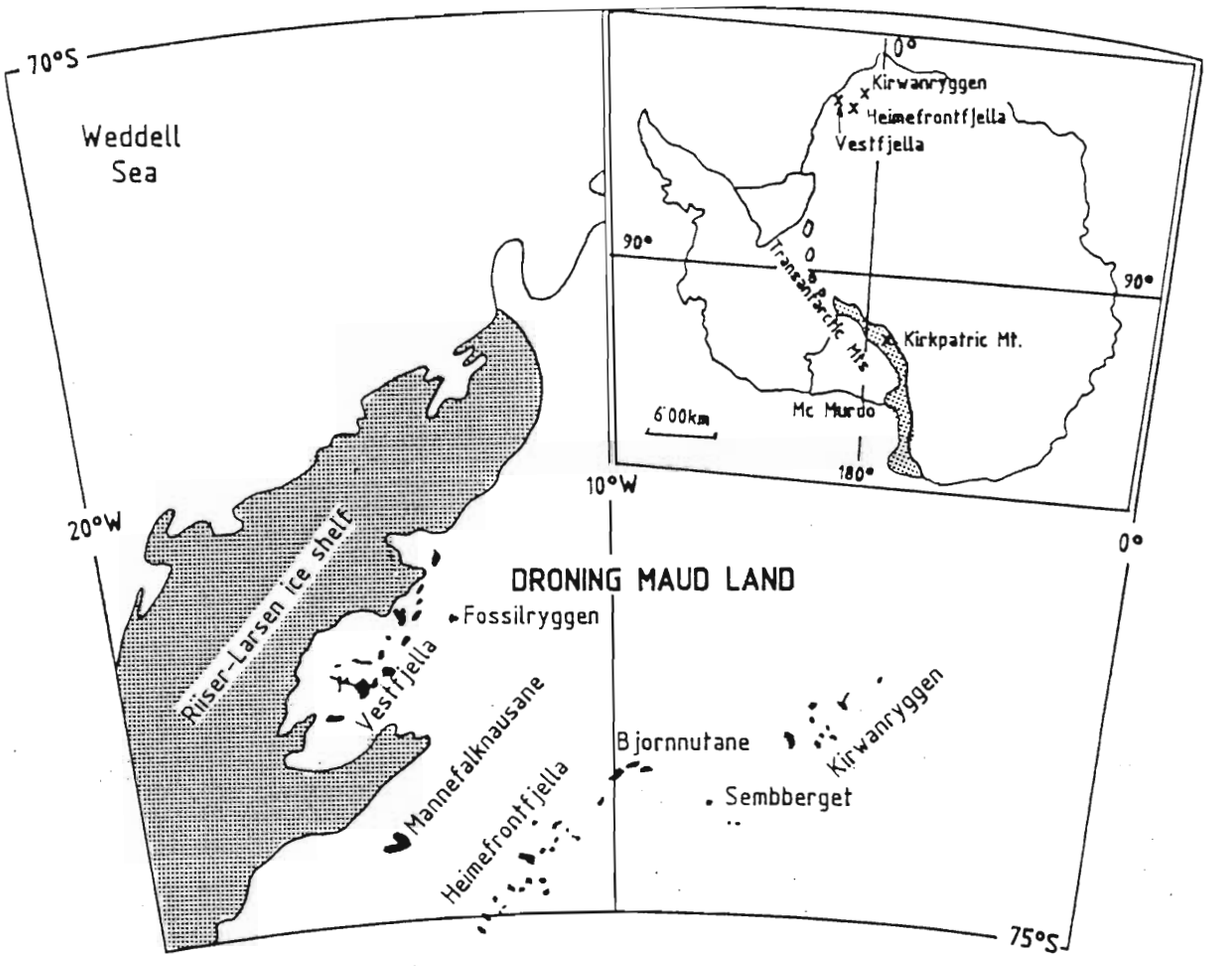

Fig. 12.2 Map of Dronning Maud Land showing location of basalt nunataks at Kirwanveggan, Vestfjella and Heimefrontfjella. Map has been adopted from Furnes et al., (1987).

from aphyric to highly porphyritic, the phenocrysts being plagioclase, Ca-rich pyroxene, Ca-poor pyroxene and olivine (Furnes *et al.*, 1987).

In general, the Kirwan basalts show a restricted range in composition, particularly regarding the major elements, whereas the trace elements show rather more variation with incompatible elements varying by factors of about two or more (Harris *et al.*, 1986; 1990). When the average Kirwan basalt chemistry is compared to that of the Vestfjella and Heimefrontfjella basalts, the latter is similar to the Kirwan basalts in both major and trace elements (see Table 12.1 and Figs. 12.3a-e). The Vestfjella basalts on the other hand, show a greater variation in chemistry, particularly for the incompatible elements K, Rb and Ba which show strong decoupling from Nb and Zr. Furnes *et al.*, (1987) suggested that the decoupling might be ascribed to the accumulation of a high proportion of phenocrysts in these rocks. Harris *et al.*, (1990) noted that the Heimefrontfjella and Kirwan basalts occupy similar compositional fields on variation diagrams as the Vestfjella basalts, and therefore, the Kirwan and Heimefrontfjella basalts might be compositionally equivalent to "uncontaminated" Vestfjella basalts.

Gabbro fractionation is the dominant differentiation process in the Kirwan basalts, but the incompatible element data require that the parent liquids of these basalts be derived by slightly different degrees of partial melting of a common source, or alternatively of open system (RTF) magma processes (Harris *et al.*, 1990). Furnes *et al.*, (1987) suggested that the Vestfjella lavas were derived from a garnet-free mantle with variable incompatible trace element ratios, by degrees of partial melting greater than 15%. The liquids were subsequently modified by crystal fractionation of olivine, clinopyroxene, plagioclase and magnetite.

12.3. Geochemical Comparison of the Dronning Maud Land basalts with the Sani Pass basalts

Comparisons between the Kirwan basalts and Karoo lavas of southern Africa have indicated many common features, particularly with the Sabie River Basalt Formation in the southern Lebombo (Harris *et al.*, 1986; 1990). These authors suggested that the composition of the

Kirwan basalts is consistent with their derivation from a source similar to that for the southern Lebombo SRBF, by slightly higher degrees of partial melting.

Similarly, the five magma types in the Sani Pass succession are compared with the Kirwan, Heimefrontfjella and Vestfjella, by means of spidergrams. For the purposes of this study average values are used for the Kirwan (data from Harris *et al.*, 1990), Heimefrontfjella (data from Furnes *et al.*, 1987) and Vestfjella (data from Juckes, 1972) basalts, and are normalized to an average Lesotho-type basalt (data from Duncan *et al.*, 1984b). In addition to the average Sani Pass magma compositions being plotted on the spidergrams, the compositional range for the element is also plotted. In plotting these parameters for the Sani Pass basalts, samples suspected of being highly altered (GC350, GC360 and AV400), contaminated (AV60 and AV70) and cumulus enriched (P180 and P227) were omitted. The unnormalized data used in the spidergrams are listed in Table 12.1.

A comparison between the Dronning Maud Land basalts and the Giant's Cup basalts, indicates that the Antarctic basalts are clearly enriched in Nb, P, Ni and less so in Ti and Cr concentrations (Fig. 12.3a). Compositional overlap for the Heimefrontfjella and Kirwan basalts with the Giant's Cup basalts is only present for K, Rb and Ba concentrations. These elements, in addition to Zr, are slightly depleted relative to the average Agate Vale basalts (Fig. 12.3b). In addition, the Agate Vale basalts are depleted in P_2O_5 and TiO_2 concentrations relative to the Dronning Maud Land basalts.

Incompatible element enrichment in the Kirwan, Heimefrontfjella, and Vestfjella basalts is clearly illustrated when compared to the Sakeng basalts (Fig. 12.3c). However, the trend is reversed when the compatible elements (Ni and Cr) are compared. Nevertheless, Marsh and Eales (1984) suggested that such parallel shifts in the incompatible element concentrations, as present in Fig. 12.3c is indicative of different degrees of melting of similar mantle source compositions. Harris *et al.*, (1990) noted a similar feature when they compared the Kirwan basalts to the southern Lebombo Sabie River Basalt Formation, and suggested that the Kirwan basalts were derived from a similar source to the southern Lebombo SRBF by slightly higher degrees of partial melting. When the average southern

Table 12.1 Average chemical compositions of basalts from Antarctica and the Sani Pass

	1	2	3	4	5	6	7	8
SiO2	51.19	51.14	49.96	53.81	53.87	52.85	52.96	51.59
TiO2	1.47	1.38	1.59	1.18	1.05	1.00	1.02	0.97
Al2O3	14.79	14.78	14.39	15.31	15.53	15.76	15.75	15.90
Fe2O3	12.53	11.87	11.99	1.77	1.69	1.62	1.58	1.69
FeO	0.00	0.00	0.00	8.87	8.46	8.08	7.90	8.43
MnO	0.20	0.20	0.21	0.18	0.16	0.16	0.16	0.17
MgO	5.88	6.59	8.47	4.94	6.20	6.96	7.32	7.02
CaO	10.48	10.91	9.64	11.01	9.51	11.09	7.84	11.16
Na2O	2.74	2.42	2.47	2.29	2.50	1.90	4.32	2.28
K2O	0.53	0.52	1.00	0.50	0.84	0.44	1.01	0.63
P2O5	0.19	0.19	0.28	0.14	0.16	0.15	0.15	0.16
TOTAL	100.00	100.00	100.00	100.00	100.00	100.00	100.00	100.00
Sr	189	232	331	190	184	137	155	195
Rb	10	10	17	14	19	8	25	13
Y	32	23	25	29	23	20	29	26
Zr	109	114	98	101	146	90	101	85
Nb	4	5	6	3	5	3	4	6
Co	—	—	—	37	44	43	44	42
V	—	—	—	253	240	241	263	232
La	—	—	—	13	13	10	11	12
Cr	123	195	—	121	205	271	339	251
Zn	—	—	—	78	100	71	86	75
Cu	—	—	—	63	87	88	98	80
Ni	75	85	—	61	83	101	115	83
Sc	—	—	—	24	25	33	37	31
Ba	147	223	489	199	311	142	262	162

1 Kirwan basalts (Harris et al., 1990)
2 Heimefrontfjella basalts (Juckes, 1972)
3 Vestfjella basalts (Furnes et al., 1987)
4 Giant's Cup
5 Agate Vale
6 Sakeng
7 Mkhomazana
8 Phinong

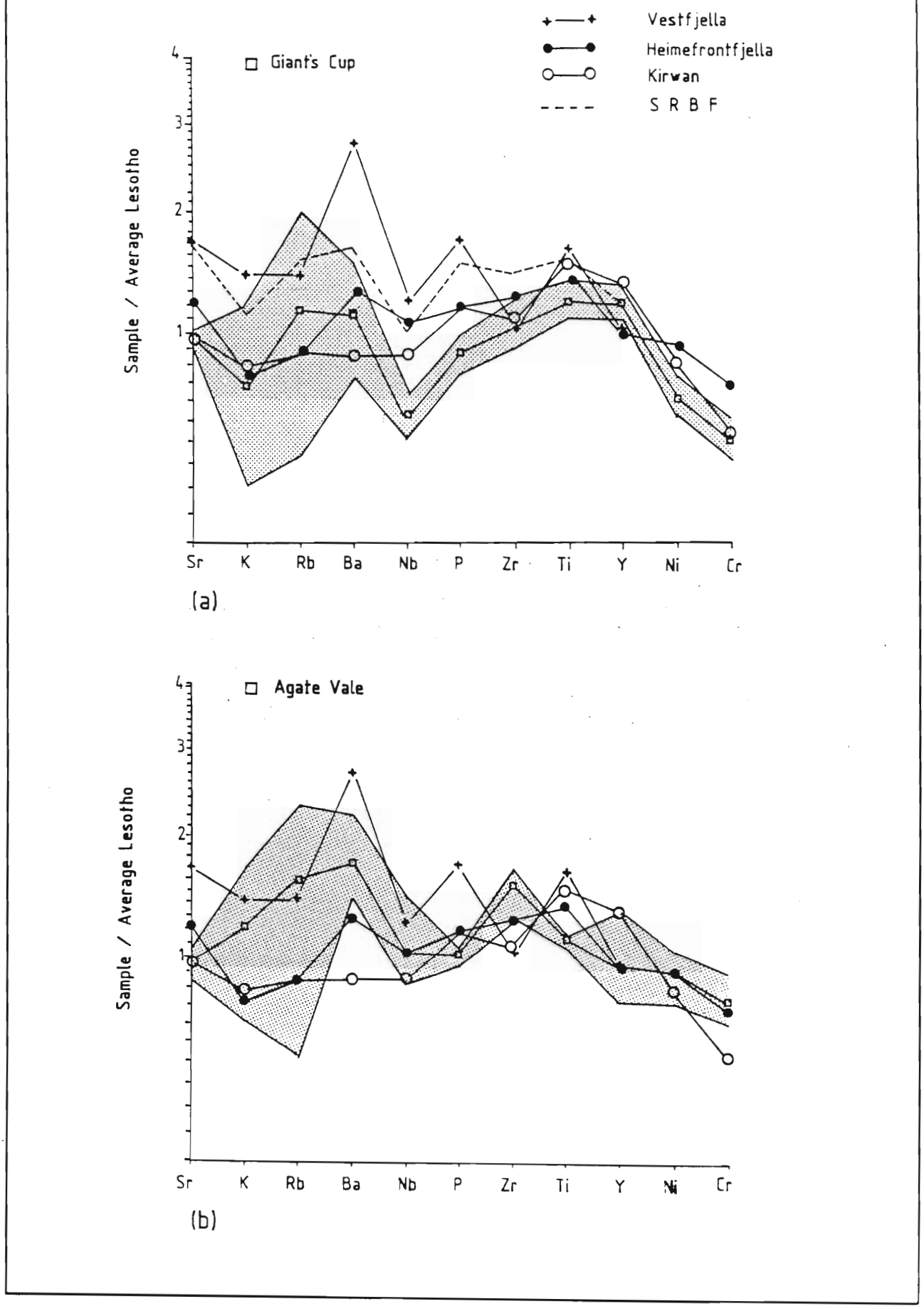

Fig. 12.3a-b Comparison of Dronning Maud Land basalts (Kirwan, Vestfjella and Heimefrontfjella) with (a) basalts of the Giant's Cup magma type and (b) the Agate Vale basalts. The shaded area is the range seen in each Sani Pass magma type.

Lebombo SRBF compositions are plotted on Fig. 12.3c, they show a similar parallel shift in the incompatible element concentrations as that in the Dronning Maud Land basalts. The inference therefore is that the Dronning Maud Land basalts, the southern Lebombo SRBF and the Sakeng basalts may have been derived by different degrees of partial melting of a similar mantle source composition. Whether it represents the same source, however is debatable, since Marsh *et al.*, (1992) have provided isotopic evidence suggesting that the Central area basalts and the Lebombo basalts were derived from separate sources and sites of eruption.

The Mkhomazana basalts do not indicate much compositional overlap with the Dronning Maud Land basalts, but substantial criss-crossing of the spidergrams is present (Fig. 12.3d). Less variability is observed in a comparison between the Dronning Maud Land basalts and the Phinong basalts (Fig. 12.3e), which have been previously shown to be a correlative of the Lesotho-type basalts. The Vestfjella basalts are clearly enriched in Sr, K, Rb, Ba, P and Ti and do not compare favourably with the Phinong basalts. However, the Kirwan basalts are broadly similar to the Phinong basalts, being slightly enriched in TiO_2 and Y concentrations. A similar enrichment in TiO_2 is exhibited by the Heimefrontfjella basalts which show marginally more variability than the Kirwan basalts, when compared to the Phinong basalts. Nevertheless, it is evident that the Kirwan, Heimefrontfjella and Phinong basalts are broadly similar in composition. However, the criss-crossing pattern of these spidergrams suggests that the Dronning Maud Land basalts could not have been directly derived from the same source as the Phinong lavas. Similar conclusions were reached by Harris *et al.*, (1990) in their comparison between the Kirwan and Lesotho Formation lavas.

12.4. Summary

Basalts of Dronning Maud Land, preserved at Kirwan, Heimefrontfjella and Vestfjella have been compared to the Sani Pass basalts. The Vestfjella basalts are generally enriched in incompatible elements, relative to the Sani Pass basalts. Broad compositional overlap is present between the Kirwan and Heimefrontfjella, and Phinong basalts.

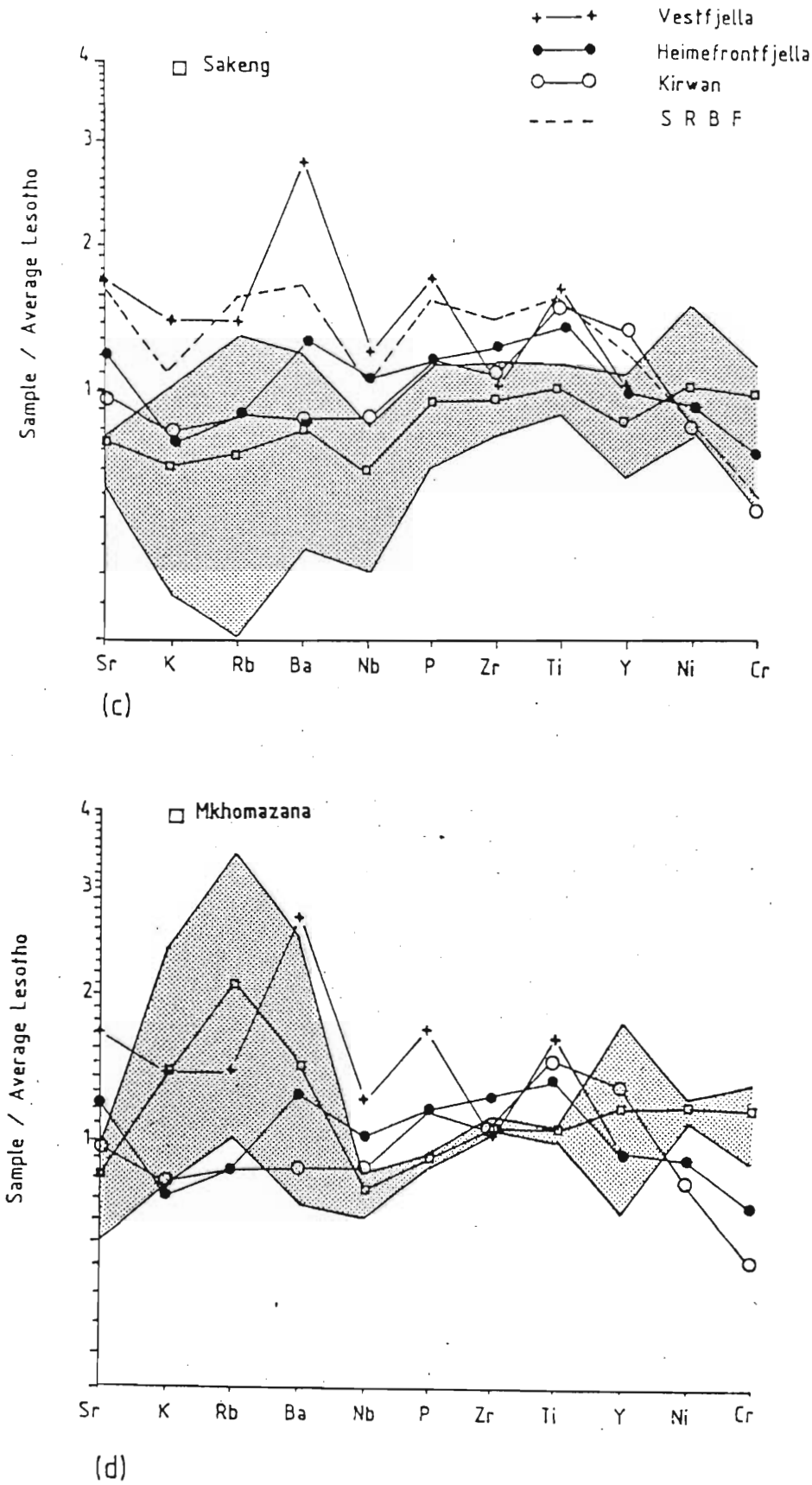

Fig. 12.4c-d Comparison of the Dronning Maud Land basalts (Kirwan, Vestfjella and Heimefrontfjella) with (c) basalts of the Sakeng magma type and (d) the Mkhomazana basalts. The shaded area is the range seen in each Sani Pass magma type.

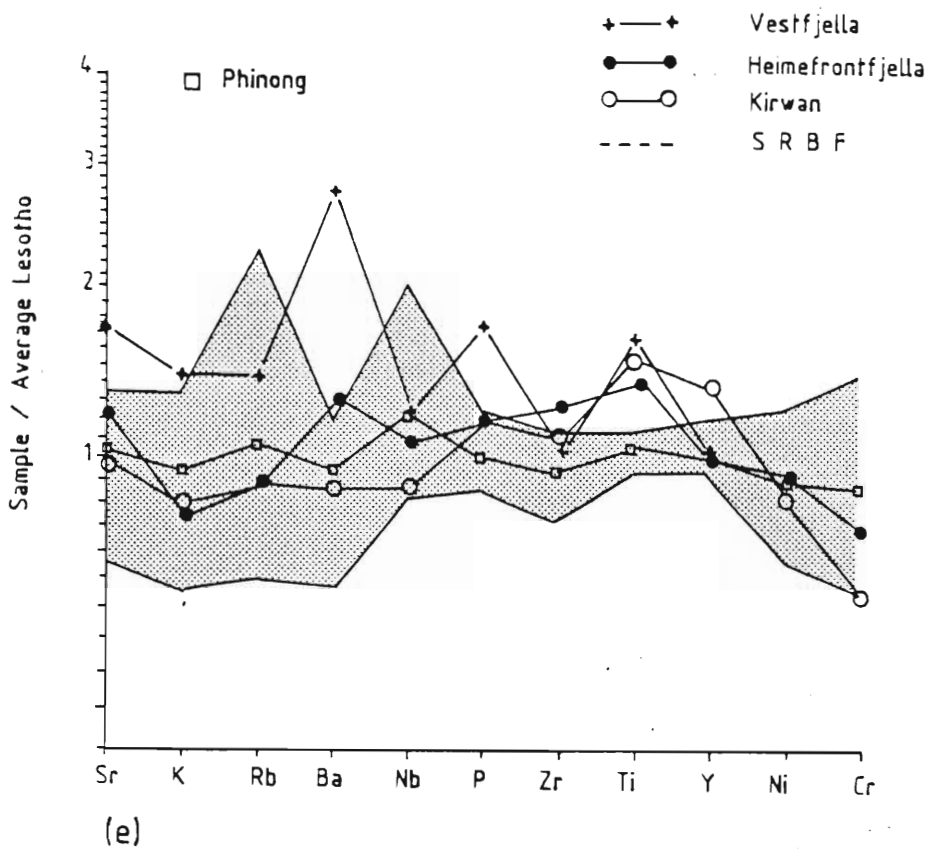

Fig. 12.2e Comparison of the Dronning Maud Land basalts (Kirwan, Vestfjella and Heimefrontfjella) with the Phinong basalts. The shaded area is the range seen in the Phinong magma type.

The similarity in spidergrams between the Sakeng, and Kirwan and Heimefrontfjella basalts, indicates that these Sani Pass basalts were probably derived by greater degrees of partial melting of a source composition similar to that responsible for the Kirwan and Heimefrontfjella basalts.

CHAPTER 13

13. CONCLUSIONS

The Lesotho highlands form a major basaltic massif which was erupted about 190 my ago. The Sani Pass, located in the Natal Drakensberg, is situated in the north-eastern sector of this massif and has exposed an approximately 800m thick succession of mainly tholeiitic basalts. The recognition of only a single diatreme, and the lack of any significant pyroclastic deposits indicates the lack of central vent-type eruptions in the Sani Pass, with fissure type eruptions being the predominant mechanism of eruption. Mapping in the area adjacent to the Sani Pass has indicated a network of dolerite dykes, which occupy feeders to the volcanic succession, and which intrude the Karoo basaltic succession as well as the underlying sediments. These dykes trend predominantly NW-SE and NE-SW.

The early phase of volcanism in the Sani Pass was punctuated by numerous short-lived episodes of quiesence, indicated by sedimentary lenses, bole surfaces and possible playa lakes. Following this precursive phase, volcanic activity was continuous and deposited thick flow units, which can be traced for many kilometers. A variety of amygdale morphologies, pahoehoe surfaces, auto-intrusive dykes and pillow lavas are preserved by the flows.

Subsequent to the eruption of the basalts, hydrothermal solutions percolated through the volcanic succession and filled the vesicles with a variety of minerals. These amygdale minerals show a zonal distibution into a lower quartz-calcite zone, followed by a laumontite zone, which is overlain by a mesolite zone. Using prevailing pressure and temperature conditions from other volcanic provinces, an original maximum thickness of 1 820m and an average fossil geothermal gradient of 111°C/km have been calculated for the Sani Pass volcanic succession. The calculated original thickness of the basaltic succession indicates that a maximum of some 413m of lavas might have been eroded from the top of Thabana Ntlenyana. In addition, it implies that felsic extrusives equivalent to those preserved in the Lebombo mountains could not have erupted in the Lesotho portion of the Central igneous province.

New major and trace element analyses for 67 basalts and 8 dolerites have been presented, and a detailed geochemical stratigraphy of the Sani Pass has been obtained. Major element geochemistry has indicated that most of the basalts, and all the dolerites are quartz tholeiites, with only eleven basalts being classified as olivine tholeiites.

The detailed geochemistry of the Sani Pass section has enabled the recognition of five different magma types, which in order of stratigraphic succession are: the Giant's Cup, Agate Vale, Sakeng, Mkhomazana and Phinong. The Phinong basalts comprise the uppermost two thirds of the volcanic succession and are generally geochemically homogeneous. Similar homogeneity is exhibited by the dolerites which are compositionally similar for most elements to the Phinong magma type. The pre-Phinong magma types are less uniform in their geochemistry and are marginally enriched in silica and have higher Zr/Nb and lower P/Zr ratios than the Phinong basalts. In the pre-Phinong succession, the lowermost Giant's Cup magma type is depleted in MgO, Cr, Ni and Co, and slightly enriched in TiO_2 content. The succeeding Agate Vale basalts are enriched in the alkalies, Rb, Sr, Ba and Zr, and depleted in CaO, while the overlying Sakeng basalts are depleted in K_2O and Sr. The Mkhomazana magma type which constitutes the three uppermost flows in the pre-Phinong succession is slightly enriched in MgO, Ni, Sc, and Cr, relative to the preceding magma types. In addition, the Mkhomazana basalts are extremely enriched in Na_2O and depleted in CaO, but this is likely to be of a secondary origin.

The pre-Phinong succession indicates a slight tendency of becoming more primitive with time. In contrast, in the Phinong succession, there is a tendency for the more fractionated rocks to be found in the uppermost 50m of the volcanic succession. Mixing calculations have indicated that 26% fractionation of plagioclase, pyroxene and olivine, in the proportions 48%, 32% and 20%, respectively from a parent composition similar to P200 can account for the more evolved chemistry of the uppermost flows in the Phinong succession. Trace element calculations, assuming Rayleigh fractionation, also suggest the possibility of differentiation having occurred within the Phinong succession.

Discriminant function analyses has only discriminated between the Phinong and Agate Vale basalts, with the remaining magma types plotting in incoherent fields. Better success

was obtained utilizing only incompatible elements, particularly the ratios Ti/Zr and P/Zr, which clearly separate all the magma types, except the Sakeng basalts. Tectonic characterization of the basalts has been unsuccessful, since the available tectonic discriminant diagrams indicate source area characteristics, rather than the prevailing tectonic regime during eruption of the lavas.

In explaining the chemical variability of the Sani Pass magma types numerous possibilities have been examined, namely, alteration, crystal fractionation with and without crustal assimilation, variation in the degree of partial melting of the source during melt extraction, and a heterogeneous source. Alteration has affected the Sani Pass rocks to varying degrees, but significant alteration has been restricted to the basal flows of the Giant's Cup and Agate Vale units. This process has also been responsible for the Sr and Na_2O depletion in the Sakeng basalts. Bulk contamination accompanied by fractionation is unlikely to have affected the basalts, but evidence for conduit contamination has been recognised in three samples of the Agate Vale magma type. Incompatible element ratios indicate that batch partial melting or continous melting of a homogeneous source are unlikely to be responsible for the chemical variation between the Sani Pass magma types. Instead, a heterogeneous mantle as the source seems to be the most likely cause of the chemical variation between the magma types.

A detailed comparison between the Sani Pass magma types and those from the the north-eastern Cape, indicates that the Phinong magma can be correlated stratigraphically and geochemically with the Lesotho magma type. Although stratigraphic similarity is present between the pre-Phinong magmas in the Sani Pass and the pre-Lesotho magmas in the north-eastern Cape, their correlation cannot be sustained in terms of geochemistry. For most of the discriminant diagrams the Agate Vale basalts are somewhat unique and might indicate a new magma type within the Karoo Central area.

A comparison of the Sani Pass magma types with basalts from Dronning Maud Land, Antarctica, indicates a broad compositional overlap between the Kirwan and Heimefrontfjella, and Phinong basalts, suggesting that the position of these Dronning Maud Land basalts in a reconstructed Gondwanaland, was close to the Karoo central province.

Incompatible element geochemistry of the Sakeng, and Kirwan and Heimefrontfjella basalts, indicates that these Sani Pass basalts were probably derived by greater degrees of partial melting of a source composition similar to that responsible for the Kirwan and Heimefrontfjella basalts.

ACKNOWLEDGEMENTS

I am grateful to my supervisor and co-supervisor, Drs. Andrew Mitchell and John Dunlevey for the time and effort they contributed during the duration of this thesis - without their effort this thesis might not have reached its culmination. Helpful suggestions and discussions with Prof. Mike Cooper, Drs. Ingo Foster, Johannes Schade and Hannes Henckel are gratefully acknowledged. Sincere appreciation is also extended to Betsy Greyling for photographic development and printing, Stanley Pillay and Ashwin Sudamah who willingly manufactured a large number of high quality thin and polished sections, and Frik van der Merwe and René Bakkes at Luipaardsvlei Geological Centre, for assisting with drafting and typing, respectively. The logistical assistance and understanding rendered by Messrs Cecil Begley and Dave Mourant (Gold Fields of S.A.) are most appreciated.

I am indebted to the Geological Survey and Natal University (Pietermaritzburg) for whole-rock chemical analyses; Dr Terry Doyle for allowing me access to the XRD at Natal University (Durban) in the period before the Durban-Westville machine was commissioned, and the Natal Parks Board for permitting me to work in the Sani Pass Game area. Bart Fokkens is thanked for his hospitality during field work and Mike Clark is thanked for transporting the writer's rock samples down the treacherous pass. Many thanks to fellow geology students, particularly, Andy and Segie for help during field work. Funding for this project was supplied by a grant from the University of Durban-Westville and a FRD grant, both these institutions are thanked for their generosity.

Finally, I am most grateful to my parents and family, who during my years of study provided a never ending amount of inspiration, encouragement and support.

REFERENCES

Adam, J. (1990). The geochemistry and experimental petrology of sodic alkaline basalts from Oatlands, Tasmania. *J. Petrology,* **31**, 1201-1223.

Ahrens, L.H. (1964). The significance of the chemical bond for controlling the chemical distribution of the elements. *Phys. Chem. Earth,* **5**, 1-54.

Anderson, J.R. (1975). Zeolite distribution-Naude's Nek. *Terra (Rhodes Univ. Geol. Soc. Journal),* **1**, 26-30.

Arculus, R.J. (1985). Oxidation states of the mantle: past and present. *Annu. Rev. Earth Planet. Sci.*, **13**, 75-95.

Armstrong, R.V., Bristow, J.W. & Cox, K.G. (1984). The Rooi Rand dyke swarm, southern Lebombo. *Geol. Soc. S. Afr., Spec. Publ.*, **13**, 77- 86.

Arth, J.G. (1976). Behaviour of trace elements during magmatic processes - a summary of theoretical models and their applications. *J. Res. U. S. Geol. Surv.*, **4**, 41-47.

Aucamp, A.P.H., Wolmarans, L.G. & Neethling, D.C. (1972). The Urfjell Group, a deformed (?) early Palaeozoic sedimentary sequence, Kirwanryggen, western Dronning Maud Land. *In:* Adie, R.J. (Ed.), *Antarctic geology and geophysics,* Universitetsforlaget, Oslo, 557-561.

Augustithus, A. (1978). *Atlas of the textural patterns of basalts and their genetic significance.* Elsevier, Amsterdam, 323pp.

Bailey, E.B., Clough, C.T., Wright, B.A., Richey, J.E. & Wilson, G.V. (1924). The Tertiary and Post-Tertiary geology of Mull, Loch Aline, and Oban. *Mem. Geol. Surv. Scotland,* 445pp.

Ballhaus, C., Berry, R.F. & Green, D.H. (1990). Oxygen fugacity controls in the Earth's upper mantle. *Nature,* **248**, 437-440.

Barberi, F., Bizouard, H. & Varet, J. (1971). Nature of the clinopyroxene and iron enrichment in alkalic and transitional basaltic magmas. *Contr. Miner. Petrol.*, **33**, 93-107.

Beckinsale, R.D., Pankhurst, R.J., Skelhorn, R.R. & Walse, J.N. (1978). Geochemistry and petrogenesis of the Early Tertiary lava pile of the Isle of Mull, Scotland. *Contr. Mineral. Petrol.*, **66**, 415-427.

Best, M.G. (1982). *Igneous and Metamorphic Petrology.* Freeman and Company, U.S.A., 650pp.

Betton, P.J. (1978). *Geochemistry of Karoo volcanic rocks in Swaziland.* D.Phil. thesis (unpubl.), Univ. Oxford, 287pp.

Bhattacharji, S. (1967). Mechanics of flow differentiation in ultramafic and mafic sills. *J. Geology,* **75**, 101-112.

Birle, J.D., Gibbs, G.V., Moore, P.B. & Smith, J.V. (1968). Crystal structure of natural olivines. *Amer. Mineral.*, **47**, 383-394.

Boles, J.R. & Coombs, D.S. (1977). Zeolite facies alteration of sandstones, South Island syncline, New Zealand. *Amer. J. Sci.*, **277**, 982-1012.

Botha, B.J.V. (1971). Kussinglawa en pypamandels in die Stormberg basalt naby Barkly-Oos. *Tydskr. Natuurw.*, **11**, 68-77.

Botha, B.J.V. & Lindstrom, W. (1976). The stratigraphy of the upper part of the Karoo sequence in the area around Giant's Castle, Natal. Ann. geol. Surv. S. Afr., **11**, 59-66.

Botha, B.J.V. & Theron, J.C. (1967). New evidence for the early commencement of Stormberg volcanism. *Tydskr. Natuurw.*, **7**, 469- 473.

Bowen, M.P. (1984). *The petrogenesis of the volcanic rocks of the Witwatersrand Triad in the Klerksdorp area, Transvaal.* M.Sc (unpubl.), Rhodes Univ., 204pp.

Bowen, N.L. (1928). *The evolution of the igneous rocks.* Princeton Univ. Press, 332pp.

Bowen, T.B. (1984). *The geochemical stratigraphy of the volcanic rocks of the Witwatersrand Triad in the Klerksdorp area, Transvaal.* M.Sc (unpubl.), Rhodes Univ., 223pp.

Bowen, T.B., Marsh, J.S., Bowen, M.P. & Eales, H.V. (1986). Volcanic rocks of the Witwatersrand Triad, South Africa: Description, classification and geochemical stratigraphy. *Precamb. Res.*, **31**, 297-324.

Boyd, F.R. & Gurney, J.J. (1986). Diamonds and the African lithosphere. *Science,* **232**, 472-477.

Bristow, J.W. (1976). *The geology and geochemistry of the southern Lebombo.* M.Sc. thesis (unpubl.), Univ. Natal, 331pp.

Bristow, J.W. (1980). *The geochronology and geochemistry of Karoo volcanics in the Lebombo and adjacent areas.* Ph.D. thesis (unpubl.), Univ. Cape Town, 256pp.

Bristow, J.W. (1984). Picritic rocks of the north Lebombo and south- east Zimbabwe. *Geol. Soc. S. Afr., Spec. Publ,* **13**, 105-124.

Bristow, J.W., Allsopp, H.L., Erlank, A.J., Marsh, J.S. & Armstrong, R.A. (1984). Strontium isotope characterization of Karoo volcanic rocks. *Geol. Soc. S. Afr., Spec. Publ.*, **13**, 295-331.

Bristow, J.W. & Saggerson, E.P. (1983). A general account of Karoo vulcanicity in Southern Africa. *Geol. Rundsch.*, **72**, 1015-1060.

Bristow, J.W., Smith, C.B., Allsopp, H.L. & Skinner, E.M.W. (1987). Exciting signatures from Earth's mantle. *Nuclear Active,* **36**, 21-25.

Brooks, C.K. (1976). The Fe_2O_3/FeO ratio of basalt analyses: An appeal for a standardised procedure. *Bull. Geol. Soc. Denmark,* **25**, 117- 120.

Brown, G.M. & Vincent, E.A. (1963). Pyroxenes from the late stages of fractionation of the Skaergaard intrusion, East Greenland. *J. Petrology,* **4**, 175-197.

Bryan, W.B., Finger, L.W. & Chayes, F. (1968). Estimating proportions in petrographic mixing equations by least-squares approximation. *Science,* **163**, 926-927.

Buddington, A.F. & Lindsley, D.H. (1964). Iron-titanium oxide minerals and synthetic equivalents. *J. Petrology,* **5**, 310-357.

Cameron, M. & Papike, J.J. (1981). Structural and chemical variations in pyroxenes. *Amer. Mineral.*, **66**, 1-50.

Campbell, I.H. & Borley, G.D. (1974). The geochemistry of pyroxenes from the lower layered series of the Jimberlana Intrusion, Western Australia. *Contr. Miner. Petrol.*, **47**, 281-297.

Campbell, I.H. & Nolan, J. (1974). Factors affecting the stability field of Ca-poor pyroxene and the origin of the Ca-poor minimum in Ca-rich pyroxenes from tholeiitic intrusions. *Contr. Miner. Petrol.*, **48**, 205-219.

Carlson, C.W., Langmuir, G.W. & MacDougal, J.D. (1981). Columbia River volcanism: the question of mantle heterogeneity or crustal contamination. *Geochim. Cosmochim. Acta,* **45**, 2483-2499.

Carmichael, I.S.E. (1964). The petrology of Thingmuli, a Tertiary volcano in eastern Iceland. *J. Petrology,* **5**, 435-460.

Carmichael, I.S.E. (1991). The redox states of basic and silicic magmas: a reflection of their source regions. *Contr. Miner. Petrol.*, **106**, 129-141.

Cawthorn, R.G. (1980). High-MgO Karoo tholeiite and the formation of nickel-copper sulphide mineralization in the Insizwa intrusion, Transkei. *S. Afr. J. Sci.*, **76**, 467-470.

Cawthorn, R.G., Maske, S., De Wet, M., Groves, D.I. & Cassidy, K.F. (1988). Contrasting magma types in the Mount Ayliff intrusion (Insizwa Complex), Transkei: Evidence from ilmenite compositions. *Canad. Mineral.*, **26**, 145-160.

Chayes, F. (1966). Alkaline and sub-alkaline basalts. *Amer. J. Sci.*, **264**, 128-145.

Chayes, F. (1990). Partitioning Fe for normative calculations. *Ann. Rept., Dir. Geophy. Inst., Carnegie Inst., Washington,* 1989-1990.

Chen, C.Y., Frey, F.A., Garcia, M.O., Dalrymple, G.B., & Hart, S.R. (1991). The tholeiite to alkalic basalt transition at Haleakala Volcano, Maui, Hawaii. *Contr. Miner. Petrol.*, **106**, 183-200.

Cleverly, R.W. (1977). *The structural and magmatic evolution of the Lebombo monocline, southern Africa, with particular reference to Swaziland.* D. Phil. thesis (unpubl.), Univ. Oxford, 316pp.

Cleverly, R.W. & Bristow, J.W. (1979). Revised volcanic stratigraphy of the Lebombo monocline. *Trans. geol. Soc. S. Afr.*, **82**, 227-230.

Cleverly, R.W. (1979). The volcanic geology of the Lebombo monocline in Swaziland. *Trans. geol. Soc. S. Afr.*, **82**, 343-348.

Collerson, K.D. (1985). Mafic dyke swarms of the East Antartic Shield. *Mafic Dyke Swarms (Abstr.),* Univ. Toronto, 199pp.

Coombs, D.S. (1963). Trends and affinities of basaltic magmas and pyroxenes as illustrated on the diopside-olivine-silica diagram. *Mineral. Soc. Amer.*, **Spec. Pp. 1**, 227-250.

Coombs, D.S. (1971). Present status of the zeolite facies in molecular sieve zeolites. *In: Advances in Chemistry series (Amer. Chem. Soc.),* **101**, 317-327.

Coombs, D.S., Ellis, A.D., Fyfe, W.S. & Taylor, A.M. (1959). The zeolite facies, with comments on the interpretation of hydrothermal syntheses. *Geochim. Cosmochim. Acta,* **17**, 1-52.

Cox, K.G. (1972). The Karroo volcanic cycle. *J. Geol. Soc. London,* **128**, 311-336.

Cox, K.G. (1978). Flood basalts, subduction and the break-up of Gondwanaland. *Nature,* **274**, 47-49.

Cox, K.G. (1980). A model for flood basalt vulcanism. *J. Petrology,* **21**, 629-650.

Cox, K.G. (1983). The Karoo Province of Southern Africa: Origin of trace element enrichment patterns. In C.J. Hawksworth & M.J. Norry, (Eds), *Continental Basalts and Mantle Xenoliths.* Shiva Press, United Kingdom, 139-157.

Cox, K.G. (1988). Numerical modelling of a randomized RTF magma chamber: A comparison with continental flood basalt sequences. *J. Petrology,* **29**, 681-697.

Cox, K.G., Bell, J.D. & Pankhurst, R.J. (1979). *The interpretation of igneous rocks.* Allen & Unwin, London, 450pp.

Cox, K.G. & Bristow, J.W. (1984). The Sabie River Basalt Formation of the Lebombo monocline and south-east Zimbabwe. *Geol. Soc. S. Afr., Spec. Publ.,* **13**, 125-148.

Cox, K.G. & Bell, J.D. (1972). A crystal fractionation model for basaltic rocks of the New Georgia Group, British Solomon Islands. *Contr. Miner. Petrol.,* **37**, 1-13.

Cox, K.G. & Clifford, P. (1982). Correlation coefficient patterns and their interpretation in three basaltic suites. *Contr. Miner. Petrol.,* **79**, 268-278.

Cox, K.G. & Hawkesworth, C.J. (1984). Relative contribution of crust and mantle to flood basalt magmatism, Mahabaleshwar area, Deccan Traps. *Phil. Trans. R. Soc. London,* **A310**, 627-641.

Cox, K.G. & Hawkesworth, C.J. (1987). Geochemical stratigraphy of the Deccan Traps at Mahabaleshwar, Western Ghats, India, with implications for open system magmatic processes. *J. Petrology,* **26**, 355-377.

Cox, K.G. & Hornung, G. (1966). Petrology of the Karoo basalts of Basutoland. *Amer. Mineral.,* **51**, 1414-1432.

Cox, K.G., MacDonald, R. & Hornung, G. (1967). Geochemical and petrographic provinces in the Karoo basalts of southern Africa. *Amer. Mineral.,* **52**, 1451-1474.

Cox, K.G. & Mitchell, C. (1988). Importance of crystal settling in the differentiation of Deccan Trap basaltic magmas. *Nature,* **333**, 447-449.

Davies, G.R. & MacDonald, R. (1987). Crustal influences in the petrogenesis of the Naivasha basalt-comendite complex: combined trace element and Sr-Nd-Pb isotope constraints. *J. Petrology,* **28**, 1009-1031.

Deer, W.A., Howie, R.A. & Zussman, S. (1966). *An introduction to the rock-forming minerals.* Longman, London-528pp.

DeLong, S.E. & Hoffman, M.A. (1975). Alkali/silica distinction between Hawaiian tholeiites and alkali basalts. *Geol. Soc. Amer. Bull.,* **86**, 1101-1108.

De Paolo, D.J. (1981). Trace element and isotopic effects of combined wallrock assimilation and fractional crystallization. *Earth Planet. Sci. Lett.,* **53**, 189-202.

Devey, C.W. & Cox, K.G. (1987). Relationships between crustal contamination and crystallization in continental flood basalt magmas, with special reference to the Deccan Traps of the Western Ghats, India. *Earth Planet. Sci. Lett.,* **84**, 59-68.

De Wit, M.J. & Bristow, J.W. (1985). Correlation and comparison of the upper Palaeozoic - Mesozoic geology of central and northern Gondwanaland with specific reference to the terminal rifting and drifting stages of the supercontinent relative to back-arc phenomena. *Gondwanaland Symp. Abstr.,* Ohio State Univ., U.S.A.

Drake, M.J. & Weill, D.F. (1975). Partition of Sr, Ba, Ca, Y, Eu^{2+}, Eu^{3+}, and other REE between plagioclase feldspar and magmatic liquid: an experimental study. *Geochim. Cosmochim. Acta,* **39**, 689-712.

Duke, J.M. (1976). Distribution of the period four transition elements among olivine, calcic clinopyroxene and mafic silicate liquid: Experimental results. *J. Petrology,* **17**, 499-521.

Duncan, A.R. (1987). The Karoo Igneous Province-A problem area for inferring tectonic setting from basalt geochemistry. In: S.D. Weaver & R.W. Johnson, (Eds.), Tectonic controls on magma chemistry. *J. Volcanol. Geotherm. Res.,* **32**, 13-34.

Duncan, A.R. & Erlank, A.J. (1979). Regional geochemistry of the Karoo volcanics. *18th Earth Science Congress. Geol. Soc. S. Afr. (Extd. Abstr.),* 128-131.

Duncan, A.R., Erlank, A.J. & Betton, P.J. (1984a). Appendix 1: Analytical techniques and database descriptions. *Geol. Soc. S. Afr., Spec. Publ.,* **13**, 389-395.

Duncan, A.R., Erlank, A.J. & Marsh, J.S. (1984b). Regional geochemistry of the Karoo Igneous Province. *Geol. Soc. S. Afr., Spec. Publ.,* **13**, 355-388.

Duncan, A.R., Marsh, J.S., Erlank, A.J. & Milner, S.C. (1990). Geochemistry and petrogenesis of basaltic rocks of the Etendeka Formation, northwestern Namibia. *23rd Earth Science Congress. Geol. Soc. S. Afr.,(Extd. Abstr.),* 139-142.

Duncan, R.A. & Green, D.H. (1987). The genesis of refractory melts in the formation of oceanic crust. *Contr. Miner. Petrol.,* **96**, 326-342.

Du Toit, A.L. (1904). Geological survey of the divisions of Aliwal North, Herschel, Barkly east and part of Wodehouse. *9th Ann. Rept. Geol. Commission, Colony of Cape of Good Hope,* 69-110.

Du Toit, A.L. (1907). Pipe amygdaloids. *Geol. Mag.,* **4**, 4-17.

Du Toit, A.L. (1911). Geological survey of parts of the Stormbergen. *16th Ann. Rept. Geol. Commission, Colony of Cape of Good Hope,* 113-136.

Du Toit, A.L. (1954). *The geology of South Africa (3rd Edn.).* Oliver & Boyd, Edinburgh, 611pp.

Eales, H.V. (1980). Contrasted trace element variations in two Karoo cumulus complexes. *Chem. Geol.,* **29**, 39-48.

Eales, H.V. & Booth, P.W.K. (1974). The Birds River Gabbro Complex, Dordrecht district. *Trans. geol. Soc. S. Afr.,* **77**, 1-15.

Eales, H.V. & Marsh, J.S. (1979). High-Mg tholeiitic rocks and their significance in the Karroo Central Province. *S. Afr. J. Sci.,* **75**, 400-404.

Eales, H.V. & Marsh, J.S. (1984). Al/Cr ratios of coexisting pyroxenes and spinelloids in the same ultramafic rocks. *Chem. Geol.,* **38**, 57-74.

Eales, H.V., Marsh, J.S. & Cox, K.G. (1984). The Karoo Igneous Province: an introduction. *Geol. Soc. S. Afr., Spec. Publ.,* **13**, 1-26.

Eales, H.V., Reynolds, I.M. & Gouws, D.A. (1980). The spinel group minerals of the central Karoo tholeiitic province. *Trans. geol. Soc. S. Afr.,* **83**, 243-252.

Eales, H.V. & Robey, J.v.A. (1976). Differentiation of tholeiitic Karoo magma at Birds River. *Contr. Miner. Petrol.,* **56**, 101- 117.

Elliot, D.H. (1975). Tectonics of Antarctica: A review. *Amer. J. Sci.,* **275a**, 45-106.

Elliot, D.H. & Watts, D.R. (1974). The nature and origin of volcaniclastic material in some Karroo and Beacon rocks. *Trans. geol. Soc. S. Afr.,* **77**, 109-111.

Eriksson, P.G. (1979). Mesozoic sheetflow and playa sediments of the Clarens Formation in the Kamberg area of the Natal Drakensberg. *Trans. geol. Soc. S. Afr.,* **82**, 257-258.

Erlank, A.J.(Ed.) (1984). *Petrogenesis of the volcanic rocks of the Karoo Igneous Province, Geol. Soc. S. Afr., Spec. Publ.* 13, 395pp.

Erlank, A.J., Allsop, H.L., Duncan, A.R. & Bristow, J.W. (1980). Mantle heterogeneity beneath southern Africa: evidence from the volcanic record. *Phil. Trans. Roy. Soc. London,* **A297**, 295-307.

Erlank, A.J., Hawkesworth, C.J. & Menzies, M.A. (1982). Chemical and isotopic characterization of upper mantle metasomatism in peridotite nodules from the Bultfontein kimberlite. *Terra Cognita,* **2**, 261-263.

Erlank, A .J., Marsh, J.S., Duncan, A.R., Miller, R.McG., Hawkesworth, C.J., Betton, P.J. & Rex, D.C. (1984). Geochemistry and petrogenesis of the Etendeka rocks from SWA/Namibia. *Geol. Soc. S. Afr., Spec. Publ.,* **13**, 195-245.

Erlank, A.J. & Rickard, R.S. (1977). Potassic richterite bearing peridotites from kimberlite and the evidence they provide for upper mantle metasomatism. *Second Int. Kimberlite Conf., (Extnd. Abstr.),* New Mexico.

Erlank, A.J., Waters, F.G., Hawkesworth, C.J., Haggerty, S.E., Allsop, H.L., Rickard, R.S. & Menzies, M.A. (1987). Evidence for mantle metasomatism in peridotite nodules from the Kimberley pipes, South Africa. *In:* Hawkesworth, C.J. and Menzies, M.A. (Eds.), *Mantle Metasomatism.* Academic Press, 472pp.

Erlank, A.J., Le Roex, A.P., Harris, C., McLachlan, C. & Miller, R. McG. (1990a). Geochemistry of basalt samples from the Kudu boreholes, offshore Namibia. *23rd Earth Science Congress. Geol. Soc. S. Afr., (Abstr.),* 153-157.

Erlank, A.J., Duncan, A.R., Sweeney, R.J., Milner, S.C., Marsh, J.S., Hawksworth, C.J., Rogers, N.W. & Miller, R.M. (1989). Is there a laterally extensive geochemical boundary in the Mesozoic basalts of southern Gondawanaland? *28th International Geological Congress, Washington D.C. (Abstr.),* 1, 458-459.

Erlank, A.J., Duncan, A.R., Marsh, J.S., Sweeney, R.J., Milner, S.C., Hawksworth, C.J., McG. Miller, R. & Rogers, N.W. (1990b). Distribution of Mesozoic Karoo basalts from southern Africa. *23rd Earth Science Congress. Geol. Soc. S. Afr. (Abstr.),* 754-757.

Ernst, W.G. (1976). *Petrologic phase equilibria.* San Francisco, W.H. Freeman and Company, 327pp.

Faure, G., Bowman, J.R., & Elliot, D.H. (1979). The initial $^{87}Sr/^{86}Sr$ ratios of the Kirwan volcanics of Dronning Maud Land: comparison with the Kirkpatrick basalts, Transantarctic mountains. *Chem. Geol.*, **26**, 77-90.

Fitch, F.J. & Miller, J.A. (1971). Potassium-argon radioages of Karoo volcanic rocks from Lesotho. *Bull. Volcanol.*, **35**, 64-84.

Fitch, F.J. & Miller, J.A. (1984). Dating Karoo igneous rocks by the conventional K-Ar and $^{40}Ar/^{39}Ar$ age spectrum methods. *Geol. Soc. S. Afr., Spec. Publ.*, **13**, 247-266.

Fodor, R.V. (1971). Fe content in pyroxenes from a calc-alkalic volcanic suite, New Mexico, U.S.A. *Earth Planet. Sci. Lett.*, **11**, 383-390.

Froidevaux, C. & Nataf, H.C. (1981). Continental drift: What driving mechanism? *Geol. Rundsch.*, **70**, 166-176.

Fuller, A.O. (1970). The occurrence of laumontite in strata of the Karoo System, South Africa. *Second Gondwana Symposium, Proc. & Pap.*, 455-456.

Furnes, H., Vad, E., Austrheim, H., Mitchell, J.G. & Garmann, L.B. (1987). Geochemistry of basalt lavas from Vestfjella and adjacent areas, Dronning Maud Land, Antarctica. *Lithos,* **20**, 337-356.

Gast, P.W. (1960). Limitations on the composition of the upper mantle. *J. Geophys. Res.*, **65**, 1287-1296.

Gast, P.W. (1968). Trace element fractionation and the origin of tholeiitic and alkaline magma types. *Geochim. Cosmochim. Acta,* **32**, 1057-1086.

Gevers, T.W. (1928). The volcanic vents of the western Stormberg. *Trans. geol. Soc. S. Afr.*, **31**, 43-62.

Gibb, F.G.F. (1973). The zoned pyroxenes of the Shiant Isles sill, Scotland. *J. Petrology,* **14**, 203-230.

Gibson, I.L., Kinsman, D.J.J., & Walker, G.P.L. (1966). Geology of the Faskrudsfjordur area, eastern Iceland. *Visindafelag Isl. Greinar,* **2**, 1-52.

Greenland, L.P. (1970). An equation for trace element distribution during magmatic crystallization. *Amer. Mineral.*, **55**, 455-465.

Groenewald, P.B., Grantham, G.H., & Watkeys, M.K. (1991). Geological evidence for a Proterozoic to Mesozoic link between southeastern Africa and Dronning Maud Land, Antarctica. *J. Geol. Soc. London.*, **148,** 1115-1123.

Grover, J.E. & Lindsley, D.H. (1972). Ca-Mg-Fe pyroxenes: subsolidus phase relations in iron-rich portions of the pyroxene quadrilateral. *Geol. Soc. Amer., Abstr. Programs,* **4**, 521-522.

Gurney, J.J. & Harte, B. (1980). Chemical variations in upper mantle nodules from southern African kimberlites. *Phil. Trans. R. Soc. London,* **A297**, 273-293.

Haggerty, S.E. (1976). Oxidation of opaque mineral oxides in basalts, Hg1-Hg98. *In:* Rumble, D. (Ed.),. *Reviews in mineralogy, Vol. 3: Oxide minerals.* Mineral. Soc. Amer.

Haggerty, S.E., Smyth, J.R., Erlank, A.J., Rickard, R.S. & Danchin, R.V. (1983). Lindsleyite (BA) and mathiasite (K): two new chrome titanates in the crichtonite series from the upper mantle. *Amer. Mineral.*, **68**, 494-505.

Hall, A. (1987). *Igneous Petrology.* John Wiley & Sons, U.S.A. 573pp.

Harris, C., Marsh, J.S., Erlank, A.J., & Duncan, A.R. (1986). Geology of the Jurassic basalts of the Kirwanveggen, Antarctica, and their significance for Gondwana volcanism. *21st Earth Science Congress. Geol. Soc. S. Afr., (Extd. Abstr.),* 731-734.

Harris, C., Erlank, A.J., Duncan, A.R. & Marsh, J.S. (1988). The geochemistry of the Kirwan and other Jurassic basalts of Dronning Maud Land and their petrogenetic significance for Gondwana reconstruction. *Proc. 5th Antarctic Earth Sci. Conf., Cambridge.*

Harris, C., Marsh, J.S., Duncan, A.R., Erlank, A.J. (1990). The petrogenesis of the Kirwan Basalts of Dronning Maud Land, Antarctica. *J. Petrology,* **31**, 341-369.

Hart, S.R., Gunn, B.M. & Watkins, N.D. (1971). Intralava variation of alkali elements in Icelandic basalts. *Amer. J. Sci.*, **270**, 315- 318.

Hart, S.R. & Davies, K.E. (1978). Nickel partitioning between olivine and silicate melt. *Earth Planet. Sci. Lett.*, **40**, 203-219.

Hatch, F.H., Wells, A.K. & Wells, M.K. (1981). *Petrology of the Igneous Rocks.* Billing and Sons Ltd., London 551pp.

Haughton, S.H. (1969). *Geological history of southern Africa.* Geol. Soc. S. Afr., 535pp.

Hawkesworth, C.J., Erlank, A.J., Marsh, J.S., Menzies, M.A. & van Calsteren, P. (1983). Evolution of the continental lithosphere: evidence from volcanics and xenoliths in southern Africa. *In:* C.J. Hawkesworth and M.J. Norry, (Eds.), *Continental Basalts and Mantle Xenoliths.* Shiva Press, United Kingdom, 111-138.

Hawkesworth, C.J., Marsh, J.S., Duncan, A.R., Erlank, A.J. & Norry, M.J. (1984). The role of the Karoo volcanic rocks: evidence from combined Nd- and Sr-isotope studies. *Geol. Soc. S. Afr., Spec. Publ.,* **13**, 341-354.

Hawkesworth, C.J. & Menzies, M. (Eds.) (1987). *Mantle metasomatism.* Academic Press, 472pp.

Hawkesworth, C.J. & Norry, M.J. (Eds.) (1983). *Continental basalts and mantle xenoliths.* Shiva Press, United Kingdom, 272pp.

Hensen, B.J. (1973). Pyroxenes and garnets as geothermometers and barometers. *Carnegie Inst. Washington, Ybk.,* **72**, 527-534.

Hergt, J.M., Peate, D.W., & Hawkesworth, C.J. (1991). The petrogenesis of Mesozoic Gondwana low-Ti flood basalts. *Earth Planet. Sci. Lett.*, **105**, 134-148.

Hess, H.H. & Poldervaart, A. (Eds.) (1967). *Basalts*: **Vol. 1**. Interscience, New York 482pp.

Hofmann, A.W. & Hart, S.R. (1978). An assessment of local and regional isotopic equilibrium in the mantle. *Earth Planet. Sci. Lett.*, **38**, 44-62.

Hooper, P.R. (1988). Crystal fractionation and recharge (RFC) in the American Bar flows of the Imnaha Basalt, Columbia River Basalt Group. *J. Petrology,* **29**, 1097-1118.

Hughes, C.J. (1979). Standardized procedure for presenting corrected Fe_2O_3/FeO ratios in analyses of finegrained mafic rocks. *Neues Jahrb. Mineral. Monatsh,* **12**, 570-572.

Hughes, C.J. & Hussey, E.M. (1976). M and Mg values in igneous rocks: proposed usage and a comment on currently employed Fe_2O_3 corrections. *Geochim. Cosmochim. Acta,* **40**, 485-486.

Humphris, S.E. & Thompson, G. (1978). Hydrothermal alteration of oceanic basalts by seawater. *Geochim. Cosmochim. Acta*, **42**, 107-125.

Huppert, H.E. & Sparks, R.S.J. (1985). Cooling and contamination of mafic and ultramafic magmas during ascent through continental crust. *Earth Planet. Sci. Lett.*, **74**, 371-386.

Hutchinson, C.S. (1974). *Laboratory handbook of petrographic techniques.* Wiley Interscience, New York.

Irvine, T.N. & Baragar, W.R.A. (1971). A guide to the chemical classification of the common volcanic rocks. *Canad. J. Earth Sci.*, **8**, 523-548.

Irving, A.J. (1978). A review of experimental studies of crystal/liquid trace element partitioning. *Geochim. Cosmochim. Acta,* **42**, 743-770.

Ivanov, I.P. & Gurevich, L.P. (1975). Experimental study of T-X_{CO2} boundaries of metamorphic zeolite facies. *Contr. Miner. Petrol.*, **53**, 55-60.

Jamieson, B.G. & Clark, D.B. (1970). Potassium and associated elements in tholeiitic basalts. *J. Petrology,* **11**, 183-204.

JCPDS (1983). *Mineral Powder Diffraction File; Group Data Book. JCPDS.* International Centre for Diffraction Data. Swartmore, U.S.A.

JCPDS (1986a). *Mineral Powder Diffraction File; Search Manual. JCPDS.* International Centre for Diffraction Data. Swartmore, U.S.A.

JCPDS (1986b). *Mineral Powder Diffraction File; Data Book. JCPDS.* International Centre for Diffraction Data. Swartmore, U.S.A.

Johnson, M.R. (1991). Sandstone petrography, provenance and plate tectonic setting in Gondwana context of the southeastern Cape-Karoo Basin. *S. Afr. J. Geol.*, **94**, 137-154.

Jones, M.Q.W. (1990). Heat anomaly in the northern Lesotho: Implications for the nature of the southern boundary of the Kaapvaal Craton. *Geocongr. '90 (Extd. Abstr.), Geol. Soc. S. Afr.*, Univ. Cape Town, Cape Town.

Juckes, L.M. (1972). The geology of northeastern Heimefrontfjella, Dronning Maud Land. *Bull. Br. Antarct. Surv. Sci. Rep.*, **65**, 45pp

Kennedy, W.Q. (1933). Trends of differentiation in basaltic magmas. *Amer. J. Sci.*, **25**, 239-256.

Kenyon, A.K. (1976). *Reaction phenomena between Karoo dolerite and Cave Sandstone xenoliths in the Bird's River Complex.* MSc thesis (unpubl.), Rhodes Univ., Grahamstown 166pp.

Kouchi, A., Tsuchiyama, A. & Sunagawa, I. (1986). Effects of stirring on crystallization kinetics of basalt: texture and element partitioning. *Contr. Miner. Petrol.*, **93**, 429-438.

Krishnamurthy, P. & Cox, K.G. (1977). Picrite basalts and related lavas from the Deccan Traps of western India. *Contr. Miner. Petrol.*, **62**, 53-75.

Kristmannsdottir, H. (1978). Alteration of basaltic rocks by hydrothermal activity at 100-300°C. *Proc. 6th Int. Clay Conf.* Elsevier, Amsterdam, 359-367.

Kristmannsdottir, H. (1982). Alteration in the IRDP drill hole compared with other drill holes in Iceland. *J. Geophys. Res.*, **87**, 6525-6531.

Kristmannsdottir, H. & Tomasson, J. (1978). Zeolite zones in geothermal areas in Iceland. *In:* Sand, L.B. & Mumpton, F.A. (Eds.), *Natural zeolites, occurrences, properties, uses.* Pergamon, New York, 277-284.

Kuno, H. (1960). High-alumina basalt. *J. Petrology,* **1**, 121-145.

Lagache, M. (1984). The exchange equilibrium distribution of alkali and alkaline elements between feldspars and hydrothermal solutions. *In:* Brown, W.L., (Ed.), *Feldspars and feldspathoids.* D. Reidel, Dordrecht, 247-279.

Langmuir, C.H., Bender, J.F., Bence, A.E. & Hanson, G.N. (1977). Petrogenesis of basalt from the FAMOUS area: Mid-Atlantic ridge. *Earth Planet. Sci. Lett.*, **36**, 133-145.

Leeman, W.P. & Lindstrom, D.J. (1978). Partitioning of Ni^{2+} between basaltic and synthetic melts and olivine: an experimental study. *Geochim. Cosmochim. Acta,* **42**, 801-816.

Le Maitre, R.W. (1976). The chemical variability of some common igneous rocks. *J. Petrology,* **17**, 589-637.

Le Roex, A.P. (1985). Geochemistry, mineralogy and magmatic evolution of the basaltic and trachytic lavas from Gough Island, South Atlantic. *J. Petrology,* **26**, 149-186.

Le Roex, A.P., Dick, H.J.B., Erlank, A.J., Reid, A.M., Frey, F.A. & Hart, S.R. (1983). Geochemistry, mineralogy and petrogenesis of lavas erupted along the southwest Indian ridge between the Bouvet triple junction and 11 degrees east. *J. Petrology,* **24**, 267-318.

Le Roex, A.P., Erlank, A.J. & Needham, H.D. (1981). Geochemical and mineralogical evidence for the occurrence of at least three distinct magma types in the FAMOUS area. *Contr. Miner. Petrol.*, **77**, 24-37.

Le Roex, A.P. & Reid, D.L. (1978). Geochemistry of Karoo dolerite sills in the Calvinia district, western Cape Province, South Africa. *Contr. Miner. Petrol.*, **66**, 351-360.

Lightfoot, P.C. & Naldrett, A.J. (1989). Assimilation and crystallization in basic magma chambers: Trace-element and Nd-isotope variations in Kerns sill, Nipissing Diabase province, Ontario. *Can. Jour. Earth Sci.*, **26**, 737-754.

Lightfoot, P.C., Sutcliffe, H. & Doherty, W. (1991). Crustal contamination identified in Keweenawan Osler Group tholeiites, Ontario: a trace element persperctive. *J. Geol.*, **99**, 739-760.

Liou, J.G. (1971). Stabilities of laumontite, wairakite, lawsonite and related minerals in the system CaO-$Al_2O_3SiO_2$-SiO_2-H_2O. *J. Petrology,* **12**, 379-411.

Lock, B.E. & Johnson, M.R. (1974). A crystal tuff from the Ecca Group near Lake Mentz, eastern Cape Province. *Trans. geol. Soc. S. Afr.*, **77**, 373-374.

Lock, B.E., Paverd, A.L. & Broderick, T.J. (1974). Stratigraphy of the Karroo volcanic rocks of the Barkly East district. *Trans. geol. Soc. S. Afr.*, **77**, 117-129.

Lock, B.E. & Wilson, J.D. (1975). Discussion of "The nature and origin of volcaniclastic material in some Karroo and Beacon rocks" by Elliot, D.H., and Watts, D.R. *Trans. geol. Soc. S. Afr.*, **78**, 170-171.

Lofgren, G.E. (1983). Effect of heterogeneous nucleation on basaltic textures: A dynamic crystallization study. *J. Petrology,* **24**, 229- 255.

Lombaard, B.V. (1952). Karoo dolerites and lavas. *Trans. geol. Soc. S. Afr.*, **55**, 175-198.

Long, P.E. & Davidson, N.J. (1981). Lithology of the Grande Ronde basalt with emphasis on the Umtanum and McCoy Canyon flows. *In:* Myers, C.W. & Price, S.M. (Eds.), *Subsurface geology of the Cold Creek syncline, Rockwell Hanford.* Richland, Washington 240pp.

Long, P.E. & Wood, B.J. (1986). Structures, textures, and cooling histories of Columbia River basalt flows. *Geol. Soc. Amer. Bull.*, **97**, 1144-1155.

Loomis, T.P. (1982). Numerical simulation of crystallization of plagioclase in complex melts: the origin of major and oscillatory zoning in plagioclase. *Contr. Miner. Petrol.*, **81**, 219-229.

MacDonald, G.A. (1967). Forms and structures of extrusive basalt rocks. *In:* Hess, H.H. & Poldervaart, A. (Eds)., *The Poldervaart Treatise on rocks of basaltic composition,* **vol. 1,** 1-61, New York, Interscience.

MacDonald, G.A. (1968). Composition and origin of Hawaiian lavas. *Geol. Soc. Amer., Mem.,* **116,** 477-522.

MacDonald, G.A. (1972). *Volcanoes.* Prentice Hall Inc., Eaglewood Cliffs, New Jersey, 510pp.

MacDonald, G.A. & Katsura, T. (1964). Chemical composition of Hawaiian lavas. *J. Petrology,* **5,** 82-133.

MacDonald, R., Crossley, R. & Waterhouse, K.S. (1983). Karroo basalts of southern Malawi and their petrological significance. *Mineral. Mag.,* **47,** 281-291.

Mantovani, M.S.M., Marques, L.S., De Sousa, M.A., Civetta, L., Atalla, L. & Innocenti, F. (1985). Trace element and strontium isotope constraints on the origin and evolution of Parana continental flood basalts of Santa Catarina State (southern Brazil). *J. Petrology,* **26,** 187-209.

Marsh, J.S. (1987). Basalt geochemistry and tectonic discrimination within continental flood basalt provinces. In: S.D. Weaver & R.W. Johnson (Eds.), Tectonic Controls on magma chemistry. *J. Volcanol. Geotherm. Res.,* **32,** 35-49.

Marsh, J.S. (1989). Geochemical constraints on coupled assimilation and fractional crystallization involving upper crustal compositions and continental tholeiitic magma. *Earth. Planet. Sci. Lett.,* **92,** 70-80.

Marsh, J.S. (1991). REE fractionation and Ce anomalies in weathered Karoo dolerite. *Chem. Geol.,* **90,** 189-194.

Marsh, J.S., Sweeney, R.J. & Armstrong, R.A. (1992). New Pb, Sr and Nd isotope data from the Karoo Province. *24th Earth Science Congress. Geol. Soc. S. Afr. (Abstr.),* 262-264.

Marsh, J.S. & Eales, H.V. (1984). The chemistry and petrogenesis of igneous rocks of the Karoo central area, southern Africa. *Geol. Soc. S. Afr., Spec. Publ.,* **13,** 27-67.

Martin, A.K., & Hartnady, C.J. (1986). Plate tectonic development of the south west Indian Ocean: a revised reconstruction of east Antarctica and Africa. *J. Geophys. Res. B,* **91,** 4767-4786.

Martini, J.E.J. (1974). On the presence of ash beds and volcanic fragments in the greywackes of the Karroo System in the southern Cape Province. *Trans. geol. Soc. S. Afr.,* **77,** 113-116.

Maske, S. (1966). The petrography of the Ingeli mountain range. *Ann. Univ. Stellenbosch,* **A41,** 1-109.

Mason, B. & Moore, C.B. (1982). *Principles of Geochemistry.* (4th Ed.). John Wiley & Sons, U.S.A., 344pp.

Mathez, E.A. (1984). Influence of degassing on oxidation states of basaltic magmas. *Nature,* **310,** 371-375.

Mathias, M., Siebert, J.C. & Ringwood, P.C. (1970). Some aspects of the mineralogy and petrology of ultramafic xenoliths in kimberlite. *Contr. Miner. Petrol.,* **26,** 75-123.

McCarthy, M.J. (1970). An occurrence of pillow lava in a basal flow of the Drakensberg volcanic stage, Ndedema valley, Natal. *IUGS, 2nd Gondwana Symposium, S. Afr., 1970, Proc. & Pap.,* 433-439.

McDougall, I. & Lovering, J.P. (1963). Fractionation of chromium, nickel, cobalt and copper in a differentiated dolerite-granophyre sequence at Red Hill, Tasmania. *Geol. Soc. Australia Jour.,* **10,** 325-338.

McLachlan, J.R. & Jonker, J.P. (1990). Tuff beds in the northwestern part of the Karoo Basin. *S. Afr. J. Geol.,* **93,** 329-338.

Mehegen, J.M., Robinson, P. & Delaney, J.R. (1982). Secondary mineralization and hydrothermal alteration in the Reydarfjordur drill core, Eastern Iceland. *J. Geophys. Res.,* **87,** 6511-6524.

Middlemost, E.A.K. (1989). Iron oxidation ratios, norms and the classification of volcanic rocks. *Chem. Geol.,* **77,** 19-26.

Mitchell, A.A. (1980). *The extrusive and intrusive basaltic rocks of the Molteno-Jamestown area.* M.Sc. thesis (unpubl.), Rhodes Univ., Grahamstown, 195pp.

Moorbath, S. & Thompson, R.N. (1980). Strontium isotope geochemistry and petrogenesis of the early Tertiary lava pile of the Isle of Skye, Scotland, and other basic rocks of the British Tertiary Province: an example of magma-crust interaction. *J. Petrology,* **21,** 295-321.

Mori, T. (1978). Experimental study of pyroxene equilibria in the system of CaO-MgO-FeO-SiO_2. *J. Petrology,* **19,** 45-65.

Mountain, E.D. (1958). Acidification of dolerite at Coedmore Quarries, Durban. *Trans. geol. Soc. S. Afr.*, **61**, 209-224.

Mountain, E.D. (1960). Felsic matereial in Karroo dolerite. *Trans. geol. Soc. S. Afr.*, **63**, 137-151.

Murata, K.J., Formoso, M.L.L. & Roisenberg, A. (1987). Distribution of zeolites in lavas of southeastern Parana Basin, State of Rio Grande do Sul, Brazil. *J. Geol.*, **95**, 455-467.

Mysen, B.O. & Kushiro, I. (1979). Pressure dependence of nickel partitioning between forsterite and aluminous silicate melts. *Earth Planet. Sci. Lett.*, **42**, 383-388.

Nag, S.K. & Mallik, S.B. (1983). Temperature and oxygen fugacity of a lava flow from Rajmahal volcanics, Bihar. *Indian J. Earth Sci.*, **10**, 30-38.

Naldrett, A.J. & Barnes, S.J. (1986). The behavior of platinum group elements during fractional crystallization and partial melting with special reference to the composition of magmatic sulphide ores. *Fortschr. Miner.*, **64**, 113-133.

Nesbitt, H.W. & Young, G.M. (1982). Early Proterozoic climates and plate motions inferred from major element chemistry of lutites. *Nature*, **299**, 715-718.

Nienaber, C.J. (1975). *Stormberg lavas in the Cathedral Peak area, Natal Drakensberg.* Unpubl. BSc project, Univ. Natal, Pietermaritzburg.

Noack, Y., Mathieu, D., Claparols, C., Loubet, M., Bernat, M., & Goncalves, N. (1990). Weathering of basalts in north Parana basin (Brazil) chemical aspects. 2nd Int. Symp.: *Geochemistry of the Earth's surface and of mineral formation.* Aix en Provence, France, 111-113.

Nockolds, S.R. & Allen, R. (1953). The geochemistry of some igneous rock series, Part 1. *Geochim. Cosmochim. Acta*, **4**, 105-142.

Nockolds, S.R. & Allen, R. (1954). Chemical composition of some igneous rocks. *Geol. Soc. Amer. Bull.*, **65**, 119-157.

Nockolds, S.R. & Allen, R. (1956). The geochemistry of some igneous rock series, Part III. *Geochim. Cosmochim. Acta*, **9**, 34-77.

Nockolds, S.R. & Le Bas, M.J. (1977). Average calc-alkali basalt. *Geol. Mag.*, **114**, 311-312.

Norrish, K. & Hutton J.T. (1969). An accurate x-ray spectrographic method for the analysis of a wide range geolical samples. *Geochim. Cosmochim. Acta*, **33**, 431-453.

Norry, M.J. & Fitton, J.G. (1983). Compositional differences between oceanic and continental basic lavas and their significance. *In:* Hawkesworth, C. J. & Norry, M. J., (eds.), *Continental basalts and mantle xenoliths.* Shiva Press, United Kingdom, 5-19.

O'Hara, M.J. (1965). Primary magmas and the origin of basalts. *Scott. J. Geol.*, **1**, 19-40.

O'Hara, M.J. (1968). The bearing of phase equilibria studies on the origin and evolution of basic and ultrabasic rocks. *Earth Sci. Rev.*, **4**, 69-133.

O'Hara, M.J. (1977). Geochemical evolution during fractional crystallization of a periodically refilled magma chamber. *Nature*, **266**, 503-507.

O'Hara, M.J. & Mathews, R.E. (1981). Geochemical evolution in an advancing periodically replenished, periodically tapped, continously fractionated magma chamber. *J. Geol. Soc. London*, **138**, 237-277.

O'Hara, M.J. & Yoder, Jr., H.J. (1967). Formation and fractionation of basic magmas at high pressures. *Scott. J. Geol.*, **3**, 67-117.

O'Nions, R.K. (1984). Isotopic abundances relevant to the identification of magma sources. *Phil. Trans. Roy. Soc. London*, **A310**, 591-603.

Palmasson, G., Arnosson, S., Fridleifsson, B.., Kristmannsdottir, H., Saemundsson, K., Stefansson, V., Steingrimsson, B., Tomasson, J. & Kristjansson, L. (1979). The Iceland crust: Evidence from drillhole data on structure and processes. *In:* Talwani, M., Harrison, C.G. & Hayes, D.E. (Eds.), *Deep drilling results in the Atlantic Ocean: Ocean crust, A.G.U.*, Washington D.C., 43-65.

Papike, J.J., Hodges, F.N., Bence, A.E., Cameron, M. & Rhodes, J.M. (1976). Mare basalts: crystal chemistry, mineralogy and petrology. *Geophys. Space Phys. Rev.*, **14**, 475-540.

Pearce, J.A. (1982). Trace element characteristics of lavas from destructive plate boundaries. *In:* Thorpe, R.S. (Ed), *Andesites.* John Wiley and Sons, New York, 525-548p.

Pearce, J.A. & Cann, J.R. (1973). Tectonic setting of basic volcanic rocks determined using trace element analyses. *Earth Planet. Sci. Lett.*, **19**, 290-300.

Pearce, J.A. & Norry, M.J. (1979). Petrogenetic implications of Ti, Zr, Y and Nb variations in volcanic rocks. *Contr. Miner. Petrol.*, **69**, 33-47.

Pedersen, A.K. (1975). New investigations of the native iron bearing volcanic rocks of Disko. *Rapp. Gronl. Geol. Unders.*, **75**, 48-51.

Pemberton, J. (1978). *The geochemistry and petrology of Karoo basalts of the Barkly East area, north-eastern Cape.* M.Sc. thesis (unpubl.), Rhodes Univ., Grahamstown 139pp.

Petrini, R., Civetta, L., Piccirillo, E.M., Bellieni, G., Comin- Chiaramonti, P., Marques, L.S. & Melfi, A.J. (1987). Mantle heterogeneity and crustal contamination in the genesis of low-Ti continental flood basalts from the Parana Plateau (Brazil): Sr-Nd isotope and geochemical. *J. Petrology,* **28**, 701-726.

Philpotts, A.R. & Reichenbach, I. (1985). Differentiation of Mesozoic basalts of the Hartford basin, Connecticut. *Geol. Soc. Amer. Bull.*, **96**, 1131-1139.

Piccirillo, E.M., Melfi, A.J., Comin-Chiaramonti, P., Bellieni, G., Ernesto, M., Marques, L.S., Nardes, A.J.R., Pacca, I.G., Roisenberg, A. & Stolfa, D. (1986). Continental flood volcanism from the Parana basin (Brazil). *In:* MacDougall, J.D. (Ed.), *Flood basalts.* Reidel, Dordrecht.

Potgieter, C.D., Snyman, C.P. & Fortsch, E.B. (1982). Epigenetic laumontite in the Jurassic Clarens and Drakensberg Formations of the Karoo Sequence. *Trans. geol. Soc. S. Afr.*, **85**, 203-210.

Presnall, D.C., Dixon, J.R., O'Donnell, T.H. & Dixon, S.A. (1979). Generation of mid-ocean ridge tholeiites. *J. Petrology,* **20**, 3-35.

Prudencio, M.I., Sequeira Brogu, M.A., and Cabral, J.M.P. (1990). Basalts weathering in the Lisbon volcanic complex (Portugal). 2nd Int. Sym.: *Geochemistry of the Earth's surface and of mineral formation.* Aix en Provence, France, 119-121.

Ramdohr, P. (1980). *The ore minerals and their intergrowths (2nd Ed.).* Pergamon, New York, 1207pp.

Ray, G.L., Shimizu, N. & Hart, S.R. (1983). An ion microprobe study of the partitioning of trace elements between clinopyroxene and liquid in the system diopside-albite-anorthite. *Geochim. Cosmochim. Acta,* **47**, 2131-2140.

Reynolds, I.M. (1983). The iron-titanium oxide mineralogy of Karoo dolerite in the eastern Cape and southern Orange Free State. *Trans. geol. Soc. S. Afr.*, **86**, 211-220.

Rhodes, J.M., Dungan, M.A., Blanchard, D.P. & Long, P.E. (1979). Magma mixing at mid-ocean ridges: Evidence from basalts drilled near 22°N on the mid-Atlantic ridge. *Tectonophysics,* **55**, 35-61.

Rhodes, R.C. & Krohn, D.H. (1972). Tectonic control over regional geochemical variation in the Karoo basaltic province of southern Africa. *Trans. geol. Soc. S. Afr.*, **75**, 11-21.

Richardson, S.H., Gurney, J.J., Erlank, A.J., & Harris, J.W. (1984). Origin of diamonds in old enriched mantle. *Nature,* **310**, 198-202.

Ringwood, A.E. (1982). Phase transformations and differentiation in subducted lithosphere: implications for mantle dynamics, basalt petrogenesis and crustal evolution. *J. Geol.*, **90**, 611-643.

Robey, J.v.A. (1976). *Aspects of the geochemistry of the dolerites and basalts of the north-eastern Cape Province, South Africa. M.Sc.* thesis (unpubl.), Rhodes Univ., Grahamstown 118pp.

Robinson, P.T., Hall, J.M., Christensen, N.I., Gibson, I.L., Fridleifsson, I.B., Schmincke, H-U. & Schonnarting, G. (1982). The Iceland research drilling project: Synthesis of results and implications for the nature of Icelandic and oceanic crust. *J. Geophys. Res.*, **87**, 6657-6667.

Roeder, P.L. & Emslie, R.F. (1970). Olivine-liquid equilibrium. *Contr. Miner. Petrol.*, **29**, 275-289.

Rumble, K.C. (1979). *The geochemistry and petrology of the Karoo andesites and associated basalts of the north-eastern Cape Province.* M.Sc. thesis (unpubl.), Rhodes Univ., Grahamstown, 174pp.

Saggerson, E.P., Bristow, J.W. & Armstrong, R.A. (1983). The Rooi Rand dyke swarm. *S. Afr. J. Sci.*, **79**, 365-369.

Sato, H. (1977). Ni content of basaltic magmas and a measure of the degree of olivine fractionation. *Lithos,* **10**, 113-120.

Sato, M. (1978). Oxygen fugacity of basaltic magmas and the role of gas-forming elements. *Geophys. Res. Lett.*, **5**, 447-449.

Schutte, S.S., & Cornell, D.H. (1990). Spilitization Processes in the Proterozoic Ongeluk Andesite Formation in Griqualand West, South Africa. *Geocongr. '90 (extd. Abstr.), Geol. Soc. S. Afr.*, Univ. Cape Town, Cape Town, 505-508.

Schweitzer, E. L., Papike, J.J. & Bence, A.E. (1979). Statistical analysis of clinopyroxenes from deep-sea basalts. *Amer. Min.*, 64, 501-513.

Seyfried, W. & Bischoff, J.L. (1977). Hydothermal transport of heavy metals by seawater: The role of seawater/basalt ratio. *Earth Planet. Sci. Lett.*, **34**, 71-77.

Sen, G. (1986). Mineralogy and petrogenesis of the Deccan Trap lava flows around Mahabaleshwar, India. *J. Petrology*, **27**, 627-663.

Shaw, D.M. (1970). Trace element fractionation during anatexis. *Geochim. Cosmochim. Acta*, **34**, 237-243.

South African Committee for Stratigraphy (SACS), (1980). Stratigraphy of South Africa. Part 1. (Comp. L.E. Kent). Lithostratigraphy of the Republic of South Africa, South West Africa/Namibia, and the Republics of Bophuthatswana, Transkei and Venda. *Handbk. Geol. Surv. S. Afr.*, **8**, 690pp.

Stockley, G.M. (1940). The geology of Basutoland. *Geol. Mag.*, **77**, 444- 460.

Stockley, G.M. (1947). *Report on the geology of Basutoland.* Basutoland Govt. Printer, Maseru.

Stolper, E. (1980). A phase diagram for Mid-Ocean Ridge Basalts: Preliminary results and implications for petrogenesis. *Contr. Miner. Petrol.*, **74**, 13-27.

Stolper, E. & Walker, D. (1980). Melt Density and the average composition of basalt. *Contri. Mineral. Petrol.*, **74**, 7-12.

Sukheswala, R.W., Avasia, R.K. & Gangopadhyay, M. (1974). Zeolites and associated minerals in the Deccan Traps of western India. *Min. Mag.*, **39**, 658-671.

Sweeney, R.J. (1988). *Geochemistry of the Sabie River Basalt Formation in the central Lebombo, Karoo Igneous Province.* Ph.D. thesis (unpubl.), Univ. Cape Town, 309pp.

Tankard, A.J., Jackson, M.P.A., Eriksson, K.A., Hobday, D.K., Hunter, D.R. & Minter, W.E.L. (1982). *Crustal evolution of southern Africa.* Springer Verlag, New York 523pp.

Thompson, A.B. (1971). P_{CO2} in low-grade metamorphism, zeolites, carbonates, clay minerals, prehnite relations in the system CaO- Al_2O_3-SiO_2-CO_2-H_2O. *Contr. Miner. Petrol.*, **33**, 145-161.

Tilley, C.E. (1950). Some aspects of magmatic evolution. *Quart. J. Geol. Soc. London*, **106**, 37-61.

Turner, F.J. (1970). Uniqueness versus conformity to pattern in petrogenesis. *Amer. Mineral.*, **55**, 339-348.

Vallance, T. G. (1974). Spilitic Degradation of a Tholeiitic Basalt. *J. Petrology*, **15**, 79-96.

von Gruenewaldt, G., Klemm, D.D., Henckel, J. & Dehm, R.M. (1985). Exsolution features in titanomagnetites from massive magnetite layers and their host rocks of the Upper Zone, eastern Bushveld Complex. *Econ. Geol.*, **80**, 1049-1061.

Walker, D., Shibata, T. & Delong, S.E. (1979). Abyssal tholeiites from the oceanographer fracture Zone: II. Phase equilibria and mixing.*Contr. Miner. Petrol.*, **70**, 111-125.

Walker, F. & Poldervaart, A. (1949). Karoo dolerites of the Union of South Africa. *Geol. Soc. Amer. Bull.*, **60**, 591-706.

Walker, G.P.L. (1960). Zeolite zones and dike distribution in relation to the structure of basalts of eastern Iceland. *J. Geology*, **68**, 515-528.

Washington, H.S. (1922). Deccan Traps and other plateau basalts. *Geol. Soc. Amer. Bull.*, **33**, 765-804.

Waters, A.C. (1960). Determining direction of flow in basalts. *Amer. J. Sci.*, **258a**, 350-366.

Watson, E.B.C. (1977). Partitioning of manganese between forsterite and silicate liquid. *Geochim. Cosmochim. Acta*, **41**, 1363-1374.

Wheelock, G. (1978). The geochemical distribution of zeolites from basalts of the Mfolozi River Formation, Lebombo. *Petros*, **8**, 6-11.

White, R.S. & McKenzie, D.P. (1989). Magmatism at rift zones: The generation of volcanic continental margins and flood basalts. *J. Geophys. Res.*, **94**, 7685-7729.

Wilkinson, J.F.G. (1968). The magmatic affinities of some volcanic rocks from the Tweed shield volcano, S.E. Queensland-N.E. New South Wales. *Geol. Mag.*, **105**, 275-289.

Wilkinson, J.F.G. (1986). Classification and average chemical compositions of common basalts and andesites. *J. Petrology*, **27**, 31-62.

Wolmarans, L.G. & Kent, L.E. (1982). Geological investigations in western Dronning Maud Land, Antarctica-a synthesis. *S. Afr. Antarct. Res. Suppl.*, **2**, 93pp.

Wood, B.J., Bryndzia, L.T. & Johnson, K.E. (1990). Mantle oxidation state and its relationship to tectonic environment and fluid speciation. *Science.*, **248**, 337-345.

Wood, D.A., Joron, J.C., Treuil, M., Norry, M. & Tarney, J. (1979). Elemental and Sr isotope variations in basic lavas from Iceland and the surrounding ocean floor. *Contr. Miner. Petrol.*, **70**, 319-339.

Woolley, A.R. & Garson, M.J. (1970). Petrochemical and tectonic relationships of the Malawi carbonatite-alkaline province and the Lupata-Lebombo volcanics. *In:* Clifford, T.N. and Gass, I.G., (Eds.), *African magmatism and tectonics*. Oliver & Boyd, Edinburgh, 237-262.

Wright, T.L. (1974). Presentation and interpretation of chemical data for igneous rocks. *Contr. Miner. Petrol.*, **48**, 233-248.

Yoder, H.S. (1988). The great basaltic "floods". *S. Afr. J. Geol.*, **91**, 139-154.

Yoder, H.S. & Chayes, F. (1986). Linear alkali correlation in oceanic alkali basalts. *Bull. Geol. Soc. Finland*, **58**, 81-94.

Yoder, H.S. & Tilley, C.E. (1962). Origin of basalt magmas: an experimental study of natural and synthetic rock systems. *J. Petrology,* **3**, 342-532.

Zindler, A. & Jagoutz, E. (1988). Mantle cryptology. *Geochim. Cosmochim. Acta,* **52**, 319-333.

APPENDIX 1

SAMPLE LOCALITIES AND EXPERIMENTAL WORK

A stratigraphic column of the Sani Pass volcanic succession with corresponding sample stratigraphic localities is indicated in Fig. A1.1. Also, sample numbers with corresponding stratigraphic height are listed in a composite tabulation (Table A1.1). In this tabulation, samples are listed starting from the bottom of the stratigraphic sequence and working upward. Included in the tabulation is a concise list of experimental work undertaken on each sample. Sample numbers are prefixed to indicate magma-type affinities.

Sampling of the dolerite dykes has been restricted to the area adjacent to the Sani Pass, and only of dykes following major structural trends in the area. The choice of which dyke to sample was done during the air-photo interpretation. In the field, the dykes were sampled in the most central and accessible portion of the dyke. Localities of the dolerite samples are indicated in Fig. A1.2.

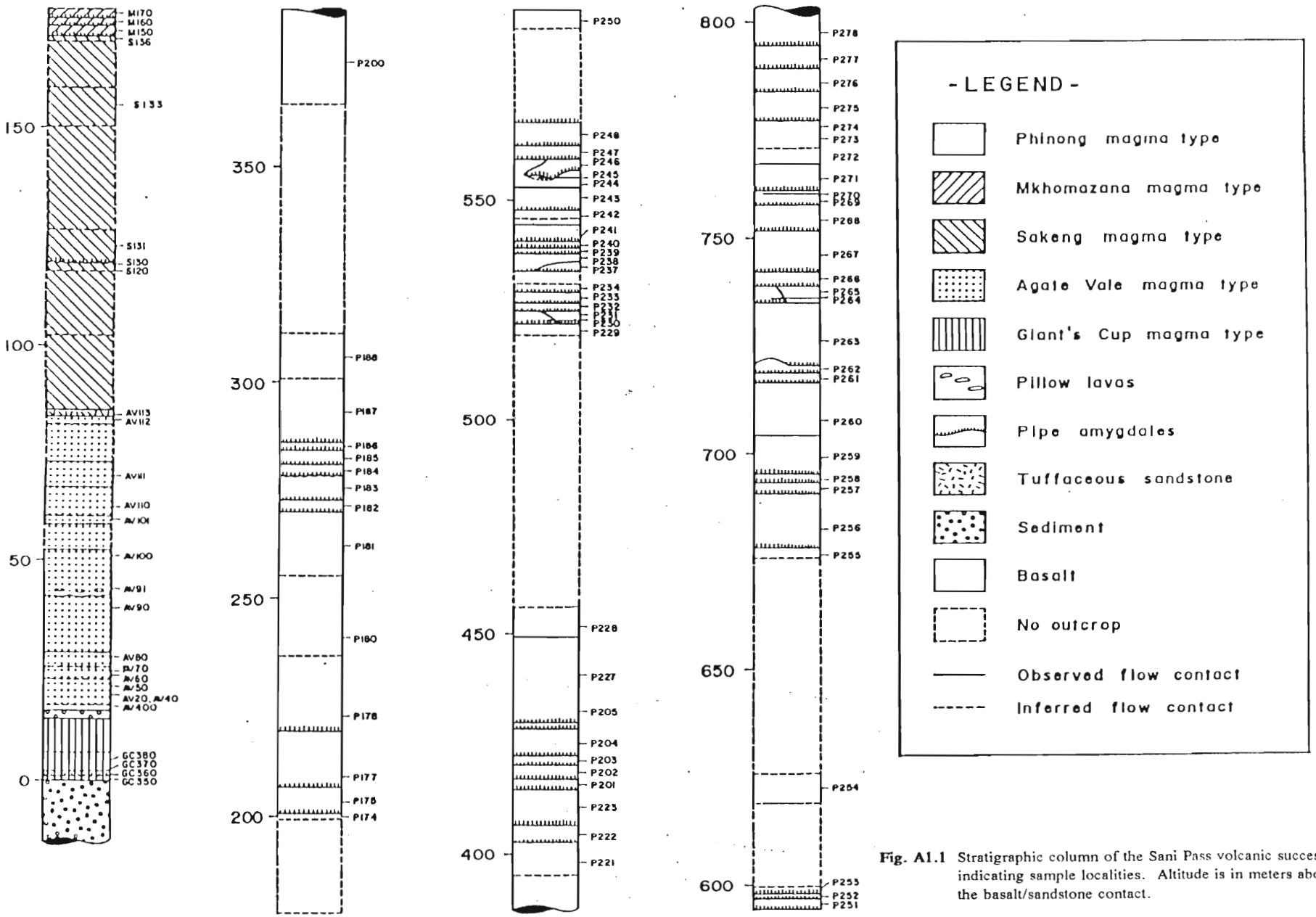

Fig. A1.1 Stratigraphic column of the Sani Pass volcanic succession, indicating sample localities. Altitude is in meters above the basalt/sandstone contact.

Table A1.1. List of experimental work done on the Sani Pass rocks

sample number	stratigraphic height (meters)	petrographic investigation		X–ray flourescence	microprobe analyses	X–ray diffraction
		normal light	reflected light			
P278	797	X	X	X		X
P277	789	X	X	X		X
P276	784	X		X		
P275	780	X				X
P274	777	X				X
P273	773	X		X		
P272	770	X		X		X
P271	765	X		X	X	X
P270	761	X				
P269	760	X		X		
P268	755	X		X		
P267	746	X		X		X
P266	741	X				
P265	738	X				
P264	736	X				
P263	728	X		X		X
P262	721	X				X
P261	719	X				
P260	708	X				
P259	697	X	X	X		X
P258	695	X				
P257	691	X		X		X
P256	680	X		X		
P255	676	X		X		X
P254	623	X	X	X		
P253	597	X				
P252	595	X				
P251	594	X				X
P250	590	X	X	X		X
P248	564	X				X
P247	560	X	X	X		
P246	557	X			X	X
P245	554	X				X
P244	552	X		X		
P243	550	X				X
P242	545	X		X		X
P241	541	X				
P240	540	X		X		X
P239	539	X				
P238	536	X		X		X
P236	535	X		X		
P234	530	X		X		
P233	527	X		X		X
P232	525	X		X		
P231	522	X				
P230	522	X				X
P229	518	X				

X = completed

Table A1.1. List of experimental work done on the Sani Pass rocks

sample number	stratigraphic height (meters)	petrographic investigation		X-ray flourescence	microprobe analyses	X-ray diffraction
		normal light	reflected light			
P228	451	X		X		
P227	440	X	X	X	X	
P205	432	X		X	X	
P204	422	X		X		X
P203	420	X		X		X
P202	416	X				
P201	414	X		X		X
P223	409	X		X		
P222	403	X		X		X
P221	396	X				
P200	372	X		X	X	
P188	304	X	X	X		X
P187	289	X		X	X	
P186	285	X				
P185	281	X		X		
P184	278	X				
P183	274	X		X		
P182	269	X		X		
P181	262	X		X		
P180	239	X	X	X	X	X
P178	222	X		X		
P177	213	X		X		X
P175	203	X				
P174	200	X		X		
P172	173	X				
M170	173	X		X		
M160	171	X		X		X
M150	170	X		X		X
S136	169	X		X		
S133	150	X		X		X
S131	125	X		X		
S130	119	X		X		
S120	118	X	X	X		X
AV112	82	X				
AV111	70	X				
AV110	62	X		X		X
AV100	51	X		X		
AV91	43	X	X	X		
AV90	38	X		X	X	X
AV80	28	X		X		
AV70	25	X		X		
AV60	23	X		X		
AV50	21	X		X	X	
AV40	20	X	X	X		
AV20	19	X		X	X	
AV400	16	X		X		
GC380	4	X	X	X		
GC370	2	X		X		
GC360	1	X	X	X		
GC350	0	X	X	X		X

X=completed

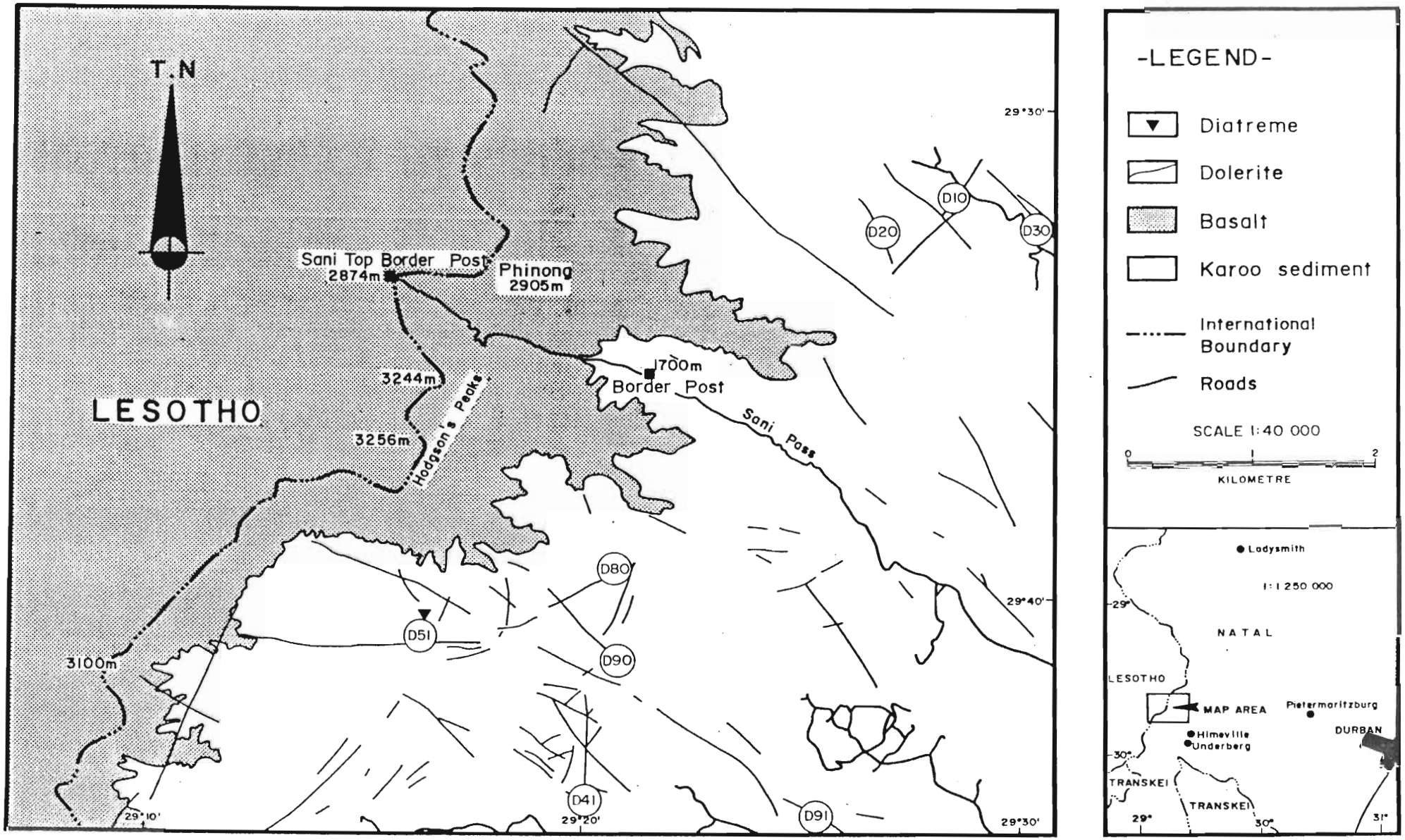

Fig. A1.2 Geological map of the Sani Pass area, indicating sample localities of the dolerite dykes.

APPENDIX 2

X-RAY FLUORESCENCE SPECTROMETRY

Major and trace element analyses for 67 basalts and 8 dolerites were carried out at the University of Natal (Pietermaritzburg). Analytical conditions are tabulated in Table A2.1. All major elements were analysed on fusion discs, prepared after the method described by Norris and Hutton (1969). Trace elements were analysed on pressed powder briquettes. FeO, CO_2, S, H_2O^+ and H_2O^- were analysed by the Geological Survey in Pretoria. CO_2, S, H_2O^+ and H_2O^- were determined by infrared spectroscopy and FeO by redox titration.

Tables A2.2 and A2.3 list the unnormalised major element data for the basalts and dolerites, respectively. A brief description of each sample is included with these tabulations. The analyses are presented in numerical order in which they were sampled, and prefixed to indicate magma-type affinities. Tables A2.4 and A2.5 are tabulations for the basalts and dolerites respectively, of major and trace element data recalculated to a 100% volatile-free, using $Fe_2O_3/FeO=0.2$. Included in these tables are unnormalised trace element concentrations and selected trace element ratios. Data listed in Tables A2.4 and A2.5 have been used in explaining major and trace element variation.

Tables A2.6 and A2.7 list the CIPW normative data for the basalts and dolerites, respectively. These tabulations include the major element data used in calculating the norms, which include CO_2 and have been recalculated using $Fe_2O_3/FeO=0.2$. The normative mineralogy has been calculated in weight percent.

TABLE A2.1 Analytical conditions for XRF analyses

Element	Tube	KV	Ma	Analytical Line	Analysing Crystal	Collimator	Counter	Peak 2θ	Count Time Sec.	Background 2θ	Count Time Sec.	Standard	Blanks	Detection Limits	Analytical Accuracy
SiO_2	Cr	50	50	Ka	Pet	Coarse	Flow	109.165	60	106.000	30	SiO_2 100% NIMD 37.02%		0.004%	0.2%
Al_2O_3	Cr	50	50	Ka	"	"	"	145.040	60	139.160	30	NIML 13.90%	SiO_2	0.005%	0.5%
Fe_2O_3	Au	50	50	Ka	Lif200	Fine	"	57.525	40	Blank standards used to calibrate background.		NIML 10.28%	SiO_2 and $60CaO+40SiO_2$	0.001%	0.5%
MnO	Au	50	50	Ka	Lif200	"	"	62.990	40			NIML 0.78%	SiO_2 and $60CaO+40SiO_2$	0.001%	0.5%
MgO	Cr	50	50	Ka	PX-1	Coarse	"	23.300	60	25.300	30	W-1 6.55%	SiO_2	0.011%	0.3%
CaO	Cr	50	50	Ka	pet	Fine	"	45.240	40	Blank standards		NIML 3.32%	SiO_2 and $40Fe_2O_3 60SiO_2$	0.0003%	0.2%
K_2O	Cr	50	50	Ka	Pet	"	"	50.720	40	used to calibrate		W-1 0.65%	SiO_2 and $60CaO+40SiO_2$	0.0003%	0.2%
TiO_2	Cr	50	50	Ka	Pet	"	"	36.720	40	background		W-1 1.05%	SiO_2 and $60CaO+40SiO_2$	0.0004%	0.2%
P_2O_5	Cr	50	50	Ka	Ge	Coarse	"	141.040	60	138.000 143.000	30 30	BR 1.10%	SiO_2	0.001%	0.2%
Na_2O	Cr	50	50	Ka	PX-1	Fine	"	28.170	60	30.000	30	BR 3.12%	SiO_2	0.018%	2%
Sc	Cr	50	50	Ka	Lif200	"	"	97.730	60	95.850 98.555	30 30	BCR 33 ppm	SiO_2 and $CaCO_3$	0.3 ppm	10%
Ba	Cr	50	50	La	Lif220	"	"	115.275	60	114.500 116.500	30 30	W-1 160 ppm	SiO_2 and MgO	1 ppm	± 20%
Zn	Au	50	50	Ka	Lif200	"	"	41.795	60	39.65 46.70	30 30	NIMP 100 ppm	SiO_2 and $CaCo_3$	0.3 ppm	± 10%
Cu	Au	50	50	Ka	Lif200	"	"	45.040	60	39.65 46.70	30 30	W-1 110 ppm	SiO_2 and $CaCo_3$	0.2 ppm	± 10%
Ni	Au	50	50	Ka	Lif200	"	"	48.690	60	46.70 50.00	30 30	BR 260 ppm	SiO_2 and $CaCo_3$	0.1 ppm	± 10%
Cr	Au	50	50	Ka	Lif200	"	"	69.375	60	68.10 70.80	30 30	JB1 400 ppm	SiO_2	0.6 ppm	10%
V	Au	50	50	Ka	Lif220	"	"	123.220	60	117.10 123.80	30 30	W-1 260 ppm	SiO_2	0.5 ppm	± 10%
La	Au	50	50	Ka	Lif220	"	"	138.920	60	132.60 141.80	30 30	BR 80 ppm	SiO_2	1.5 ppm	15%
Zr	Rh	50	50	Ka	Lif220	"	Scint	32.045	60	29.30 34.89	30 30	AGV 230 ppm	SiO_2	0.3 ppm	3%
Sr	Rh	50	50	Ka	Lif220	"	"	35.830	60	34.89 36.90	30 30	W-1 190 ppm	SiO_2	0.2 ppm	3%
Nb	Rh	50	50	Ka	Lif220	"	"	30.420	60	29.45 34.80	30 30	GSP 23 ppm	SiO_2	0.1 ppm	3%
Y	Rh	50	50	Ka	Lif220	"	"	33.855	60	29.45 34.80	30 30	NIMG 145 ppm	SiO_2	0.3 ppm	3%
Rb	Rh	50	50	Ka	Lif220	"	"	37.960	60	34.80 41.10	30 30	NIMG 320 ppm	SiO_2	0.4 ppm	2%
U	Rh	50	50	Ka	Lif220	"	"	37.300	100	36.90 41.10	30 30	NIMG 15 ppm	SiO_2	0.1 ppm	20%
Th	Rh	50	50	Ka	Lif220	"	"	39.250	100	36.90 41.10	30 30	GSP 105 ppm	SiO_2	0.5 ppm	20%
Pb	Au	50	50	Ka	Lif220	"	Flow/ Scint	40.225	60	39.80 41.50	30 30	GSP 54 ppm	SiO_2	1 ppm	± 10%
Ga	Au	50	50	Ka	Lif220	"	"	56.165	60	55.50 57.20	30 30	GSP 23 ppm	SiO_2	0.2 ppm	10%
Co	Au	50	50	Ka	Lif220	"	"	77.890	60	77.40 79.00	30 30	NIMD 210 ppm	SiO_2	1 ppm	± 10%

Table A2.2. Unnormalised major element data for the Sani Pass volcanics

	GC350	GC360	GC370	GC380	AV400	AV20	AV40	AV50	AV60
SiO2	47.04	54.59	52.75	53.12	47.68	53.76	53.97	54.60	55.90
TiO2	1.25	1.01	1.02	1.30	1.13	1.05	1.07	1.08	0.96
Al2O3	16.35	14.48	15.57	14.55	16.49	15.74	15.72	15.46	15.45
Fe2O3	10.15	10.53	10.78	12.11	10.73	11.61	11.24	10.91	10.78
MnO	0.21	0.13	0.17	0.18	0.25	0.17	0.16	0.17	0.16
MgO	3.12	2.70	5.14	4.57	4.54	6.42	6.39	5.99	6.26
CaO	17.88	10.98	11.62	10.04	10.37	9.43	9.06	9.45	6.88
Na2O	3.37	2.31	2.13	2.39	1.06	2.16	2.62	2.56	2.80
K2O	0.35	0.52	0.14	0.83	7.22	0.72	1.13	1.11	1.98
P2O5	0.16	0.12	0.12	0.16	0.17	0.17	0.17	0.16	0.16
TOTAL	99.88	97.37	99.44	99.25	99.64	101.23	100.57	101.49	101.33
FeO	6.35	6.52	7.97	6.23	4.57	6.37	5.76	6.77	4.34
S	0.04	1.27	0.07	0.69	0.03	0.02	0.02	0.02	0.01
CO2	9.74	5.11	1.77	0.03	5.93	0.28	0.20	0.44	0.10
H2O+	3.09	2.65	1.89	0.71	3.19	1.27	1.18	0.58	1.60
H2O−	1.07	1.10	3.09	0.40	0.42	2.47	2.75	1.18	3.35
volatiles	12.87	9.03	3.73	1.43	9.15	1.57	1.40	1.04	1.71

SAMPLE	PHENOCRYSTS	GROUNDMASS	AMYGDALES	ALTERATION
GC350	Plag	Plag + glass (fine)	Abund. cc/qz	+
GC360	Plag	Plag + glass + minor qz (fgr)	Abund. cc/qz	+
GC370	Plag	Plag + aug + glass (mgr)	Abund. small cc/qz	+-
GC380	Glom. plag	Plag + aug + glass + oxd (mgr)	Minor chl.	-
AV400	Glom. plag	Plag + aug + glass + cc (fgr)	Abund. cc/chl.	+
AV20	-	Plag, suboph. aug, int. glass	Small qz/zeol	+-
AV40	Glom. plag	Plag, suboph. aug, int. glass	V.small cc/chl.	+-
AV50	Glom. plag	Plag, aug, int. glass	Minor cc/chl.	-
AV60	Plag	Plag, aug, int. glass, qz	V. small qz	++

ABBREVIATIONS:

++, +, +-, - : indicate decreasing degrees of alteration

aug. : augite
chl. : chlorite
glom. : glomeroporphyritic
int. : interstitial
oph. : ophitic
plag. : plagioclase
zeol. : zeolite
cc : calcite
fgr. : finegrained
GM : groundmass
mgr. : medium-grained
oxd. : oxide
qz. : quartz

Table A2.2. Unnormalised major element data for the Sani Pass volcanics

	AV70	AV80	AV90	AV91	AV100	AV110	S120	S130	S131
SiO2	52.94	52.04	53.39	55.35	54.01	54.33	53.77	51.55	52.44
TiO2	1.09	1.08	1.00	1.04	1.03	1.05	0.85	1.05	1.09
Al2O3	16.24	16.36	15.29	15.18	15.33	15.33	16.01	15.90	15.52
Fe2O3	11.43	12.00	11.23	9.98	11.19	10.74	10.26	11.45	10.95
MnO	0.13	0.17	0.16	0.12	0.17	0.18	0.15	0.16	0.17
MgO	6.39	6.81	6.69	5.77	5.97	5.64	7.32	6.56	6.77
CaO	8.87	9.32	10.05	8.24	10.18	10.43	10.94	12.08	11.40
Na2O	2.21	2.65	2.33	2.69	2.56	2.49	1.66	1.86	2.12
K2O	1.79	0.40	0.75	1.19	0.48	0.99	0.10	0.45	0.58
P2O5	0.16	0.17	0.15	0.16	0.16	0.16	0.10	0.18	0.18
TOTAL	101.25	101.00	101.04	99.72	101.08	101.34	101.16	101.24	101.22
FeO	3.88	6.07	8.33	5.09	5.42	7.05	8.68	6.51	7.83
S	0.02	0.01	0.02	0.46	0.05	0.03	0.17	0.03	0.01
CO2	0.36	0.79	0.47	0.15	0.54	1.11	1.15	1.92	1.76
H2O+	1.59	1.94	0.82	1.77	1.11	0.66	1.69	1.49	0.65
H2O−	3.68	3.35	1.00	2.84	0.68	0.71	2.96	1.88	0.76
volatiles	1.97	2.74	1.31	2.38	1.70	1.80	3.01	3.44	2.42

SAMPLE	PHENOCRYSTS	GROUNDMASS	AMYGDALES	ALTERATION
AV70	-	Plag, aug, glass	Abund. qz/cc	++
AV80	Glom. plag	Plag, glass (fgr)	Small cc/chl.	++
AV90	Glom. plag	Plag, aug, oxd (mgr)	GM cc, chl.	-
AV91	Plag, minor aug	Glass	Abund. cc, minor qz	+-
AV100	-	Plag, suboph. aug, glass (mgr)	GM cc, chl.	-
AV110	-	Plag, suboph. aug, glass, oxd	Small isol. cc/chl.	-
S120	-	Plag, suboph. aug,glass	Abund. chl, cc, qz	+-
S130	Plag	Plag, aug, glass, oxd	GM chl.	+-
S131	-	Plag, oph. aug, glass, oxd	Abund. cc,qz, chl.	+-

Table A2.2. Unnormalised major element data for the Sani Pass volcanics

	S133	S136	M150	M160	M170	P174	P177	P178	P180
SiO2	53.22	52.33	53.69	51.35	53.33	50.22	51.64	50.93	49.00
TiO2	0.97	1.03	1.03	1.03	0.98	0.93	1.00	1.09	0.67
Al2O3	15.79	15.29	16.12	15.47	15.50	15.52	15.60	16.40	15.27
Fe2O3	9.66	10.49	10.31	10.56	10.09	10.35	10.19	10.30	10.91
MnO	0.18	0.12	0.18	0.16	0.15	0.22	0.15	0.15	0.16
MgO	6.99	7.04	7.47	7.21	7.20	6.23	7.07	5.92	11.08
CaO	10.52	10.26	6.39	8.61	8.41	13.12	11.28	10.62	9.71
Na2O	2.08	1.75	4.17	4.22	4.51	2.25	2.09	3.24	2.01
K2O	0.33	0.72	1.71	0.77	0.53	0.65	0.56	0.91	0.38
P2O5	0.16	0.14	0.15	0.15	0.14	0.16	0.16	0.20	0.11
TOTAL	99.96	99.17	101.22	99.53	100.84	99.65	99.74	99.76	99.30
FeO	5.00	6.57	7.97	6.70	6.61	3.72	6.35	5.15	8.30
S	0.01	0.76	0.02	0.24	0.02	0.05	0.00	0.00	0.00
CO2	0.24	0.85	0.37	0.24	0.26	2.73	0.06	1.26	0.10
H2O+	1.30	2.05	2.48	3.34	3.19	1.88	3.82	1.69	1.32
H2O−	2.20	2.72	0.93	0.62	0.71	3.66	1.02	1.21	0.65
volatiles	1.55	3.66	2.87	3.82	3.47	4.66	3.88	2.95	1.42

SAMPLE	PHENOCRYSTS	GROUNDMASS	AMYGDALES	ALTERATION
S133	-	Plag, oph. aug, glass, oxd	Abund. cc, qz, chl.	+-
S136	Glom. plag	Plag, aug, glass (fgr)	Abund. large cc, qz.	+-
M150	Glom. plag	Plag, suboph. aug, glass	Abund. cc, qz, chl.	++
M160	Glom. plag	Plag, suboph. aug, glass	GM zeol, chl.	++
M170	Glom. plag	Plag, suboph. aug, glass	GM zeol, chl.	++
P174	-	Plag, suboph. aug, abund. glass	Abund. cc/zeol/chl.	+-
P177	-	Plag, oph. aug, minor glass	GM cc, chl.	+-
P178	Glom. plag	Plag, aug, abund. glass	Abund. zeol, chl.	+
P180	-	Plag, suboph. aug, oliv, oxd	-	-

Table A2.2. Unnormalised major element data for the Sani Pass volcanics

	P181	P182	P183	P185	P187	P188	P200	P222	P223
SiO2	52.49	51.48	51.63	51.24	51.11	50.48	50.82	51.06	50.27
TiO2	1.11	1.01	1.03	1.00	0.92	0.99	0.91	0.97	0.91
Al2O3	15.42	16.00	16.49	15.36	15.40	15.47	15.18	15.54	16.19
Fe2O3	11.19	10.91	10.07	10.97	10.92	11.12	10.96	10.96	10.92
MnO	0.18	0.16	0.20	0.17	0.17	0.17	0.18	0.19	0.17
MgO	5.92	7.32	5.89	6.77	7.83	7.23	7.72	6.86	7.60
CaO	10.07	10.57	11.69	11.20	10.85	11.41	10.90	11.39	11.23
Na2O	2.55	2.08	2.22	1.93	2.22	2.34	2.06	2.37	2.19
K2O	0.72	0.50	0.50	0.54	0.49	0.56	0.51	0.56	0.45
P2O5	0.19	0.16	0.16	0.17	0.14	0.15	0.15	0.17	0.14
TOTAL	99.84	100.19	99.88	99.35	100.05	99.92	99.39	100.07	100.07
FeO	5.41	5.30	5.19	6.33	7.15	6.48	6.57	6.75	7.15
S	0.00	0.00	0.00	0.00	0.00	0.02	0.02	0.01	0.00
CO2	0.30	0.29	1.10	0.26	0.10	0.23	0.06	0.15	0.07
H2O+	1.23	1.07	1.20	0.90	0.96	0.92	0.72	1.45	0.73
H2O−	2.28	1.11	1.80	1.66	0.45	0.79	0.75	2.95	0.74
volatiles	1.53	1.36	2.30	1.16	1.60	1.17	0.80	1.61	0.80

SAMPLE	PHENOCRYSTS	GROUNDMASS	AMYGDALES	ALTERATION
P181	Plag	Plag, suboph. aug, oxd, glass	cc, chl.	+
P182	-	Plag, suboph. aug, glass	cc	++
P183	-	Plag, suboph. aug, glass	Abund. cc, chl.	++
P185	-	Plag, oph. aug glass	GM chl., cc	+-
P187	-	Plag, oph. aug (cgr)	GM chl.	-
P188	-	Plag, oph. aug, glass	Zeol, chl.	+
P200	-	Oliv, plag, suboph. aug (cgr)	-	-
P222	-	Plag, oph. aug, glass	Abund. zeol, chl.	+
P223	-	Oliv, plag, suboph. aug	GM chl.	-

Table A2.2. Unnormalised major element data for the Sani Pass volcanics

	P201	P203	P204	P205	P227	P228	P232	P233	P234
SiO2	50.22	51.73	50.98	50.53	49.33	51.01	49.66	50.32	50.68
TiO2	0.89	1.11	0.89	0.88	0.88	1.04	0.95	0.96	0.92
Al2O3	15.85	15.46	15.75	14.74	13.34	15.07	16.20	15.93	16.39
Fe2O3	10.68	11.22	10.67	10.94	12.24	11.03	10.93	10.96	10.55
MnO	0.19	0.17	0.16	0.17	0.19	0.18	0.17	0.17	0.19
MgO	7.42	6.09	7.13	8.60	11.92	7.14	7.81	7.29	6.77
CaO	11.58	10.79	11.05	10.95	8.70	11.22	10.93	11.08	11.06
Na2O	2.35	2.34	2.31	1.94	1.60	2.12	2.05	2.15	2.22
K2O	0.52	0.75	0.54	0.48	1.11	0.71	0.85	0.73	0.76
P2O5	0.14	0.20	0.14	0.14	0.16	0.20	0.17	0.17	0.16
TOTAL	99.84	99.86	99.62	99.37	99.47	99.72	99.72	99.76	99.70
FeO	5.19	7.18	8.92	6.13	9.62	1.61	4.47	4.74	5.45
S	0.00	0.00	0.00	0.00	0.01	0.00	0.03	0.00	0.02
CO2	0.51	0.28	0.34	0.08	0.12	0.32	0.32	0.19	0.16
H2O+	1.61	1.51	1.47	0.91	1.36	1.34	1.49	1.49	0.79
H2O−	3.42	2.45	2.57	0.43	0.68	2.46	1.88	3.29	0.68
volatiles	2.12	1.79	1.81	0.99	1.49	1.66	1.84	1.68	0.97

SAMPLE	PHENOCRYSTS	GROUNDMASS	AMYGDALES	ALTERATION
P201	-	Plag, oph. aug	Chl., zeol	+-
P203	-	Plag, oph. aug, glass	Chl., zeol	+
P204	-	Plag, oph. aug, glass	Chl/zeol/cc	+-
P205	-	Oliv, plag, suboph. aug	GM chl.	+-
P227	oliv (cumul)	Plag, suboph. aug	GM chl.	+-
P228	-	Plag, oph. aug, glass	cc,chl., zeol	+-
P232	-	Plag, suboph. aug, glass	chl., zeol	+
P233	-	Plag, suboph. aug, glass	Chl., zeol	+-
P234	Glom. plag	Plag, aug, glass	Chl., zeol	+-

Table A2.2. Unnormalised major element data for the Sani Pass volcanics

	P236	P238	P240	P242	P244	P247	P250	P254	P255
SiO2	51.09	50.38	51.57	51.43	50.44	50.21	52.12	51.32	51.44
TiO2	0.97	0.99	0.96	0.96	0.93	0.97	0.93	1.01	0.96
Al2O3	15.59	16.32	15.82	15.57	16.18	15.99	15.31	15.26	16.15
Fe2O3	10.79	11.13	10.87	10.75	10.82	10.95	10.85	11.15	10.56
MnO	0.16	0.18	0.16	0.15	0.18	0.18	0.17	0.18	0.16
MgO	6.79	6.86	6.27	6.73	6.95	7.27	7.16	6.99	6.52
CaO	10.68	11.08	11.07	10.10	11.35	11.28	10.28	10.65	11.12
Na2O	2.43	2.18	2.31	2.71	2.24	2.28	2.68	2.37	2.24
K2O	0.88	0.75	0.51	0.88	0.51	0.71	0.37	0.77	0.67
P2O5	0.17	0.18	0.17	0.17	0.16	0.17	0.15	0.16	0.15
TOTAL	99.55	100.05	99.71	99.45	99.76	100.01	100.02	99.86	99.97
FeO	5.56	4.46	5.98	4.46	5.30	5.66	6.95	6.40	6.10
S	0.03	0.00	0.03	0.00	0.00	0.02	0.03	0.03	0.02
CO2	0.31	0.13	0.13	0.15	0.20	0.11	0.10	0.23	0.09
H2O+	2.25	1.17	4.13	1.31	3.07	1.33	3.29	1.06	2.66
H2O−	2.39	1.38	1.55	1.49	2.98	2.21	1.56	1.46	0.86
volatiles	2.59	1.30	4.29	1.46	3.27	1.46	3.42	1.32	2.77

SAMPLE	PHENOCRYSTS	GROUNDMASS	AMYGDALES	ALTERATION
P236	Glom. plag	Plag, aug, glass	Abund. zeol, cc	++
P238	-	Plag, aug glass	GM chl., zeol	+
P240	Glom. plag	Plag, aug, glass	Zeol, cc	+
P242	-	Plag, oph. aug, glass	Zeol, chl.	+
P244	-	Plag, suboph. aug, glass	Zeol, chl.	+
P247	Glom. plag	Plag, aug, glass	Zeol, chl.	+
P250	Glom. plag	Plag, oph. aug, glass	Zeol	++
P254	-	Plag, oph. aug, glass	Zeol, cc	+
P255	-	Plag, oph. aug, glass	Zeol, qz	++

Table A2.2. Unnormalised major element data for the Sani Pass volcanics

	P256	P257	P259	P263	P267	P268	P269	P271	P272
SiO2	50.97	50.78	51.08	51.40	51.11	51.59	50.88	51.00	51.45
TiO2	0.94	0.91	0.88	0.92	0.83	0.89	0.90	0.91	1.01
Al2O3	15.67	16.15	15.53	15.25	16.60	15.55	15.70	15.74	14.99
Fe2O3	10.73	11.00	10.90	11.20	10.51	10.97	11.12	11.20	12.01
MnO	0.16	0.17	0.17	0.18	0.16	0.17	0.18	0.19	0.17
MgO	7.47	6.73	7.43	7.36	6.63	7.45	7.21	6.98	7.02
CaO	11.09	11.45	11.07	11.01	11.36	11.01	11.17	11.13	10.25
Na2O	2.03	1.99	2.05	1.99	2.05	2.27	2.07	2.27	2.17
K2O	0.59	0.84	0.51	0.65	0.75	0.47	0.44	0.57	0.57
P2O5	0.15	0.15	0.15	0.15	0.13	0.15	0.15	0.15	0.17
TOTAL	99.80	100.00	99.77	100.11	100.13	100.52	99.82	100.14	99.81
FeO	6.39	5.03	7.18	4.47	4.77	7.23	5.92	4.16	6.66
S	0.00	0.04	0.01	0.00	0.00	0.00	0.00	0.00	0.00
CO2	0.13	0.11	0.09	0.14	0.11	0.10	0.09	0.07	0.17
H2O+	1.11	4.25	0.55	0.45	4.31	0.76	0.88	1.12	1.93
H2O−	1.97	1.81	0.33	0.95	1.77	0.84	2.02	1.76	1.17
volatiles	1.24	4.40	0.65	0.59	4.42	0.86	0.97	1.19	2.10

SAMPLE	PHENOCRYSTS	GROUNDMASS	AMYGDALES	ALTERATION
P256	-	Plag, aug, glass	Zeol, chl.	++
P257	-	Plag, oph. aug, glass	Zeol, chl.	++
P259	Glom. plag	Plag, aug, oxd, (fgr)	Chl. (minor)	-
P263	-	Plag, aug, oxd, glass (fgr)	Zeol, chl.	+-
P267	-	Plag, aug, glass	Abund. zeol, chl.	++
P268	Glom. plag	Plag, aug, oxd (fgr)	Zeol, chl.	+-
P269	Glom. plag	Plag, aug, glass, oxd	Zeol, chl.	++
P271	-	Plag, suboph. aug, glass	Zeol, chl.	+
P272	Glom. plag(acic)	Plag, aug, glass (fgr)	Zeol, chl.	+

Table A2.2. Unnormalised major element data for the Sani Pass volcanics

	P273	P276	P277	P278
SiO2	51.71	50.99	50.03	52.13
TiO2	0.99	0.99	1.00	0.99
Al2O3	15.41	16.00	16.18	15.38
Fe2O3	11.56	11.49	11.78	11.20
MnO	0.18	0.16	0.19	0.17
MgO	6.02	6.67	6.53	6.11
CaO	10.62	10.47	11.73	10.50
Na2O	2.26	2.46	2.03	2.40
K2O	0.76	0.79	0.31	0.69
P2O5	0.16	0.17	0.16	0.18
TOTAL	99.67	100.19	99.94	99.75
FeO	8.29	6.91	6.35	5.82
S	0.00	0.08	0.00	0.01
CO2	0.08	0.00	0.06	0.05
H2O+	0.51	0.98	3.82	0.78
H2O−	0.51	0.77	1.02	0.48
volatiles	0.59	1.06	3.88	0.84

SAMPLE	PHENOCRYSTS	GROUNDMASS	AMYGDALES	ALTERATION
P273	Glom. plag	Plag, aug, oxd	Zeol, chl.	+-
P276	Glom. plag	Plag, aug, oxd	Zeol, chl.	+
P277	Glom. plag	Plag, aug, oxd, glass	Zeol, chl.	++
P278	-	Plag, oph. aug, glass (mgr)	GM zeol, chl.	+

Table A2.3. Unnormalised major elements for the Sani Pass dolerites

	D10	D20	D30	D41	D51	D80	D90	D91
SiO2	51.56	52.22	52.15	51.23	51.74	51.36	51.79	51.99
TiO2	1.13	0.96	1.16	1.08	0.98	1.02	0.97	0.98
Al2O3	14.72	15.61	14.41	14.80	15.30	15.24	15.32	15.21
Fe2O3	12.52	10.39	12.86	12.18	10.80	11.90	10.93	10.88
MnO	0.19	0.16	0.20	0.20	0.18	0.20	0.18	0.18
MgO	6.07	6.89	5.69	6.30	7.39	6.34	7.34	7.19
CaO	10.73	10.91	10.15	10.26	10.20	10.92	10.45	10.58
Na2O	2.25	2.19	2.17	2.25	2.23	2.26	2.44	2.41
K2O	0.61	0.54	0.64	0.56	0.56	0.48	0.55	0.47
P2O5	0.14	0.13	0.19	0.16	0.16	0.15	0.17	0.17
TOTAL	99.89	99.97	99.61	100.03	100.86	99.82	100.15	100.15
FeO	7.51	7.16	10.72	8.73	8.36	8.74	8.30	8.10
S	0.04	0.03	0.00	0.04	0.01	0.03	0.04	0.01
CO2	0.11	0.09	0.03	0.05	0.05	0.07	0.06	0.06
H2O+	0.62	0.79	0.93	0.72	0.88	0.62	0.77	0.97
H2O−	0.51	0.31	0.51	0.77	0.48	0.42	0.21	0.47
volatiles	0.77	0.91	0.96	0.81	0.94	0.72	0.87	1.04

Table A2.4. Normalised major and unnormalised trace element data for the Sani Pass volcanics

	GC350	GC360	GC370	GC380	AV400	AV20	AV40	AV50	AV60
SiO2	47.50	56.59	53.53	54.09	48.30	53.64	53.66	54.29	55.67
TiO2	1.26	1.05	1.04	1.32	1.14	1.05	1.06	1.07	0.96
Al2O3	16.52	15.01	15.81	14.81	16.70	15.70	15.63	15.37	15.39
Fe2O3	1.56	1.66	1.67	1.88	1.65	1.76	1.70	1.66	1.64
FeO	7.82	8.32	8.35	9.40	8.29	8.83	8.53	8.28	8.19
MnO	0.21	0.13	0.17	0.18	0.25	0.17	0.16	0.17	0.16
MgO	3.15	2.80	5.22	4.65	4.60	6.40	6.35	5.96	6.24
CaO	18.06	11.39	11.80	10.22	10.50	9.41	9.01	9.40	6.85
Na2O	3.40	2.40	2.16	2.43	1.07	2.15	2.61	2.54	2.78
K2O	0.35	0.54	0.14	0.85	7.31	0.71	1.12	1.10	1.97
P2O5	0.16	0.13	0.12	0.16	0.17	0.17	0.17	0.16	0.16
TOTAL	100.00	100.00	100.00	100.00	100.00	100.00	100.00	100.00	100.00
Sr	238	175	192	187	70	191	209	179	200
Rb	8	12	4	24	109	14	25	28	51
Y	28	22	26	32	25	23	23	23	16
Zr	96	91	85	117	146	150	150	159	132
Nb	3	3	3	2	4	7	5	4	4
Co	28	38	36	38	40	46	43	44	51
V	279	246	263	242	241	243	257	228	261
La	13	10	9	17	10	15	12	16	19
Cr	127	137	152	89	190	193	187	167	407
Zn	98	78	66	90	97	112	97	99	74
Cu	72	57	61	65	59	65	149	84	53
Ni	65	62	69	53	66	79	72	66	141
Sc	27	25	26	22	27	26	28	24	29
Ba	170	196	130	268	868	330	386	307	670
Selected trace element ratios									
Zr/Nb	32.00	30.33	28.33	58.50	36.50	21.43	30.00	39.75	33.00
Zr/Y	3.43	4.14	3.27	3.66	5.84	6.52	6.52	6.91	8.25
Ti/Zr	78.88	69.29	73.23	67.66	47.01	42.09	42.45	40.53	43.65
P/Zr	7.49	6.05	6.27	5.97	5.07	4.96	4.96	4.41	5.30
Ti/P	10.53	11.45	11.68	11.33	9.27	8.48	8.56	9.19	8.24
Sc/Ni	0.42	0.40	0.38	0.42	0.41	0.33	0.39	0.36	0.21
Cr/Ni	1.95	2.21	2.20	1.68	2.88	2.44	2.60	2.53	2.89

Table A2.4. Normalised major and unnormalised trace element data for the Sani Pass volcanics

	AV70	AV80	AV90	AV91	AV100	AV110	S120	S130	S131
SiO2	52.80	52.04	53.36	55.97	53.95	54.08	53.62	51.40	52.28
TiO2	1.09	1.08	0.99	1.05	1.02	1.05	0.85	1.05	1.09
Al2O3	16.19	16.37	15.27	15.35	15.31	15.27	15.95	15.86	15.47
Fe2O3	1.74	1.83	1.71	1.54	1.71	1.63	1.56	1.74	1.67
FeO	8.69	9.15	8.55	7.70	8.53	8.15	7.80	8.71	8.33
MnO	0.13	0.17	0.16	0.12	0.17	0.18	0.15	0.16	0.17
MgO	6.37	6.80	6.68	5.84	5.96	5.62	7.30	6.54	6.75
CaO	8.84	9.32	10.05	8.33	10.16	10.39	10.91	12.05	11.37
Na2O	2.20	2.65	2.33	2.72	2.55	2.48	1.66	1.86	2.11
K2O	1.79	0.40	0.74	1.20	0.47	0.99	0.10	0.45	0.58
P2O5	0.16	0.17	0.15	0.16	0.16	0.16	0.10	0.18	0.18
TOTAL	100.00	100.00	100.00	100.00	100.00	100.00	100.00	100.00	100.00
Sr	214	181	176	164	206	168	109	136	145
Rb	42	5	19	23	16	22	0	6	13
Y	24	22	17	32	22	22	15	14	18
Zr	152	147	123	152	144	143	73	89	95
Nb	4	6	4	5	5	4	3	2	4
Co	47	48	42	44	41	41	51	47	43
V	274	257	214	274	221	222	262	245	211
La	16	20	3	10	13	14	7	9	8
Cr	289	256	214	180	221	222	262	245	211
Zn	101	98	75	91	130	95	80	70	67
Cu	103	62	63	74	140	60	72	133	60
Ni	96	95	97	87	84	82	90	144	101
Sc	31	27	23	29	20	26	35	33	28
Ba	751	333	281	254	312	285	51	138	168
Selected trace element ratios									
Zr/Nb	38.00	24.50	30.75	30.40	28.80	35.75	24.33	44.50	23.75
Zr/Y	6.33	6.68	7.24	4.75	6.55	6.50	4.87	6.36	5.28
Ti/Zr	43.15	43.99	48.49	41.48	42.28	44.09	69.79	70.73	68.73
P/Zr	4.61	5.09	5.35	4.60	4.88	4.94	6.05	9.00	8.42
Ti/P	9.36	8.65	9.07	9.01	8.67	8.93	11.54	7.86	8.17
Sc/Ni	0.32	0.28	0.24	0.33	0.24	0.32	0.39	0.23	0.28
Cr/Ni	3.01	2.69	2.21	2.07	2.63	2.71	2.91	1.70	2.09

Table A2.4. Normalised major and unnormalised trace element data for the Sani Pass volcanics

	S133	S136	M150	M160	M170	P174	P177	P178	P180
SiO2	53.70	53.25	53.50	52.05	53.33	50.83	52.22	51.49	49.82
TiO2	0.98	1.05	1.02	1.04	0.98	0.94	1.01	1.10	0.68
Al2O3	15.93	15.56	16.07	15.69	15.50	15.71	15.78	16.59	15.53
Fe2O3	1.48	1.62	1.57	1.63	1.54	1.60	1.57	1.59	1.69
FeO	7.43	8.14	7.84	8.17	7.70	7.99	7.86	7.94	8.46
MnO	0.18	0.12	0.18	0.16	0.15	0.23	0.15	0.15	0.16
MgO	7.05	7.16	7.45	7.31	7.20	6.31	7.15	5.99	11.26
CaO	10.67	10.44	6.36	8.73	8.41	13.29	11.41	10.75	9.87
Na2O	2.10	1.78	4.16	4.28	4.51	2.28	2.12	3.28	2.04
K2O	0.33	0.74	1.71	0.78	0.53	0.66	0.56	0.92	0.38
P2O5	0.16	0.14	0.15	0.15	0.14	0.16	0.16	0.20	0.11
TOTAL	100.00	100.00	100.00	100.00	100.00	100.00	100.00	100.00	100.00
Sr	150	144	190	179	96	187	228	248	218
Rb	7	16	43	20	13	11	10	19	8
Y	25	27	43	28	16	25	26	23	19
Zr	86	105	101	105	96	79	91	87	55
Nb	1	4	4	3	4	8	7	10	2
Co	33	43	40	47	44	35	42	39	62
V	223	262	259	285	246	264	226	265	163
La	11	15	6	18	8	13	12	14	6
Cr	303	333	259	368	390	265	261	239	477
Zn	51	85	87	83	87	76	70	81	67
Cu	75	99	79	79	135	86	77	83	52
Ni	70	99	116	108	122	84	92	91	250
Sc	33	35	37	38	35	31	29	33	22
Ba	129	224	468	197	122	154	154	189	143
Selected trace element ratios									
Zr/Nb	61.71	26.25	25.25	35.00	24.00	9.88	13.00	8.70	27.50
Zr/Y	3.51	3.89	2.35	3.75	6.00	3.16	3.50	3.78	2.89
Ti/Zr	68.17	59.90	60.78	59.53	61.37	70.97	66.59	76.08	74.20
P/Zr	8.10	5.87	6.51	6.25	6.38	9.08	7.68	10.16	8.74
Ti/P	8.41	10.20	9.34	9.52	9.62	7.81	8.67	7.49	8.49
Sc/Ni	0.47	0.35	0.32	0.35	0.29	0.37	0.32	0.36	0.09
Cr/Ni	4.33	3.36	2.23	3.41	3.20	3.15	2.84	2.63	1.91

Table A2.4. Normalised major and unnormalised trace element data for the Sani Pass volcanics

	P181	P182	P183	P185	P187	P188	P200	P222	P223
SiO2	53.08	51.85	52.14	52.07	51.57	51.01	51.60	51.51	50.71
TiO2	1.12	1.02	1.04	1.02	0.93	1.00	0.93	0.98	0.92
Al2O3	15.59	16.12	16.65	15.61	15.54	15.63	15.42	15.67	16.33
Fe2O3	1.73	1.67	1.55	1.70	1.68	1.71	1.70	1.68	1.68
FeO	8.64	8.38	7.76	8.50	8.40	8.57	8.50	8.43	8.40
MnO	0.18	0.16	0.20	0.17	0.17	0.17	0.18	0.19	0.17
MgO	5.99	7.38	5.96	6.88	7.90	7.31	7.84	6.92	7.67
CaO	10.19	10.65	11.80	11.38	10.94	11.53	11.08	11.49	11.33
Na2O	2.58	2.10	2.23	1.96	2.24	2.37	2.09	2.39	2.21
K2O	0.72	0.50	0.51	0.54	0.49	0.56	0.51	0.56	0.45
P2O5	0.19	0.16	0.16	0.17	0.14	0.15	0.15	0.17	0.14
TOTAL	100.00	100.00	100.00	100.00	100.00	100.00	100.00	100.00	100.00
Sr	220	217	229	210	212	202	209	198	197
Rb	14	9	8	10	12	13	11	12	11
Y	29	26	25	26	25	26	25	23	24
Zr	91	72	73	82	70	73	74	70	73
Nb	6	6	6	6	5	5	5	5	5
Co	38	48	39	22	47	41	40	47	45
V	247	235	216	211	216	224	224	239	210
La	11	13	9	15	10	11	11	13	11
Cr	187	239	212	238	326	268	336	304	400
Zn	81	72	72	72	62	64	64	76	65
Cu	104	64	83	71	68	79	76	68	74
Ni	52	85	74	80	97	72	96	93	119
Sc	37	29	28	27	27	29	27	31	26
Ba	204	131	110	141	192	184	158	127	151
Selected trace element ratios									
Zr/Nb	15.17	12.00	12.17	13.67	14.00	14.60	14.80	14.00	14.60
Zr/Y	3.14	2.77	2.92	3.15	2.80	2.81	2.96	3.04	3.04
Ti/Zr	74.02	85.19	85.54	74.78	79.56	82.32	75.40	84.07	75.62
P/Zr	9.14	9.73	9.67	9.07	8.73	8.99	8.85	10.62	8.38
Ti/P	8.10	8.76	8.84	8.24	9.12	9.16	8.52	7.92	9.03
Sc/Ni	0.71	0.34	0.38	0.34	0.29	0.40	0.28	0.33	0.22
Cr/Ni	3.60	2.81	2.86	2.98	3.36	3.72	3.50	3.27	3.36

Table A2.4. Normalised major and unnormalised trace element data for the Sani Pass volcanics

	P201	P203	P204	P205	P227	P228	P232	P233	P234
SiO2	50.77	52.29	51.67	51.33	50.10	51.64	50.26	50.91	51.29
TiO2	0.89	1.12	0.90	0.90	0.89	1.05	0.96	0.97	0.93
Al2O3	16.02	15.63	15.95	14.97	13.56	15.26	16.40	16.12	16.59
Fe2O3	1.65	1.73	1.65	1.69	1.90	1.71	1.69	1.69	1.63
FeO	8.23	8.65	8.24	8.48	9.49	8.52	8.44	8.46	8.14
MnO	0.19	0.17	0.16	0.17	0.19	0.18	0.17	0.17	0.19
MgO	7.50	6.16	7.22	8.74	12.10	7.23	7.91	7.37	6.85
CaO	11.71	10.91	11.19	11.13	8.84	11.36	11.07	11.21	11.19
Na2O	2.37	2.37	2.34	1.97	1.63	2.15	2.08	2.18	2.25
K2O	0.52	0.76	0.54	0.48	1.13	0.71	0.86	0.74	0.77
P2O5	0.14	0.20	0.14	0.14	0.16	0.20	0.17	0.17	0.16
TOTAL	100.00	100.00	100.00	100.00	100.00	100.00	100.00	100.00	100.00
Sr	207	196	191	254	246	234	200	210	208
Rb	12	6	10	15	22	14	15	11	15
Y	28	24	23	28	22	26	25	25	24
Zr	83	71	68	95	73	92	91	93	88
Nb	6	5	4	8	7	9	9	9	8
Co	43	44	49	41	64	41	49	50	41
V	202	252	238	195	195	191	235	221	212
La	9	7	17	13	13	14	15	16	19
Cr	256	315	322	175	232	240	328	312	203
Zn	58	74	76	64	78	74	80	80	68
Cu	75	71	67	124	55	75	71	65	65
Ni	70	90	93	63	188	76	117	104	74
Sc	26	30	29	25	27	25	30	28	27
Ba	164	135	140	211	282	213	169	175	162
Selected trace element ratios									
Zr/Nb	13.83	14.20	17.00	11.88	10.43	10.22	10.11	10.33	11.00
Zr/Y	2.96	2.96	2.96	3.39	3.32	3.54	3.64	3.72	3.67
Ti/Zr	64.62	94.85	79.63	56.85	73.19	68.65	63.45	62.66	63.47
P/Zr	7.40	12.33	9.02	6.44	9.58	9.52	8.18	7.99	7.95
Ti/P	8.73	7.69	8.83	8.83	7.64	7.21	7.76	7.84	7.98
Sc/Ni	0.37	0.33	0.31	0.40	0.14	0.33	0.26	0.27	0.36
Cr/Ni	3.66	3.50	3.46	2.78	1.23	3.16	2.80	3.00	2.74

Table A2.4. Normalised major and unnormalised trace element data for the Sani Pass volcanics

	P236	P238	P240	P242	P244	P247	P250	P254	P255
SiO2	51.79	50.83	52.20	52.19	51.02	50.68	52.59	51.88	51.84
TiO2	0.98	1.00	0.97	0.98	0.94	0.98	0.94	1.02	0.97
Al2O3	15.81	16.47	16.02	15.80	16.37	16.14	15.46	15.43	16.39
Fe2O3	1.67	1.71	1.68	1.66	1.67	1.68	1.67	1.72	1.62
FeO	8.35	8.56	8.39	8.32	8.35	8.43	8.35	8.60	8.13
MnO	0.16	0.18	0.16	0.15	0.18	0.18	0.17	0.18	0.16
MgO	6.88	6.93	6.35	6.83	7.03	7.34	7.23	7.07	6.58
CaO	10.83	11.17	11.20	10.26	11.48	11.38	10.37	10.76	11.22
Na2O	2.47	2.20	2.34	2.74	2.27	2.30	2.70	2.40	2.26
K2O	0.89	0.76	0.51	0.89	0.51	0.72	0.37	0.78	0.68
P2O5	0.17	0.18	0.17	0.17	0.16	0.17	0.15	0.16	0.15
TOTAL	100.00	100.00	100.00	100.00	100.00	100.00	100.00	100.00	100.00
Sr	186	207	150	214	183	200	180	187	170
Rb	14	14	10	13	7	10	7	17	14
Y	26	27	25	26	25	26	25	28	25
Zr	92	97	90	92	83	88	80	90	79
Nb	8	9	8	8	8	7	4	5	4
Co	42	43	40	38	42	46	44	37	43
V	230	215	238	247	240	245	243	232	235
La	17	15	11	12	13	13	15	13	10
Cr	215	185	233	225	258	262	287	247	274
Zn	79	68	82	82	78	81	79	59	75
Cu	78	92	76	73	74	70	74	72	80
Ni	67	69	74	62	89	78	88	73	87
Sc	30	27	31	33	31	33	35	29	31
Ba	189	175	163	212	159	160	146	187	143
Selected trace element ratios									
Zr/Nb	11.50	10.78	11.25	11.50	10.38	12.57	20.00	18.00	19.75
Zr/Y	3.54	3.59	3.60	3.54	3.32	3.38	3.20	3.21	3.16
Ti/Zr	64.07	61.89	64.70	63.96	68.04	66.84	70.52	68.11	73.68
P/Zr	8.09	8.11	8.26	8.08	8.43	8.44	8.19	7.78	8.30
Ti/P	7.92	7.63	7.84	7.92	8.07	7.92	8.61	8.76	8.88
Sc/Ni	0.45	0.39	0.42	0.53	0.35	0.42	0.40	0.40	0.36
Cr/Ni	3.21	2.68	3.15	3.63	2.90	3.36	3.26	3.38	3.15

Table A2.4. Normalised major and unnormalised trace element data for the Sani Pass volcanics

	P256	P257	P259	P263	P267	P268	P269	P271	P272
SiO2	51.56	51.17	51.69	51.82	51.49	51.80	51.47	51.42	52.10
TiO2	0.95	0.92	0.89	0.93	0.84	0.90	0.91	0.92	1.02
Al2O3	15.85	16.27	15.71	15.37	16.73	15.62	15.88	15.87	15.18
Fe2O3	1.65	1.69	1.68	1.72	1.61	1.68	1.71	1.72	1.85
FeO	8.27	8.45	8.41	8.61	8.08	8.40	8.58	8.61	9.27
MnO	0.16	0.17	0.17	0.18	0.16	0.17	0.18	0.19	0.17
MgO	7.55	6.79	7.52	7.42	6.68	7.48	7.29	7.03	7.10
CaO	11.21	11.53	11.20	11.12	11.45	11.05	11.30	11.22	10.38
Na2O	2.05	2.01	2.07	2.01	2.07	2.28	2.09	2.29	2.19
K2O	0.59	0.85	0.51	0.66	0.76	0.47	0.44	0.58	0.57
P2O5	0.15	0.15	0.15	0.15	0.13	0.15	0.15	0.15	0.17
TOTAL	100.00	100.00	100.00	100.00	100.00	100.00	100.00	100.00	100.00
Sr	184	112	194	178	115	191	183	190	171
Rb	10	28	8	16	24	7	7	10	21
Y	26	25	25	26	23	25	26	26	29
Zr	83	83	85	82	74	85	93	93	103
Nb	4	5	5	4	5	4	6	5	7
Co	48	47	42	46	39	29	45	47	45
V	224	260	230	232	237	234	225	218	276
La	6	14	9	7	8	8	14	12	15
Cr	251	288	284	271	330	282	204	181	211
Zn	74	81	79	81	74	82	81	66	89
Cu	77	79	81	80	73	102	82	128	100
Ni	95	89	90	93	97	110	91	92	66
Sc	29	35	35	34	34	33	31	27	39
Ba	147	102	150	150	143	180	149	158	160
Selected trace element ratios									
Zr/Nb	20.75	16.60	17.00	20.50	14.80	21.25	15.50	18.60	14.71
Zr/Y	3.19	3.32	3.40	3.15	3.22	3.40	3.58	3.58	3.55
Ti/Zr	68.72	66.53	62.84	68.10	68.13	63.55	58.72	59.35	59.48
P/Zr	7.90	7.90	7.71	8.00	7.68	7.71	7.05	7.05	7.22
Ti/P	8.70	8.42	8.15	8.52	8.88	8.24	8.33	8.42	8.24
Sc/Ni	0.31	0.39	0.39	0.37	0.35	0.30	0.34	0.29	0.59
Cr/Ni	2.64	3.24	3.16	2.91	3.40	2.56	2.24	1.97	3.20

Table A2.4. Normalised major and unnormalised trace element data for the Sani Pass volcanics

	P273	P276	P277	P278
SiO2	52.38	51.39	50.57	52.76
TiO2	1.00	1.00	1.01	1.00
Al2O3	15.61	16.13	16.35	15.57
Fe2O3	1.79	1.77	1.82	1.73
FeO	8.94	8.83	9.09	8.64
MnO	0.18	0.16	0.19	0.17
MgO	6.10	6.72	6.59	6.19
CaO	10.77	10.55	11.86	10.63
Na2O	2.29	2.48	2.05	2.43
K2O	0.77	0.80	0.31	0.70
P2O5	0.16	0.17	0.16	0.18
TOTAL	100.00	100.00	100.00	100.00
Sr	189	189	147	202
Rb	16	16	8	12
Y	29	29	27	27
Zr	100	101	98	93
Nb	5	6	6	7
Co	34	41	40	38
V	244	248	263	215
La	10	8	12	8
Cr	164	174	172	133
Zn	84	86	83	78
Cu	99	77	81	83
Ni	62	61	61	55
Sc	33	36	36	31
Ba	192	225	81	182
Selected trace element ratios				
Zr/Nb	20.00	16.83	16.33	13.29
Zr/Y	3.45	3.48	3.63	3.44
Ti/Zr	60.01	59.36	61.83	64.50
P/Zr	6.99	7.35	7.13	8.45
Ti/P	8.58	8.08	8.67	7.63
Sc/Ni	0.53	0.59	0.59	0.56
Cr/Ni	2.65	2.85	2.82	2.42

Table A2.5. Normalised major and unnormalised trace element data for the Sani Pass dolerites

	D10	D20	D30	D41	D51	D80	D90	D91
SiO2	52.19	52.68	52.92	52.53	52.21	51.96	52.21	52.40
TiO2	1.09	0.97	1.17	1.10	0.99	1.03	0.98	0.99
Al2O3	14.90	15.74	14.63	15.03	15.43	15.42	15.44	15.33
Fe2O3	1.93	1.60	1.99	1.89	1.66	1.84	1.68	1.67
FeO	9.67	8.00	9.96	9.43	8.30	9.19	8.40	8.36
MnO	0.19	0.16	0.20	0.20	0.18	0.20	0.19	0.18
MgO	6.15	6.96	5.77	6.39	7.45	6.41	7.39	7.24
CaO	10.85	11.01	10.31	10.42	10.81	11.04	10.53	10.76
Na2O	2.27	2.21	2.20	2.28	2.25	2.28	2.46	2.43
K2O	0.62	0.54	0.65	0.57	0.56	0.48	0.55	0.47
P2O5	0.14	0.13	0.19	0.16	0.16	0.15	0.17	0.17
TOTAL	100.00	100.00	100.00	100.00	100.00	100.00	100.00	100.00
Sr	166	190	188	183	214	174	207	203
Rb	15	13	17	16	14	13	13	12
Y	29	25	32	28	27	28	26	28
Zr	92	86	108	96	82	87	83	83
Nb	4	5	5	3	4	4	3	3
Co	44	39	40	35	31	35	36	41
V	280	226	266	231	216	242	215	221
La	15	5	20	15	6	5	11	6
Cr	111	272	142	93	252	125	277	248
Zn	93	79	138	65	67	75	70	73
Cu	113	84	110	92	77	92	76	79
Ni	58	101	43	45	69	53	85	76
Sc	33	27	32	28	31	32	30	32
Ba	194	134	219	197	202	198	377	186
Selected trace element ratios								
Zr/Nb	25.47	19.00	21.54	31.83	20.50	21.75	27.67	24.47
Zr/Y	3.16	3.43	3.37	3.40	3.04	3.09	3.23	3.03
Ti/Zr	71.35	68.08	65.19	69.10	72.42	71.03	70.84	71.39
P/Zr	6.67	6.64	7.71	7.32	8.52	7.53	8.95	8.92
Ti/P	10.69	10.25	8.46	9.44	8.50	9.43	7.92	8.00
Sc/Ni	0.56	0.26	0.75	0.62	0.45	0.60	0.35	0.42
Cr/Ni	1.91	2.68	3.30	2.07	3.65	2.36	3.26	3.26

Table A2.6. C.I.P.W. weight percent norms for the Sani Pass volcanics

	GC350	GC360	GC370	GC380	AV400	AV20	AV40	AV50	AV60
SiO2	43.25	53.81	52.59	54.07	45.57	53.49	53.55	54.05	55.61
TiO2	1.15	1.00	1.02	1.32	1.08	1.05	1.06	1.07	0.96
Al2O3	15.04	14.27	15.53	14.81	15.76	15.66	15.60	15.30	15.37
Fe2O3	1.42	1.58	1.64	1.88	1.56	1.76	1.70	1.65	1.64
FeO	7.12	7.91	8.20	9.40	7.82	8.81	8.51	8.24	8.18
MnO	0.19	0.12	0.17	0.18	0.24	0.17	0.16	0.17	0.16
MgO	2.87	2.66	5.13	4.65	4.34	6.38	6.34	5.93	6.23
CaO	16.44	10.83	11.59	10.22	9.91	9.38	8.99	9.36	6.84
Na2O	3.10	2.28	2.12	2.43	1.01	2.14	2.60	2.53	2.78
K2O	0.32	0.51	0.14	0.85	6.90	0.71	1.12	1.10	1.97
P2O5	0.15	0.12	0.12	0.16	0.16	0.17	0.17	0.16	0.16
CO2	8.95	4.91	1.75	0.03	5.65	0.28	0.20	0.44	0.10
TOTAL	100.00	100.00	100.00	100.00	100.00	100.00	100.00	100.00	100.00
Ap	0.35	0.27	0.28	0.38	0.38	0.41	0.41	0.38	0.38
Cc	20.35	11.16	3.99	0.07	12.84	0.64	0.46	1.01	0.23
Il	2.18	1.90	1.94	2.51	2.04	1.99	2.01	2.02	1.82
Or	1.90	3.01	0.82	5.01	40.80	4.22	6.61	6.47	11.62
Ab	26.19	19.25	17.95	20.60	8.54	18.15	22.00	21.43	23.54
An	24.05	21.96	32.43	26.98	12.42	30.99	27.59	27.16	23.65
C	0.78	1.93	0.00	0.00	2.07	0.00	0.00	0.00	0.00
Mt	2.06	2.29	2.38	2.73	2.27	2.55	2.47	2.39	2.37
En (Di)	0.00	0.00	2.75	4.25	0.00	2.79	3.26	3.40	1.93
Fs (Di)	0.00	0.00	2.65	5.09	0.00	2.34	2.64	2.84	1.54
Wo (Di)	0.00	0.00	5.51	9.39	0.00	5.29	6.10	6.43	3.60
En (Hy)	7.14	6.62	10.02	7.33	3.65	13.11	12.52	11.37	13.58
Fs (Hy)	10.36	11.81	9.67	8.77	3.96	10.97	10.13	9.49	10.84
Q	4.65	19.81	9.61	6.90	0.00	6.56	3.82	5.63	4.90
Fo	0.00	0.00	0.00	0.00	5.02	0.00	0.00	0.00	0.00
Fa	0.00	0.00	0.00	0.00	6.01	0.00	0.00	0.00	0.00
Total	100.01	100.01	100.00	100.01	100.00	100.01	100.02	100.02	100.00

Ap – Apatite
Cc – Calcite
Il – Ilmenite
Or – Orthoclase
Ab – Albite
C – Corundum
Mt – Magnetite
En – Enstatite
Fs – Ferrosillite
Wo – Wollastonite
Q – Quartz
Fo – Fosterite
Fa – Fayalite
Di – Diopside
Hy – Hyperstene

Table A2.6. C.I.P.W. weight percent norms for the Sani Pass volcanics

	AV70	AV80	AV90	AV91	AV100	AV110	S120	S130	S131
SiO2	52.61	51.63	53.11	55.89	53.66	53.48	53.00	50.42	51.37
TiO2	1.09	1.07	0.99	1.05	1.01	1.04	0.84	1.03	1.07
Al2O3	16.13	16.24	15.20	15.33	15.23	15.10	15.77	15.56	15.20
Fe2O3	1.73	1.82	1.70	1.54	1.70	1.61	1.54	1.71	1.64
FeO	8.66	9.08	8.51	7.69	8.48	8.06	7.71	8.54	8.18
MnO	0.13	0.17	0.16	0.12	0.17	0.18	0.15	0.16	0.17
MgO	6.35	6.75	6.65	5.83	5.93	5.56	7.22	6.42	6.63
CaO	8.81	9.25	10.00	8.32	10.11	10.27	10.78	11.82	11.17
Na2O	2.19	2.63	2.32	2.72	2.54	2.45	1.64	1.82	2.07
K2O	1.78	0.40	0.74	1.20	0.47	0.98	0.10	0.44	0.57
P2O5	0.16	0.17	0.15	0.16	0.16	0.16	0.10	0.18	0.18
CO2	0.36	0.79	0.47	0.15	0.54	1.11	1.15	1.90	1.75
TOTAL	100.00	100.00	100.00	100.00	100.00	100.00	100.00	100.00	100.00
Ap	0.38	0.40	0.36	0.38	0.38	0.38	0.24	0.42	0.42
Cc	0.82	1.80	1.07	0.34	1.23	2.52	2.61	4.32	3.97
Il	2.06	2.04	1.89	1.99	1.93	1.97	1.59	1.96	2.03
Or	10.52	2.37	4.39	7.08	2.79	5.78	0.59	2.58	3.34
Ab	18.56	22.22	19.64	23.01	21.49	20.77	13.84	15.42	17.54
An	28.93	31.33	28.87	26.08	28.76	27.29	35.44	32.99	30.51
C	0.00	0.00	0.00	0.00	0.00	0.00	0.00	0.00	0.00
Mt	2.51	2.63	2.47	2.23	2.46	2.34	2.24	2.48	2.37
En]	2.55	1.88	3.80	2.98	3.68	3.38	2.44	2.78	2.93
Fs] Di	2.08	1.53	2.95	2.33	3.19	2.96	1.60	2.24	2.17
Wo]	4.78	3.52	7.00	5.50	7.06	6.52	4.23	5.20	5.30
En]	13.26	14.95	12.77	11.54	11.10	10.46	15.54	13.20	13.60
Fs] Hy	10.84	12.19	9.93	9.01	9.62	9.14	10.18	10.63	10.05
Q	2.71	3.15	4.87	7.53	6.31	6.52	9.48	5.80	5.78
Fo	0.00	0.00	0.00	0.00	0.00	0.00	0.00	0.00	0.00
Fa	0.00	0.00	0.00	0.00	0.00	0.00	0.00	0.00	0.00
Total	100.00	100.01	100.01	100.00	100.00	100.03	100.02	100.02	100.01

Ap – Apatite
Cc – Calcite
Il – Ilmenite
Or – Orthodase
Ab – Albite
C – Corundum
Mt – Magnetite
En – Enstatite
Fs – Ferrosillite
Wo – Wollastonite
Q – Quartz
Fo – Fosterite
Fa – Fayalite
Di – Diopside
Hy – Hyperstene

Table A2.6. C.I.P.W. weight percent norms for the Sani Pass volcanics

	S133	S136	M150	M160	M170	P174	P177	P178	P180
SiO2	53.57	52.80	53.30	51.93	53.19	49.47	52.19	50.84	49.77
TiO2	0.98	1.04	1.02	1.04	0.98	0.91	1.01	1.09	0.68
Al2O3	15.89	15.43	16.01	15.65	15.46	15.29	15.77	16.38	15.51
Fe2O3	1.48	1.61	1.56	1.63	1.54	1.56	1.57	1.57	1.69
FeO	7.41	8.07	7.81	8.15	7.68	7.78	7.86	7.84	8.45
MnO	0.18	0.12	0.18	0.16	0.15	0.22	0.15	0.15	0.16
MgO	7.03	7.10	7.42	7.29	7.18	6.14	7.15	5.91	11.25
CaO	10.64	10.35	6.34	8.71	8.39	12.93	11.40	10.61	9.86
Na2O	2.09	1.76	4.14	4.27	4.50	2.22	2.12	3.24	2.04
K2O	0.33	0.73	1.70	0.78	0.53	0.64	0.56	0.91	0.38
P2O5	0.16	0.14	0.15	0.15	0.14	0.16	0.16	0.20	0.11
CO2	0.24	0.85	0.37	0.24	0.26	2.68	0.06	1.26	0.10
TOTAL	100.00	100.00	100.00	100.00	100.00	100.00	100.00	100.00	100.00
Ap	0.38	0.33	0.36	0.36	0.33	0.37	0.38	0.47	0.26
Cc	0.55	1.93	0.85	0.55	0.59	6.10	0.14	2.85	0.23
Il	1.85	1.98	1.95	1.97	1.85	1.73	1.91	2.06	1.28
Or	1.96	4.32	10.04	4.58	3.15	3.77	3.34	5.36	2.26
Ab	17.7	14.90	35.03	36.13	38.05	18.78	17.92	27.40	17.24
An	32.99	32.03	20.08	21.24	20.43	29.87	31.85	27.48	32.04
C	0	0.00	0.00	0.00	0.00	0.00	0.00	0.00	0.00
Mt	2.15	2.34	2.26	2.36	2.23	2.26	2.28	2.27	2.45
En (Di)	4.19	3.11	1.96	4.64	4.51	3.70	5.59	3.59	4.11
Fs (Di)	2.66	2.10	1.24	3.12	2.90	2.88	3.69	2.83	1.95
Wo (Di)	7.19	5.45	3.36	8.12	7.77	6.81	9.72	6.65	6.48
En (Hy)	13.32	14.59	7.32	1.00	4.88	11.59	12.21	9.37	15.12
Fs (Hy)	8.45	9.89	4.63	0.67	3.14	9.02	8.06	7.38	7.18
Q	6.61	7.05	0.00	0.00	0.00	3.14	2.92	0.00	0.00
Fo	0	0.00	6.44	8.77	5.95	0.00	0.00	1.23	6.17
Fa	0	0.00	4.50	6.49	4.22	0.00	0.00	1.07	3.23
Total	100.00	100.02	100.02	100.00	100.00	100.02	100.01	100.01	100.00

Ap – Apatite
Cc – Calcite
Il – Ilmenite
Or – Orthoclase
Ab – Albite
C – Corundum
Mt – Magnetite
En – Enstatite
Fs – Ferrosillite
Wo – Wollastonite
Q – Quartz
Fo – Fosterite
Fa – Fayalite
Di – Diopside
Hy – Hyperstene

Table A2.6. C.I.P.W. weight percent norms for the Sani Pass volcanics

	P181	P182	P183	P185	P187	P188	P200	P222	P223
SiO2	52.92	51.70	51.57	51.93	51.57	50.89	51.57	51.43	50.67
TiO2	1.12	1.02	1.03	1.02	0.93	1.00	0.93	0.98	0.92
Al2O3	15.54	16.07	16.47	15.57	15.54	15.59	15.41	15.65	16.32
Fe2O3	1.72	1.67	1.53	1.70	1.68	1.71	1.70	1.68	1.68
FeO	8.61	8.36	7.67	8.48	8.40	8.55	8.49	8.42	8.39
MnO	0.18	0.16	0.20	0.17	0.17	0.17	0.18	0.19	0.17
MgO	5.97	7.36	5.89	6.86	7.90	7.29	7.84	6.91	7.66
CaO	10.16	10.62	11.67	11.35	10.94	11.50	11.07	11.47	11.32
Na2O	2.57	2.09	2.21	1.95	2.24	2.36	2.09	2.39	2.21
K2O	0.72	0.50	0.50	0.54	0.49	0.56	0.51	0.56	0.45
P2O5	0.19	0.16	0.16	0.17	0.14	0.15	0.15	0.17	0.14
CO2	0.30	0.29	1.10	0.26	0.00	0.23	0.06	0.15	0.07
TOTAL	100.00	100.00	100.00	100.00	100.00	100.00	100.00	100.00	100.00
Ap	0.45	0.38	0.38	0.41	0.33	0.36	0.36	0.41	0.33
Cc	0.69	0.66	2.50	0.60	0.00	0.53	0.14	0.34	0.16
Il	2.12	1.93	1.95	1.93	1.76	1.89	1.76	1.86	1.74
Or	4.28	2.97	2.95	3.21	2.92	3.33	3.04	3.34	2.68
Ab	21.72	17.71	18.74	16.53	18.96	19.94	17.67	20.21	18.69
An	28.75	32.97	33.53	32.10	30.87	30.30	31.14	30.32	33.28
C	0.00	0.00	0.00	0.00	0.00	0.00	0.00	0.00	0.00
Mt	2.50	2.42	2.22	2.46	2.44	2.48	2.46	2.44	2.43
En (Di)	4.02	3.98	3.71	4.92	5.43	5.69	5.36	5.65	5.13
Fs (Di)	3.48	2.73	2.90	3.69	3.53	4.06	3.57	4.20	3.45
Wo (Di)	7.72	7.02	6.85	8.94	9.39	10.15	9.35	10.23	8.98
En (Hy)	10.85	14.34	10.96	12.16	14.26	12.27	14.16	11.58	13.51
Fs (Hy)	9.39	9.85	8.58	9.12	9.29	8.75	9.42	8.61	9.08
Q	4.04	3.03	4.74	3.94	0.82	0.00	1.58	0.84	0.00
Fo	0.00	0.00	0.00	0.00	0.00	0.15	0.00	0.00	0.30
Fa	0.00	0.00	0.00	0.00	0.00	0.12	0.00	0.00	0.23
Total	100.01	99.99	100.01	100.01	100.00	100.02	100.01	100.03	99.99

Ap – Apatite
Cc – Calcite
Il – Ilmenite
Or – Orthodase
Ab – Albite
C – Corundum
Mt – Magnetite
En – Enstatite
Fs – Ferrosillite
Wo – Wollastonite
Q – Quartz
Fo – Fosterite
Fa – Fayalite
Di – Diopside
Hy – Hyperstene

Table A2.6. C.I.P.W. weight percent norms for the Sani Pass volcanics

	P201	P203	P204	P205	P227	P228	P232	P233	P234
SiO2	50.51	52.14	51.49	51.29	50.04	51.47	50.10	50.81	51.21
TiO2	0.89	1.12	0.90	0.90	0.89	1.05	0.96	0.97	0.93
Al2O3	15.94	15.59	15.90	14.96	13.54	15.21	16.35	16.09	16.56
Fe2O3	1.64	1.73	1.64	1.69	1.90	1.70	1.68	1.69	1.63
FeO	8.19	8.63	8.21	8.47	9.48	8.49	8.41	8.44	8.13
MnO	0.19	0.17	0.16	0.17	0.19	0.18	0.17	0.17	0.19
MgO	7.46	6.14	7.20	8.73	12.09	7.21	7.88	7.36	6.84
CaO	11.65	10.88	11.15	11.12	8.83	11.32	11.03	11.19	11.17
Na2O	2.36	2.36	2.33	1.97	1.63	2.14	2.07	2.18	2.25
K2O	0.52	0.76	0.54	0.48	1.13	0.71	0.86	0.74	0.77
P2O5	0.14	0.20	0.14	0.14	0.16	0.20	0.17	0.17	0.16
CO2	0.51	0.28	0.34	0.08	0.12	0.32	0.32	0.19	0.16
TOTAL	100.00	100.00	100.00	100.00	100.00	100.00	100.00	100.00	100.00
Ap	0.33	0.48	0.33	0.33	0.38	0.48	0.41	0.41	0.38
Cc	1.16	0.64	0.78	0.18	0.28	0.73	0.73	0.44	0.37
Il	1.70	2.12	1.70	1.71	1.69	1.99	1.82	1.84	1.76
Or	3.09	4.46	3.21	2.86	6.68	4.22	5.05	4.35	4.53
Ab	19.97	19.94	19.75	16.64	13.75	18.14	17.54	18.41	19.01
An	31.37	29.72	31.31	30.56	26.30	29.74	32.78	31.96	32.85
C	0.00	0.00	0.00	0.00	0.00	0.00	0.00	0.00	0.00
Mt	2.38	2.50	2.38	2.46	2.75	2.46	2.44	2.45	2.36
En (Di)	5.30	4.66	4.93	5.74	4.13	5.39	4.53	5.00	4.76
Fs (Di)	3.59	3.92	3.45	3.43	2.02	3.84	2.95	3.50	3.47
Wo (Di)	9.29	8.84	8.75	9.67	6.55	9.69	7.84	8.87	8.56
En (Hy)	12.34	10.64	13.01	15.99	18.17	12.55	12.84	13.34	12.28
Fs (Hy)	8.35	8.97	9.10	9.56	8.88	8.95	8.37	9.33	8.94
Q	0.00	3.12	1.31	0.87	0.00	1.87	0.00	0.12	0.74
Fo	0.66	0.00	0.00	0.00	5.48	0.00	1.58	0.00	0.00
Fa	0.49	0.00	0.00	0.00	2.95	0.00	1.14	0.00	0.00
Total	100.02	100.01	100.01	100.00	100.01	100.05	100.02	100.02	100.01

Ap – Apatite
Cc – Calcite
Il – Ilmenite
Or – Orthoclase
Ab – Albite
C – Corundum
Mt – Magnetite
En – Enstatite
Fs – Ferrosillite
Wo – Wollastonite
Q – Quartz
Fo – Fosterite
Fa – Fayalite
Di – Diopside
Hy – Hyperstene

Table A2.6. C.I.P.W. weight percent norms for the Sani Pass volcanics

	P236	P238	P240	P242	P244	P247	P250	P254	P255
SiO2	51.63	50.76	52.13	52.11	50.92	50.62	52.54	51.76	51.79
TiO2	0.98	1.00	0.97	0.98	0.94	0.98	0.94	1.02	0.97
Al2O3	15.76	16.45	16.00	15.78	16.34	16.12	15.44	15.39	16.38
Fe2O3	1.66	1.71	1.68	1.66	1.67	1.68	1.67	1.72	1.62
FeO	8.32	8.55	8.38	8.31	8.33	8.42	8.34	8.58	8.12
MnO	0.16	0.18	0.16	0.15	0.18	0.18	0.17	0.18	0.16
MgO	6.86	6.92	6.34	6.82	7.02	7.33	7.22	7.05	6.57
CaO	10.80	11.16	11.19	10.24	11.46	11.37	10.36	10.74	11.21
Na2O	2.46	2.20	2.34	2.74	2.27	2.30	2.70	2.39	2.26
K2O	0.89	0.76	0.51	0.89	0.51	0.72	0.37	0.78	0.68
P2O5	0.17	0.18	0.17	0.17	0.16	0.17	0.15	0.16	0.15
CO2	0.31	0.13	0.13	0.15	0.20	0.11	0.10	0.23	0.09
TOTAL	100.00	100.00	100.00	100.00	100.00	100.00	100.00	100.00	100.00
Ap	0.41	0.43	0.41	0.41	0.38	0.41	0.36	0.38	0.36
Cc	0.71	0.30	0.30	0.34	0.46	0.25	0.23	0.53	0.21
Il	1.85	1.90	1.84	1.86	1.78	1.86	1.78	1.93	1.84
Or	5.23	4.47	3.04	5.24	3.04	4.23	2.20	4.58	3.99
Ab	20.78	18.60	19.79	23.19	19.18	19.45	22.86	20.20	19.11
An	29.36	32.77	31.64	28.14	32.89	31.56	28.89	28.99	32.30
C	0.00	0.00	0.00	0.00	0.00	0.00	0.00	0.00	0.00
Mt	2.41	2.48	2.43	2.41	2.42	2.44	2.42	2.49	2.35
En]	4.88	4.72	4.91	4.75	5.03	5.42	4.90	5.02	5.00
Fs] Di	3.60	3.56	3.95	3.51	3.66	3.80	3.47	3.72	3.75
Wo]	8.82	8.60	9.16	8.59	9.04	9.62	8.73	9.09	9.09
En]	12.21	12.51	10.89	12.24	12.46	10.96	13.08	12.54	11.37
Fs] Hy	8.99	9.42	8.76	9.04	9.06	7.68	9.24	9.28	8.52
Q	0.76	0.26	2.92	0.28	0.63	0.00	1.85	1.25	2.12
Fo	0.00	0.00	0.00	0.00	0.00	1.32	0.00	0.00	0.00
Fa	0.00	0.00	0.00	0.00	0.00	1.02	0.00	0.00	0.00
Total	100.01	100.02	100.04	100.00	100.03	100.02	100.01	100.00	100.01

Ap – Apatite
Cc – Calcite
Il – Ilmenite
Or – Orthodase
Ab – Albite
C – Corundum
Mt – Magnetite
En – Enstatite
Fs – Ferrosillite
Wo – Wollastonite
Q – Quartz
Fo – Fosterite
Fa – Fayalite
Di – Diopside
Hy – Hyperstene

Table A2.6. C.I.P.W. weight percent norms for the Sani Pass volcanics

	P256	P257	P259	P263	P267	P268	P269	P271	P272
SiO2	51.49	51.11	51.64	51.75	51.43	51.75	51.42	51.38	52.01
TiO2	0.95	0.92	0.89	0.93	0.84	0.90	0.91	0.92	1.02
Al2O3	15.83	16.25	15.70	15.35	16.71	15.60	15.87	15.86	15.15
Fe2O3	1.65	1.69	1.68	1.72	1.61	1.68	1.71	1.72	1.85
FeO	8.26	8.44	8.40	8.60	8.07	8.39	8.57	8.60	9.25
MnO	0.16	0.17	0.17	0.18	0.16	0.17	0.18	0.19	0.17
MgO	7.54	6.78	7.51	7.41	6.67	7.47	7.28	7.03	7.09
CaO	11.20	11.52	11.19	11.10	11.44	11.04	11.29	11.21	10.36
Na2O	2.05	2.01	2.07	2.01	2.07	2.28	2.09	2.29	2.19
K2O	0.59	0.85	0.51	0.66	0.76	0.47	0.44	0.58	0.57
P2O5	0.15	0.15	0.15	0.15	0.13	0.15	0.15	0.15	0.17
CO2	0.13	0.11	0.09	0.14	0.11	0.10	0.09	0.07	0.17
TOTAL	100.00	100.00	100.00	100.00	100.00	100.00	100.00	100.00	100.00
Ap	0.36	0.36	0.36	0.36	0.31	0.36	0.36	0.36	0.41
Cc	0.30	0.25	0.21	0.32	0.25	0.23	0.21	0.16	0.39
Il	1.80	1.74	1.69	1.76	1.59	1.70	1.72	1.74	1.93
Or	3.51	5.01	3.04	3.87	4.47	2.80	2.62	3.40	3.40
Ab	17.32	16.98	17.49	16.98	17.48	19.28	17.67	19.38	18.52
An	32.24	32.84	32.04	30.95	34.09	30.94	32.61	31.30	29.82
C	0.00	0.00	0.00	0.00	0.00	0.00	0.00	0.00	0.00
Mt	2.40	2.45	2.44	2.49	2.34	2.43	2.49	2.49	2.68
En (Di)	5.14	5.16	5.19	5.20	4.86	5.25	5.07	5.24	4.35
Fs (Di)	3.44	3.95	3.58	3.71	3.62	3.63	3.68	3.96	3.47
Wo (Di)	8.98	9.45	9.15	9.28	8.81	9.28	9.11	9.55	8.09
En (Hy)	13.64	11.71	13.52	13.26	11.76	13.36	13.07	12.27	13.32
Fs (Hy)	9.11	8.96	9.32	9.47	8.78	9.23	9.48	9.26	10.63
Q	1.77	1.14	1.98	2.35	1.65	1.52	1.92	0.90	3.01
Fo	0.00	0.00	0.00	0.00	0.00	0.00	0.00	0.00	0.00
Fa	0.00	0.00	0.00	0.00	0.00	0.00	0.00	0.00	0.00
Total	100.01	100.00	100.01	100.00	100.01	100.01	100.01	100.01	100.02

Ap – Apatite
Cc – Calcite
Il – Ilmenite
Or – Orthoclase
Ab – Albite
C – Corundum
Mt – Magnetite
En – Enstatite
Fs – Ferrosillite
Wo – Wollastonite
Q – Quartz
Fo – Fosterite
Fa – Fayalite
Di – Diopside
Hy – Hyperstene

Table A2.6. C.I.P.W. weight percent norms for the Sani Pass volcanics

	P273	P276	P277	P278
SiO2	52.34	51.39	50.54	52.73
TiO2	1.00	1.00	1.01	1.00
Al2O3	15.60	16.13	16.34	15.56
Fe2O3	1.79	1.77	1.82	1.73
FeO	8.93	8.83	9.08	8.64
MnO	0.18	0.16	0.19	0.17
MgO	6.10	6.72	6.59	6.19
CaO	10.76	10.55	11.85	10.62
Na2O	2.29	2.48	2.05	2.43
K2O	0.77	0.80	0.31	0.70
P2O5	0.16	0.17	0.16	0.18
CO2	0.08	0.00	0.06	0.05
TOTAL	100.00	100.00	100.00	100.00
Ap	0.38	0.41	0.38	0.43
Cc	0.18	0.00	0.14	0.11
Il	1.90	1.90	1.92	1.90
Or	4.53	4.71	1.85	4.11
Ab	19.38	21.02	17.34	20.58
An	30.02	30.50	34.47	29.48
C	0.00	0.00	0.00	0.00
Mt	2.59	2.56	2.63	2.51
En]	4.67	4.65	5.03	4.76
Fs] Di	4.19	3.72	4.24	4.05
Wo]	9.09	8.66	9.56	9.07
En]	10.51	12.10	11.39	10.65
Fs] Hy	9.42	9.69	9.61	9.06
Q	3.14	0.10	1.44	3.30
Fo	0.00	0.00	0.00	0.00
Fa	0.00	0.00	0.00	0.00
Total	100.00	100.02	100.00	100.01

Ap – Apatite
Cc – Calcite
Il – Ilmenite
Or – Orthoclase
Ab – Albite
C – Corundum
Mt – Magnetite
En – Enstatite
Fs – Ferrosillite
Wo – Wollastonite
Q – Quartz
Fo – Fosterite
Fa – Fayalite
Di – Diopside
Hy – Hyperstene

Table A2.7. C.I.P.W. weight percent norms for the Sani Pass dolerites

	D10	D20	D30	D41	D51	D80	D90	D91
SiO2	52.13	52.63	52.88	52.50	52.18	51.92	52.18	52.37
TiO2	1.09	0.97	1.17	1.10	0.99	1.03	0.98	0.99
Al2O3	14.88	15.73	14.62	15.02	15.42	15.41	15.43	15.32
Fe2O3	1.93	1.60	1.99	1.89	1.66	1.84	1.68	1.67
FeO	9.66	7.99	9.95	9.43	8.30	9.18	8.39	8.35
MnO	0.19	0.16	0.20	0.20	0.18	0.20	0.19	0.18
MgO	6.14	6.95	5.77	6.39	7.45	6.41	7.39	7.24
CaO	10.84	11.00	10.30	10.41	10.80	11.03	10.52	10.75
Na2O	2.27	2.21	2.20	2.28	2.25	2.28	2.46	2.43
K2O	0.62	0.54	0.65	0.57	0.56	0.48	0.55	0.47
P2O5	0.14	0.13	0.19	0.16	0.16	0.15	0.17	0.17
CO2	0.11	0.09	0.08	0.05	0.05	0.07	0.06	0.06
TOTAL	100.00	100.00	100.00	100.00	100.00	100.00	100.00	100.00
Ap	0.33	0.31	0.46	0.38	0.38	0.36	0.41	0.41
Cc	0.25	0.21	0.07	0.11	0.11	0.16	0.14	0.14
Il	2.07	1.84	2.23	2.09	1.88	1.96	1.86	1.88
Or	3.64	3.22	3.82	3.34	3.34	2.86	3.28	2.80
Ab	19.22	18.68	18.65	19.32	19.04	19.31	20.83	20.57
An	28.59	31.42	28.08	29.06	30.32	30.36	29.43	29.49
C	0.00	0.00	0.00	0.00	0.00	0.00	0.00	0.00
Mt	2.80	2.32	2.89	2.73	2.41	2.66	2.43	2.42
En (Di)	4.91	5.12	4.33	4.55	5.22	4.96	5.02	5.26
Fs (Di)	4.72	3.57	4.54	4.09	3.53	4.36	3.48	3.69
Wo (Di)	9.84	9.06	9.01	8.86	9.15	9.58	8.88	9.33
En (Hy)	10.38	12.18	10.05	11.38	13.35	11.00	13.39	12.78
Fs (Hy)	9.97	8.48	10.53	10.22	9.04	9.65	9.28	8.97
Q	3.27	3.61	5.36	3.87	2.24	2.78	1.58	2.27
Fo	0.00	0.00	0.00	0.00	0.00	0.00	0.00	0.00
Fa	0.00	0.00	0.00	0.00	0.00	0.00	0.00	0.00
Total	99.99	100.02	100.02	100.00	100.01	100.00	100.01	100.01

Ap – Apatite
Cc – Calcite
Il – Ilmenite
Or – Orthoclase
Ab – Albite
C – Corundum
Mt – Magnetite
En – Enstatite
Fs – Ferrosillite
Wo – Wollastonite
Q – Quartz
Fo – Fosterite
Fa – Fayalite
Di – Diopside
Hy – Hyperstene

APPENDIX 3

ELECTRON MICROPROBE

Mineral analyses were performed by Dr A A Mitchell, using the JEOL SUPERPROBE 733 at Rhodes University, utilizing wavelength dispersive spectrometers. Accelerating potential was 15 kV, and beam current 25 nA. Samples were prepared as polished thin sections on glass slides at the University of Durban-Westville.

APPENDIX 4

X-RAY DIFFRACTION ANALYSIS

X-Ray diffraction measurements were undertaken on 58 samples of amygdale minerals. The aliquot of pure mineral analysed was hand-picked from each sample and crushed to a fine ($<63\mu$) powder using an agate mortar and pestle.

Measurements were made at the Physics Department, University of Natal (Durban) and the Geology Department, University of Durban-Westville. The University of Natal equipment consisted of a Phillips PW1370/20 generator with a PW1316/60 tube head containing a Rigaku-Denki RK291800LF copper target tube (run at 40 Kv and 30 or 20 Ma) with a nickel filter and a scanning goniometer controlled by a PW1390 channel controller unit. At the University of Durban-Westville a Phillips PW1310/08 generator with a PW1316/10n tube head containing a PW2276/20 cobalt target tube (run at 35 Kv and 20 Ma) with iron filter and a Debey-Scherrer powder camera (114.6 mm diameter) were used.

The 2 theta values recorded on the difractograms and films were measured manually and converted to d spacing using tables derived from the Bragg's equation. Mineral identification was undertaken using J.C.P.D.S. search manual and mineral data books (J.C.P.D.S. 1983, 1986a, 1986b).

Table A4.1. Amygdales from the Sani Pass analysed by x−ray diffraction

sample #	method	K−alpha	filter	volts	amps
350a	difractometer	Cu	Ni	40	20
360a	camera	Co	Fe	35	20
400a	camera	Co	Fe	35	20
20a	camera	Co	Fe	35	20
70b	difractometer	Co	Fe	40	30
90a	camera	Co	Fe	35	20
110a	difractometer	Cu	Ni	40	20
112a	difractometer	Co	Fe	40	30
112b	difractometer	Co	Fe	40	30
120a	difractometer	Cu	Ni	40	20
133a	difractometer	Co	Fe	40	30
150a	difractometer	Cu	Ni	40	20
160a	difractometer	Co	Fe	40	30
177a	difractometer	Cu	Ni	40	20
180a	difractometer	Cu	Ni	40	20
188a	difractometer	Cu	Ni	40	20
201a	difractometer	Co	Fe	40	30
203a	difractometer	Co	Fe	40	30
204a	difractometer	Co	Fe	40	30
222a	difractometer	Co	Fe	40	30
230a	difractometer	Cu	Ni	40	20
233a	difractometer	Co	Fe	40	30
238a	difractometer	Cu	Ni	40	20
240a	difractometer	Cu	Ni	40	20
242a	difractometer	Co	Fe	40	30
243a	difractometer	Co	Fe	40	30
245a	difractometer	Co	Fe	40	30
246a	difractometer	Cu	Ni	40	30
246b	difractometer	Cu	Ni	40	20
248a	difractometer	Co	Fe	40	30
248p	difractometer	Cu	Ni	40	20
250a	difractometer	Co	Fe	40	20
250p	difractometer	Co	Fe	40	30
251a	difractometer	Cu	Ni	40	20
253p	difractometer	Cu	Ni	40	20
255a	difractometer	Co	Fe	40	30
257a	difractometer	Cu	Ni	40	20
259a	difractometer	Co	Fe	40	30
259p	difractometer	Cu	Ni	40	20
262a	difractometer	Cu	Ni	40	20
263a	difractometer	Co	Fe	40	30

263a,b,c=spherical amygdale
259p=pipe amygdale

Table A4.1. Amygdales from the Sani Pass analysed by x−ray diffraction

sample #	method	K−alpha	filter	volts	amps
267a	difractometer	Cu	Ni	40	20
269p	difractometer	Cu	Ni	40	20
271p	difractometer	Cu	Ni	40	30
271b	difractometer	Co	Fe	40	20
272a	difractometer	Co	Fe	40	30
272p	difractometer	Co	Fe	40	30
272c	difractometer	Co	Fe	40	30
274a	difractometer	Cu	Ni	40	20
274p	difractometer	Cu	Ni	40	20
275a	difractometer	Cu	Ni	40	20
277a	difractometer	Co	Fe	40	30
278a	difractometer	Co	Fe	40	30
278b	difractometer	Cu	Ni	40	20
278c	difractometer	Cu	Ni	40	20

263a,b,c=spherical amygdale
259p=pipe amygdale

APPENDIX 5

DISTRIBUTION COEFFICIENTS

Distribution coefficients used in this study are tabulated in Table A5.1, and all have been obtained from the literature, which is appropriately listed in the references.

TABLE A 5.1

SELECTED PARTITION COEFFICIENTS FOR TRACE ELEMENTS IN THE BASALTIC ASSEMBLAGE

	PLAGIOCLASE	CLINOPYROXENE	OLIVINE
Ba	0.10	0.01[1]	0.01[1]
Nb	0.01[1] 0.01[2]	0.10[1] 0.10[2]	0.01[1] 0.01[2]
Zr	0.01[1] 0.01[2]	0.25[1] 0.10[2]	0.01[1] 0.01[2]
Y	0.10[1] 0.03[2]	0.55[1] 0.50[2]	0.01[1] 0.01[2]
Ti	0.04[2]	0.3[2]	0.02[2]
Sr	2.00[1]	0.10[1]	0.01[1]
Rb	0.05[1]	0.01[1]	0.01[1]
Ni	0.01[1]	2.00[1]	20.00[1]
Cr	0.05[1]	5.00[1]	0.60[1]
V	0.01[1]	1.5[1]	0.01[1]

1 = Le Roex (1985)
2 = Pearce and Norry (1979)